Geometry of River Networks

by

Peter Sheridan Dodds

M.Sc., University of Melbourne, 1994
B.Eng. (Elec.), University of Melbourne, 1993
B.Sc., University of Melbourne, 1993

Submitted to the Department of Mathematics
in partial fulfillment of the requirements for the degree of

DOCTOR OF PHILOSOPHY

AT THE

MASSACHUSETTS INSTITUTE OF TECHNOLOGY

JUNE 2000

Author . . . .
Department of Mathematics
May 10, 2000

Certified by. . . . .
Daniel H. Rothman
Professor of Geophysics
Department of Earth, Atmospheric and Planetary Sciences
Thesis Supervisor

Accepted by . . . .
Michael Sipser
Chairman, Applied Mathematics Committee

Accepted by . . . .
Tomasz S. Mrowka
Chairman, Departmental Committee on Graduate Students

Geometry of River Networks

by

Peter Sheridan Dodds

Abstract

Networks are intrinsic to a broad spectrum of complex phenomena in the
world around us: thoughts and memory emerge from the interconnection
of neurons in the brain, nutrients and waste are transported through the
cardiovascular system, and social and business networks link people. River
networks stand as an archetypal example of branching networks, an impor-
tant sub-class of all network structures. Of significant physical interest in
and of themselves, river networks thus also provide an opportunity to de-
velop results which are extendable to branching networks in general. To this
end, this thesis carries out a thorough examination of river network geom-
etry. The work combines analytic results, numerical simulations of simple
models and measurements of real river networks. We focus on scaling laws
which are central to the description of river networks. Starting from a few
simple assumptions about network architecture, we derive all known scaling
laws showing that only two scaling exponents are independent. Having thus
simplified the description of networks we pursue the precise measurement
of real network structure and the further refining of our descriptive tools.
We address the key issue of universality, the possibility that scaling expo-
nents of river networks take on specific values independent of region. We find
that deviations from scaling are significant enough to preclude exact, defini-
tive measurements. Importantly, geology matters as the externality of basin
shape is shown to be part of the reason for these deviations. This implies that
theories that do not incorporate boundary conditions are unable to produce
realistic river network structures. We also extend a number of scaling laws
to incorporate fluctuations about simple scaling. Going further than this, we
find we are able to identify joint probability distributions that underlie these
scaling laws. We generalize a well-known description of the size and number
of network components as well as a description of network architecture, how

these network components fit together. Both of these generalizations demonstrate that the spatial distribution of network components is random and, in this sense, we obtain the most basic level of network description.

Thesis Supervisor: Daniel H. Rothman
Title: Professor of Geophysics
Department of Earth, Atmospheric and Planetary Sciences

Acknowledgments

Let's see. First billing goes to Dan Rothman as the esteemed fulfiller of the supervisory tasks. Dan has created a wonderful environment where all sorts of scientific directions are possible. Alongside the provision of this academic freedom, Dan also manages to pass on the necessary discipline of thinking as well as an even requirement of quality. The atmosphere of Dan's group is collegial after his own nature and encourages, if not requires, a great broadening of ones skill base. I am delighted to have had the opportunity to do so.

Given these thoughts, it is not surprising that over the years, Dan has gathered together an intriguing and eclectic bunch of students and postdocs. Not the least of these characters is the irrepressible Josh Weitz, a fellow drifter, in his case from physics. With elements of the bizzaro world Dodds, our scientific interaction has been tremendous and will hopefully extend out over a longer time scale. Josh is also to be commended on the fact that he is an excellent human being.

Other members: the affable Olav van Genabeek, an escapee to Wall Street, from whom much knowledge of coding was absorbed (extracted); the roaming Romualdo Pastor-Satorras, whose passing interest in the earth sciences led us to many useful ideas and discussions in the middle part of my research time; and it is pleasing to note the arrival of Norbert Schorghofer, whose charter in part is to clean up the thoughts we and others have generated on river networks.

Thanks go to many from whom I have sort advice on or discussed the matters of science and otherwise: Michael Brenner (for providing the right measures of excitement, encouragement, and doubt), Kelin Whipple (both the irascible and non-irascible versions are appreciated as well as the chance to tag along on field trips and hence see the real world), Andrea Rinaldo (for unbounded enthusiasm and many network discussions), Simon McClusky (for much discussion of the intricacies of Linux and cricket issues), Duncan Watts (for being a good bloke), Hung Cheng, and Gil Strang (the latter two for their sagacity). Much gratitude goes also to Michael and Kelin along with Martin Bazant for committing to be on my thesis committee.

Terri Macloon and Jane Shapiro have both provided steady good humor as well as infinite skill in dealing with the bureaucracy of MIT and elsewhere. Thanks to Shirley Entzminger-Merritt for showing unflagging spirit and good humour. Linda Okun deserves much credit for keeping an eye on graduate researchers in the Mathematics Department.

Aimee is a champ. Brave too, in that our relationship has spanned much of my PhD and even included a wedding. Her ability to tackle any situation and get the job done continues to give me clues about the way forward. An infinite supplier of companionship and confidence. Well met, indeed.

Ah, yes, Mum and Dad, who are asleep at the moment on the other side of the world on their farm in rural Australia, 180 degrees out of phase. They have been remarkably happy to see me wander off on this strange path. A sentence, not even a carefully crafted self-referential one, can capture their influence on my life. Or can it? To Chris and Ritchie, who are two of the funniest blokes around, uproariously amusing, and are also my two younger yet larger brothers; for sharing in all the great things about growing up in the country. Plaudits to Mandy for her collusion with Chris. To Grandma for being an amazing and continual source of inspiration and for her unbounded curiosity and love of crosswords.

To those who come with Aimee: Bernie, Nancy, Sarah and Kalea. Their inclusion of me into their family makes things that much more solid.

And some good mates: Peter Trapa (the raving f'wit), Richard Stone, Radica Šipčić, Chrysanthe Spyropolous, Anthony Brockwell, Susie Brennan, Fleur Johns and Pete Hammond, Carl McCamish, and Rach Haverfield.

Miscellaneous thanks also go to the existence of `cricinfo.org`, LaTeX, Promite, Linux (Linus Torvalds, well done), the majesty of Perl, Tadasana through to Sirasana, Asthanga Yoga, K. Pattabhi Jois, Pilates, Moira Stott, chocolate-coated almonds, running trails, Toshiba (Satellite Pro 420CDS), the Peter Pan Bus service, touch rugby, Bridgestone Bicycles, `slashdot.org`, the London Times cryptic, the word "lull," Kate, Garfield, Fred, Red, Whiskey, Sylvester, Blackie, Charlie and Freida, Michael Leunig.

And while we are here, I must recommend some books for the thesis scribe. Have a read of "Writing Your Dissertation in Fifteen Minutes a Day" by Joan Bolker, [14]. It is not the detrimental pseudo-self-help book that its title would suggest. A wonderful and inspirational treatise on writing is "On Writing Well" by William Zinnser, [158]. Of course, the writing in this thesis is not at the level aspired to by Zinsser but it is perhaps better than it would have been otherwise.

Finally, in preparing this work, many scribbles of thoughts have been recorded elsewhere in two ways. The first method has produced a collection

of the traditional handwritten notebooks which now reside on the shelf and contain streams of often impenetrable confusion. Indeed, these are yellow pages that are immediately aged, imbued with strokes of pale blue fantasy. The second storage of 'work done' has employed the higher level of the imperious LaTeX. What has evolved are yearly journals with daily entries of ideas, findings, graphs and so on. These works contain indexes for citations, people, authors and subject. These I would suggest for the truly interested reader who is after the rough material from which papers are hewn. Not surprisingly, the most probable number of such truly interested readers will be one, namely me. I hasten to add such a record has proved time and time again to be of great benefit. Didn't I do this before? What went wrong there? When did we think to do all of that? Pleased with the idea, I have created a template which has been passed on to various fellow researchers who will presumably improve upon the original in all manner of ways.

Contents

CHAPTER 1

Introduction

This is a thesis about the geometry of river networks.

Let us first take a moment to enjoy the etymological foundations of the title. River networks pattern the earth's surface, their form constantly being reaffirmed and rearranged by the many physical actions that conspire together to create erosion. The study of river networks is thus a subject placed in the box marked "Earth Sciences," bundled up in a small package with the word "Geomorphology" written across one end. In its entirety, geomorphology is the study of the surfaces of planets, their form and the physical processes at work [114]. Thus, in discerning the spatial structure of river networks, we are performing geometry in its most obvious and obsolete sense, the measurement of the earth.

While the work of this thesis does technically reside somewhere in the geomorphology package, the study of river networks lends itself to more general applications. First and foremost, a river network stands as an archetypal example of a branching network. Branching networks appear throughout the world around us and often their tasks revolve around the distribution or collection of material. Myriad examples appear in biology such as the bronchial structure of the lungs [44, 53], the arterial and venous blood networks [23, 43, 71], and the external forms of all tree-like biological organisms.

Moving out beyond branching networks, we see them as an important sub-class of the broad spectrum of all networks. Having restrained ourselves from saying the same for branching networks, we give in to the temptation and suggest that networks are ubiquitous. Moreover, they play many important roles. There is the Internet [3], power grids [148], road systems, leaf patterns [103], computer chip architecture, social networks [149], and the wiring of the brain [5, 17].

It seems reasonable that networks become a focus of the much vaunted study of complex systems (in other words, science). Indeed, the study of networks is showing signs of developing into a science of its own. Although graph theory is a mature field, results there lean towards topological information. There appears to be much room for general theories of network structure, network evolution and dynamics on networks.

1.1   A few rules of the game

Against the sage advice of Heraclitus,[1] we largely view river networks as static structures. While their dynamic origin is of great interest, as it is for branching networks in general, we find a profound richness in the description of river network geometry. Indeed, it is only after a static description of network form has been properly developed that we may begin to reasonably ask about network growth. Furthermore, in the case of river networks, we have access only to the present day's single snapshot of the earth's topographic evolution. Dynamic models are thus guided by physical reasoning and inspired computer modeling. While this is enjoyable, comparisons between models and real data tend to be ambiguous and will remain so until we have a better picture of real data.

A particular feature that sets river networks apart within the class of branching networks is that they are embedded in a two-dimensional surface. Going one step further, the work presented here focuses on the planform structure of river networks, i.e., the network as viewed from directly above as on a map. There is a simple reason for doing this: precipitation falls downwards. If we want to equate the area of a basin with how much water is flowing out of it, then the area we need is not the integral of $\mathrm{d}S$ over the basin's surface. Rather, it is the area of the basin as projected onto the horizontal plane. In truth, the connection between precipitation and river water levels is more complicated but nevertheless we have good motivation to study the planform structure of river networks. These remarks are made all the more academic by our choice to study large-scale river networks such as the Amazon and the Mississippi. These networks lie on what are effectively gravitationally flat surfaces and our planar treatment of river networks becomes the logical approach.

---

[1]You could not step twice into the same rivers; for waters are ever flowing on to you—Heraclitus c. 540–c. 480 B.C. [12].

1.2   A nutshelling of major results

Two central notions in the study of river networks are *scaling* and *universality*. In brief, the presence of scaling in a system means that at different scales, a representation of the system looks the same when an appropriate transformation is made. This general definition often reduces to the statement of a set of power laws relating a system's variables. This in turn gives a set of scaling exponents. Universality arises when disparate systems are described by the same set of scaling exponents which are said to define a universality class. Importantly, such an equivalence is usually reflected in a congruence between high-level descriptions of the processes creating systems while the low-level or microscopic details appear to bear little resemblance to each other.

Now, it is observed that the basic structure of river networks is described by scaling laws. So the question is this: what is the universality class of river networks?

Our findings indicate the answer is there is no such beast. We observe deviations from scaling that range from subtle to strong and no fixed exponent can be justified. Moreover, an important source of these deviations comes from the boundary condition of basin shape which is always imposed at large scales by geology. The effects and history of geology are not simply removed by the process of averaging.

Along the road to this finding, we achieve a variety of other results, three of which are bold enough to step forward here. First, from a few simple assumptions about network architecture, we derive the gamut of river network scaling laws. This greatly simplifies and clarifies the amount of information needed to fully describe network structure.

Next, we generalize the description of network components. We find distributions, where before only mean quantities have been used, for the size and number of different types of network fragments. Moreover, we show in depth how these distributions are connected to each other.

Finally, we fully generalize the accepted view of river network architecture. We show in particular that streams and their tributaries are randomly distributed in space. We thus identify the lowest level of meaningful network description.

Having briefly canvassed the major results, we provide a more detailed and linear tour through the thesis.

1.3   Detailed outline of the thesis

First off, we fully describe scaling and universality later in the **Introduction**. We round this discussion out with a presentation of a number of theoretical networks. Each network is a representative of a specific universality class, i.e., a set of networks whose geometries are described by identical scaling exponents. This discussion is adapted from our review paper "Scaling, Universality and Geomorphology" [35].

The thesis proper then comprises four main chapters. Each of these is presented as a separate paper and may be read independent of the others and, indeed, this introduction. However, they are strongly interrelated and are arranged in an order most natural for reading. There is therefore also a degree of overlap in the introductory material to each chapter which, after having read some of the others, may prove tiresome and judicious skimming is advised.

In **chapter 2** we develop connections between the large number of scaling laws found in the description of river networks. This provides a base of understanding upon which the following chapters build. In connecting these scaling laws we obtain a set of scaling relations, i.e., simple algebraic expressions involving scaling exponents. Some of these scaling relations agree with those already known, others are new, and yet others provide corrections to previous calculations. Our approach is the first to connect all exponents starting from a few simple assumptions.

We are thereby able to reduce the scaling law description of river networks to the content of two independent scaling exponents. One of these exponents is further seen to depend on two parameters that describe the details of network architecture. As far as description by scaling laws goes, universality classes of river networks may therefore be identified by a pair of exponents.

The chapter is for the most part theoretical with some modest comparisons with data from real networks and models. This imbalance is addressed in the ensuing three chapters (which have been created as a three part series of papers) with each presenting an even mixture of theory and empirical observations. Specifically, we examine networks for the Mississippi, Amazon, Nile, Congo and Kansas rivers basins. We also motivate our theory with a model of random networks originally introduced by Scheidegger [112]. This model also appears with less fanfare in **chapter 2** and is described later on in the introduction.

In **chapter 3** we focus on the scaling law relating drainage basin area and main stream length. Known as Hack's law, we understand it be of central

importance due to the work we have done in **chapter 2**. There are several
goals of this chapter. First, we examine fluctuations around Hack's law. We
go further than fluctuations and are in fact able to postulate a full joint
probability distribution between basin areas and main stream lengths.

Having established this broader view of Hack's law, we carry out a detailed
investigation of the actual form of Hack's law found in real networks. The aim
is to measure the scaling exponent of Hack's law as accurately as possible.
What we find, however, is that scaling is only approximately obeyed.

We find Hack's law has three regimes pertaining to small, intermediate
and large scales. At small scales, the presence of linear basin shapes gives rise
to a linear relationship between areas and lengths. This linearity gives way to
an approximate scaling at intermediate scales. Here, we find slow, systematic
drifts in exponents. This is significant: we are unable to associate a unique
exponent with the intermediate regime. A further surprise is the extent to
which deviations at small and large scales limit this region of approximate
scaling.

At large scales, Hack's law breaks down, in part due to growing fluctu-
ations coupled with exponentially decreasing sample space. However, this
breakdown is not random and we find deviations to be strongly correlated
with overall basin shape. It is this last observation that brings geology back
into the picture. Basin shapes at large scales are set by tectonic processes
such as orogenesis, i.e., the formation of mountains, and at smaller scales by
geologic processes such as faulting. Even where such effects are not strong,
statistical fluctuations in basin shape still occur.

Taken in total, these deviations from scaling, subtle as they are at in-
termediate scales, are enough to prevent us from determining exact scaling
exponents. River network structure is thus suggested to be subtly more com-
plicated then the form suggested by a single universality class. The results
attest to the difficulty of comparing theory, models and real networks.

Nevertheless, the approximate scaling we do observe is good enough to aid
the development of our geometric picture of river networks. In **chapter 4**
we uncover distributions for the size and number of network components.
Networks are inherently discrete and can be seen as compositions of stream
segments. Equivalently, they can be broken down into a discrete set of nested
sub-basins. These network components may then be systematically classified
according to the way they fit together. The relationships between the average
features of network components belonging to different classes is known as
Horton's laws [58]. What we provide here is a full generalization of these
relationships, extending their arguments from averages to distributions.

The underlying assumptions of **chapter 2** concern network architecture, i.e., how network components fit together, and a generalization of these ideas appears in **chapter 5**. This network description is originally due to Tokunaga [144, 145, 146]. Here we develop a fundamental picture of river network structure showing that the distribution of stream segments is random. Hence, in this final chapter, we reach the most basic level of description of river network geometry.

A summary with a few thoughts on future directions and the nature of research is provided in the **Conclusion**. The summary, having the thesis behind it, is more specific in its statements (and has more jargon) and those well versed in river networks may find it useful to read ahead of time.

Appendix A, we provide detailed calculations pertaining to the work of **Chapter 4**. In **Appendix B**, inspired by Hack's law and the Scheidegger model, we perform some calculations involving random walks. We examine the joint distribution between area and time to first return. In **Appendix C**, we provide details of our analysis of digitized topography and in **Appendix D** we provide some extra data from our analysis not included in the main body of the thesis. Finally, a full bibliography is naturally provided along with indices for the citations as well as notation and subject matter.

We now turn to our discussion of scaling and universality. This is followed by a brief overview of known universality classes of river networks. The reader is invited to engage in these preliminaries as he or she deems necessary.

1.4   Scaling

Consider the following questions regarding the structure of river networks. If one doubles the length of a stream, how does the area drained by that stream change? Or, inversely, how does basin shape change when we compare basins of different drainage areas? The concept of scaling addresses such questions.

1.4.1   Basin allometry

Figure 1.1 shows two river basins along with a sub-basin of each. A basin can be defined at any point on a landscape. Embedded within any basin are a multitude of sub-basins. In considering our simple question above we must first define some dimensions. A reasonable way to do this is to enclose each basin by a rectangle with dimensions $L_\parallel$ and $L_\perp$ as illustrated in Figure 1.1a. $L_\parallel$ is the longitudinal extent of the basin and $L_\perp$ is the basin's characteristic
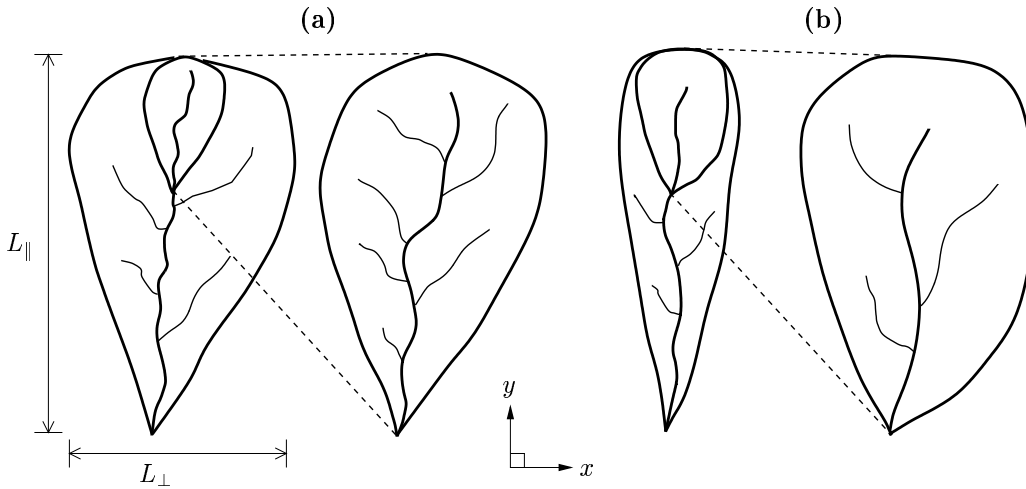
Figure 1.1: A pair of river basins, each with a sub-basin scaled up for comparison with the original. The basins in (a) are self-similar. The basins in (b) are not.

width. By this construction, the area a of a basin is related to these lengths by

$$a \propto L_{\parallel} L_{\perp}. \tag{1.1}$$

Measurements made from real river basins show that $L_{\perp}$ scales like a power H of $L_{\parallel}$ [63, 87]. In symbols,

$$L_{\perp} \propto L_{\parallel}^{H}. \tag{1.2}$$

Substituting equation (1.2) into (1.1), we obtain

$$a \propto L_{\parallel}^{1+H}. \tag{1.3}$$

Equations (1.2) and (1.3) are *scaling laws*. Respectively, they describe how one length scales with respect to another, and how the total area scales with respect to one of the lengths.

Figure 1.1a corresponds to $H = 1$, known as *geometric similarity* or *self-similarity*. As the latter appellation implies, regardless of the basin's size, it looks the same. More prosaically, lengths scale like widths.

The case $H \neq 1$ is called *allometric* scaling. Originally introduced in biology by Huxley and Teissier [62] "to denote growth of a part at a different rate from that of a body as a whole," its meaning for basin size is illustrated

by Figure 1.1b. Here $0 \leq H < 1$, which means that if we examine basins of increasing area, basin *shape* becomes more elongate. In other words, because and $(1 - H)/(1 + H) > 0$ and

$$L_\perp/L_\parallel \propto L_\parallel^{-(1-H)} \propto a^{-(1-H)/(1+H)}, \tag{1.4}$$

the aspect ratio $L_\perp/L_\parallel$ decreases as basin size increases.

1.4.2   Random walks

Our next example is a random walk [39, 91]. We describe it straightforwardly here noting that random walks and their geomorphological applications will reappear throughout the review.

The basic random walk may be defined in terms of a person, who has had too much to drink, stumbling home along a sidewalk. The disoriented walker moves a unit distance along the sidewalk in a fixed time step. After each time step, our inebriated friend spontaneously and with an even chance turns about face or maintains the same course and then wanders another unit distance only to repeat the same erratic decision process. The walker's position x_n after the nth step, relative to the front door of his or her local establishment, is given by

$$x_n = x_{n-1} + s_{n-1} = \sum_{k=0}^{n-1} s_k \tag{1.5}$$

where each $s_k = \pm 1$ with equal probability and $x_0 = 0$.

There are many scaling laws associated with random walks. Probably the most important of these describes the root-mean-square distance that the average walker has traveled after n steps. Since x_n is the sum of independent increments, its variance $\langle x_n^2 \rangle$ is given by the sum of the individual variances,

$$\langle x_n^2 \rangle = \sum_{i=1}^{n} \langle s_i^2 - \langle s_i \rangle^2 \rangle, \tag{1.6}$$

where $\langle \cdot \rangle$ indicates an average over an ensemble of walkers. Since $\langle s_i \rangle = 0$ and $s_i^2 = 1$, we have $\langle x_n^2 \rangle = n$. Defining $r_n = \langle x_n^2 \rangle^{1/2}$, we obtain

$$r_n = n^{1/2}. \tag{1.7}$$
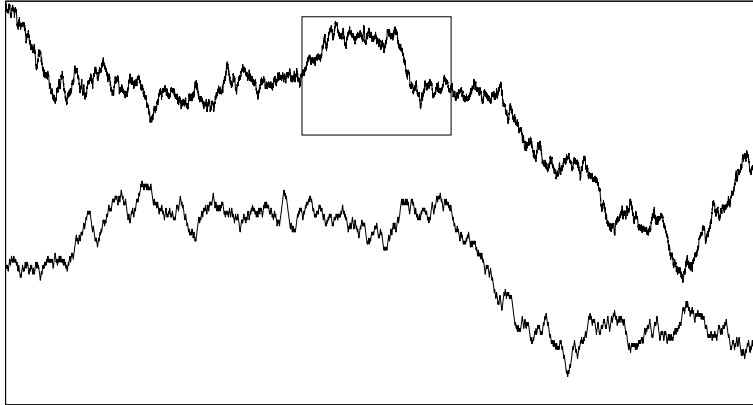
Figure 1.2: Two example random walks where the lower walk is the inset section of the upper walk "blown up." Random walks are statistically equivalent under the rescaling of equation (1.8). Here, $b = 1/5$ so the rescaling is obtained by stretching the horizontal axis by a factor of 5 and the vertical one by $5^{1/2}$.

Generalizing the scaling (1.7) to continuous time t and space x, one has $r(t) \propto t^{1/2}$. Now note that

$$r(t) = b^{-1/2}r(bt). \tag{1.8}$$

In other words, if one rescales time and space such that $t \to bt$ and $x \to b^{1/2}x$, the statistics of the random walk are unchanged. Figure 1.2 illustrates the meaning of these rescalings. The two random walks shown, the lower being a portion of the upper rescaled, are said to be *statistically equivalent*.

More generally, functions $f(x)$ that satisfy equations of the form $f(x) = b^{-\alpha}f(bx)$ are called *self-affine* [83]. This relation need not be exact and indeed usually only holds in a statistical sense. An example already given is the scaling of basin widths found in equation (1.2). Also, when f measures the elevation of a surface at position x, α is called the *roughness exponent* [10].

1.4.3   Probability distributions

What is the size distribution of river basins? In other words, if you pick a random position on a landscape, what is the probability that an area a drains into that point? As we shall see, scaling laws appear once again, this time in the form of probability distributions.

Imagine that the boundaries on each side of a basin are *directed random walks*. In this context, a directed random walk is one in which the random motion is always in the x-direction of Figure 1.1 while the y-direction plays the role of time. Taking the left boundary to be $\phi_l(y)$ and the right boundary to be $\phi_r(y)$, a basin is formed when these two walks intersect (i.e., a pair of sots collide). Since ϕ_l and ϕ_r are independent, the difference $\phi(y) = \phi_r(y) - \phi_l(y)$ is yet another random walk. We see then that the distribution of basin sizes may be related to the probability that the random walk $\phi(y)$ returns to its initial position after n steps for the first time. This is the classic problem of the first return time of a random walk. As the number of steps becomes large, the asymptotic form of the solution is [39]

$$P(n) = \frac{1}{2\sqrt{\pi}} n^{-3/2}. \tag{1.9}$$

In terms of basin parameters, we may take $n \propto l \propto L_\parallel$, where l is the length of the main stream. Note that the assumption $l \propto L_\parallel$ is only valid for directed random walks; this will be discussed further in the following section on networks. We therefore have the distribution of main stream lengths

$$P_l(l) \propto l^{-3/2}. \tag{1.10}$$

Since the typical width of such a basin of length l scales like $l^{1/2}$ (see equation (1.7)), the typical area $a \propto l^{3/2}$. Thus the probability of basin areas is

$$\begin{aligned} P_a(a) &= P_l[l(a)]\frac{\mathrm{d}l}{\mathrm{d}a} \\ &\propto a^{-4/3}. \end{aligned} \tag{1.11}$$

As expressed by equation (1.2), basin widths scale in general like $L_\parallel^H$, where $0 \leq H < 1$ rather than the fixed $H = 1/2$ of random walks. In keeping with this observation, the distributions for area and main stream also generalize. Thus we write

$$P_l(l) \propto l^{-\gamma} \qquad \text{and} \qquad P_a(a) \propto a^{-\tau}. \tag{1.12}$$

Furthermore, the exponents τ and γ are not independent and their connection lies in the aforementioned Hack's law, one of the most well-known scaling laws of river networks. Hack's law expresses the variation of average main stream length $\bar{l}$ with area a,

$$\bar{l} \propto a^h \tag{1.13}$$

where h is known as Hack's exponent. The averaged value $\bar{l}$ is required here since there are noticeable statistical fluctuations in Hack's law [32, 33, 34, 87, 106]. For the simple random model we have $\bar{l} \propto a^{2/3}$, and therefore Hack's exponent $h = 2/3$ [61, 138]. Now, as per equation (1.11), we can write

$$
P_a(a) \;\; = \;\; P_l[\bar{l}(a)]\frac{\mathrm{d}\bar{l}}{\mathrm{d}a} \tag{1.14}
$$

$$
\propto \;\; a^{h(1-\gamma)-1}. \tag{1.15}
$$

Using equation (1.12), this gives our first *scaling relation*

$$
\tau = h(1-\gamma) - 1. \tag{1.16}
$$

In general, scaling relations express exponents as algebraic combinations of other exponents. Such relations abound in theories involving scaling laws and as such provide important tests for both theory and experiment.

1.4.4   Scaling functions

In any physical system, scaling is restricted to a certain range. For example, basins on the size of a water molecule are clearly out of sanity's bounds. At the other extreme, drainage areas are capped by the size of the overall basin which is dictated by geology. In the customary terminology, one says that scaling breaks down at such upper cut-offs due to *finite-size effects*.

As it turns out, this feature of scaling is important both in theory and in practice. Measurements of exponents are made more rigorous and more can be achieved with limited system size. In the case of river networks, Maritan et al. [87] demonstrate how finite-size scaling can be used to derive a number of scaling relations. We outline the basic principle below.

Consider the probability distribution of basin areas $P_a(a) \propto a^{-\tau}$. We can more generally write it as

$$
P_a(a) = a^{-\tau} f(a/a_*) \tag{1.17}
$$

where f is referred to as a *scaling function* and a_* is the typical largest basin area. The behavior of the present scaling function is

$$
f(x) \propto \begin{cases} c & \text{for} \quad x \ll 1 \\ 0 & \text{for} \quad x \gg 1. \end{cases} \tag{1.18}
$$

So for $a \ll a_*$ we have the power law scaling of $P_a(a)$ while for $a \gg a_*$, the probability vanishes.

We enjoy the full worth of this construction when we are able to examine systems of varying overall size. We can recast the form of $P_a(a)$ with lengths by noting from equation (1.3) that $a_* \propto L_\parallel^D$ where we have set $1 + H = D$. This gives

$$P_a(a|L_\parallel) = L_\parallel^{-D\tau} \tilde{f}(a/L_\parallel^D) \tag{1.19}$$

where $\tilde{f}$ is a new scaling function which, due to equation (1.12), has the limiting forms

$$\tilde{f}(x) \propto \begin{cases} x^{-\tau} & \text{for } x \ll 1 \\ 0 & \text{for } x \gg 1. \end{cases} \tag{1.20}$$

We now have two exponents involved. By examining basins of different overall size L we obtain a family of distributions upon which we perform a *scaling collapse*. Rewriting equation (1.19) we have

$$L_\parallel^{\tau D} P_a(a|L_\parallel) = \tilde{f}(a/L_\parallel^D) \tag{1.21}$$

so that plots of $L_\parallel^{D\tau} P_a$ against $a/L_\parallel^D$ should lie along one curve, namely the graph of the scaling function $\tilde{f}$. Thus, by tuning the two exponents τ and D to obtain the best data collapse we are able to arrive at strong estimates for both.

1.5 Universality

One would like to know precisely what aspects of a system are responsible for observed scaling laws. Sometimes seemingly different mechanisms lead to the same behavior. If there is truly a connection between these mechanisms then it must be at a level abstract from raw details. In scaling theory, such connections exist and are heralded by the title of *universality*. In the present section, we consider several examples of universality. This will then lead us into problems in geomorphology proper.

1.5.1 More random walks: crossover phenomena

First, consider once again the drunkard's walk. Suppose that instead of describing the walk as one of discrete steps of unit length, the walker instead lurches a distance s_n at time n with s_n now drawn from some probability

distribution $P(s)$. Take, for example, $P(s) \propto \exp\{-s^2/2\sigma^2\}$, a Gaussian with variance σ^2. One then finds from equation (1.6) that $\langle x_n^2 \rangle = n\sigma^2$, and once again the characteristic excursion $r_n \propto n^{1/2}$. Thus the scaling is the same in both cases, even though the details of the motion differ. Loosely stated, any choice of $P(s)$ will yield the same result, as long as the probability of an extremely large step is extremely small. This is an especially simple but nonetheless powerful instance of universality, which in this case derives directly from the central limit theorem.

Real random walks may of course be more complicated. The archetypal case is Brownian motion. Here one considers the random path taken by a microscopically small object, say a tiny sphere of radius r and mass m, immersed in a liquid of viscosity μ. Within the fluid, random molecular motions induced by thermal agitations act to give the particle random kicks, thus creating a random walk. A classical model of the process, due to Langevin, is expressed by the stochastic differential equation [45, 105]

$$m\frac{\mathrm{d}v}{\mathrm{d}t} = -\alpha v + \eta(t). \tag{1.22}$$

Here v is the velocity of the particle, $\eta(t)$ is uncorrelated Gaussian noise, and $\alpha = 6\pi r \mu$ is the hydrodynamic drag that resists the motion of the sphere. Now note that the existence of the drag force creates a characteristic time scale $\tau = \alpha/m$. For times $t \ll \tau$, we expect viscous damping to be sufficiently unimportant that the particle moves in free flight with the thermal velocity characteristic of molecular motion. On the other hand, for times $t \gg \tau$, the effect of any single kick should damp out.[2] Solving equation (1.22) for the mean-square excursion $\langle x^2 \rangle$, one finds [45, 105]

$$\langle x^2 \rangle \propto \begin{cases} t^2 & t \ll \tau \\ t & t \gg \tau, \end{cases} \tag{1.23}$$

The first of these relations describes the *ballistic* phase of Brownian motion while the second describes the *diffusive* phase. The point here is that there is a *crossover* from one type of behavior to another, each characterized by a particular exponent. The existence of the ballistic phase at small times, like the diffusive phase at large times, is independent of the details of the motion. Brownian motion thus provides an elementary example of a dynamical process that can fall into one of two classes of motion, depending on which

---

[2]While the essence of the problem is captured here, the full story is in truth richer [e.g., 4].

processes dominate at which times. In general, such crossover transitions range from being sharp to being long and drawn out. Later, we will argue that crossovers are an important feature of Hack's law.

1.5.2   A little history

Scaling and universality are deep ideas with an illustrious past. Therefore a brief historical perspective is in order.

In essence, scaling may be viewed as an extension of classical dimensional analysis [11]. Our interest, however, is strongly influenced by studies of phase transitions and critical phenomena that began in the 1960's. Analogous to the present situation with river networks, equilibrium critical phenomena at that time presented a plethora of empirical scaling exponents for which there was no fundamental "first principles" understanding. Kadanoff and others then showed how an analysis of a simple model of phase transitions— the famous Ising model of statistical mechanics—could yield the solution to these problems [68]. Their innovation was to view the problem at different length scales and search for solutions that satisfied scale invariance.

These ideas were richly extended by Wilson's development of the calculational tool known as the renormalization group [155]. This provided a formal way to eliminate short-wavelength components from problems while at the same time finding a "fixed point" from which the appropriate scaling laws could be derived. The renormalization group method then showed explicitly how different microscopic models could yield the same macroscopic dynamics, i.e., fall within the same universality class.

These ideas turned out to have tremendous significance well beyond equilibrium critical phenomena. (See, for example, the brief modern review by Kadanoff [67] and the pedagogical book by Goldenfeld [49].) Of particular relevance to geomorphology are the applications in dynamical systems theory. An outstanding example is the famous period-doubling transition to chaos, which occurs in systems ranging from the forced pendulum to Rayleigh-Bénard convection [129]. By performing a mathematical analysis similar to that of the renormalization group, Feigenbaum [38] was able to quantitatively predict the way in which a system undergoes period-doubling bifurcations. The theory applies not only to a host of models, but also to widely disparate experimental systems.

Underlying all of this work is an effort to look for classes of problems having common solutions. This is the essence of universality: if a problem satisfies qualitative criteria, then its quantitative behavior—scaling laws and

scaling relations—may be predicted.

1.6   Known universality classes of river networks

We next describe basic network models that exemplify various universality classes of river networks. These classes will form the basis of our ensuing discussion of Hack's law. We consider networks for non-convergent flow, random networks of directed and undirected nature, self-similar networks and "optimal channel networks." We also discuss binary trees to illustrate the requirement that networks be connected with surfaces. We take universality classes to be defined by the pair (h, d), these exponents being sufficient to give the exponents of all macroscopic scaling laws. The networks classes described below are provided in Table 1.1, along with results for real river networks.

Note that in some cases, different models belong to the same universality class. Indeed, this is the very spirit of universality. The details of the models that we outline below are important only to the models themselves.

1.6.1   Non-convergent flow $[(h, d) = (1, 1)]$

Figure 1.3a shows the trivial case of non-convergent flow where $(h, d) = (1, 1)$. By non-convergent, we mean the flow is either parallel or divergent. Basins are effectively linear objects and thus we have that drainage area is proportional to length. This universality class corresponds to flow over convex hillslopes, structures that are typically dominated by diffusive processes rather than erosive ones.

1.6.2   Directed random networks $[(h, d) = (2/3, 1)]$

We next have what we deem to be the simplest, physically reasonable network entailing convergent flow. This is the directed random network first introduced by Scheidegger [112]. Scheidegger originally considered the ensemble of networks formed on a triangular lattice when flow from each site is randomly chosen to be in one of two directions. This may be reformulated on a regular square lattice with the choices as given in Figure 1.3b. Due to universality, the same scaling arises independent of the underlying lattice. Now, these networks are essentially the same as that which we discussed in
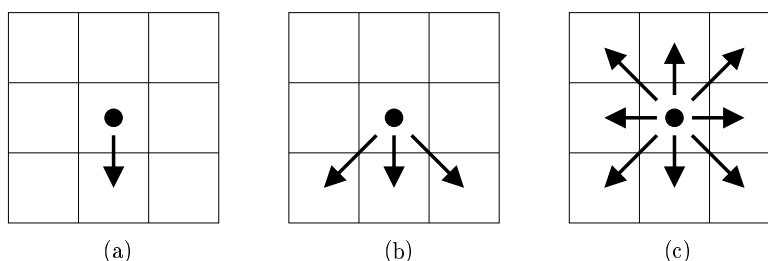
Figure 1.3: Possible directions of flow for three networks whose statistics belong to differing universality classes. Diagram (a) provides the trivial hillslope class where overland flow is essentially non-convergent; diagram (b) corresponds to directed random networks; and diagram (c) to undirected random networks. Note that while diagram (a) literally pictures perfect parallel flow, it figuratively symbolizes any set of flow lines that do not converge.

the introductory section on scaling. In both cases basin boundaries and main streams are directed random walks. We have thus already derived the results $h = 2/3$, $\tau = 4/3$ and $\gamma = 3/2$. Other exponents follow from the scaling relations. Furthermore, $d = 1$ since the networks are directed. Our first universality class is therefore defined by the pair of exponents $(h, d) = (2/3, 1)$.

At present, the Tokunaga and Horton parameters may only been obtained from numerical simulations.

The dynamics here appear to be back-to-front. River networks extend upwards into a surface as a fracture propagates into rock. Of course, the dynamics here are merely "dynamics" and only serve the purpose of describing what is a essentially a static model. But we can think of the model as having a growth of sorts by considering the divides. Starting from the bottom of our artificial slope, we can picture the divides between basins as random walks moving upwards. When two such divides meet then they continue on as one single boundary. The network of divides formed is exactly the same as the network of rivers but oriented in the opposite direction. Moreover, the two networks mesh together—like the visual illusion of the corner cube, one can see either but not both at the same time.

An alternative view of Scheidegger networks is to consider the surfaces from which they may be derived. There is an infinitude of such since networks are essentially only defined by the sign of differences in heights. One can, for example, always define a surface with all heights in $[0, 1]$ that will yield a given network (directed or not). It is clear that much information is lost when
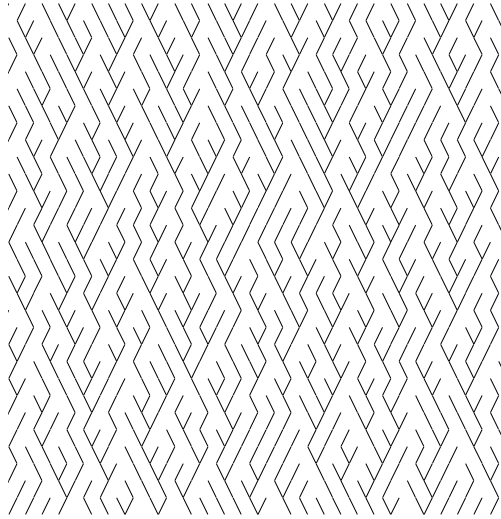
Figure 1.4: The simplest, physically reasonable model of a river network. Flow is down the page and from each site the direction of flow is randomly chosen to be one of the two neighbors below.

a surface is replaced by its drainage network. In the case of Scheidegger, we can make a surface slightly more aesthetically pleasing by adding an overall tilt to a lattice of random heights chosen uniformly from $[0, 1]$. Providing the tilt is sufficient to make the derivative network a directed one then the output will be a Scheidegger one.

So a Scheidegger network being random and uncorrelated is derived from a surface of the same nature with the sole identifiable characteristic being an overall trend.

1.6.3   Undirected random networks $[(h, d) = (5/8, 5/4)]$

If we relax the condition of directedness, then we move to a set of networks belonging to a different universality class. These networks were first explored by Leopold and Langbein [82]. They were later theoretically studied under the moniker of random spanning trees by Manna et al. [84] who found that the universality class is described by $(h, d) = (5/8, 5/4)$. The possible flow directions are shown for both directed and undirected random networks in Figures 1.3b and 1.3c.
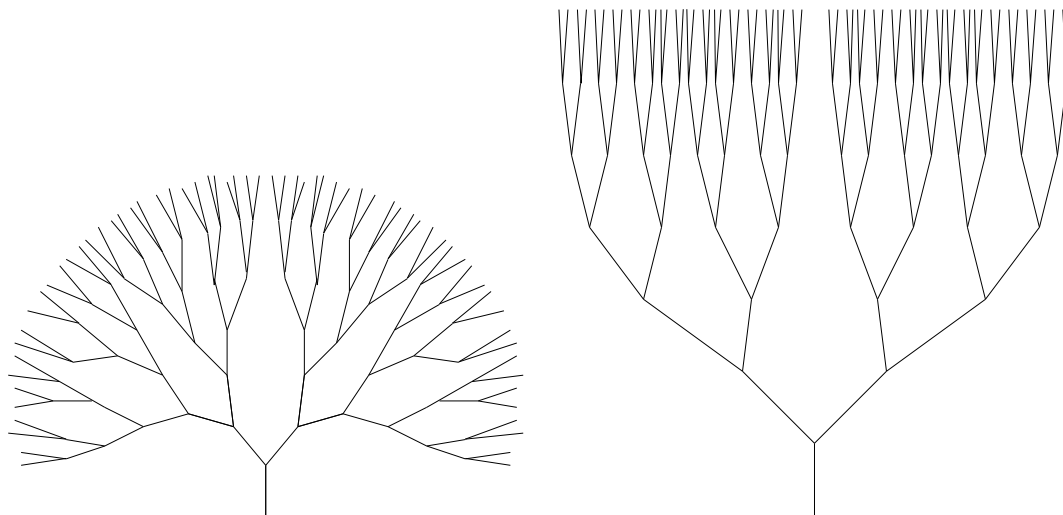
Figure 1.5: Two examples of a binary tree rendered onto a plane. The exponential growth of the number of branches means that the networks fill up space too quickly. The two usual assumptions of binary trees that individual links are similar in length and that drainage density is uniform cannot be both maintained.

1.6.4   Branching trees $[(h, d) = (?, ?)]$

The networks above are built on two-dimensional lattices. We take an aside here to discuss a case where no clear link to a two-dimensional substrate exists. Consider then a binary branching tree and all of its possible subnetworks [117, 118]. This seems a logical model since most river networks are comprised of confluences of two streams at forks—very rarely does one see even trifurcations let alone the conjoining of four streams.

However, binary trees are not as general as one might think. That river networks are trees is evident but they are special trees in that they fill all space (uniform drainage density again, see Figure 1.5). If links between forks are assumed to be roughly constant throughout a network then drainage density increases exponentially. Conversely, if drainage density is held constant, then links grow exponentially in length as one moves away from the outlet into the network. Thus, one cannot consider the binary tree model to be a representation of real river networks.[3]

---

[3]Binary trees are examples of Bethe lattices which have been well studied in percolation theory [126]. Solutions to percolation problems show that they resemble infinite-dimensional space, much less two-dimensional space.
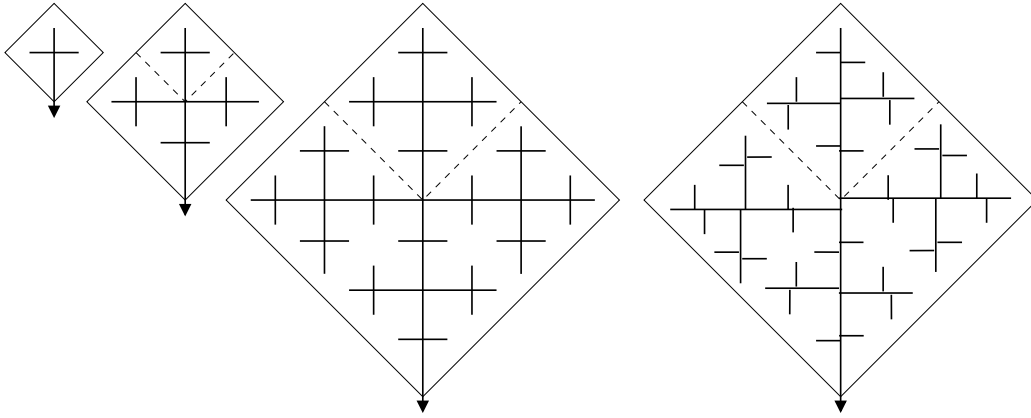
Figure 1.6: The Peano basin, a member of the $(h, d) = (1/2, 1)$ universality class. The first three basin show the basic construction with each larger basin being built out of four of those from the previous level. The rightmost basin shows a slight perturbation to remove the trifurcations. Each basin's outlet is at its bottom.

Nevertheless, we briefly persist with this unrealizable model since it is of historic importance and does allow for some interesting analysis. If we do make the unphysical assumption that we may ascribe unit lengths and areas to each link then the Horton ratios can be calculated to be $R_n = 4$ and $R_l = 2$ [117, 118, 145]. This gives the Hack exponent $h = \log R_l / \log R_n = 1/2$. Other avenues have arrived at this same result which came to be known as Moon's conjecture [92, 150]. Since main stream lengths are proportional to basin length, we have the universality class $(h, d) = (1/2, 1)$.

One final comment regarding binary trees concerns the work of Kirchner [72] who found that river network scaling laws are "statistically inevitable." The problem with this seemingly general and hence rather damning result is that the basis of the study was the examination of binary tree sub-networks. Thus, no conclusions may be drawn from this work regarding real river networks. As we hope has been clearly demonstrated, any reasonable method for producing general ensembles of networks *must* have them associated with surfaces. Moreover, work by Costa-Cabral and Burges [21] has confirmed variability of network laws for one particular model that works along these lines.

1.6.5   Self-similar basins $[(h, d) = (1/2, 1)]$

An example of a network that belongs to the universality class $(h, d) = (1/2, 1)$ and is embedded in a surface is the so-called Peano basin [110]. Its definition is an iterative one demonstrated by the first three "basins" in Figure 1.6. A modified version without trifurcations is illustrated on the right so that all junctions are the usual forks of river networks. Technically, this also allows for the proper application of Tokunaga's description which quite reasonably presumes that all junctions are forks.

Since main stream length rapidly approaches $L_\parallel$, we have essentially that $l = L_\parallel$ so that $d = 1$. The important point to note here is that, by construction, the basins are of unit aspect ratio. As $d = 1$, we see that Hack's exponent is by necessity $1/2$.

Thus, the Peano basin belongs to what we will call the self-similar universality class defined by $(h, d) = (1/2, 1)$. As with other simple models, the Peano basin is not something we would expect to find in nature. Nevertheless, the general class of self-similar basins is a very reasonable one. Indeed, that basins of all sizes be geometrically similar is what would be expected by straightforward dimensional analysis.

1.6.6   Optimal channel networks $[(h, d) = (2/3, 1)$, $(1/2, 1)$, or $(3/5, 1)]$

Another collection of networks with well understood universality classes comprises *optimal channel networks* [see 108, 110, and references therein]. These models, known as OCN's, are based on the conjecture that landscapes evolve to a stationary state characterized by the minimization of the energy dissipation rate $\dot{\varepsilon}$, where

$$\dot{\varepsilon} \sim \sum_i a_i s_i \sim \sum_i a_i^{1-\theta}. \tag{1.24}$$

Here a_i and s_i are the contributing area and the slope at the ith location on a map, and are identified with a thermodynamic flux and force, respectively. The second approximation comes from the empirical observation that $\langle s \rangle_a \sim a^{-\theta}$, where the average is taken over locations with the same contributing area and, typically, $\theta \simeq 0.5$ [41, 58, 110].

The conjecture of optimality is controversial. Although it is appealing to seek a variational formulation of fluvial erosion [9, 119], it seems unlikely

that its existence could be proven or disproved.[4] It remains nevertheless interesting to consider its ramifications.

   Maritan et al. [86] have shown that OCN's based on the formulation (1.24) fall into two distinct universality classes, denoted respectively here by (I) and (II), depending on the value of θ. In the simplest case ($\theta = 0$), one finds that the OCN's belong to the universality class of directed random networks. On the other hand, for $0 < \theta \leq 1/2$, the OCN's fall into the self-similar class. A third class (III) is made possible by extending the model to include a fixed, random erosivity at each site. This final class is deduced to be $(h, d) = (3/5, 1)$.

   Much of the literature on OCN's is devoted to numerical investigations. As it turns out, the universality classes given above are not necessarily obtained and differing exponents are reported. The reason lies in that fact that the minimization process is fraught with local minima. Further, the results depend on the details of the numerical method itself. As we will discuss below, the actual scaling of real networks may be somewhat deceptively masked by long crossovers between distinct regimes of scaling. It is conceivable that a similar effect occurs with OCN's. Locally, physical processes such as the one suggested in the OCN formulation may conspire to produce certain scaling exponents whereas at large scales, exponents in keeping with random networks may become apparent.

1.6.7   Summary

Table 1.1 provides a summary of the foregoing networks and their corresponding universality classes. As the table shows, we have identified five distinct universality classes for river networks. Ranges for h and d for real river networks are also indicated. In scaling theory, the importance of exact results cannot be overlooked. The measurement of scaling exponents is a notoriously fickle exercise. For example, one might find that regression analysis gives a tight error bound over any given variable range but that the choice of the range greatly affects the estimate. Thus we need persuasive reasoning to reject these known universality classes of networks and composite versions thereof.

---

[4]A comparison with fluid mechanics is instructive. Here one starts with the Navier-Stokes equations, so precise derivations are possible. For example, in the case of creeping (Stokes) flow with fixed boundaries, the flow field does indeed minimize energy dissipation rate [see 77, art. 344]. On the other hand, if the boundaries can move, cases may be found in which the flow field *maximizes*, rather than minimizes, dissipation [57].

network	h	d
Non-convergent flow	1	1
Directed random	2/3	1
Undirected random	5/8	5/4
Self-similar	1/2	1
OCN's (I)	1/2	1
OCN's (II)	2/3	1
OCN's (III)	3/5	1
Real rivers	0.5–0.7	1.0–1.2

Table 1.1: Theoretical networks with analytically known universality classes. The universality class of river networks is defined by the pair of exponents (h, d) where h is Hack's exponent (1.13) and d is the scaling exponent that represents stream sinuosity. Each network is detailed in the text. The range of these exponents for real river networks is shown for comparison.

CHAPTER **2**

Unified view of network scaling laws

Abstract. Scaling laws that describe the structure of river networks are shown to follow from three simple assumptions. These assumptions are: (1) river networks are structurally self-similar, (2) single channels are self-affine, and (3) overland flow into channels occurs over a characteristic distance (drainage density is uniform). We obtain a complete set of scaling relations connecting the exponents of these scaling laws and find that only two of these exponents are independent. We further demonstrate that the two predominant descriptions of network structure (Tokunaga's law and Horton's laws) are equivalent in the case of landscapes with uniform drainage density. The results are tested with data from both real landscapes and a special class of random networks.

2.1   Introduction

If it is true that scaling laws abound in nature [83], then river networks stand as a superb epitome of this phenomenon. For over half a century, researchers have uncovered numerous power laws and scaling behaviors in the mathematical description of river networks [54, 58, 74, 78, 87, 127, 141, 143]. These scaling laws, which are usually parameterized by exponents or ratios of fundamental quantities, have been used to validate scores of numerical and theoretical models of landscape evolution [59, 73, 80, 82, 88, 110, 117, 122, 124, 130, 131, 152, 153, 154] and have even been invoked as evidence of self-organized criticality [7, 110]. However, despite this widespread usage,

there is as yet no fundamental understanding of the origin of scaling laws in river networks.

It is the principal aim of this paper to bring together a large family of these scaling laws within a simple, logical framework. In particular, we demonstrate that from a base of three assumptions regarding network geometry, all scaling laws involving planform quantities may be obtained. The worth of these consequent scaling laws is then seen to rest squarely upon the shoulders of the structural assumptions themselves. We also simplify the relations between the derived laws, demonstrating that only two scaling exponents are independent.

The paper is composed in the following manner. We first present preliminary definitions of network quantities and a list of empirically observed scaling laws. Our assumptions will next be fully stated along with evidence for their validity. Several sections will then detail the derivations of the various scaling laws, being a combination of both new insights of our own as well as previous results. Progressing in a systematic way from our assumptions, we will also be required to amend several inconsistencies persistent in other analyses. The theory will be tested with comparisons to data taken from real landscapes and Scheidegger's random network model [112, 115].

2.2 The ordering of streams

A basic tool used in the analysis of river networks is the device of stream ordering. A stream ordering is any scheme that attaches levels of significance to streams throughout a basin. Most orderings identify the smallest tributaries as lowest order streams and the main or 'trunk' stream as being of highest order with the intermediary 'stream segments' spanning this range in some systematic fashion. Stream orderings allow for logical comparisons between different parts of a network and provide a basic language for the description of network structure.

Here, we build our theory using the most common ordering scheme, one that was first introduced by Horton in his seminal work on erosion [58]. Strahler later improved this method [128] and the resulting technique is commonly referred to as Horton-Strahler stream ordering [110]. The most natural description of this stream ordering, due to Melton [89], is based on an iterative pruning of a tree representing a network as shown in Figure 2.1. All source (or external) streams are pared away from the tree, these being defined as the network's first order 'stream segments'. A new tree is thus created
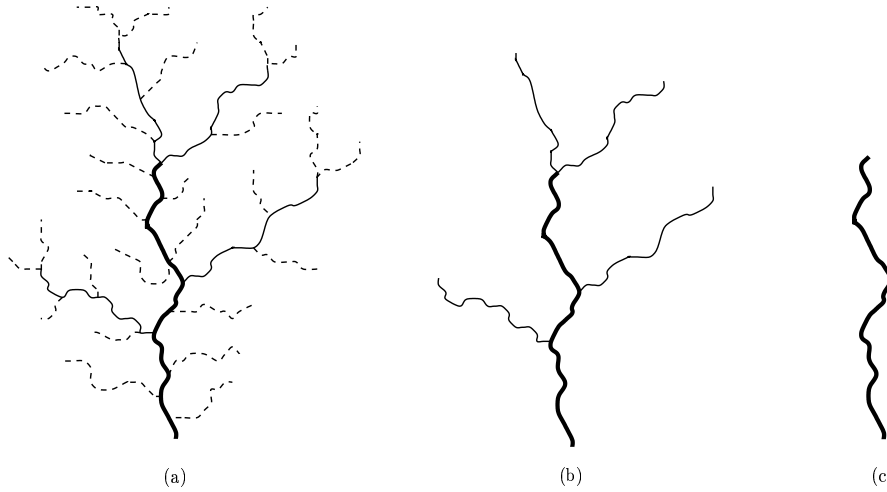
Figure 2.1: Horton-Strahler stream ordering. (a) shows the basic network. (b) is created by removing all source streams from the network in (a), these same streams being denoted as first order 'stream segments'. The new source streams in the pruned network of (b) are labelled as second order stream segments and are themselves removed to give (c), a third order stream segment.

along with a new collection of source streams and these are precisely the second order stream segments of the original network. The pruning and order identification continues in like fashion until only the trunk stream segment of the river network is left. The overall order of the basin itself is identified with the highest stream order present.

The usual and equivalent description details how stream orders change at junctions [110]. When a stream segment of order ω_1 merges with a stream segment of order ω_2, the outgoing stream will have an order of ω given by

$$\omega = \max(\omega_1, \omega_2) + \delta_{\omega_1, \omega_2} \tag{2.1}$$

where δ is the Kronecker delta. In other words, stream order only increases when two stream segments of the same order come together and, otherwise, the highest order is maintained by the outflowing stream.

2.3   Planform network quantities and scaling laws

The results of this paper pertain to networks as viewed in planform. As such, any effects involving relief, the vertical dimension, are ignored. Nevertheless, we show that a coherent theory of planform quantities may still be obtained. This section defines the relevant quantities and their various permutations along with scaling laws observed to hold between them. The descriptions of these laws will be short and more detail will be provided in later sections.

The two essential features in river networks are basins and the streams that drain them. The two basic planform quantities associated with these are drainage area and stream length. An understanding of the distribution of these quantities is of fundamental importance in geomorphology. Drainage area, for example, serves as a measure of average discharge of a basin while its relationship with the length of the main stream gives a sense of how basins are shaped.

2.3.1   General network quantities

Figure 2.2 shows a typical drainage basin. The basin features are a, the area, l, the length of the main stream, and $L_{\parallel}$ and $L_{\perp}$, the overall dimensions. The main (or trunk) stream is the dominant stream of the network—it is traced out by moving all the way upstream from the outlet to the start of a source stream by choosing at each junction (or fork) the incoming stream with the largest drainage area. This is not to be confused with stream segment length which only makes sense in the context of stream ordering. We will usually write L for $L_{\parallel}$. Note that any point on a network has its own basin and associated main stream. The sub-basin in Figure 2.2 illustrates this and has its own primed versions of a, l, $L_{\parallel}$ and $L_{\perp}$. The scaling laws usually involve comparisons between basins of varying size. These basins must be from the same landscape and may or may not be contained within each other.

Several scaling laws connect these quantities. One of the most well known is Hack's law [54]. Hack's law states that l scales with a as

$$l \sim a^{h} \tag{2.2}$$

where h is often referred to as Hack's exponent. The important feature of Hack's law is that $h \neq 1/2$. In particular, it has been observed that for a reasonable span of basin sizes that $0.57 < h < 0.60$ [52, 54, 87, 106].

The actual range of this scaling is an unresolved issue with some studies demonstrating that very large basins exhibit the more expected scaling of $h = 1/2$ [94, 95, 96]. We simply show later that while the assumptions of this paper hold so too does Hack's law.

Further comparisons of drainage basins of different sizes yield scaling in terms of $L(= L_\parallel)$, the overall basin length. Area, main stream length, and basin width are all observed to scale with L [74, 75, 87, 141, 143],

$$a \sim L^D, \qquad l \sim L^d, \qquad L_\perp \sim L^H. \qquad (2.3)$$

Turning our attention to the entire landscape, it is also observed that histograms of stream lengths and basin areas reveal power law distributions [87, 110]:

$$P(a) \sim a^{-\tau} \qquad \text{and} \qquad P(l) \sim l^{-\gamma}. \qquad (2.4)$$

There are any number of other definable quantities and we will limit ourselves to a few that are closely related to each other. We write λ for the average distance from a point on the network to the outlet of a basin (along streams) and Λ for the unnormalized total of these distances. A minor variation of these are $\tilde{\lambda}$ and $\tilde{\Lambda}$, where only distances from junctions in the network to the outlet are included in the averages.

The scaling law involving these particular quantities is Langbein's law [78] which states that

$$\Lambda \sim a^\beta. \qquad (2.5)$$

Similarly, we have $\lambda \sim L^\varphi$, $\tilde{\Lambda} \sim a^{\tilde{\beta}}$ and $\tilde{\lambda} \sim L^{\tilde{\varphi}}$, [87].

2.3.2   Network quantities associated with stream ordering

With the introduction of stream ordering, a whole new collection of network quantities appear. Here, we present the most important ones and discuss them in the context of what we identify as the principal structural laws of river networks: Tokunaga's law and Horton's laws.

2.3.3   Tokunaga's law

Tokunaga's law concerns the set of ratios, $\{T_{\omega,\omega'}\}$, first introduced by Tokunaga [97, 102, 144, 145, 146]. These 'Tokunaga ratios' represent the average
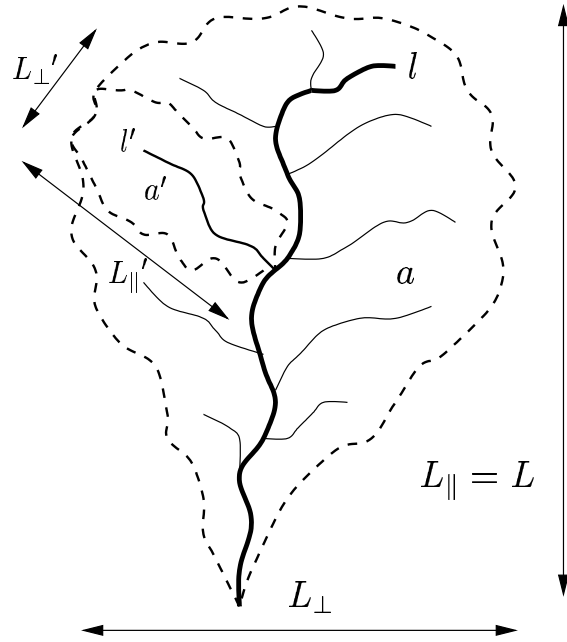
Figure 2.2: A planform view of an example basin. The main defining parameters of a basin are a, the drainage area, l, the length of the main stream, and $L_\parallel$ and $L_\perp$, the overall Euclidean dimensions. The sub-basin with primed quantities demonstrates that a basin exists at every point in a network.

number of streams of order ω' flowing into a stream of order ω as side tributaries. In the case of what we will call a 'structurally self-similar network', we have that $T_{\omega,\omega'} = T_{\omega-\omega'} = T_\nu$ where $\nu = \omega - \omega'$ since quantities involving comparisons between features at different scales should only depend on the relative separation of those scales. These T_ν, in turn, are observed to be dependent such that [144],

$$T_{\nu+1}/T_\nu = R_T \tag{2.6}$$

where R_T is a fixed constant for a given network. Thus, all of Tokunaga's ratios may be specified by two fundamental parameters T_1 and R_T:

$$T_\nu = T_1(R_T)^{\nu-1}. \tag{2.7}$$

We refer to this last identity as Tokunaga's law.

    The network parameter T_1 is the average number of major side tributaries per stream segment. So for a collection of stream segments of order ω, there

will be on average T_1 side tributaries of order $\omega - 1$ for each stream segment. The second network parameter R_T describes how numbers of side tributaries of successively lower orders increase, again, on average. As an example, consider that the network in Figure 2.1 is part of a much larger network for which $T_1 = 2$ and $R_T = 4$. Figure 2.1 (b) shows that the third order stream segment has two major side tributaries of second order which fits exactly with $T_1 = 2$ (Note that the two second order stream segments that come together to create the third order stream segment are not side tributaries). Figure 2.1 (a) further shows nine first order tributaries, slightly above the average eight suggested by $T_2 = T_1 R_T^1 = 8$. Finally, again referring to Figure 2.1 (a), there are $9/4 = 2.25$ first order tributaries for each second order stream segment, not far from the expected number $T_1 = 2$.

2.3.4   Horton's laws

Horton introduced several important measurements for networks in conjunction with his stream ordering [58]. The first is the bifurcation ratio, R_n. This is the ratio of the number n_ω of streams of order ω to the number $n_{\omega+1}$ of streams of order $\omega+1$ and is, moreover, observed to be independent of ω over a large range. There is next the stream length ratio, $R_{l^{(\mathrm{s})}} = \bar{l^{(\mathrm{s})}}_{\omega+1}/\bar{l^{(\mathrm{s})}}_\omega$, where $\bar{l^{(\mathrm{s})}}_\omega$ is the average length of stream segments of order ω. These lengths only exist within the context of stream ordering. In contrast to these are the main stream lengths, which we have denoted by l and described in section 2.3.1. Main stream lengths are defined regardless of stream ordering and, as such, are a more natural quantity. Note that stream ordering gives rise to a discrete set of basins, one for each junction in the network. We therefore also have a set of basin areas and main stream lengths defined at each junction. Taking averages over basins of the same order we have $\bar{a}_\omega$ and $\bar{l}_\omega$ to add to the previously defined $\bar{l^{(\mathrm{s})}}_\omega$ and n_ω.

The connection between the two measures of stream length is an important, if simple, exercise [113]. Assuming $\bar{l^{(\mathrm{s})}}_{\omega+1} = R_{l^{(\mathrm{s})}} \bar{l^{(\mathrm{s})}}_\omega$ holds for all ω, one has

$$\bar{l}_\omega = \sum_{i=1}^{\omega} \bar{l^{(\mathrm{s})}}_i = \sum_{i=1}^{\omega} (R_{l^{(\mathrm{s})}})^{i-1} \bar{l^{(\mathrm{s})}}_1 = \bar{l}_1 \frac{(R_{l^{(\mathrm{s})}})^\omega - 1}{R_{l^{(\mathrm{s})}} - 1} \tag{2.8}$$

where $\bar{l}_1 = \bar{l^{(\mathrm{s})}}_1$ has been used. Since typically $R_{l^{(\mathrm{s})}} > 2$ [72], $\bar{l}_{\omega+1}/\bar{l}_\omega \to R_{l^{(\mathrm{s})}}$ rapidly. For $\omega = 4$ and $R_{l^{(\mathrm{s})}} = 2$, the error is only three per cent. On the other hand, starting with the assumption that main stream lengths satisfy

Horton's law of stream lengths for all ω implies that the same is true for stream segments.

Thus, for most calculations, Horton's law of stream lengths may involve either stream segments or main streams and, for convenience, we will assume that the law is fully satisfied by the former. Furthermore, this small calculation suggests that studies involving only third- or fourth-order networks cannot be presumed to have reached asymptotic regimes of scaling laws. We will return to this point throughout the paper.

Schumm [116] is attributed with the concrete introduction of a third and final law that was also suggested by Horton. This last ratio is for drainage areas and states that $R_a = \bar{a}_{\omega+1}/\bar{a}_\omega$. We will later show in section 2.7 that our assumptions lead to the result that $R_a \equiv R_n$. At this stage, however, we write Horton's laws as the three statements

$$\frac{n_\omega}{n_{\omega+1}} = R_n, \ \ \frac{\bar{l^{(\mathrm{s})}}_{\omega+1}}{\bar{l^{(\mathrm{s})}}_\omega} = R_{l^{(\mathrm{s})}}, \ \text{and} \ \frac{\bar{a}_{\omega+1}}{\bar{a}_\omega} = R_a. \tag{2.9}$$

A summary of all of the scaling laws presented in this section is provided in Table 2.1. Empirically observed values for the relevant exponents and ratios are presented in Table 2.2.

2.3.5   Scheidegger's random networks

To end this introductory section, we detail some of the features of the random network model of Scheidegger [112, 115]. Although originally defined without reference to a real surface, Scheidegger networks may be obtained from a completely uncorrelated landscape as follows. Assign a random height between 0 and 1 at every point on a triangular lattice and then tilt the lattice so that no local minima (lakes) remain. Scheidegger networks are then traced out by following paths of steepest descent.

Surprisingly, these networks still exhibit all of the scaling laws observed in real networks. It thus provides an important point in 'network space' and accordingly, also provides an elementary test for any theory of scaling laws. Exact analytical results for various exponents are known due to the work of Takayasu et al. on the aggregation of particles with injection [61, 135, 136, 138, 139, 140]. While there are no analytic results for the Tokunaga ratio T_1 or the Horton ratios R_n and $R_{l^{(\mathrm{s})}}$, our own simulations show that these stream order laws are strictly obeyed. Table 2.2 lists the relevant exponents and their values for the Scheidegger model along with those found in real networks.

Law:	Name or description:
$T_\nu = T_1(R_T)^{\nu-1}$	**Tokunaga's law**
$l \sim L^d$	**self-affinity of single channels**
$\bar{n}_{\omega+1}/\bar{n}_\omega = R_n$	Horton's law of stream numbers
$\bar{l^{(\mathrm{s})}}_{\omega+1}/\bar{l^{(\mathrm{s})}}_\omega = R_{l^{(\mathrm{s})}}$	Horton's law of stream segment lengths
$\bar{l}_{\omega+1}/\bar{l}_\omega = R_{l^{(\mathrm{s})}}$	Horton's law of main stream lengths
$\bar{a}_{\omega+1}/\bar{a}_\omega = R_a$	Horton's law of stream areas
$l \sim a^h$	Hack's law
$a \sim L^D$	scaling of basin areas
$L_\perp \sim L^H$	scaling of basin widths
$P(a) \sim a^{-\tau}$	probability of basin areas
$P(l) \sim l^{-\gamma}$	probability of stream lengths
$\Lambda \sim a^\beta$	Langbein's law
$\lambda \sim L^\varphi$	variation of Langbein's law
$\tilde{\Lambda} \sim a^{\tilde{\beta}}$	as above
$\tilde{\lambda} \sim L^{\tilde{\varphi}}$	as above

Table 2.1: A general list of scaling laws for river networks. All laws and quantities are defined in section 2.3. The principal finding of this paper is that these scaling laws follow from the first two relations, Tokunaga's law (structural self-similarity) and the self-affinity of single channels, and the assumption of uniform drainage density (defined in section 2.4.3).

2.4   Assumptions

We start from three basic assumptions about the structure of river networks: structural self-similarity, self-affinity of individual streams and uniformity of drainage density. We define these assumptions and their relevant parameters and then discuss their mutual consistency. We end with a discussion of the correspondence between the laws of Tokunaga and Horton. It should be stressed that while we make a case for each assumption there is also considerable proof to ponder in the pudding that these ingredients create.

2.4.1   Structural self-similarity

Our first assumption is that networks are structurally self-similar. It has been observed that river networks exhibit self-similarity over a large range of scales [83, 110, 141]. Naturally, the physical range of this self-similarity is

Quantity:	Scheidegger:	Real networks:
R_n	$5.20 \pm .05$	3.0–5.0 [1]
R_a	$5.20 \pm .05$	3.0–6.0 [1]
$R_{l^{(\mathrm{s})}}$	$3.00 \pm .05$	1.5–3.0 [1]
T_1	$1.30 \pm .05$	1.0–1.5 [145]
d	1	1.1 ± 0.01 [87]
D	3/2	1.8 ± 0.1 [87]
h	2/3	0.57–0.60 [87]
τ	4/3	1.43 ± 0.02 [87]
γ	3/2	1.8 ± 0.1 [106]
φ	1	1.05 ± 0.01 [87]
H	1/2	0.75–0.80 [87]
β	5/3	1.56 [78]
φ	1	1.05 ± 0.01 [87]

Table 2.2: Ratios and scaling exponents for Scheidegger's random network model and real networks. For Scheidegger's model, exact values are known due to the work of Takayasu et al. [61, 135, 136, 138, 139, 140] and approximate results are taken from our own simulations. For real networks, the references given are generally the most recent and further appropriate references may be found within them and also in section 2.3.

restricted to lie between two scales. The large scale cutoff is the overall size of the landscape and the small scale cutoff is of the order of the characteristic separation of channels [90].

In order to quantify this phenomenon, we look to laws of network structure such as Tokunaga's law and Horton's laws of stream number and length. We demonstrate in the following section that these descriptions are mutually consistent within the context of our third assumption, uniformity of drainage density. Thus, we may assume a network where both Tokunaga's and Horton's laws hold. For convenience, we write these laws as if they hold for all orders down to the first order. Any actual deviations from these laws for low orders will not affect the results since we are interested in how laws behave for increasing stream order.

2.4.2   Self-affinity of individual streams

Our second assumption is that individual streams are self-affine curves possessing a dimension $d > 1$, as introduced in equation (2.3). Empirical support for this premise is to be found in [74, 87, 110, 141, 142, 143]. In reality, this is at best a weak fractality with measurements generally finding d to be around 1.1 [87]. We assume d to be constant throughout a given network, true for each stream independent of order.

In general, it is most reasonable to consider this in the sense of a growing fractal: stream length l will grow like L^d where L is the overall length of a box containing a portion of a stream. So, rather than examine one fixed section of a stream, we take larger and larger pieces of it. Moreover, this is the most reasonable method for actually measuring d for a real network.

2.4.3   Uniform drainage density

Our third and final assumption is that drainage density is uniform throughout a network. For a given basin, the drainage density, ρ, is a measure of the average area drained per unit length of stream by overland flow (i.e., excluding contributions from tributary streams). Its usual form is that given by Horton [58]:

$$\rho = \frac{\sum l^{(s)}}{a} \qquad (2.10)$$

where, for a given basin, $\sum l^{(s)}$ represents the summed total length of all stream segments of all orders and a is the drainage area. More generally, one can in the same way measure a local drainage density for any connected sections of a network within a landscape. Such sections should cover a region at least $l^{(s)}{}_1$ in diameter, the typical length of a first order stream. Drainage density being uniform means that the variation of this local drainage density is negligible. There is good support in the literature for the uniformity of drainage density in real networks [24, 46, 54, 55, 93, 118] while there are some suggestions that it may vary slightly with order [54, 145].

Uniform drainage density may also be interpreted as the observation that the average distance between channels is roughly constant throughout a landscape [58, 110], an estimate of this distance being simply $1/\rho$. This is due to the fact that there is a finite limit to the channelization of a landscape determined by a combination of soil properties, climate and so on. Implicit in this assumption is that the channel network has reached its maximum extension

into a landscape [48, 118]. Indeed, In the bold words of Glock [48], we are considering river networks at the "time of completed territorial conquest." Furthermore, Shreve [118] notes that drainage density would be uniform in a "mature topography developed in a homogeneous environment."

Importantly, our third assumption connects the planform description to the surface within which the network lies. Computationally, the uniformity of drainage density allows for the use of the length of a stream as a proxy for drainage area [24]. Further, the average distance between streams being roughly constant implies that, on average, tributaries are spaced evenly along a stream.

2.5   Tokunaga's law and Horton's laws are equivalent

This section demonstrates an equivalence between Tokunaga's law and Horton's two laws of stream number and stream length in the case of a landscape with uniform drainage density.

2.5.1   From Tokunaga's law to Horton's laws

Tokunaga has shown that Horton's law for stream numbers follows from Tokunaga's law (given in equation (2.7)) [102, 145]. This follows from the observation that n_ω, the number of streams of order ω, in a basin of order Ω may be expressed as

$$n_\omega = 2n_{\omega+1} + \sum_{\nu=1}^{\Omega-\omega} T_\nu n_{\omega+\nu}. \qquad (2.11)$$

The $2n_{\omega+1}$ accounts for the fact that each order $\omega + 1$ stream is initiated by the confluence of two streams of order ω. Presuming Tokunaga's law, a simple analysis of equation (2.11) shows that in the limit of large Ω, the ratio $n_\omega/n_{\omega+1}$ does indeed approach a constant. This leads to an expression for the Horton ratio R_n in terms of the two Tokunaga parameters T_1 and R_T (first obtained by Tokunaga in [145]):

$$2R_n = (2 + R_T + T_1) + \left[(2 + R_T + T_1)^2 - 8R_T\right]^{1/2}. \qquad (2.12)$$

Tokunaga's work has been recently generalized by Peckham who deduces links to the other Horton ratios $R_{l^{(s)}}$ and R_a [102]. In contrast to the purely

algebraic calculation of R_n, these results require the step of equating topological properties to metric basin quantities. In determining $R_{l(\mathrm{s})}$, Peckham uses the number of side tributaries to a stream as an estimate of stream segment length. This is based on the assumption that tributaries are evenly spaced. As discussed in section 2.4.3, this even spacing of tributaries follows for networks with uniform drainage density. Therefore, we may write, after Peckham, that

$$l^{\overline{(\mathrm{s})}}_{\,\omega} \propto 1 + \sum_{\nu=1}^{\omega-1} T_\nu \tag{2.13}$$

where the dimension of length absent on the right-hand side is carried by an appropriate constant of proportionality. This sum is simply the total number of tributaries that, on average, enter a stream of order ω. The number of lengths of stream between tributaries is then simply one more in number.

Using Tokunaga's law (equation (2.7)) we find that

$$l^{\overline{(\mathrm{s})}}_{\,\omega+1}/l^{\overline{(\mathrm{s})}}_{\,\omega} = R_T \left(1 + O(R_T)^{-\omega}\right), \tag{2.14}$$

obtaining Horton's stream length ratio with the simple identification:

$$R_{l(\mathrm{s})} = R_T \tag{2.15}$$

and we will use $R_{l(\mathrm{s})}$ in place of R_T throughout the rest of the paper. As already noted we will see that $R_a \equiv R_n$ for landscapes where drainage density is uniform. This redundancy means that there are only two independent Horton ratios, $R_{l(\mathrm{s})}$ and R_n, which sits well with the two independent quantities required for Tokunaga's law, T_1 and R_T. Presupposing this result, we can invert equations (2.12) and (2.15) to obtain Tokunaga's parameters from the two independent Horton ratios:

$$
\begin{aligned}
R_T &= R_{l(\mathrm{s})} & (2.16)\\
T_1 &= R_n - R_{l(\mathrm{s})} - 2 + 2R_{l(\mathrm{s})}/R_n. & (2.17)
\end{aligned}
$$

2.5.2   From Horton's laws to Tokunaga's law

We now provide an heuristic argument to show that Tokunaga's law in the form of equation (2.7) follows from Horton's laws of stream number and length and uniform drainage density. Note that even though we have shown in equations (2.12), (2.15), and (2.17) that the parameters of Tokunaga's law

and those of Horton's laws may be obtained from each other, it is not a priori clear that this result would be true. Indeed, Tokunaga's law contains more direct information about network structure than Horton's laws and it is the additional constraint of uniform drainage density that provides the key.

Consider a stream of order ω along with its side tributaries of order $\omega' = 1$ through $\omega' = \omega - 1$, the numbers of which are given by the usual T_ν where $\nu = \omega - \omega'$ (see Figure 2.3). Since the presumed adherence to Horton's laws implies that a network is self-similar we need only consider the form of the T_ν and not the more general $T_{\omega',\omega}$. Now, again since networks are self-similar, a typical stream of order $\omega + 1$ can be obtained by scaling up the picture of this order ω stream. As per Horton's law of stream lengths, this is done by increasing the length of each stream by a factor of $R_{l(\mathrm{s})}$ (Figure 2.3 (a) becomes Figure 2.3 (b)).

However, since order ω' streams become $\omega' + 1$ streams in this rescaling, the picture in Figure 2.3 (b) is missing first order streams. Also, the average distance between tributaries has grown by a factor of $R_{l(\mathrm{s})}$. Therefore, to retain the same drainage density, an extra $(R_{l(\mathrm{s})} - 1)$ first order streams must be added for each link (one more than the number of tributaries) along this new order $\omega + 1$ stream (Figure 2.3 (c)). Since the number of first order streams is now given by $T_{\omega+1}$ we have

$$T_{\omega+1} = (R_{l(\mathrm{s})} - 1) \left(\sum_{\nu=1}^{\omega} T_\nu + 1 \right). \tag{2.18}$$

It may be simply checked that this equation is satisfied, for large ω, by Tokunaga ratios given by equation (2.7). Thus, Horton's laws of stream number and stream length and the uniform drainage density are seen to imply Tokunaga's law.

In general, Horton's ratios rather than the parameters of Tokunaga's law will be the most useful parameters in what follows. In particular, we will see that the two independent quantities R_n and $R_{l(\mathrm{s})}$ will be needed only in the form $\ln R_n / \ln R_{l(\mathrm{s})}$. All other exponents will be expressible as algebraic combinations of $\ln R_n / \ln R_{l(\mathrm{s})}$ and d, the fractal dimension of an individual stream.

Furthermore, example (or modal) values for the parameters of Horton and Tokunaga are [72, 145]

$$T_1 = 1, \ R_T = R_{l(\mathrm{s})} = 2, \ \text{and} \ R_n = 4. \tag{2.19}$$

The parameters have been chosen so as to satisfy the inversion relations of equation (2.17). As shown in Table 2.2, real networks provide some variation
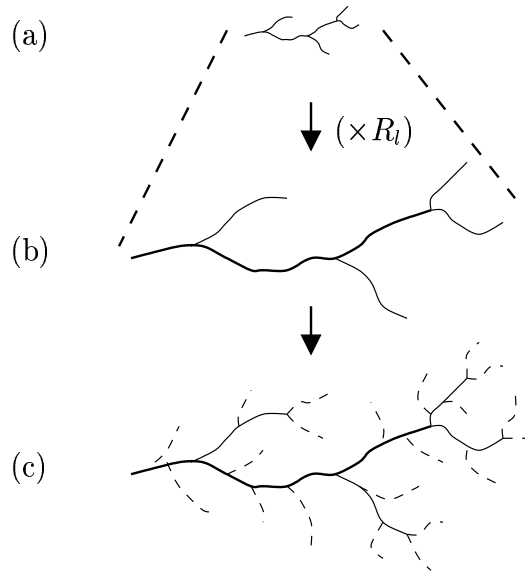
Figure 2.3: An example rescaling of a basin to demonstrate how Tokunaga's law follows from Horton's laws and uniform drainage density. In the first step from (a) to (b), the streams of the small network are rescaled in length by a factor of $R_{l(\mathrm{s})}$. The second step from (b) to (c) demonstrates that for drainage density to remain constant and uniform, a sufficient number of first order tributaries must be added.

around these modal values. These will be used as rough checks of accuracy throughout the rest of the paper.

2.6   Hack's law

One of the most intriguing scalings found in river networks is Hack's law [54] which relates main stream length to basin area as $l \sim a^h$. This equation has been empirically shown to hold true for a large range of drainage basin sizes on many field sites [110]. The salient feature is that for smaller basins [106], h is typically found to be in the range $(0.56, 0.60)$, whereas 0.5 would be expected from simple dimensional analysis [110].

It should be emphasized that Hack's law is only true on average as are, for that matter, Tokunaga's law and Horton's laws. An extension of Hack's law to a more natural statistical description of the connection between stream lengths and drainage areas was suggested by Maritan et al. [87] with some further developments to be found in [30].

2.6.1 Horton's other law of stream numbers

In order to obtain Hack's law, we will use the uniformity of drainage density to estimate the area of an order Ω basin by calculating the total length of streams within the same basin. So we simply need the typical length and number of each stream order present. Taking the length of a source stream, $l^{(\mathrm{s})}{}_1$, to be the finest resolution of the network and the basic unit of length, the length of a stream segment of order ω is $l^{(\mathrm{s})}{}_\omega = (R_{l^{(\mathrm{s})}})^{\omega-1} l^{(\mathrm{s})}{}_1$. However, in finding the frequency of such streams we find that some care must be taken for the following reasons.

Horton's law of stream numbers is potentially misleading in that it suggests, at first glance, that within a basin of order ω there should be one stream of order ω, R_n streams of order $\omega - 1$, R_n^2 streams of order $\omega - 2$ and so on. Indeed, many calculations involving Horton's laws use this assumption [24, 74, 110, 111].

But Horton's R_n actually provides the ratio of the number of streams of consecutive orders as totalled for a *whole basin*. To illustrate this fact, consider streams of order ω and $\omega + 1$ within a basin of order $\Omega \gg \omega$. As Tokunaga's law makes clear, streams of order ω are not all found within sub-basins of order $\omega + 1$. Indeed, a certain number of order ω streams will be tributaries to streams of order greater than $\omega + 1$ (see the example network of Figure 2.1 (a)). Tokunaga's law shows that we should in fact expect $T_1 + 2$ rather than than R_n streams of order ω entering into a stream of order $\omega + 1$. For the typical values $T_1 = 1$ and $R_n = 4$ in (2.19) this is a substantial error.

We proceed then to find a corrected version of Horton's law of stream numbers. Returning to equation (2.11), we see that it is only valid in the limit $\Omega \to \infty$. Defining $n'(\omega, \Omega)$ as the actual number of streams of order ω *within* a basin of order Ω, we have

$$n'(\omega, \Omega) = 2n'(\omega + 1, \Omega) + \sum_{\nu=1}^{\Omega - \omega} T_\nu n'(\omega + \nu, \Omega). \qquad (2.20)$$

This equation may be exactly solved. Considering the above expression for $n'(\omega, \Omega)$ and the corresponding one for $n'(\omega + 1, \Omega)$ we can reduce this to a simple difference equation,

$$n'(\omega, \Omega) = (2 + R_{l^{(\mathrm{s})}} + T_1)n'(\omega + 1, \Omega) - 2R_{l^{(\mathrm{s})}}n'(\omega + 2, \Omega) \qquad (2.21)$$

which has solutions of the form μ^k. Applying the constraints that $n'(\Omega, \Omega) = 1$ and $n'(\Omega - 1, \Omega) = T_1 + 2$, we obtain

$$n'(\omega, \Omega) = c(\mu_+)^{\Omega - \omega} + (1 - c)(\mu_-)^{\Omega - \omega} \qquad (2.22)$$

where

$$2\mu_\pm = (2 + R_{l(s)} + T_1) \pm \left[(2 + R_{l(s)} + T_1)^2 - 8R_{l(s)}\right]^{1/2} \qquad (2.23)$$

and

$$c = R_n(R_n - R_{l(s)})/(R_n^2 - 2R_{l(s)}). \qquad (2.24)$$

Note that $R_n = \mu_+$ and we will use the notation R_n^* in place of μ_-. This observation regarding Horton's law of stream numbers was first made by Tokunaga [144] and later by Smart [120]. In particular, Tokunaga noted that this would explain the deviation of Horton's law for the highest orders of a basin, a strong motivation for his work.

We can now define an effective Horton ratio, $R_n'(\omega, \Omega)$ as follows:

$$\begin{aligned}
R_n'(\omega, \Omega) &= n'(\omega - 1, \Omega)/n'(\omega, \Omega) \\
&= R_n \left(1 + O(R_n^*/R_n)^{(\Omega - \omega)}\right) \qquad (2.25)
\end{aligned}$$

The typical values of Horton's ratios in (2.19) give $R_n^* = 1$. In this case, $R_n'(\omega, \Omega)$ converges rapidly to R_n with an error of around one per cent for $\omega = \Omega - 3$.

2.6.2   Stream ordering version of Hack's law

As discussed in section 2.4.3, an estimate of total drainage area of a basin is given by the total length of all streams within the basin. Summing over all stream orders and using the numbers $n'(\omega, \Omega)$ given by equations (2.22) and (2.23) we have that

$$\begin{aligned}
\bar{a}_\Omega &\propto \sum_{\omega=1}^{\Omega} n'(\omega, \Omega)(R_{l(s)})^{\omega-1} \\
&= c_1(R_n)^\Omega + c_2(R_{l(s)})^\Omega - c_3(R_n^*)^\Omega \qquad (2.26)
\end{aligned}$$

where $c_1 = c/(R_n - R_{l(s)})$, $c_3 = (1 - c)/(R_{l(s)} - R_n^*)$ and $c_2 = c_3 - c_1$ with c being given in equation (2.24). Slightly more complicated is the estimate of $\bar{a}(\omega, \Omega)$, the drainage area of a basin of order ω within a basin of order Ω:

$$\begin{aligned}
\bar{a}(\omega, \Omega) &\propto 1/n'(\omega, \Omega) \sum_{\omega'=1}^{\omega} n'(\omega', \Omega)(R_{l(s)})^{\omega'-1} \\
&= 1/n'(\omega, \Omega) \left[c_1(R_n)^\Omega(1 - (R_{l(s)}/R_n)^\omega) \right. \\
&\qquad \left. + c_3(R_{l(s)})^\omega (R_n^*)^{\Omega-\omega}(1 - (R_n^*/R_{l(s)})^\omega)\right]. \qquad (2.27)
\end{aligned}$$

Now, for $1 \ll \omega \ll \Omega$ (typically, $3 < \omega < \Omega - 2$ is sufficient), this expression is well approximated as

$$\bar{a}(\omega, \Omega) \sim (R_n)^\omega. \tag{2.28}$$

since $R_n > R_{l(\mathrm{s})} > R_n^*$.

Thus, we have also shown here that $R_a \equiv R_n$. While it is true that we would have obtained the same with a naive use of Horton's laws, we have both made the derivation thorough and established the correction terms found in equation (2.27). This will be investigated further in the next section.

Finally, using this result and the estimate $\bar{l}_\omega \propto (R_{l(\mathrm{s})})^\omega$ from equation (2.8), it follows that

$$\bar{l}_\omega \propto (R_{l(\mathrm{s})})^\omega = (R_n)^{\omega \ln R_{l(\mathrm{s})} / \ln R_n} \sim (\bar{a}_\omega)^{\ln R_{l(\mathrm{s})} / \ln R_n} \tag{2.29}$$

which is precisely Hack's law. Comparing equations (2.29) and (2.2), Hack's exponent is found in terms of the Horton ratios R_n and $R_{l(\mathrm{s})}$ as

$$h = \frac{\ln R_{l(\mathrm{s})}}{\ln R_n}. \tag{2.30}$$

There is one minor caveat to the derivation in (2.29) and, for that matter, to most other derivations in this paper. Equation (2.29) only holds for the characteristic areas and lengths $\bar{a}_\omega$ and $\bar{l}_\omega$. Since these quantities grow exponentially with ω, the derivation gives evenly spaced points on a log-log plot lying on a straight line. Clearly, this would indicate that the actual relationship is continuous and linear on a log-log plot. Indeed, there is no obvious reason that a network would prefer certain lengths and areas. The averaging of stream lengths and areas brought about by the imposition of stream ordering necessarily removes all information contained in higher order statistics. Motivated by this observation, generalizations of the laws of Tokunaga, Horton and Hack to laws of distributions rather than averages is in progress [30].

2.7   There are only two Horton ratios

In deriving Hack's law in the previous section we obtained from equation (2.28) that $R_a \equiv R_n$. This redundancy in Horton's laws is implicit in, amongst others, the works of Horton [58] and Hack [54] but has never been stated outright. As noted previously, Peckham also obtains a similar result for a topological

quantity, the number of source streams in a basin, that is used as an estimate of area. Thus, we see that for a landscape with uniform drainage density, Horton's laws are fully specified by only two parameters R_n and $R_{l^{(s)}}$. This further supports our claim that Tokunaga's law and Horton's laws are equivalent since we have shown that there is an invertible transformation between (T_1, R_T), the parameters of Tokunaga's law, and $(R_n, R_{l^{(s)}})$ (equations (2.12), (2.15) and (2.17)). In this section, we present data from real networks that support the finding $R_n = R_a$. We also address reported cases that do not conform to this result and consider a possible explanation in light of the correction terms established in equation (2.26).

Excellent agreement for the result $R_n = R_a$ in real networks is to be found in the data of Peckham [102]. The data is taken from an analysis of digital elevation models (DEM's) for the Kentucky River, Kentucky and the Powder River, Wyoming. Figure 2.4 shows average area and stream number plotted as a function of order for the Kentucky River while Figure 2.5 shows the same for the Powder river. Note that stream number has been plotted against decreasing stream order to make the comparison clear. The exponents R_a and R_n are indistinguishable in both cases. For the Kentucky river, $R_n \approx R_a = 4.65 \pm 0.05$ and for the Powder river, $R_n \approx R_a = 4.55 \pm 0.05$. Also of note here is that the same equality is well satisfied by Scheidegger's model where numerical simulations yield values of $R_a = 5.20 \pm 0.05$ and $R_n = 5.20 \pm 0.05$.

Note the slight deviation from a linear form for stream numbers for large ω in both cases. This upwards concavity is as predicted by the modified version of Horton's law of stream numbers for a single basin, equation (2.22).

At the other extreme, the fit for both stream areas and stream numbers extends to $\omega = 1$. While this may seem remarkable, it is conceivable that at the resolution of the DEM's used, some orders of smaller streams may have been removed by coarse-graining. Thus, $\omega = 1$ may actually be, for example, a third order stream. Note that such a translation in the value of ω does not affect the determination of the ratios as it merely results in the change of an unimportant multiplicative constant. If ω_r is the true order and $\omega = \omega_r - m$, where m is some integer, then, for example,

$$n_\omega \propto (R_n)^\omega \sim (R_n)^{\omega_r - m} = \text{const} \times (R_n)^{\omega_r}. \qquad (2.31)$$

This is only a rough argument as coarse-graining does not necessarily remove all streams of low orders.

At odds with the result that $R_n \equiv R_a$ are past measurements that uniformly find $R_a > R_n$ at a number of sites. For example, Rosso et al. in [111]
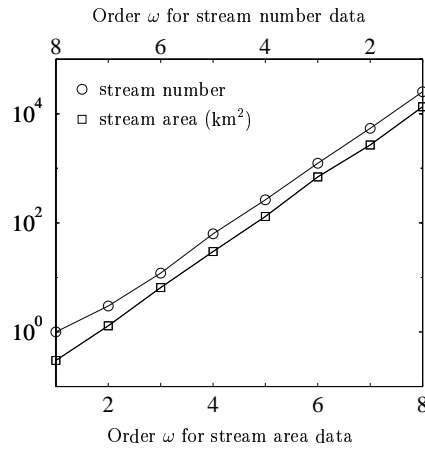
Figure 2.4: Average area and stream number as functions of stream order for Kentucky River, Kentucky (data taken from Peckham [102]). The stream number data is reversed for simpler comparison with the area data. The Horton ratios are estimated to be $R_n \approx R_a = 4.65 \pm 0.05$.
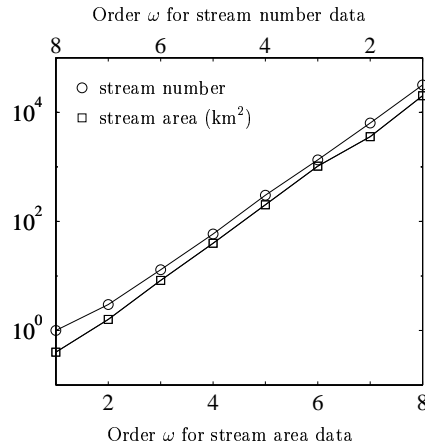
Figure 2.5: Average area and stream number as functions of stream order for Powder River, Wyoming (data taken from Peckham [102]). Here the ratios are $R_n \approx R_a = 4.55 \pm 0.05$.

examine eight river networks and find R_a to be on average 40 % greater than R_n. Clearly, this may be solely due to one or more of the our assumptions not being satisfied. The most likely would be that drainage density is not uniform. However, the limited size of the data sets points to a stronger possibility which we now discuss.
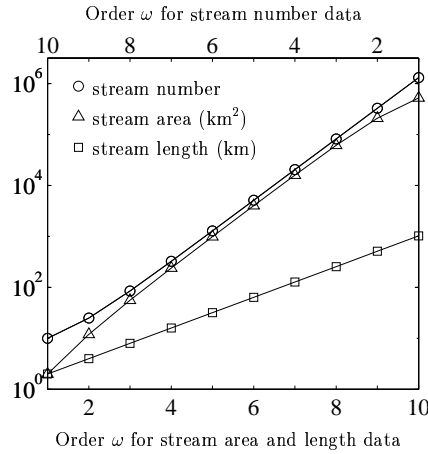
Figure 2.6: An explanation for the empirical finding that $R_n < R_a$. Fitting a line to the stream area for only low ω would result in an overestimate of its asymptotic slope. For stream number, its slope would be underestimated.

In the case of [111], the networks considered are all third or fourth order basins with one exception of a fifth order basin. As shown by equation (2.26), if Horton's laws of stream number and length are exactly followed for all orders, Horton's law of area is not obeyed for lower orders. Moreover, the former are most likely asymptotic relations themselves. It is thus unsatisfactory to make estimates of Horton's ratios from only three or four data points taken from the lowest order basins. Note that the Kentucky and Powder rivers are both eighth order networks and thus provide a sufficient range of data.

We consider more precisely how the corrections to the scaling of area given in equation (2.27) would affect the measurement of the Horton ratios. Figure 2.6 shows an example of how stream number, length and area might vary with ω. It is assumed, for the sake of argument, that stream number and length scale exactly as per Horton's laws and that area behaves as in equation (2.27), satisfying Horton's law of area only for higher values of ω. The plot is made for the example values $R_n = 4$ and $R_{l(\mathrm{s})} = 2$. The prefactors are chosen arbitrarily so the ordinate is of no real significance.

A measurement of R_a from a few data points in the low ω range will overestimate its asymptotic value as will a similar measurement of R_n underestimate its true value. Estimates of R_n and R_a from a simple least squares fit for various ranges of data are provided in Table 2.3.

Thus, the validity of the methods and results from past work are cast in

ω range	$1, 2, 3$	$1, 2, 3, 4$	$1, 2, 3, 4, 5$	$4, 5, 6, 7, 8$
R_n	2.92	3.21	3.41	3.99
R_a	5.29	4.90	4.67	4.00

Table 2.3: Values of Horton ratios obtained from least squares estimates of slopes for data represented in Figure 2.6. The range indicates the data points used in the estimate of the slopes. The ratios obtained from the low order data demonstrate substantial error whereas those obtained from the middle data essentially give the true values of $R_n = R_a = 4$.

some doubt. A reexamination of data which has yielded $R_a \gg R_n$ appears warranted with an added focus on drainage density. Moreover, it is clear that networks of a much higher order must be studied to produce any reasonable results.

2.8 Fractal dimensions of networks: a revision

A number of papers and works over the past decade have analyzed the relationships that exist between Horton's laws and two fractal dimensions used to describe river networks [37, 74, 76, 111, 125, 141, 143]. These are D, the dimension which describes the scaling of the total mass of a network, and d, the fractal dimension of individual streams that comprises one of our assumptions. In this section, we briefly review these results and point out several inconsistencies. We then provide a revision that fits within the context of our assumptions.

Our starting point is the work of La Barbera and Rosso [74] which was improved by Tarboton et al. to give [143]

$$D = d\frac{\ln R_n}{\ln R_{l^{(s)}}}. \tag{2.32}$$

We find this relation to be correct but that the assumptions and derivations involved need to be redressed. To see this, note that equation (2.32) was shown to follow from two observations. The first was the estimation of $N(l^{(\bar{s})}{}_1)$, the number of boxes of size $l^{(\bar{s})}{}_1 \times l^{(\bar{s})}{}_1$ required to cover the network [74]:

$$N(l^{(\bar{s})}{}_1) \sim (l^{(\bar{s})}{}_1)^{-\ln R_n / \ln R_{l^{(s)}}} \tag{2.33}$$

where $l^{(\mathrm{s})}_1$ is the mean length of first order stream segments. Note that Horton's laws were directly used in this derivation rather than the correctly modified law of stream numbers for single basins (equation (2.22)). Nevertheless, the results are the same asymptotically. The next was the inclusion of our second assumption, that single channels are self-affine [143]. Thus, it was claimed, $\bar{l^{(\mathrm{s})}}_1 \sim \delta^{-d}$ where δ is now the length of the measuring stick. Substitution of this into equation (2.33) gave

$$N(\delta) \sim \delta^{-d \ln R_n / \ln R_{l^{(\mathrm{s})}}}, \tag{2.34}$$

yielding the stated expression for D, equation (2.32).

However, there is one major assumption in this work that needs to be more carefully examined. The network is assumed to be of infinite order, i.e., one can keep finding smaller and smaller streams. As we have stated, there is a finite limit to the extension of any real network. The possible practical effects of this are pictorially represented in Figure 2.7. Consider that the network in question is of actual order Ω. Then there are three possible scaling regimes. Firstly, for a ruler of length $\delta \gg \bar{l^{(\mathrm{s})}}_1$, only the network structure may be detected, given that individual streams are almost one-dimensional. Here, the scaling exponent will be $\ln R_n / \ln R_{l^{(\mathrm{s})}}$. Next, as δ decreases, the fractal structure of individual streams may come into play and the exponent would approach that of equation (2.34). Depending on the given network, this middle section may not even be present or, if so, perhaps only as a small deviation as depicted. Finally, the contribution due to the overall network structure must vanish by the time δ falls below $\bar{l^{(\mathrm{s})}}_1$. From this point on, the measurement can only detect the fractal nature of individual streams and so the exponent must fall back to d.

We therefore must rework this derivation of equation (2.32). As suggested in the definition of d in section 2.4.2, it is more reasonable to treat networks as growing fractals. Indeed, since there is a finite limit to the extent of channelization of a landscape, there is a lower cut-off length scale beyond which most network quantities have no meaning. The only reasonable way to examine scaling behavior is to consider how these quantities change with increasing basin size. This in turn can only be done by comparing different basins of increasing order as opposed to examining one particular basin alone.

With this in mind, the claim that equation (2.32) is the correct scaling can be argued as follows. Within some basin of order Ω, take a sub-basin of order ω. Consider $N(\omega)$, the number of boxes of side length $\bar{l^{(\mathrm{s})}}_1$ required to cover the sub-network. This is essentially given by the total length of all the streams in the network. This is given by the approximation of equation (2.28)
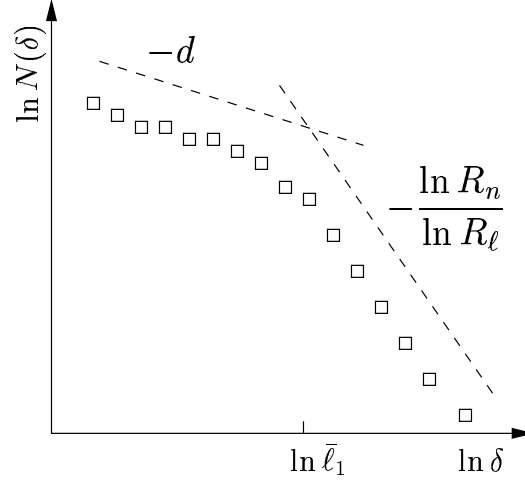
Figure 2.7: A schematic representing the problems associated with measuring the fractal dimension of *a single river network*. Here, the box counting method is assumed and δ, which has the units of length, is the side length of the $N(\delta)$ boxes needed to cover the network. For box sizes much greater than $l^{(\mathrm{s})}{}_1 \times l^{(\mathrm{s})}{}_1$, only the network structure is detected while for box sizes smaller than $l^{(\mathrm{s})}{}_1 \times l^{(\mathrm{s})}{}_1$, the measurement picks out the fractal dimension of individual streams. Some deviation towards the scaling suggested by equation (2.34) may occur between these two limits.

and so we have that $N(\omega) \propto (R_n)^\omega$. Using the fact that $\bar{l}^{(\mathrm{s})}{}_\omega = (R_{l^{(\mathrm{s})}})^{\omega-1} \bar{l}^{(\mathrm{s})}{}_1$ we then have that $N(\omega) \propto (l^{(\mathrm{s})}{}_\omega / \bar{l}^{(\mathrm{s})}{}_1)^{\ln R_n / \ln R_{l^{(\mathrm{s})}}}$. The difference here is that $\bar{l}^{(\mathrm{s})}{}_1$ is fixed and pertains to the actual first order streams of the network. By assumption, we have that $l^{(\mathrm{s})}{}_\omega \propto L^d$ and thus

$$N(L) \propto L^{d \ln R_n / \ln R_{l^{(\mathrm{s})}}}, \tag{2.35}$$

which gives the same value for D as equation (2.32).

There are two other relations involving fractal dimensions that also need to be reexamined. Firstly Rosso et al. [111] found that

$$d = 2 \frac{\ln R_{l^{(\mathrm{s})}}}{\ln R_a}. \tag{2.36}$$

Combining equations (2.32) and (2.36), they then obtained

$$D = 2 \frac{\ln R_n}{\ln R_a}. \tag{2.37}$$

However, equation (2.36) and hence equation (2.37) are both incorrect.

There is a simple explanation for this discrepancy. In deriving equation (2.36), Rosso et al. make the assumption that $h = d/2$, a hypothesis first suggested by Mandelbrot [83]. In arriving at the relation $h = d/2$, Mandelbrot states in [83] that "(basin area)$^{1/2}$ should be proportional to (distance from source to mouth as the crow flies)." In other words, $a \propto L^{1/2}$. However, as noted in equation (2.3), observations of real networks show that $a \propto L^D$ where $D < 2$ [87]. Furthermore, on examining the result $h = \ln R_{l^{(s)}} / \ln R_n$ with the expression for D in equation (2.32) we see that

$$h = \frac{d}{D}, \tag{2.38}$$

which suggests that this hypothesis is valid only when $D = 2$. Consider also the test case of the Scheidegger model where $h = 2/3$, $D = 3/2$ and $d = 1$ (see Table 2.2). Using these values, we see that equation (2.38) is exactly satisfied while the relation $h = d/2$ gives $h = 1/2 \neq 2/3$.

Now, if $h = d/D$ is used in place of $h = d/2$ in deriving equation (2.36) then equation (2.32) is recovered. It also follows that equation (2.37) simplifies to the statement $R_a = R_n$, further demonstrating the consistency of our derivations. Thus, the two equations (2.36) and (2.37) become redundant and the only connection between Horton's ratios and network dimensions is given by equation (2.32).

An important point is that $D < 2$ *does not imply* that drainage basins are not space filling. This exponent shows how basin area changes when comparing different basins with different values of L, i.e., $a \propto L^D$. Any given single basin has of course a fractal dimension of 2. The equating of the way basin sizes change with the actual dimension of any one particular basin is a confusion evident in the literature (see, for example, [141]). Incorporating the effects of measuring basin area with boxes of side length δ in the relation $a \propto L^D$ would lead to the form

$$a_L(\delta) \propto \delta^{-2} L^D, \tag{2.39}$$

where the subscript L has been used to emphasize that different values of L correspond to different basins. Thus, for any given basin (i.e., for fixed L), the area scales with δ while for a fixed δ, areas of different basins scale as per equation (2.3).

It should also be emphasized that the relationship found here between Hack's exponent and the fractal dimensions d and D is one that is explicitly

derived from the assumptions made. The observation that basin areas scale non-trivially with L follows from these starting points and thus there is no need to assume it here.

2.9 Other scaling laws

We now address three remaining sets of scaling laws. These are probability distributions for areas and stream lengths, scaling of basin shape and Langbein's law.

As introduced in equation (2.4), probability distributions for a and l are observed to be power law with exponents τ and γ [110]. Both of these laws have previously been derived from Horton's laws. De Vries et al. [24] found a relationship between τ, R_n and $R_{l(s)}$ but did not include d in their calculations while Tarboton et al. [141] obtained a result for γ that did incorporate d.

Again, both of these derivations use Horton's laws directly rather than the modified version of equation (2.22). Asymptotically, the same results are obtained from both approaches,

$$\tau = 2 - \frac{\ln R_{l(s)}}{\ln R_n} \quad \text{and} \quad \gamma = \frac{\ln R_n}{\ln R_{l(s)}}. \tag{2.40}$$

Using the form of the Hack exponent found in equation (2.38) and equation (2.32), further connections between these exponents are found:

$$\tau = 2 - h \quad \text{and} \quad \gamma = \frac{1}{h}. \tag{2.41}$$

One important outcome concerns the fact that only one of the exponents of the triplet (h, τ, γ) is independent. Previously, for the particular case of directed networks, this has been shown by Meakin et al. [88] and further developed by Colaiori et al. [19]. Directed networks are those networks in which all flow has a non-zero positive component in a given direction. In a different setting, Cieplak et al. also arrive at this same conclusion for what they deem to be the separate cases of self-similar and self-affine networks although their assumptions are that $d < 1$ and $D < 2$ are mutually exclusive contrary to empirical observations [18].[1] In the case of non-directed networks, Maritan et al. have found one scaling relation for these three exponents, $\gamma = 1 + (\tau - 1)/h$ and, therefore, that two of these three exponents

---

[1]See the discussion on allometry in Chapter 5 for an updated view.

are independent. They further noted that $\tau = 2 - h$ is an "intriguing result" suggested by real data [87]. In the present context, we have obtained this reduction of description in a very general way with, in particular, no assumption regarding the directedness of the networks.

The scaling of basin shapes has been addressed already but it remains to show how it simply follows from our assumptions and how the relevant exponents are related. It is enough to show that this scaling follows from Hack's law. Now, the area of a basin is related to the longitudinal length L and the width $L_\perp$ by $a = L_\perp L$, while the main stream length scales by assumption like $l \sim L^d$. Hence,

$$\begin{aligned}
l \sim a^h &\Rightarrow L^d \sim (L_\perp L)^h \\
&\Rightarrow L_\perp \sim L^{d/h-1} = L^{D-1}
\end{aligned} \qquad (2.42)$$

where the fact that $h = d/D$ has been used. Comparing this to equation (2.3) we obtain the scaling relation

$$H = D - 1. \qquad (2.43)$$

The last set of exponents we discuss are those relating to Langbein's law [78]. Langbein found that $\tilde{\Lambda}$, the sum of the distances (along streams) from stream junctions to the outlet of a basin, scales with the area of the basin. Recently, Maritan et al. [87] introduced the quantity λ, which is an average of Langbein's $\tilde{\Lambda}$ except now the sum is taken over all points of the network. Citing the case of self-organized critical networks, they made the claim that

$$\lambda \propto L^\varphi. \qquad (2.44)$$

Further, they assumed that $\varphi = d$ although it was noted that there is no clear reason why this may be so since there are evident differences in definition (λ involves distances downstream while d involves distances upstream). We find this scaling relation to hold in the present framework. We further consider the two related quantities Λ and $\tilde{\lambda}$, respectively the sum over all points and the average over all junctions of distances along streams to the basin outlet.

The calculations are straightforward and follow the manner of previous sections. We first calculate $\lambda(\omega, \Omega)$, the typical distance to the outlet from a stream of order ω in an order Ω basin. Langbein's $\tilde{\Lambda}$, for example, is then obtained as $\sum_{\omega=1}^{\Omega} n(\omega, \Omega)\lambda(\omega, \Omega)$. We find the same scaling behavior regardless of whether sums are taken over all points or all junctions. Specifically

we find

$$\Lambda \sim \tilde{\Lambda} \sim a^{1+\ln R_{l(s)}/\ln R_n} \quad \text{and} \quad \lambda \sim \tilde{\lambda} \sim L^d \qquad (2.45)$$

yielding the scaling relations

$$\beta = \tilde{\beta} = 1 + \ln R_{l(s)}/\ln R_n \quad \text{and} \quad \tilde{\varphi} = \varphi = d. \qquad (2.46)$$

Note that the second pair of scaling relations admit other methods of measuring d. The large amount of averaging inherent in the definition of the quantity λ would suggest that it is a more robust method for measuring d than one based on measurements of the sole main stream of the basins.

Maritan et al. [87] provide a list of real world measurements for various exponents upon which several comments should be made. Of particular note is the relationship between $\tau = 2 - h$. This is well met by the cited values $1.41 < \tau < 1.45$ and $0.57 < h < 0.60$. Also reasonable is the estimate of h given by d/D ($D = \phi$ in their notation) which is $0.58 < h < 0.65$.

The values of γ and φ, however, do not work quite so well. The latter does not match d within error bars, although they are close in absolute value with $\varphi = 1.05 \pm 0.01$ and $d = 1.10 \pm 0.01$. The length distribution exponent γ may be found via 3 separate routes: $\gamma = 1/h = D/d = 1/(2-\tau)$. The second and third equalities have been noted to be well satisfied and so any one of the 3 estimates of γ may be used. Take, for example, the range $0.58 < h < 0.59$, which falls within that given by $h = 2 - \tau$, $h = d/D$ and the range given for h itself. This points to the possibility that the measured range $1.8 < \gamma < 1.9$ is too high, since using $\gamma = 1/h$ yields $\gamma = 1.74 \pm .02$. Also of note is that Maritan et al.'s own scaling relation $\gamma = 1 + (\tau - 1)/h$ would suggest $\gamma = 1.74 \pm .05$.

Better general agreement with the scaling relations is to be found in [106] in which Rigon et al. detail specific values of h, τ and γ for some thirteen river networks. Here, the relations $\tau = 2 - h$ and $\gamma = 1/h$ are both well satisfied. Comparisons for this set of data show that, on average and given the cited values of h, both τ and γ are overestimated by only 2 per cent.

2.10   Concluding remarks

We have demonstrated that the various laws, exponents and parameters found in the description of river networks follow from a few simple assumptions. Further, all quantities are expressible in terms of two fundamental

numbers. These are a ratio of logarithms of Horton's ratios, $\ln R_n / \ln R_{l^{(s)}}$, and the fractal dimension of individual streams, d. There are *only two* independent parameters in network scaling laws. These Horton ratios were shown to be equivalent to Tokunaga's law in informational content with the attendant assumption of uniform drainage density. Further support for this observation is that both the Horton and Tokunaga descriptions depend on two parameters each and an invertible transformation between them exists (see equations (2.12), (2.15) and (2.17)). A summary of the connections found between the various exponents is presented in Table 2.4.

It should be emphasized that the importance of laws like that of Tokunaga and Horton in the description of networks is that they provide explicit structural information. Other measurements such as the power law probability distributions for length and area provide little information about how a network fits together. Indeed, information is lost in the derivations as the Horton ratios cannot be recovered from knowledge of $\ln R_n / \ln R_{l^{(s)}}$ and d only.

The basic assumptions of this work need to be critically examined. Determining how often they hold and why they hold will follow through to a greater understanding of all river network laws. One vital part of any river network theory that is lacking here is the inclusion of the effects of relief, the third dimension. Another is the dynamics of network growth: why do mature river networks exhibit a self-similarity that gives rise to these scaling laws with these particular values of exponents? Also, extensive studies of variations in drainage density are required. The assumption of its uniformity plays a critical role in the derivations and needs to be reexamined. Lastly, in those cases where these assumptions are valid, the scaling relations gathered here provide a powerful method of cross-checking measurements.

Finally, we note that work of a similar nature has recently been applied to biological networks [151]. The assumption analogous to network self-similarity used in the biological setting is considerably weaker as it requires only that the network is a hierarchy. A principle of minimal work is then claimed to constrain this hierarchy to be self-similar. It is conceivable that a similar approach may be found in river networks. However, a generalization of the concept of a hierarchy and perhaps stream ordering needs to be developed since a 'Tokunagic network' is not itself a simple hierarchy.

law:	parameter in terms of R_n, $R_{l(\mathrm{s})}$ and d:
$T_\nu = T_1 (R_T)^{\nu-1}$	$T_1 = R_n - R_{l(\mathrm{s})} - 2 + 2 R_{l(\mathrm{s})}/R_n$
	$R_T = R_{l(\mathrm{s})}$
$l \sim L^d$	—
$n_{\omega+1}/n_\omega = R_n$	—
$\bar{l^{(\mathrm{s})}}_{\omega+1}/\bar{l^{(\mathrm{s})}}_\omega = R_{l(\mathrm{s})}$	—
$\bar{l}_{\omega+1}/\bar{l}_\omega = R_{l(\mathrm{s})}$	—
$\bar{a}_{\omega+1}/\bar{a}_\omega \sim R_a$	$R_a = R_n$
$l \sim a^h$	$h = \ln R_{l(\mathrm{s})}/\ln R_n$
$a \sim L^D$	$D = d \ln R_n/\ln R_{l(\mathrm{s})}$
$L_\perp \sim L^H$	$H = d \ln R_n/\ln R_{l(\mathrm{s})} - 1$
$P(a) \sim a^{-\tau}$	$\tau = 2 - \ln R_{l(\mathrm{s})}/\ln R_n$
$P(l) \sim l^{-\gamma}$	$\gamma = \ln R_n/\ln R_{l(\mathrm{s})}$
$\Lambda \sim a^\beta$	$\beta = 1 + \ln R_{l(\mathrm{s})}/\ln R_n$
$\lambda \sim L^\varphi$	$\varphi = d$
$\tilde{\Lambda} \sim a^{\tilde{\beta}}$	$\tilde{\beta} = 1 + \ln R_{l(\mathrm{s})}/\ln R_n$
$\tilde{\lambda} \sim L^{\tilde{\varphi}}$	$\tilde{\varphi} = d$

Table 2.4: Summary of scaling laws and the scaling relations found between the various exponents. Compare with table 2.1.

Acknowledgements

CHAPTER **3**

Fluctuations and deviations for scaling laws

Abstract. This article is the first in a series of three papers investigating
the detailed geometry of river networks. Branching networks are a universal
structure employed in the distribution and collection of material. Large-
scale river networks mark an important class of two-dimensional branching
networks, being not only of intrinsic interest but also a pervasive natural
phenomenon. In the description of river network structure, scaling laws are
uniformly observed. Reported values of scaling exponents vary suggesting
that no unique set of scaling exponents exists. To improve this current un-
derstanding of scaling in river networks and to provide a fuller description
of branching network structure, here we report a theoretical and empirical
study of fluctuations about and deviations from scaling. We examine data
for continent-scale river networks such as the Mississippi and the Amazon
and draw inspiration from a simple model of directed, random networks. We
center our investigations on the scaling of the length of sub-basin's domi-
nant stream with its area, a characterization of basin shape known as Hack's
law. We generalize this relationship to a joint probability density and pro-
vide observations and explanations of deviations from scaling. We show that
fluctuations about scaling are substantial and grow with system size. We
find strong deviations from scaling at small scales which can be explained
by the existence of linear network structure. At intermediate scales, we find
slow drifts in exponent values indicating that scaling is only approximately
obeyed and that universality remains indeterminate. At large scales, we ob-
serve a breakdown in scaling due to decreasing sample space and correlations
with overall basin shape. The extent of approximate scaling is significantly

restricted by these deviations and will not be improved by increases in network resolution.

3.1   Introduction

Networks are intrinsic to a vast number of complex forms observed in the natural and man-made world. Networks repeatedly arise in the distribution and sharing of information, stresses and materials. Complex networks give rise to interesting mathematical and physical properties as observed in the Internet [3], the "small-world" phenomenon [149], the cardiovascular system [156], force chains in granular media [20], and the wiring of the brain [17].

Branching, hierarchical geometries make up an important subclass of all networks. Our present investigations concern the paradigmatic example of river networks. The study of river networks, though more general in application, is an integral part of geomorphology, the theory of earth surface processes and form. Furthermore, river networks are held to be natural exemplars of allometry, i.e., how the dimensions of different parts of a structure scale or grow with respect to each other [8, 35, 83, 108, 110]. The shapes of drainage basins, for example, are reported to elongate with increasing basin size [54, 87, 106].

At present, there is no generally accepted theory explaining the origin of this allometric scaling. The fundamental problem is that an equation of motion for erosion, formulated from first principles, is lacking. The situation is somewhat analogous to issues surrounding the description of the dynamics of granular media [65, 66], noting that erosion is arguably far more complex. Nevertheless, a number of erosion equations have been proposed ranging from deterministic [64, 73, 119, 121] to stochastic theories [9, 18, 47, 98, 99, 122]. Each of these models attempts to describe how eroding surfaces evolve dynamically. In addition, various heuristic models of both surface and network evolution also exist. Examples include simple lattice-based models of erosion [15, 73, 79, 137], an analogy to invasion percolation [124], the use of optimality principles and self-organized criticality [110, 130, 132], and even uncorrelated random networks [35, 82, 112]. Since river networks are an essential feature of eroding landscapes, any appropriate theory of erosoion must yield surfaces with network structures comparable to that of the real world. However, no model of eroding landscapes or even simply of network evolution unambiguously reproduces the wide range of scaling behavior reported for real river networks.

A considerable problem facing these theories and models is that the values of scaling exponents for river network scaling laws are not precisely known. One of the issues we address in this work is universality [35, 87]. Do the scaling exponents of all river networks belong to a unique universality class or are there a set of classes obtained for various geomorphological conditions? For example, theoretical models suggest a variety of exponent values for networks that are directed versus non-directed, created on landscapes with heterogeneous versus homogeneous erosivity and so on [35, 85, 86]. Clearly, refined measurements of scaling exponents are imperative if we are to be sure of any network belonging to a particular universality class. Moreover, given that there is no accepted theory derivable from simple physics, more detailed phenomenological studies are required.

Motivated by this situation, we perform here a detailed investigation of the scaling properties of river networks. We analytically characterize fluctuations about scaling showing that they grow with system size. We also report significant and ubiquitous deviations from scaling in real river networks. This implies surprisingly strong restrictions on the parameter regimes where scaling holds and cautions against measurements of exponents that ignore such limitations. In the case of the Mississippi basin, for example, we find that although our study region span four orders of magnitude in length, scaling may be deemed valid over no more than 1.5 orders of magnitude. Furthermore, we repeatedly find the scaling within these bounds to be only approximate and that no exact, single exponent can be deduced. We show that scaling breaks down at small scales due to the presence of linear basins and at large scales due to the inherent discreteness of network structure and correlations with overall basin shape. Significantly, this latter correlation imprints upon river network structure the effects and history of geology.

This paper is the first of a series of three on river-network geometry. Having addressed scaling laws in the present work, we proceed in second and third articles [33, 34] to consider river network structure at a more detailed level. In [33] we examine the statistics of the "building blocks" of river networks, i.e., segments of streams and sub-networks. In particular, we analytically connect distributions of various kinds of stream length. Part of this material is employed in the present article and is a direct generalization of Horton's laws [31, 58]. In the third article [34], we proceed from the findings of [33] to characterize how these building blocks fit together. Central to this last work is the study of the frequency and spatial distributions of tributary branches along the length of a stream and is itself a generalization of the descriptive picture of Tokunaga [144, 145, 146].

3.2   Basin allometry

3.2.1   Hack's law

In addressing these broader issues of scaling in branching networks, we set as our goal to understand the river network scaling relationship between basin area a and the length l of a basin's main stream:

$$l \propto a^h. \tag{3.1}$$

Known as Hack's law [54], this relation is central to the study of scaling in river networks [31, 87]. Hack's exponent h is empirically found to lie in the range from 0.5 to 0.7 [52, 54, 87, 90, 94, 95, 96, 106, 107]. Here, we postulate a generalized form of Hack's law that shows good agreement with data from real world networks.

We focus on Hack's law because of its intrinsic interest and also because many interrelationships between a large number of scaling laws are known and only a small subset are understood to be independent [31, 87]. Thus, our results for Hack's law will be in principle extendable to other scaling laws. With this in mind, we will also discuss probability densities of stream length and drainage area.

Hack's law is stated rather loosely in equation (3.1) and implicitly involves some type of averaging which needs to be made explicit. It is most usually considered to be the relationship between *mean* main stream length and drainage area, i.e.,

$$\langle l \rangle \propto a^h. \tag{3.2}$$

Here, $\langle \cdot \rangle$ denotes ensemble average and $\langle l \rangle = \langle l(a) \rangle$ is the mean main stream length of all basins of area a. Typically, one performs regression analysis on $\log \langle l \rangle$ against $\log a$ to obtain the exponent h.

3.2.2   Fluctuations and deviations

In seeking to understand Hack's law, we are naturally led to wonder about the underlying distribution that gives rise to this mean relationship. By considering fluctuations, we begin to see Hack's law as an expression of basin morphology. What shapes of basins characterized by (a, l) are possible and with what probability do they occur?

An important point here is that Hack's law does not exactly specify basin shapes. An additional connection to Euclidean dimensions of the basin is
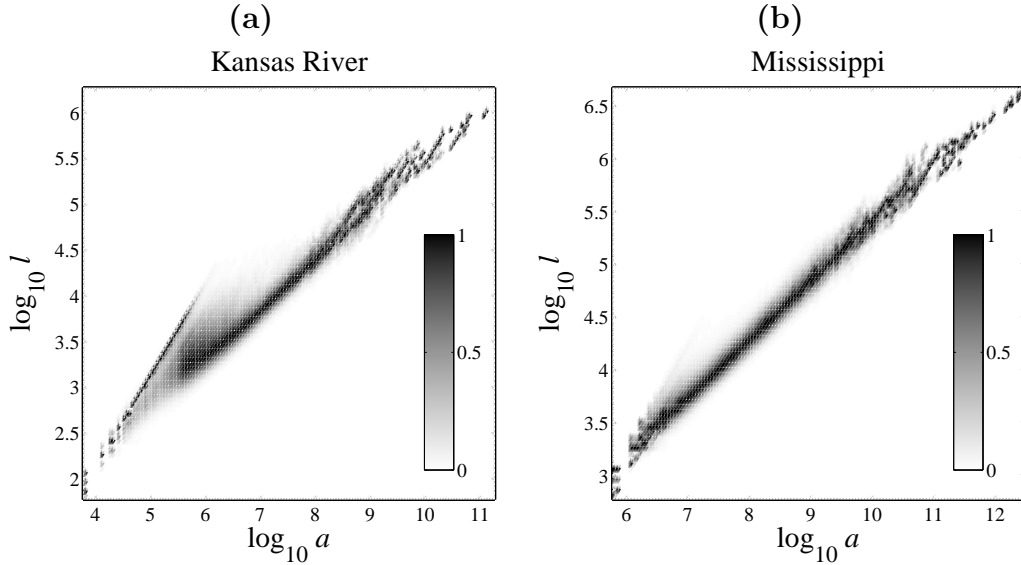
Figure 3.1: The Full Hack distribution for the Kansas, (a), and Mississippi, (b), river basins. For each value of a, the distribution has been normalized along the l direction by $\max_l P(a, l)$. The topography used to extract areas and stream lengths is a composite of United States Geological Survey three-arc-second digital elevation models available on the Internet at `www.usgs.gov`. These datasets provide grids of elevation data with horizontal resolution on the order of 90 meters. The Kansas river was analyzed directly from the data while the Mississippi basin was studied on a coarse-grained version with horizontal resolution of approximately 1000 meters.

required. We may think of a basin's longitudinal length $L_{\parallel}$ and its width $L_{\perp}$. The main stream length l is reported to scale with $L_{\parallel}$ as

$$l \propto L_{\parallel}^d, \tag{3.3}$$

where typically $1.0 \lesssim d \lesssim 1.1$, [87, 143]. Hence, we have $a \propto l^{1/h} \propto L_{\parallel}^{d/h}$. All other relevant scaling laws exponents can be related to the pair of exponents (d, h) which therefore characterize the universality class of a river network [31, 35]. If $d/h = 2$ we have that basins are self-similar whereas if $d/h < 2$, we have that basins are elongating. So, while Hack's law gives a sense of basin allometry, the fractal properties of main stream lengths need also be known in order to properly quantify the scaling of basin shape.

In addition to fluctuations, complementary insights are provided by the observation and understanding of deviations from scaling. We are thus in-

terested in discerning the regularities and quirks of the joint probability distribution $P(a, l)$. We will refer to $P(a, l)$ as the *Hack distribution*.

Hack distributions for the Kansas river basin and the Mississippi river basin are given in Figures 3.1(a) and 3.1(b). Fluctuations about and deviations from scaling are immediately evident for the Kansas and to a lesser extent for the Mississippi. The first section of the paper will propose and derive analytic forms for the Hack distribution under the assumption of uniform scaling with no deviations. Here, as well as in the following two papers of this series [33, 34], we will motivate our results with a random network model originally due to Scheidegger [112].

We then expand our discussion to consider deviations from exact scaling. In the case of the Kansas river, a striking example of deviations from scaling is the linear branch separated from the body of the main distribution shown in Figure 3.1(a). This feature is less prominent in the lower resolution Mississippi data. Note that this linear branch is not an artifact of the measurement technique or data set used. This will be explained in our discussion of deviations at small scales in the paper's second section.

We then consider the more subtle deviations associated with intermediate scales. At first inspection, the scaling appears to be robust. However, we find gradual drifts in "exponents" that prevent us from identifying a precise value of h and hence a corresponding universality class.

Both distributions also show breakdowns in scaling for large areas and stream lengths and this is addressed in the final part of our section on deviations. The reason for such deviations is partly due to the decrease in number of samples and hence self-averaging, as area and stream lengths are increased. However, we will show that the direction of the deviations depends on the overall basin shape. We will quantify the extent to which such deviations can occur and the effect that they have on measurements of Hack's exponent h.

Throughout the paper, we will return to the Hack distributions for the Kansas and the Mississippi rivers as well as data obtained for the Amazon, the Nile and the Congo rivers.

3.3 Fluctuations: an analytic form for the Hack distribution

To provide some insight into the nature of the underlying Hack distribution, we present a line of reasoning that will build up from Hack's law to a scaling

form of $P(a, l)$. First let us assume for the present discussion of fluctuations that an exact form of Hack's law holds:

$$\langle l \rangle = \theta a^h \tag{3.4}$$

where we have introduced the coefficient θ which we discuss fully later on. Now, since Hack's law is a power law, it is reasonable to postulate a generalization of the form

$$P(l \,|\, a) = \frac{1}{a^h} F_l \left(\frac{l}{a^h} \right). \tag{3.5}$$

The prefactor $1/a^h$ provides the correct normalization and F_l is the "scaling function" we hope to understand. The above will be our notation for all conditional probabilities. Implicit in equation (3.5) is the assumption that all moments and the distribution itself also scale. For example, the qth moment of $P(l \,|\, a)$ is

$$\langle l^q(a) \rangle \propto a^{qh}, \tag{3.6}$$

which implies

$$\langle l^q(a) \rangle = k^{-qh} \langle l^q(ak) \rangle . \tag{3.7}$$

where $k \in \mathbb{R}$. Also, for the distribution $P(l \,|\, a)$ it follows from equation (3.5) that

$$k^h P(lk^h \,|\, ak) = \frac{k^h}{a^h k^h} F_l \left(\frac{lk^h}{a^h k^h} \right) = P(l \,|\, a). \tag{3.8}$$

We note that previous investigations of Hack's law [87, 106] consider the generalization in equation (3.5). Rigon et al. [107] also examine the behavior of the moments of the distribution $P(l \,|\, a)$ for real networks. Here, we will go further to characterize the full distribution $P(a, l)$ as well as both $P(l \,|\, a)$ and $P(a \,|\, l)$. Along these lines, Rigon et al. [106] suggest that the function $F_l(x)$ is a "finite-size" scaling function analogous to those found in statistical mechanics, i.e.: $F_l(x) \to 0$ as $x \to \infty$ and $F_l(x) \to c$ as $x \to 0$. However, as we will detail below, the restrictions on $F_l(x)$ can be made stronger and we will postulate a simple Gaussian form. More generally, $F_l(x)$ should be a unimodal distribution that is non-zero for an interval $[x_1, x_2]$ where $x_1 > 0$. This is so because for any given fixed basin area a, there is a minimum and

maximum l beyond which no basin exists. This is also clear upon inspection of Figures 3.1(a) and 3.1(b).

We observe that neither drainage area nor main stream length possess any obvious features so as to be deemed the independent variable. Hence, we can also view Hack's law as its inversion $\langle a \rangle \propto l^{1/h}$. Note that the constant of proportionality is not necessarily $\theta^{1/h}$ and is dependent on the nature of the full Hack distribution. We thus have another scaling ansatz as per equation (3.5)

$$P(a\,|\,l) = 1/l^{1/h}F_a(a/l^{1/h}). \tag{3.9}$$

The conditional probabilities $P(l\,|\,a)$ and $P(a\,|\,l)$ are related to the joint probability distribution as

$$P(a,l) = P(a)P(l\,|\,a) = P(l)P(a\,|\,l), \tag{3.10}$$

where $P(l)$ and $P(a)$ are the probability densities of main stream length and area. These distributions are in turn observed to be power laws both in real world networks and models [88, 110, 138]:

$$P(a) \sim N_a a^{-\tau} \qquad \text{and} \qquad P(l) \sim N_l l^{-\gamma}. \tag{3.11}$$

where N_a and N_l are appropriate prefactors and the tilde indicates asymptotic agreement between both sides for large values of the argument. Furthermore, the exponents τ and γ are related to Hack's exponent h via the scaling relations [31, 87]

$$\tau = 2 - h \qquad \text{and} \qquad \gamma = 1/h. \tag{3.12}$$

Equations (3.5), (3.9), (3.10), (3.11), and (3.12) combine to give us two forms for $P(a,l)$,

$$P(a,l) = 1/a^2F(l/a^h) = 1/l^{2/h}G(a/l^{1/h}), \tag{3.13}$$

where $x^{-2}F(x^{-h}) = G(x)$ and, equivalently, $F(y) = y^{-2}G(y^{-1/h})$.

3.4   Random directed networks

We will use results from the Scheidegger model [112] to motivate the forms of these distributions. In doing so, we will also connect with some problems in the theory of random walks.
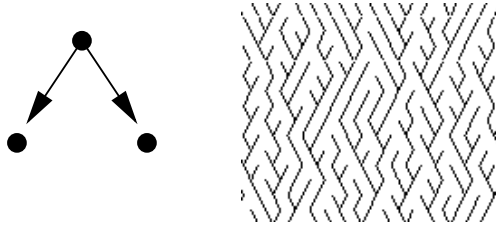
Figure 3.2: Scheidegger's model of random, directed networks. Flow is down the page and at each site, stream flow is randomly chosen to be in one of the two downward diagonals. Stream paths and basin boundaries are thus discrete random walks.

Scheidegger's model of river networks is defined on a triangular lattice as indicated by Figure 3.2. Flow in the figure is directed down the page. At each site, the stream flow direction is randomly chosen between the two diagonal directions shown. Periodic boundary conditions are applied in all of our simulations. Each site locally drains an area of α^2, where the lattice unit α is the distance between neighboring sites, and each segment of stream has a length α. For simplicity, we will take α to be unity. We note that connections exist between the Scheidegger model and models of particle aggregation [61, 138], Abelian sandpiles [25, 26, 27] and limiting cases of force chain models in granular media [20].

Since Scheidegger's model is based on random flow directions, the Hack distributions have simple interpretations. The boundaries of drainage basins in the model are random walks. Understanding Hack's law therefore amounts to understanding the first collision time of two random walks that share the same origin in one dimension. If we subtract the graph of one walk from the other, we see that the latter problem is itself equivalent to the first return problem of random walks [39].

Many facets of the first return problem are well understood. In particular, the probability of n, the number of steps taken by a random walk until it first returns to the origin, is asymptotically given by

$$P(n) \sim \frac{1}{\sqrt{2\pi}} n^{-3/2}.$$ (3.14)

But this number of steps is also the length of the basin l. Therefore, we have

$$P(l) \sim \frac{2}{\pi} l^{-3/2},$$ (3.15)
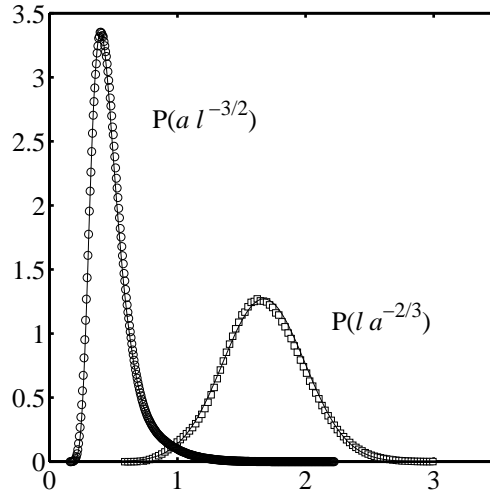
Figure 3.3: Cross-Sectional scaling functions of the Hack distribution for the Scheidegger model with lattice constant equal to unity. Both distributions are normalized. The right distribution is for l fixed and a varying and is postulated to be a normal distribution. The left distribution for a fixed and l varying and is a form of an inverse Gaussian [40]. The data used was obtained for all sites with with $l \geq 100$ and $a \geq 500$ respectively. Each distribution was obtained from ten realizations of the Scheidegger model on a $10^4 \times 10^4$ lattice.

where because we are considering the difference of two walks, we use $P(l) = P(n/2)|_{n=l}$. Also, we have found the prefactor $N_l = 2/\pi$.

We thus have that $\gamma = 3/2$ for the Scheidegger model. The scaling relations of equation (3.12) then give $h = 2/3$ and $\tau = 4/3$. The value of h is also readily obtained by noting that the typical area of a basin of length l is $a \propto l \cdot l^{1/2} = l^{3/2} = l^{1/h}$ since the boundaries are random walks.

3.5 Area-length distribution for random, directed networks

Something that is less well studied is the joint distribution of the area enclosed by a random walk and the number of steps to its first return. In terms of the Scheidegger model, this is precisely the Hack distribution.

We motivate some general results based on observations of the Scheidegger model. Figure 3.3 shows the normalized distributions $P(al^{-3/2})$ and

$P(la^{-2/3})$ as derived from simulations of the model. Given the scaling ansatzes for $P(l\,|\,a)$ and $P(a\,|\,l)$ in equations (3.5) and (3.9), we see that $P(y = la^{-2/3}) = F_l(y)$ and $P(x = al^{-3/2}) = F_a(x)$.

Note that we have already used Hack's law for the Scheidegger model with $h = 2/3$ to obtain these distributions. The results are for ten realizations of the model on a 10^4 by 10^4 lattice, taking 10^7 samples from each of the ten instances. For $P(a\,|\,l)$, only sites where $l \geq 100$ were taken, and similarly, for $P(l\,|\,a)$, only sites where $a \geq 500$ were included in the histogram.

We postulate that the distribution $P(y = la^{-2/3})$ is a Gaussian having the form

$$P(l\,|\,a) = \frac{1}{\sqrt{2\pi a^{2/3}}\eta} \exp\{-(la^{-2/3} - \theta)^2/2\eta^2\} \qquad (3.16)$$

We estimate the mean of F_l to be $\theta \simeq 1.675$ (this is the same θ as found in equation (3.4)) and the standard deviation to be $\eta \simeq 0.321$. The fit is shown in Figure 3.3 as a solid line. The above equation agrees with the form of the scaling ansatz of equation (3.5) and we now have the assertion that F_l is a Gaussian defined by the two parameters θ and η.

Note that the θ and η are coefficients for the actual mean and standard deviation. In other words, for fixed a, the mean of $P(l\,|\,a)$ is $\theta a^{2/3}$ and its standard deviation is $\eta a^{2/3}$. Having observed their context, we will refer to θ and η as the Hack mean coefficient and Hack standard deviation coefficient.

From this starting point we can create $P(a, l)$ and $P(a\,|\,l)$, the latter providing a useful test. Since $P(a) \sim N_a a^{-\tau} = N_a a^{-4/3}$, as per equation (3.11), we have

$$
\begin{aligned}
P(a, l) &= \frac{N_a}{a^{4/3}} \frac{1}{\sqrt{2\pi a^{2/3}}\eta} \exp\{-(la^{-2/3} - \theta)^2/2\eta^2\}, \\
&= \frac{N_a}{\sqrt{2\pi a^2}\eta} \exp\{-(la^{-2/3} - \theta)^2/2\eta^2\}. \qquad (3.17)
\end{aligned}
$$

As expected, we observe the form of equation (3.17) to be in accordance with that of equation (3.13). Note that the scaling function F (and equivalently G) is defined by the three parameters θ, η and N_a, the latter of which may be determined in terms of the former as we will show below. Also, since we expect all scaling functions to be only asymptotically correct, we cannot use equation (3.17) to find an expression for the normalization N_a. Equation (3.17) ceases to be valid for small a and l. However, we will be able to do so once we have $P(a\,|\,l)$ since we are able to presume l is large and

therefore that the scaling form is exact. Using equation (3.15) and the fact that $P(a\,|\,l) = P(a, l)/P(l)$ from equation (3.10) we then have

$$
\begin{aligned}
P(a\,|\,l) &= \frac{\pi l^{3/2}}{2} \frac{N_a}{\sqrt{2\pi} a^2 \eta} \exp\{-(l/a^{2/3} - \theta)^2/2\eta^2\}, \\
&= \frac{N_a \sqrt{\pi} l^{3/2}}{2^{3/2} a^2 \eta} \exp\{-(l/a^{2/3} - \theta)^2/2\eta^2\}, \\
&= \frac{1}{l^{3/2}} \frac{N_a \sqrt{\pi}}{2^{3/2} \eta} (a/l^{3/2})^{-2} \\
&\quad \times \exp\{-((a/l^{3/2})^{-2/3} - \theta)^2/2\eta^2\}.
\end{aligned}
\tag{3.18}
$$

In rearranging the expression of $P(a\,|\,l)$, we have made clear that its form matches that of equation (3.5).

A closed form expression for the normalization factor N_a may now be determined by employing the fact that $\int_{a=0}^{\infty} \mathrm{d}a P(a\,|\,l) = 1$.

$$
\begin{aligned}
1 &= \int_{a=0}^{\infty} \mathrm{d}a P(a\,|\,l), \\
&= \int_{a=0}^{\infty} \frac{\mathrm{d}a}{l^{3/2}} \frac{N_a \sqrt{\pi}}{2^{3/2} \eta} (a/l^{3/2})^{-2} \\
&\quad \times \exp\{-((a/l^{3/2})^{-2/3} - \theta)^2/2\eta^2\}, \\
&= \frac{N_a \sqrt{3\pi}}{2^{5/2} \eta} \int_{u=0}^{\infty} \mathrm{d}u u^{1/2} \exp\{-(u - \theta)^2/2\eta^2\},
\end{aligned}
\tag{3.19}
$$

where we have used the substitution $a/l^{3/2} = u^{-3/2}$ and hence also $l^{-3/2}\,\mathrm{d}a = (-3/2)u^{-5/2}\,\mathrm{d}u$. We therefore have

$$
N_a = \frac{2^{5/2} \eta}{\sqrt{3\pi}} \left[\int_{u=0}^{\infty} \mathrm{d}u u^{1/2} \exp\{-(u - \theta)^2/2\eta^2\} \right]^{-1}.
\tag{3.20}
$$

We may thus write down all of the scaling functions F_l, F_a, F and G for the Scheidegger model:

$$
\begin{aligned}
F_l(z) &= \frac{1}{\sqrt{2\pi}\eta} \exp\{-(z - \theta)^2/2\eta^2\}, &\tag{3.21} \\
F_a(z) &= \frac{N_a \sqrt{\pi}}{2^{3/2} \eta} z^{-2} \exp\{-(z^{-2/3} - \theta)^2/2\eta^2\}, &\tag{3.22} \\
F(z) &= \frac{N_a}{\sqrt{2\pi}\eta} \exp\{-(z - \theta)^2/2\eta^2\}, \text{ and} &\tag{3.23} \\
G(z) &= \frac{2N_a}{\sqrt{\pi}2^{3/2}\eta} z^{-2} \exp\{-(z^{-2/3} - \theta)^2/2\eta^2\}. &\tag{3.24}
\end{aligned}
$$

   Recall that all of these forms rest on the assumption that $F_l(z)$ is a Gaussian. In order to check this assumption, we return to Figure 3.3. The empirical distribution $P(z = a/l^{3/2})$ is shown on the left marked with circles. The solid line through these points is $F_a(z)$ as given above in equation (3.21). There is an excellent match so we may be confident about our proposed form for $F_a(z)$. We note that the function $F_a(z)$ may be thought of as a fractional inverse Gaussian distribution, the inverse Gaussian being a well known distribution arising in the study of first passage times for random walks [39]. It is worth contemplating the peculiar form of $P(a \,|\, l)$ in terms of first return random walks. Here, we have been able to postulate the functional form of the distribution of areas bound by random walks that first return after n steps. If one could understand the origin of the Gaussian and find analytic expressions for θ and η, then the problem would be fully solved.

3.6   Area-length distribution extended to real networks

We now seek to extend these results for Scheidegger's model to real world networks. We will look for the same functional forms for the Hack distributions that we have found above. The conditional probability distributions pertaining to Hack's law take on the forms

$$P(l \,|\, a) = 1/a^{-h} F_l(la^{-h}) = \frac{a^{-h}}{\sqrt{2\pi}\eta} \exp\{-(la^{-h} - \theta)^2/2\eta^2\}, \qquad (3.25)$$

and

$$P(a \,|\, l) = l^{-1/h} F_a(al^{-1/h}) = l^{-1/h} \frac{N_a}{\sqrt{2\pi}N_l \eta}(al^{-1/h})^{-2} \exp\{-((al^{-1/h})^{-h} - \theta)^2/2\eta^2\},$$
$$(3.26)$$

and the full Hack distribution is given by

$$\begin{aligned} P(a,l) &= a^2 F(la^{-h}) = l^{-2/h} G(al^{-1/h}) \\ &= \frac{N_a}{\sqrt{2\pi}\eta a^2} \exp\{-(la^{-h} - \theta)^2/2\eta^2\}. \qquad (3.27) \end{aligned}$$

with N_a determined by equation (3.20). The three parameters h, the Hack exponent, θ, the Hack mean coefficient, and η, the Hack standard deviation
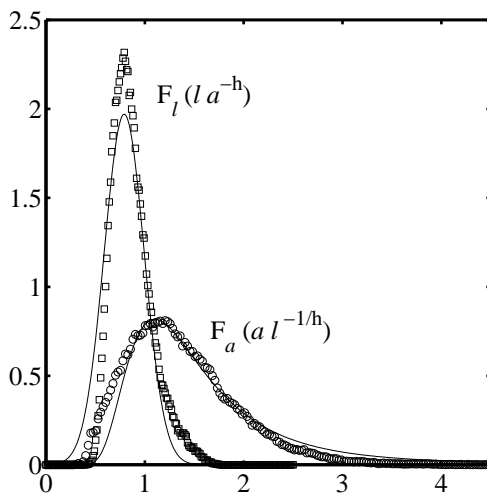
Figure 3.4: Cross-sectional scaling functions of the Hack distribution for the Mississippi. The estimates used for Hack's exponent are $h = 0.55$ and $h = 0.50$ respectively, the determination of which is discussed in section 3.7. The fits indicated by the smooth curves to the data are made as per the Scheidegger model in Figure 3.3 and according to equations (3.25) and (3.25). The values of the Hack mean coefficient and standard deviation coefficient are estimated to be $\theta \simeq 0.80$ and $\eta \simeq 0.20$.

coefficient, are in principle landscape dependent. Furthermore, in η we have a basic measure of fluctuations in the morphology of basins.

Figures 3.4 and 3.5 present Hack scaling functions for the Mississippi and Nile river basins. These Figures is to be compared with the results for the Scheidegger model in Figure 3.3.

For both rivers, Hack's exponent h was determined first from a stream ordering analysis (we discuss stream ordering later in Section 3.10). Estimates of the parameters θ and η were then made using the scaling function F_l presuming a Gaussian form.

We observe the Gaussian fit for the Mississippi is more satisfactory than that for the Nile. These fits are not rigorously made because even though we have chosen data ranges where deviations (which we address in the following section) are minimal, deviations from scaling do still skew the distributions. The specific ranges used to obtain F_l and F_a respectively are for the Mississippi: $8.5 < \log_{10} a < 9.5$ and $4.75 < \log_{10} l < 6$, and for the Nile: $9 < \log_{10} a < 11$ and $5.5 < \log_{10} l < 6$ (areas are in km^2 and lengths km).
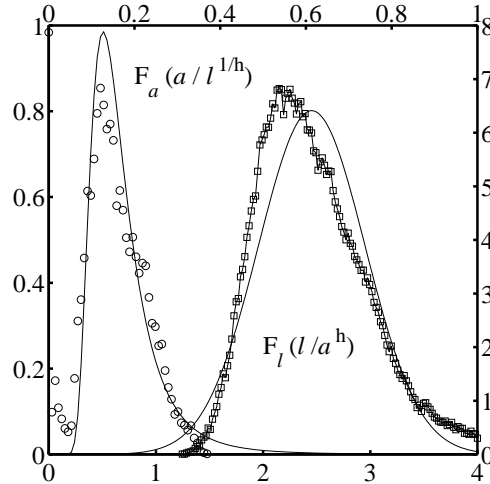
Figure 3.5: Cross-sectional scaling functions of the Hack distribution for the Nile. The top and right axes correspond to F_a and the bottom and left to F_l. The Hack exponent used is $h = 0.50$ and the values of the Hack mean coefficient and standard deviation coefficient are estimate to be $\theta \simeq 2.45$ and $\eta \simeq 0.50$. The data for the Nile and Congo was obtained from the United States Geological Survey's 30-arc-second Hydro1K dataset which may be accessed on Internet at `edcftp.cr.usgs.gov`. Note that these Hydro1K datasets have undergone the extra processing of projection onto a uniform grid.

Furthermore, we observe that the estimate of h has an effect in the resulting forms of F_l and F_a. Nevertheless, here we are attempting to capture the essence of the generalized form of Hack's law in real networks.

We then use the parameters h, θ and η and equation (3.26) to construct our theoretical F_a, the smooth curves in Figures 3.4 and 3.5. As for the Scheidegger model data in Figure 3.3, we see in both examples approximate agreement between the measured F_a and the one predicted from the form of F_l. Table 3.1 shows estimates of h, θ and η for the five major river basins studied.

Given our reservations about the precision of these values of θ and η, we are nevertheless able to make qualitative distinctions. Recalling that $\langle l \rangle = \theta a^h$, we see that, for fixed h, higher values of θ indicate relatively longer stream lengths for a given area and hence longer and thinner basins. The results therefore suggest the Nile, and to a lesser degree the Amazon, have basins with thinner profiles than the Congo and, in particular, the Mis-

River network	θ	η	h
Mississippi	0.80	0.20	0.55
Amazon	1.90	0.35	0.52
Nile	2.45	0.50	0.50
Kansas	0.70	0.15	0.57
Congo	0.89	0.18	0.54

Table 3.1: Estimates of Hack distribution parameters for real river networks. The scaling exponent h is Hack's exponent. The parameters θ and η are coefficients of the mean and standard deviation of the conditional probability density function $P(l\,|\,a)$ and are fully discussed in the text. The dataset used for the Amazon has a horizontal resolution of approximately 1000 meters and comes from 30 arc second terrain data provided by the National Imagery and Mapping Agency available on the Internet at `www.nima.mil`.

sissippi and Kansas. This seems not unreasonable since the Nile is a strongly directed network constrained within a relatively narrow overall shape. This is somewhat in spite of the fact that the shape of an overall river basin is not necessarily related to its internal basin morphology, an observation we will address later in Section 3.10.

The importance of θ is tempered by the value of h. Hack's exponent affects not only the absolute measure of stream length for a given area but also how basin shapes change with increasing area. So, in the case of the Kansas the higher value of h suggests basin profiles thin with increasing size. This is in keeping with overall directedness of the network. Note that our measurements of the fractal dimension d of stream lengths for the Kansas place it to be $d = 1.04 \pm 0.02$. Therefore, $d/h \simeq 1.9 < 2$ and elongation is still expected when we factor in the scaling of l with $L_\parallel$.

The Nile and Amazon also all have relatively high η indicating greater fluctuations in basin shape. In comparison, the Mississippi, Kansas and Congo appear to have less variation. Note that the variability of the Kansas is in reasonable agreement with that of the whole Mississippi river network for which it is a sub-basin.

Finally, regardless of the actual form of the distribution underlying Hack's law, fluctuations are always present and an estimate of their extent is an important measurement. Thus, the Hack mean and standard deviation coefficients, θ and η, are suggested to be of sufficient worth so as to be included with any measurement of the Hack exponent h.
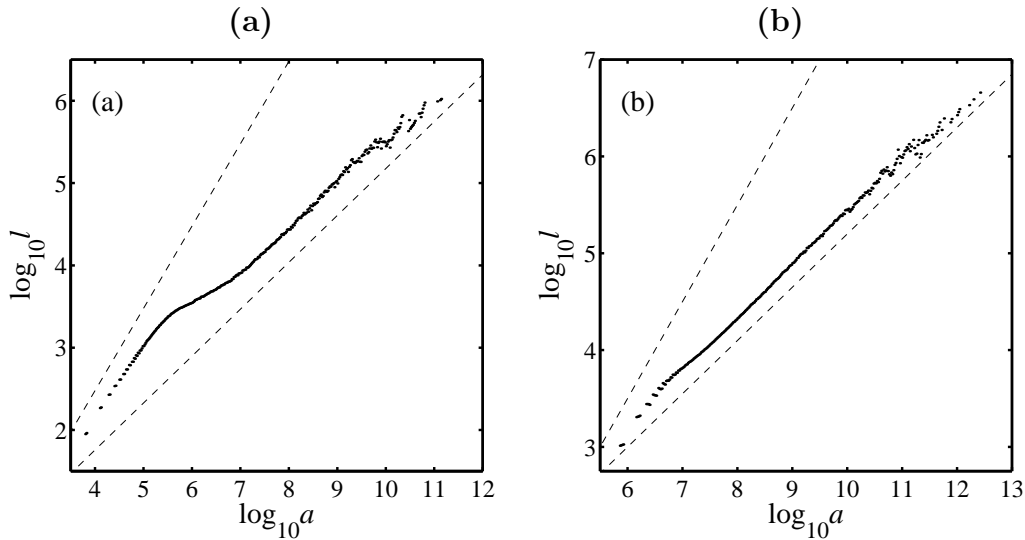
Figure 3.6: The mean version of Hack's law for the Kansas, (a), and the Mississippi, (b). The units of lengths and areas are meters and square meters. These are calculated from the full Hack distributions shown in Figures 3.1(a) and 3.1(b) by finding $\langle l \rangle$ for each value of basin area a. Area samples are taken every 0.02 orders of magnitude in logarithmic space. The upper dashed lines represent a slope of unity in both plots and the lower lines the Hack exponents 0.57 and 0.55 for the Kansas and Mississippi respectively. For the Kansas, there is a clear deviation for small area which rolls over into a region of very slowly changing derivative before breaking up at large scales. Deviations from scaling are present for the lower resolution dataset of the Mississippi but to a lesser extent.

3.7   Deviations from scaling

In generalizing Hack's law, we have sought out regions of robust scaling, discarding ranges where deviations become prominent. We now bring our attention to the nature of the deviations themselves.

We observe three major classes of deviations which we will define by the scales at which they occur: small, intermediate and large. Throughout the following sections we primarily consider deviations from the mean version of Hack's law, $\langle l \rangle = \theta a^h$, given in equation (3.4). Much of the understanding we gain from this will be extendable to deviations for higher moments.

To provide an overview of what follows, examples of mean-Hack distributions for the Kansas river and the Mississippi are shown in Figures 3.6(a)
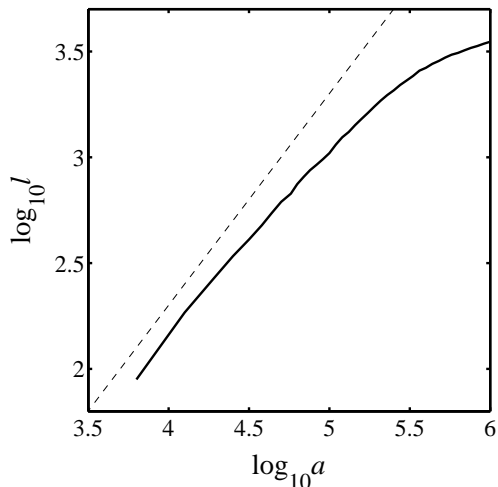
Figure 3.7: The linearity of Hack's law at small scales for the Kansas river. The linear regime enters a crossover region after almost 1.5 orders of magnitude in area. This is an expanded detail of the mean Hack's law given in Figure 3.6(a) and areas and lengths are in square meters and meters.

and 3.6(b). Hack's law for the Kansas river exhibits a marked deviation for small areas, starting with a near linear relationship between stream length and area. A long crossover region of several orders of magnitude in area then leads to an intermediate scaling regime wherein we attempt to determine the Hack exponent h. In doing so, we show that such regions of robust scaling are surprisingly limited for river network quantities. Moreover, we observe that, where present, scaling is only approximate and that no exact exponents can be ascribed to the networks we study here. It follows that the identification of universality classes based on empirical evidence is a hazardous step.

Finally, the approximate scaling of this intermediate region then gives way to a break down in scaling at larger scales due to low sampling and correlations with basin shape. The same deviations are present in the relatively coarse-grained Mississippi data but are less pronounced.

3.8   Deviations at small scales

At small scales, we find the mean-Hack distribution to follow a linear relationship, i.e., $l \propto a^1$. This feature is most evident for the Kansas river as
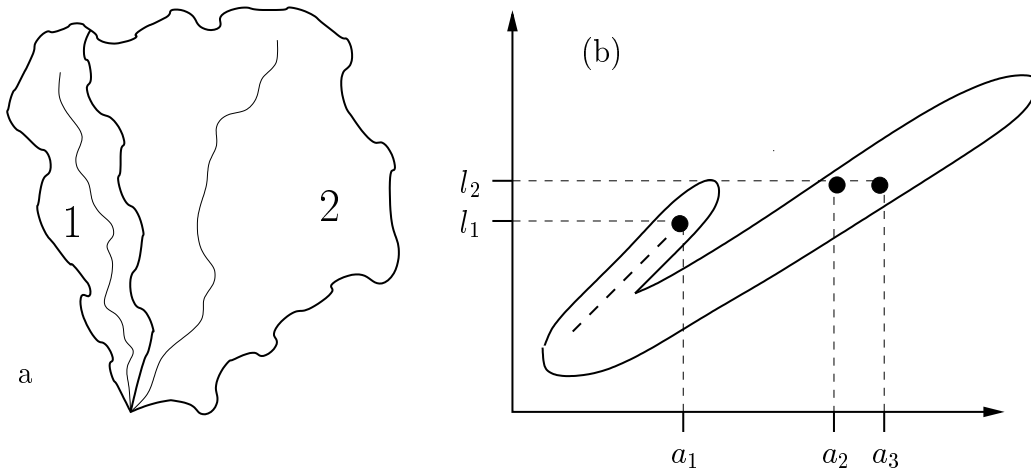
Figure 3.8: Origin of the linear branch in the Hack distribution. The sub-basins labeled 1 and 2 depicted on the left have areas a_1 and a_2 and lengths l_1 and l_2. These sub-basins combine to form a basin of area $a_3 = a_1 + a_2$ and main stream length $l_3 = \max l_1, l_2 = l_2$. Since sub-basin 1 is a linear sub-network (a valley) the pair (a_1, l_1) lie along the linear branch of the Hack distribution as shown on the right. Points along the main stream of sub-basin 1 lie along the dashed line leading to the coordinate (a_1, l_1). On combining with the second basin, the jump in the resultant area creates a jump from $(a_1, l_1$ to (a_3, l_2) in the main body of the Hack distribution.

shown in Figure 3.6(a) and in more detail in Figure 3.7. The linear regime persists for nearly 1.5 orders of magnitude in basin area. To a lesser extent, the same trend is apparent in the Mississippi data, Figure 3.6(b).

Returning to the full Hack distribution of Figures 3.1(a) and 3.1(b), we begin to see the origin of this linear regime. In both instances, a linear branch separates from the body of the main distribution. Since l cannot grow faster than a^1, the linear branch marks an upper bound on the extent of the distribution in (a, l) coordinates. When averaged to give the mean-Hack distribution, this linear data dominates the result for small scales.

We find this branch evident in all Hack distributions. It is not an artifact of resolution and in fact becomes more pronounced with increased map precision. The origin of this linear branch is simple: data points along the branch correspond to positions in narrow sub-networks, i.e., long, thin "valleys." To understand the separation of this linear branch from the main body of the distribution, consider Figure 3.8 which depicts a stream draining such a

valley with length and area (l_1, a_1) that meets a stream from a basin with characteristics (l_2, a_2). The area and length of the basin formed at this junction is thus $(a_3, l_3) = (a_1 + a_2, \max(l_1, l_2))$ (in the Figure, $\max(l_1, l_2) = l_2$). The greater jump in area moves the point across into the main body of the Hack distribution, creating the separation of the linear branch.

In fact, the full Hack distribution is itself comprised of many such linear segments. As in the above example, until a stream does not meet any streams of comparable size, then its area and length will roughly increase in linear fashion. When it does meet such a stream, there is a jump in area and the trace of a new linear segment is started in the distribution. We will see this most clearly later on when we study deviations at large scales.

For very fine scale maps, on the order of meters, we might expect to pick up the scale of the unchannelized, convex regions of a landscape, i.e., "hillslopes" [28]. This length scale represents the typical separation of branches at a network's finest scale. The computation of stream networks for these hillslope regions would result in largely non-convergent (divergent or parallel) flow. Therefore, we would have linear "basins" that would in theory contribute to the linear branch we observe [35]. Potentially, the crossover in Hack's law could be used as a determinant of hillslope scale, a crucial parameter in geomorphology [28, 29]. However, when long, thin network structures are present in a network, this hillslope scale is masked by their contribution.

Whether because of the hillslope scale or linear network structure, we see that at small scales, Hack's law will show a crossover in scaling from $h = 1$ to a lower exponent. The crossover's position depends on the extent of linear basins in the network. For example, in the Kansas River basin, the crossover occurs when $(l, a) = (4 \times 10^3 \text{m}, 10^7 \text{m}^2)$. Since increased map resolution can only increase measures of length, the crossover's position must occur at least at such a length scale which may be many orders of magnitude greater than the scale of the map.

However, the measurement of the area of such linear basins will potentially grow with coarse-graining. Note that for the Mississippi mean-Hack distribution, the crossover begins around $a = 10^{6.5}$ m^2 whereas for the Kansas, the crossover initiates near $a = 10^{5.5}$ m^2 but the ends of the crossovers in both cases appear to agree, occurring at around $a = 10^7$ m^2. Continued coarse-graining will of course eventually destroy all statistics and introduce spurious deviations. Nevertheless, we see here that the deviation which would only be suggested in the Mississippi data is well confirmed in the finer-grain Kansas data.
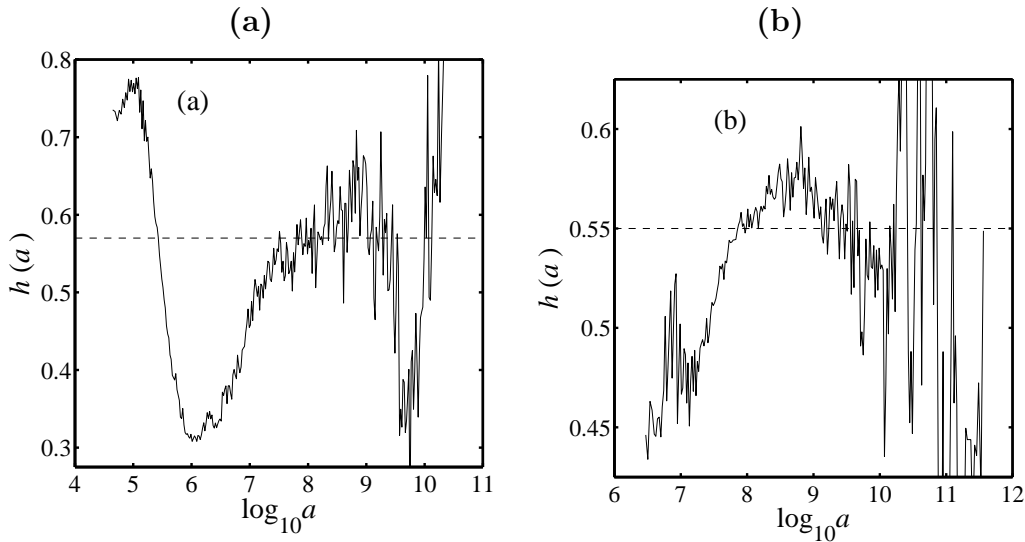
Figure 3.9: Variation in Hack's exponent for the Kansas, (a), and the Mississippi, (b). The area a is in m^2. The plots are derivatives of the mean-Hack distributions given in Figures 3.6(a) and 3.6(b). Both derivatives have been smoothed by taking running averages over 0.64 orders of magnitude in a. For the Kansas, the dashed line is set at $h = 0.57$, Hack's exponent estimated via simple regression analysis for points with $10^7 < a < 10^{10}$ m^2. The local exponent is seen to gradually rise through the $h = 0.57$ level indicating scaling is not robust. For the Mississippi in (b), the dashed line is a Hack exponent of 0.55 calculated from regression on data in the interval $10^9 < a < 10^{11.5}$ m^2. The local Hack exponent is seen to gradually rise and fall about this value.

3.9   Deviations at intermediate scales

As basin area increases, we move out of the linear regime, observing a crossover to what would be considered the normal scaling region of Hack's law. We detail our attempts to measure the Hack exponents for the Kansas and Mississippi examples. Rather than relying solely on a single regression on a mean-Hack distribution, we employ a more precise technique that examines the distribution's derivative. As we will show, we will not be able to find a definite value for the Hack exponent in either case, an important result in our efforts to determine whether or not river networks belong to specific universality classes.

To determine h, we consider Hack's law (equation (3.4)) explicitly in

logarithmic coordinates,

$$\log_{10} \langle l(a) \rangle = \log_{10} \theta + h \log_{10} a. \tag{3.28}$$

The derivative of this equation with respect to $\log_{10} a$ then gives Hack's exponent as a function of area,

$$h(a) = \frac{\mathrm{d}}{\mathrm{d} \log_{10} a} \log_{10} \langle l(a) \rangle. \tag{3.29}$$

We may think of $h(a)$ as a "local Hack exponent." Note that non-constant trends in $h(a)$ indicate scaling does not hold. We calculate the discrete derivative as above for the Kansas and Mississippi. We smooth the data by taking running averages with varying window sizes of n samples, the results for $n = 32$ being shown in Figures 3.9(a) and 3.9(b) where the spacing of $\log a$ is 0.02 orders of magnitude. Thus, the running averages for the figures are taken over corresponding area ranges 0.64 orders of magnitude.

Now, if the scaling law in question is truly a scaling law, the above type of derivative will fluctuate around a constant value of exponent over several orders of magnitude. With increasing n, these fluctuations will necessarily decrease and we should see the derivative holding steady around the exponent's value.

At first glance, we notice considerable variation in $h(a)$ for both data sets with the Kansas standing out. Fluctuations are reduced with increasing n but we observe continuous variation of the local Hack exponent with area. For the example of the Kansas, the linear regime and ensuing crossover appear as a steep rise followed by a drop and then another rise during all of which the local Hack exponent moves well below $1/2$.

It is after these small scale fluctuations that we would expect to find Hack's exponent. For the Kansas river data, we see the derivative gradually climbs for all values of n before reaching the end of the intermediate regime where the putative scaling breaks down altogether.

For the Kansas show in Figure 3.9(a), the dashed line represents $h = 0.57$, our estimate of Hack's exponent from simple regression on the mean-Hack distribution of Figure 3.6(a). For the regression calculation, the intermediate region was identified from the figure to be $10^7 < a < 10^{10}$ m^2. We see from the smoothed derivative in Figure 3.9(a) that the value $h = 0.57$ is not precise. After the crossover from the linear region has been completed, we observe a slow rise from $h \simeq 0.54$ to $h \simeq 0.63$. Thus, the local Hack exponent $h(a)$ gradually climbs above $h = 0.57$ rather than fluctuate around it.

A similar slow change in $h(a)$ is observed for the Mississippi data. We see in Figure 3.9(b) a gradual rise and then fall in $h(a)$. The dashed line here represents $h = 0.55$, the value of which was determined from Figure 3.6(b) using regression on the range $10^9 < a < 10^{11.5}$ m^2. The range of $h(a)$ is roughly $[0.52, 0.58]$. Again, while $h = 0.55$ approximates the derivative throughout this intermediate range of Hack's law, we cannot claim it to be a precise value.

We observe the same drifts in $h(a)$ in other datasets and for varying window size n of the running average. The results suggest that we cannot assign specific Hack exponents to these river networks and are therefore unable to even consider what might be an appropriate universality class. The value of h obtained by regression analysis is clearly sensitive to the the range of a used. Furthermore, these results indicate that we should maintain healthy reservations about the exact values of other reported exponents.

3.10   Deviations at large scales

We turn now to deviations from Hack's law at large scales. As we move beyond the intermediate region of approximate scaling, fluctuations in $h(a)$ begin to grow rapidly. This is clear on inspection of the derivatives of Hack's law in Figures 3.9(a) and 3.9(b). There are two main factors conspiring to drive these fluctuations up. The first is that the number of samples of sub-basins with area a decays algebraically in a. This is just the observation that $P(a) \propto a^{-\tau}$ as per equation (3.11). The second factor is that fluctuations in l and a are on the order of the parameters themselves. This follows from our generalization of Hack's law which shows, for example, that the moments $\langle l^q \rangle$ of $P(l \mid a)$ grow like a^{qh}. Thus, the standard deviation grows like the mean: $\sigma(l) = (\langle l^2 \rangle - \langle l \rangle^2)^{1/2} \propto a^h \propto \langle l \rangle$.

3.10.1   Stream ordering and Horton's laws

So as to understand these large scale deviations from Hack's law, we need to examine network structure in depth. One way to do this is by using Horton-Strahler stream ordering [58, 128] and a generalization of the well-known Horton's laws [31, 33, 58, 101, 116]. This will naturally allow us to deal with the discrete nature of a network that is most apparent at large scales.

Stream ordering discretizes a network into a set of stream segments (or, equivalently, a set of nested basins) by an iterative pruning. Source streams

(i.e., those without tributaries) are designated as stream segments of order $\omega = 1$. These are removed from the network and the new source streams are then labelled as order $\omega = 2$ stream segments. The process is repeated until a single stream segment of order $\omega = \Omega$ is left and the basin itself is defined to be of order Ω.

Natural metrics for an ordered river network are n_ω, the number of order ω stream segments (or basins), $\bar{a}_\omega$, the average area of order ω basins, $\bar{l}_\omega$, the average main stream length of order ω basins, and $\bar{l}_\omega^{(\mathrm{s})}$, the average length of order ω stream segments. Horton's laws state that these quantities change regularly from order to order, i.e.,

$$\frac{n_\omega}{n_{\omega+1}} = R_n \quad \text{and} \quad \frac{\bar{X}_{\omega+1}}{\bar{X}_\omega} = R_X, \tag{3.30}$$

where $X = a$, l or $l^{(\mathrm{s})}$. Note that all ratios are defined to be greater than unity since areas and lengths increase but number decreases. Also, there are only two independent ratios since $R_a \equiv R_n$ and $R_l \equiv R_{l^{(\mathrm{s})}}$ [31]. Horton's laws mean that stream-order quantities change exponentially with order. For example, (3.30) gives that $l_\omega \propto (R_l)^\omega$.

3.10.2 Discrete version of Hack's law

Returning to Hack's law, we examine its large scale fluctuations with the help of stream ordering. We are interested in the size of these fluctuations and also how they might correlate with the overall shape of a basin. First, we note that the structure of the network at large scales is explicitly discrete. Figure 3.10 demonstrates this by plotting the distribution of (a, l) without the usual logarithmic transformation. Hack's law is seen to be composed of linear fragments. As explained above in Figure 3.8, areas and length increase in proportion to each other along streams where no major tributaries enter. As soon as a stream does combine with a comparable one, a jump in drainage area occurs. Thus, we see in Figure 3.10 isolated linear segments which upon ending at a point (a_1, l_1) begin again at $(a_1 + a_2, l_1)$, i.e., the main stream length stays the same but the area is shifted.

We consider a stream ordering version of Hack's law given by the points $(\bar{a}_\omega, \bar{l}_\omega)$. The scaling of these data points is equivalent to scaling in the usual Hack's law. Also, given Horton's laws, it follows that $h = \ln R_l / \ln R_n$ (using $R_a \equiv R_n$). Along the lines of the derivative we introduced to study intermediate scale fluctuations in equation (3.29), we have here an order-
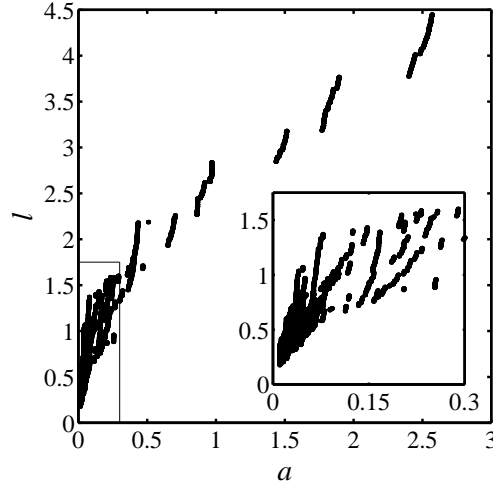
Figure 3.10: Hack distribution for the Mississippi plotted in linear space. The area units a is 10^{12} m^2 and length l is 10^6 m. The discreteness of the basin structure is clearly indicated by the isolated, linear fragments. The inset is a blow-up of the box on the main graph.

based difference:

$$h_{\omega,\omega-1} = \frac{\log \bar{l}_\omega/\bar{l}_{\omega-1}}{\log \bar{a}_\omega/\bar{a}_{\omega-1}}. \tag{3.31}$$

We can further extend this definition to differences between non-adjacent orders:

$$h_{\omega,\omega'} = \frac{\log \bar{l}_\omega/\bar{l}_{\omega'}}{\log \bar{a}_\omega/\bar{a}_{\omega'}}. \tag{3.32}$$

This type of difference, where $\omega' < \omega$, may be best thought of as a measure of trends rather than an approximate discrete derivative.

Using these discrete differences, we examine two features of the order-based versions of Hack's law. First we consider correlations between large scale deviations within an individual basin and second, correlations between overall deviations and basin shape. For the latter, we will also consider deviations as they move back into the intermediate scale. This will help to explain the gradual deviations from scaling we have observed at intermediate scales.

Since deviations at large scales are reflective of only a few basins, we require an ensemble of basins to provide sufficient statistics. As an example of such an ensemble, we take the set of order $\Omega = 7$ basins of the Mississippi basin. For the dataset used here where the overall basin itself is of order $\Omega = 11$, we have 104 order $\Omega = 7$ sub-basins. The Horton averages for these basins are $\bar{a}_7 \simeq 16600$ km^2, $\bar{l}_7 \simeq 350$ km, and $\bar{L}_7 \simeq 210$ km.
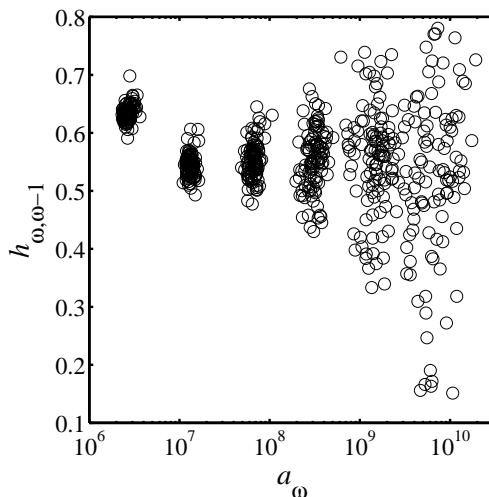
Figure 3.11: Differences of the stream order-based version of Hack's law for 104 order $\Omega = 7$ basins of the Mississippi (compare the continous versions given in Figure 3.9) The plots are overlaid to give a sense of the increase in fluctuations of the local Hack exponent $h_{\omega,\omega-1}$ with increasing order ω. The clusters correspond to $\omega = 1, 2, \dots, 7$, moving across from left to right.

For each basin, we first calculate the Horton averages $(\bar{a}_\omega, \bar{l}_\omega)$. We then compute $h_{\omega,\omega-1}$, the Hack difference given in equation (3.31). To give a rough picture of what is observed, Figure 3.11 shows a scatter plot of $h_{\omega,\omega-1}$ for all order $\Omega = 7$ basins. Note the increase in fluctuations with increasing ω. This increase is qualitatively consistent with the smooth versions found in the single basin examples of Figures 3.9(a) and 3.9(b). In part, less self-averaging for larger ω results in a greater spread in this discrete derivative. However, as we will show, these fluctuations are also correlated with fluctuations in basin shape.

3.10.3   Effect of basin shape on Hack's law

In what follows, we extract two statistical measures of correlations between deviations in Hack's law and overall basin shape. These are r, the standard linear correlation coefficient and r_s, the Spearman rank-order correlation coefficient [81, 104, 123]. For N observations of data pairs (u_i, v_i), r is defined to be

$$r = \frac{\sum_{i=1}^{N}(u_i - \mu_u)(v_i - \mu_v)}{\sum_{i=1}^{N}(x_i - \mu_u)^2 \sum_{i=1}^{N}(y_i - \mu_v)^2} = \frac{C(u,v)}{\sigma_u \sigma_v}, \tag{3.33}$$

where $C(u,v)$ is the covariance of the u_i's and v_i's, μ_u and μ_v their means, and σ_u and σ_v their standard deviations. The value of Spearman's r_s is determined in the same way but for the u_i and v_i replaced by their ranks. From r_s, we determine a two-sided significance p_s via Student's t-distribution [104].

We define κ, a measure of basin aspect ratio, as

$$\kappa = L^2/a. \tag{3.34}$$

Long and narrow basins correspond to $\kappa \gg 1$ while for short and wide basins, we have $\kappa \ll 1$

We now examine the discrete derivatives of Hack's law in more detail. In order to discern correlations between large scale fluctuations within individual basins, we specifically look at the last two differences in a basin: $h_{\Omega,\Omega-1}$ and $h_{\Omega-1,\Omega-2}$. For each of the Mississippi's 104 order $\Omega = 7$ basins, these values are plotted against each other in Figure 3.12. Both our correlation measurements strongly suggest these differences are uncorrelated. The linear correlation coefficient is $r = -0.06 \simeq 0$ and, similarly, we have $r_s = -0.08 \simeq 0$. The significance $p_s = 0.43$ implies that the null hypothesis of uncorrelated data cannot be rejected.

Thus, for Hack's law in an individual basin, large scale fluctuations are seen to be uncorrelated. However, correlations between these fluctuations and other factors may still exist. This leads us to our second test which concerns the relationship between trends in Hack's law and overall basin shape.

Figure 3.13 shows a comparison of the aspect ratio κ and $h_{7,5}$ for the order $\Omega = 7$ basins of the Mississippi. The measured correlation coefficients are $r = 0.50$ and $r_s = 0.53$, giving a significance of $p_s < 10^{-8}$. Furthermore, we find the differences $h_{7,6}$ ($r = 0.34$, $r_s = 0.39$ and $p_s < 10^{-4}$) and $h_{6,5}$ ($r = 0.35$, $r_s = 0.34$ and $p_s < 10^{-3}$) are individually correlated with basin
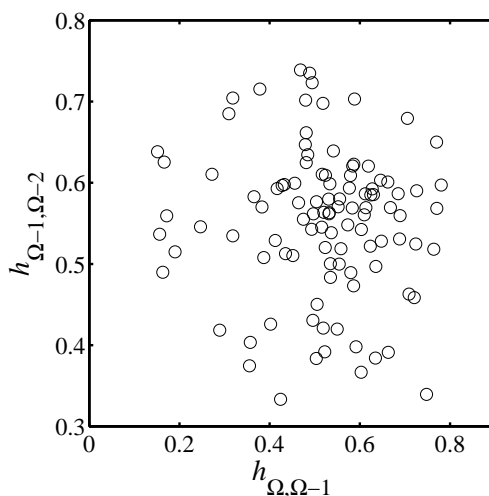
Figure 3.12: A comparison of the stream order Hack derivatives $h_{\Omega,\Omega-1}$ and $h_{\Omega-1,\Omega-2}$ for each of the 104 order $\Omega = 7$ basins of the Mississippi. The linear correlation coefficient is $r = -0.06$ and the Spearman correlation coefficient is $r_s = -0.08$. The latter has probability $p_s = 0.43$ indicating there are no significant correlations.

shape. We observe this correlation between basin shape and trends in Hack's law at large scales, namely $h_{\Omega,\Omega-1}$, $h_{\Omega-1,\Omega-2}$ and $h_{\Omega,\Omega-2}$, repeatedly in our other data sets. In some cases, correlations extend further to $h_{\Omega-2,\Omega-3}$.

Since the area ratio R_a is typically in the range 4–5, Hack's law is affected by boundary conditions set by the geometry of the overall basin down to sub-basins one to two orders of magnitude smaller in area than the overall basin. These deviations are present regardless of the absolute size of the overall basin. Furthermore, the origin of the basin boundaries being geologic or chance or both is irrelevant—large scale deviations will still occur. However, it is reasonable to suggest that particularly strong deviations are more likely the result of geologic structure rather than simple fluctuations.

3.11   Conclusion

Hack's law is a central relation in the study of river networks and branching networks in general. We have shown Hack's law to have a more complicated structure than is typically given attention. The starting generalization is to
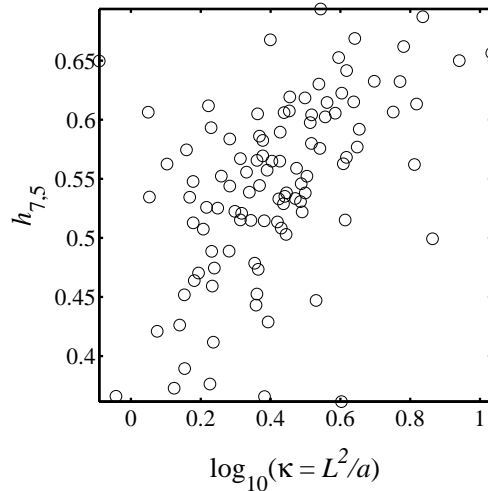
Figure 3.13: Correlation between trends in Hack's law and the aspect ratio of a basin as estimated by $\kappa = L^2/a$. The data is for the order $\Omega = 7$ basins of the Mississippi and the specific trend is $h_{7,5}$. The correlation measurements give $r = 0.50$, $r_s = 0.53$ and $p_s < 10^{-8}$.

consider fluctuations around scaling. Using the directed, random network model, a form for the Hack distribution underlying Hack's law may be postulated and reasonable agreement with real networks is observed. Questions of the validity of the distribution aside, the Hack mean coefficient θ and the Hack standard deviation coefficient η should be standard measurements because they provide further points of comparison between theory and other basins.

With the idealized Hack distribution proposed, we may begin to understand deviations from its form. As with any scaling law pertaining to a physical system, cutoffs in scaling must exist and need to be understood. For small scales, we have identified the presence of linear sub-basins as the source of an initial linear relation between area and stream length. At large scales, statistical fluctuations and geologic boundaries give rise to basins whose overall shape produces deviations in Hack's laws. Both deviations extend over a considerable range of areas as do the crossovers which link them to the region of intermediate scales, particularly the crossover from small scales.

Finally, by focusing in detail on a few large-scale examples networks, we have found evidence that river networks do not belong to well defined

universality classes. The relationship between basin area and stream length may be approximately, and in some cases very well, described by scaling laws but not exactly so. The gradual drift in exponents we observe suggests a more complicated picture, one where subtle correlations between basin shape and geologic features are intrinsic to river network structure.

Acknowledgements

Fluctuations in the size and number of network components

Abstract. The structure of a river network may be seen as a discrete set of nested sub-networks built out of individual stream segments. These network components are assigned an integral stream order via a hierarchical and discrete ordering method. Exponential relationships, known as Horton's laws, between stream order and ensemble-averaged quantities pertaining to network components are observed. We extend these observations to incorporate fluctuations and all higher moments by developing functional relationships between distributions. The relationships determined are drawn from a combination of theoretical analysis, analysis of real river networks including the Mississippi, Amazon and Nile, and numerical simulations on a model of directed, random networks. Underlying distributions of stream segment lengths are identified as exponential. Combinations of these distributions form single-humped distributions with exponential tails, the sums of which are in turn shown to give power law distributions of stream lengths. Distributions of basin area and stream segment frequency are also addressed. The calculations identify a single length-scale as a measure of size fluctuations in network components. This article is the second in a series of three addressing the geometry of river networks.

4.1   Introduction

Branching networks are an important category of all networks with river networks being a paradigmatic example. Probably as much as any other

natural phenomena, river networks are a rich source of scaling laws [35, 108, 110]. Central quantities such as drainage basin area and stream lengths are reported to closely obey power-law statistics [1, 31, 35, 54, 78, 87, 108, 110]. The origin of this scaling has been attributed to a variety of mechanisms including, among others: principles of optimality [110, 130], self-organized criticality [109], invasion percolation [124], and random fluctuations [35, 82, 84, 112]. One of the difficulties in establishing any theory is that the reported values of scaling exponents show some variation [1, 86, 87].

With this variation in mind, we have in [32] extensively examined Hack's law, the scaling relationship between basin shape and stream length. Such scaling laws are inherently broad-brushed in their descriptive content. In an effort to further improve comparisons between theory and data and, more importantly, between networks themselves, we consider here a generalization of Horton's laws [58, 116]. Defined fully in the following section, Horton's laws describe how average values of network parameters change with a certain discrete renormalization of the network. The introduction of these laws by Horton may be seen as one of many examples that presaged the theory of fractal geometry [83]. In essence, they express the relative frequency and size of network components such as stream segments and drainage basins.

Here, we extend Horton's laws to functional relationships between probability distributions rather than simply average values. The recent work of Peckham and Gupta was the first to address this natural generalization of Horton's laws [101]. Our work agrees with their findings but goes further to characterize the distributions and develop theoretical links between the distributions of several different parameters. We also present empirical studies that reveal underlying scaling functions with a focus on fluctuations and further consider deviations due to finite-size effects.

We examine continent-scale networks: the Mississippi, Amazon, Congo, Nile and Kansas river basins. As in [32], we also examine Scheidegger's model of directed, random networks [112]. Both real and model networks provide important tests and motivations for our generalizations of Horton's laws.

We begin with definitions of stream ordering and Horton's laws. Thereafter, the paper is divided into two main sections. In Section 4.3, we first sketch the theoretical generalization of Horton's laws. Estimates of the Horton ratios are carried out in Section 4.4 and these provide basic parameters of the generalized laws. Empirical evidence from real continent-scale networks is then provided along with data from Scheidegger's random network model in Section 4.5. In Section 4.6 we derive the higher order moments for stream length distributions and in Section 4.7, we consider deviations from

Horton's laws for large basins. In the Appendix A.1, we expand on some of
the connections outlined in Section 4.5, presenting a number of mathematical
considerations on these generalized Horton distributions.

This paper is the second in a series of three on the geometry of river
networks. In the first [32] we address issues of scaling and universality and
provide further motivation for our general investigation. In the third article
of the series [34] we extend the work of the present paper by examining how
the detailed architecture of river networks, i.e., how network components fit
together.

4.2   Stream ordering and Horton's laws

Stream ordering was first introduced by Horton in an effort to quantify the
features of river networks [58]. The method was later improved by Strahler to
give the present technique of Horton-Strahler stream ordering [128]. Stream
ordering is a method applicable to any field where branching, hierarchical
networks are important. Indeed, much use of stream ordering has been made
outside of the context of river networks, a good example being the study of
venous and arterial blood networks in biology [2, 42, 69, 70, 71, 147, 156, 157].
We describe two conceptions of the method and then discuss empirical laws
defined with in the context of stream ordering.

A network's constituent stream segments are ordered by an iterative prun-
ing. An example of stream ordering for the Mississippi basin is shown in
Figure 4.1. A source stream is defined as a section of stream that runs from
a channel head to a junction with another stream (for an arboreal analogy,
think of the leaves of a tree). These source streams are classified as the first
order stream segments of the network. Next, remove these source streams
and identify the new source streams of the remaining network. These are
the second order stream segments. The process is repeated until one stream
segment is left of order Ω. The order of the network is then defined to be Ω.

Once stream ordering on a network has been done, a number of natural
quantities arise. These include n_ω, the number of basins (or equivalently
stream segments) for a given order ω; $\langle l_\omega \rangle$, the average main stream length;
$\langle l_\omega^{(s)} \rangle$, the average stream segment length; $\langle a_\omega \rangle$, the average basin area; and
the variation in these numbers from order to order. Horton [58] and later
Schumm [116] observed that the following ratios are generally independent
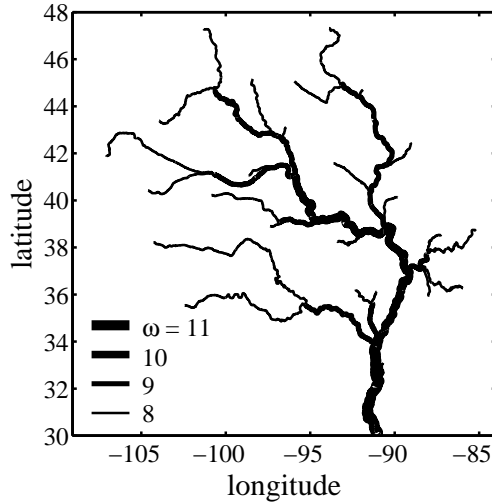
Figure 4.1: Stream segments for $\omega = 8$ up to $\omega = \Omega = 11$ for the Mississippi River. The spherical coordinates of latitude and longitude are used and the scale corresponds to roughly 2000 km along each axis.

of order ω:

$$\frac{n_\omega}{n_{\omega+1}} = R_n, \qquad \frac{\langle l \rangle_{\omega+1}}{\langle l \rangle_\omega} = R_l, \qquad \text{and} \qquad \frac{\langle a \rangle_{\omega+1}}{\langle a \rangle_\omega} = R_a. \qquad (4.1)$$

Since the main stream length averages $\bar{l}_\omega$ are combinations of stream segment lengths $\bar{l}_\omega = \sum_{\nu=1}^{\omega} \bar{l}_\omega^{(s)}$ we have that the Horton ratio for stream segment lengths $R_{l^{(s)}}$ is equivalent to R_l. Because our theory will start with the distributions of $l^{(s)}$, we will generally use the ratio $R_{l^{(s)}}$ in place of R_l.

Horton's laws have remained something of a mystery in geomorphology—the study of earth surface processes and form—due to their apparent robustness and hence perceived lack of physical (or geological) content. However, statements that Horton's laws are "statistically inevitable" [72], while possibly true, have not yet been based on reasonable assumptions [35]. Furthermore, many other scaling laws can be shown to follow in part from Horton's laws [31]. Thus, Horton's laws being without content would imply the same is true for those scaling laws that follow from them. Other sufficient assumptions include uniform drainage density (i.e., networks are space-filling) and self-affinity of single channels. The latter can be expressed as the rela-

tion [74, 87, 141, 143]

$$l \propto L_{\parallel}^{d}, \tag{4.2}$$

where $L_{\parallel}$ is the longitudinal diameter of a basin. Scaling relations may be derived and the set of relevant scaling exponents can be reduced to just two: d as given above and the ratio $\ln R_{l^{(s)}} / \ln R_n$ [31]. Note that one obtains $R_a \equiv R_n$ so that only the two Horton ratios R_n and $R_{l^{(s)}}$ are independent. Horton ratios are thus of central importance in the full theory of scaling for river networks.

4.3   Postulated form of Horton distributions

Horton's laws relate quantities which are indexed by a discrete set of numbers, namely the stream orders. They also algebraically relate mean quantities such as $\bar{a}_\omega$. Hence we may consider a generalization to functional relationships between probability distributions. In other words, for stream lengths and drainage areas we can explore the relationships between probability distributions defined for each order.

Furthermore, as we have noted, Horton's laws can be used to derive power laws of continuous variables such as the probability distributions of drainage area a and main stream length l [24, 31, 87]:

$$P(a) \propto a^{-\tau} \qquad \text{and} \qquad P(l) \propto l^{-\gamma}. \tag{4.3}$$

These derivations necessarily only give discrete points of power laws. In other words, the derivations give points as functions of the discrete stream order ω and are uniformly spaced logarithmically and we interpolate the power law from there. The distributions for stream lengths and areas must therefore have structures that when combined across orders produce smooth power laws.

For the example of the stream segment length $l_\omega^{(s)}$, Horton's laws state that the mean $\bar{l}_\omega^{(s)}$ grows by a factor of $R_{l^{(s)}}$ with each integer step in order ω. In considering $P(l_\omega^{(s)}, \omega)$, the underlying probability distribution function for $l_\omega^{(s)}$, we postulate that Horton's laws apply for every moment of the distribution and not just the mean. This generalization of Horton's laws may be encapsulated in a statement about the distribution $P(l_\omega^{(s)}, \omega)$ as

$$P(l_\omega^{(s)}, \omega) = c_{l^{(s)}} (R_n R_{l^{(s)}})^{-\omega} F_{l^{(s)}} (l_\omega^{(s)} R_{l^{(s)}}^{-\omega}). \tag{4.4}$$

The factor of $(R_n)^{-\omega}$ indicates the that $\int_{l^{(s)}=0}^{\infty} \mathrm{d}l^{(s)} P(l_\omega^{(s)}, \omega) \propto (R_n)^{-\omega}$, i.e., the frequency of stream segments of order ω decays according to Horton's law of stream number given in equation (4.1). Similarly, for l_ω, a_ω and $n_{\Omega,\omega}$, we write

$$P(l_\omega, \omega) = c_l (R_n R_{l^{(s)}})^{-\omega} F_l(l_\omega R_{l^{(s)}}^{-\omega}), \tag{4.5}$$

$$P(a_\omega, \omega) = c_a (R_n^2)^{-\omega} F_a(a_\omega R_n^{-\omega}), \tag{4.6}$$

and

$$P(n_{\Omega,\omega}) = c_n (R_n)^{\Omega-\omega} F_n(n_{\Omega,\omega} R_n^{-\omega}), \tag{4.7}$$

where constants $c_{l^{(s)}}$, c_l, c_a and c_n are appropriate normalizations. We have used the subscripted versions of the lengths and areas, $l_\omega^{(s)}$, l_ω, and a_ω, to reinforce that these parameters are for points at the outlets of order ω basins only. The quantity $n_{\Omega,\omega}$ is the number of streams of order ω within a basin of order Ω. This will help with some notational issues later on. The form of the distribution functions $F_{l^{(s)}}$, F_l, F_a and F_n and their interrelationships become the focus of our investigations. Since scaling is inherent in each of these postulated generalizations of Horton's laws, we will often refer to these distribution functions as *scaling functions*.

We further postulate that distributions of stream segment lengths are best approximated by exponential distributions. Empirical evidence for this will be provided later on in Section 4.5. The normalized scaling function $F_{l^{(s)}}(u)$ of equation (4.4) then has the form

$$F_{l^{(s)}}(u) = \frac{1}{\xi} e^{-u/\xi} = F_{l^{(s)}}(u; \xi), \tag{4.8}$$

where we have introduced a new length scale ξ and stated its appearance with the notation $F_{l^{(s)}}(u; \xi)$. The value of ξ is potentially network dependent. As we will show, distributions of main stream lengths, areas and stream number are all dependent on ξ and this is the only additional parameter necessary for their description. Note that ξ is both the mean and standard deviation of $F_{l^{(s)}}(u; \xi)$, i.e., for exponential distributions, fluctuations of a variable are on the order of its mean value. We may therefore think of ξ as a *fluctuation length scale*. Note that the presence of exponential distributions indicates a randomness in the physical distribution of streams themselves and this is largely the topic of our third paper [34].

Since main stream lengths are combinations of stream segment lengths, i.e. $l_\omega = \sum_{i=1}^{\omega} l_\omega^{(s)}$, we have that the distributions of main stream lengths of order ω basins are approximated by convolutions of the stream segment length distributions. For this step, it is more appropriate to use conditional probabilities such as $P(l_\omega^{(s)}|\omega)$ where the basin order ω is taken to be fixed. We thus write

$$P(l_\omega|\omega) = P(l^{(s)}{}_1|1) * P(l^{(s)}{}_2|2) * \cdots P(l_\omega^{(s)}|\omega). \qquad (4.9)$$

where $*$ denotes convolution. Details of the form obtained are given in Appendix A.1.1.

The next step takes us to the power law distribution for main stream lengths. Summing over all stream orders and integrating over $u = l_\omega$ we have

$$P(l) \simeq \sum_{\omega=1}^{\infty} \int_{u=l}^{\infty} \mathrm{d}u\, P(u,\omega), \qquad (4.10)$$

where we have returned to the joint probability for this calculation. The integral over u is replaced by a sum when networks are considered on discrete lattices. Note that the probability of finding a main stream of length l is independent of any sort of stream ordering since it is defined on an unordered network. The details of this calculation may be found Appendix A.1.2 where it is shown that a power law $P(l) \propto l^{-\gamma}$ follows from the deduced form of the $P(l_\omega,\omega)$ with $\gamma = \ln R_n / \ln R_{l^{(s)}}$.

4.4   Estimation of Horton ratios

We now examine the usual Horton's laws in order to estimate the Horton ratios. These ratios are seen as intrinsic parameters in the probability distribution functions given above in equations (4.4), (4.5), (4.6) and (4.7).

Figure 4.2(a) shows the stream order averages of $l^{(s)}$, l, a and n for the Mississippi basin. Deviations from exponential trends of Horton's laws are evident and indicated by deviations from straight lines on the semi-logarithmic axis. Such deviations are to be expected for the smallest and largest orders within a basin [31, 34]. For the smallest orders, the scale of the grid used becomes an issue but even with infinite resolution, the scaling of lengths, areas and number for low orders cannot all hold at the same time [31]. For large orders, the decrease in sample space contributes to these fluctuations

ω range	R_n	R_a	R_l	$R_{l(\text{s})}$	R_a/R_n	$R_l/R_{l(\text{s})}$
$[2,3]$	5.27	5.26	2.48	2.30	1.00	1.07
$[2,5]$	4.86	4.96	2.42	2.31	1.02	1.05
$[2,7]$	4.77	4.88	2.40	2.31	1.02	1.04
$[3,4]$	4.72	4.91	2.41	2.34	1.04	1.03
$[3,6]$	4.70	4.83	2.40	2.35	1.03	1.03
$[3,8]$	4.60	4.79	2.38	2.34	1.04	1.02
$[4,6]$	4.69	4.81	2.40	2.36	1.02	1.02
$[4,8]$	4.57	4.77	2.38	2.34	1.05	1.01
$[5,7]$	4.68	4.83	2.36	2.29	1.03	1.03
$[6,7]$	4.63	4.76	2.30	2.16	1.03	1.07
$[7,8]$	4.16	4.67	2.41	2.56	1.12	0.94
mean μ	4.69	4.85	2.40	2.33	1.04	1.03
std dev σ	0.21	0.13	0.04	0.07	0.03	0.03
σ/μ	0.045	0.027	0.015	0.031	0.024	0.027

Table 4.1: Horton ratios for the Mississippi River. For each range of orders (ω_1, ω_2), estimates of the ratios are obtained via simple regression analysis. (See Table D.1 for the full range). For each quantity, a mean μ, standard deviation σ and normalized deviation σ/μ are calculated. All ranges with $2 \le \omega_1 < \omega_2 \le 8$ are used in these estimates but not all are shown The values obtained for R_l are especially robust while some variation is observed for the estimates of R_n and R_a. Good agreement is observed between the ratios R_n and R_a and also between R_l and $R_{l(\text{s})}$. The Misssissippi river network was extracted from a topography dataset composed of digital elevations models obtained from the United States Geological Survey and are available on the Internet at www.usgs.gov. The dataset is decimated so as to have horizontal resolution of approximately 1000 meters leading to an order $\Omega = 11$ network.

ω range	R_n	R_a	R_l	$R_{l(\mathrm{s})}$	R_a/R_n	$R_l/R_{l(\mathrm{s})}$
$[2,3]$	5.05	4.69	2.10	1.65	0.93	1.28
$[2,5]$	4.65	4.64	2.11	1.92	1.00	1.10
$[2,7]$	4.54	4.63	2.16	2.11	1.02	1.03
$[3,4]$	4.54	4.73	2.10	2.01	1.04	1.05
$[3,6]$	4.51	4.62	2.15	2.15	1.02	1.00
$[3,8]$	4.44	4.55	2.19	2.23	1.02	0.98
$[4,6]$	4.52	4.59	2.18	2.24	1.02	0.97
$[4,8]$	4.42	4.51	2.21	2.27	1.02	0.97
$[5,7]$	4.39	4.62	2.25	2.39	1.05	0.94
$[6,7]$	4.19	4.55	2.26	2.40	1.09	0.94
$[7,8]$	4.50	4.21	2.15	2.12	0.94	1.02
mean μ	4.51	4.58	2.17	2.15	1.01	1.02
std dev σ	0.17	0.12	0.05	0.19	0.03	0.08
σ/μ	0.038	0.026	0.024	0.089	0.034	0.078

Table 4.2: Horton ratios for the Amazon. Details are as per Table 4.1. (Again, not all data is shown but is recorded later in Table D.3). The topography dataset used for the Amazon was obtained from the website of the National Imagery and Mapping Agency (`www.nima.mil`). The dataset has a horizontal resolution of approximately 1000 meters yielding and order $\Omega = 11$ network for the Amazon.
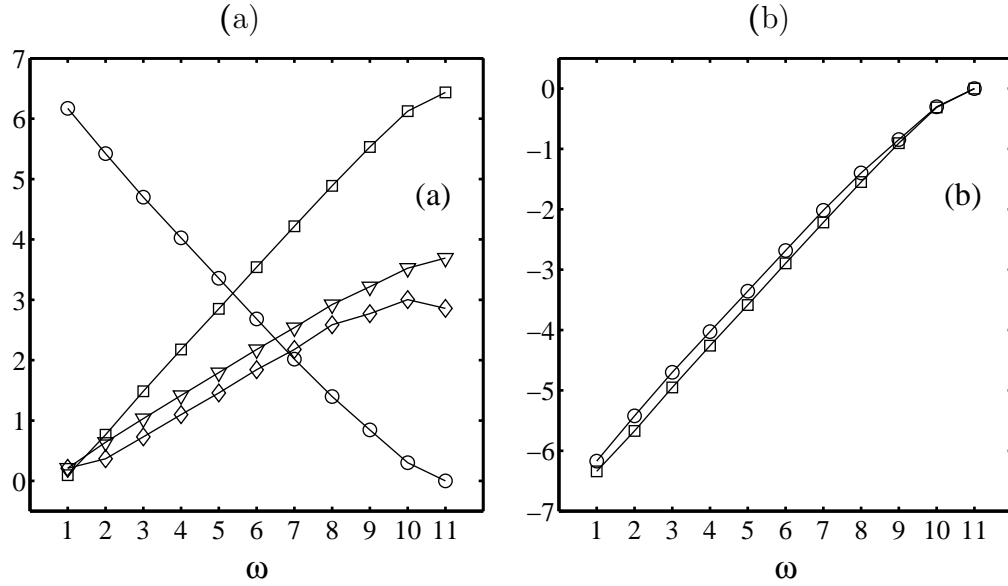
Figure 4.2: Horton's laws for the order $\Omega = 11$ Mississippi river basin network. For (a), the ordinate axis is logarithmic (base 10) representing number for stream number n_ω (circles), km^2 for area $\bar{a}_\omega$ (squares), and km for both main stream length $\bar{l}_\omega$ (triangles) and stream segment length $\bar{l}_\omega^{(s)}$ (diamonds). Note the good agreement between $\bar{l}_\omega$ and $\bar{l}_\omega^{(s)}$. In (b), the stream number data n_ω (circles) has been inverted from that in (a), i.e., the plot is of n_ω^{-1}. This is compared with the dimensionless $\bar{a}_\omega/\bar{a}_\Omega$ (squares) showing good support for the prediction the slopes are equal, i.e., $R_a \equiv R_n$.

since the number of samples of order ω streams decays exponentially with order as $(R_n)^{\Omega-\omega}$. Furthermore, correlations with overall basin shape provide another source of deviations [34]. Nevertheless, in our theoretical investigations below we will presume exact scaling. Note also that the equivalence of R_n and R_a is supported by Figure 4.2(b) where the stream numbers n_w have been inverted for comparison. Similar agreement is found for the Amazon and Nile as shown in Tables 4.1, 4.2, and 4.3 which we now discuss.

Table 4.1 shows the results of regression on the Mississippi data for various ranges of stream orders for stream number, area and lengths. Tables 4.2 and 4.3 show the same results carried out for the Amazon and Nile. Each table presents estimates of the four ratios R_n, R_a, R_l and $R_{l^{(s)}}$. Also included are the comparisons R_a/R_n and $R_l/R_{l^{(s)}}$, both of which we expect to be close

ω range	R_n	R_a	R_l	$R_{l(s)}$	R_a/R_n	$R_l/R_{l(s)}$
$[2,3]$	4.78	4.71	2.47	2.08	0.99	1.19
$[2,5]$	4.55	4.58	2.32	2.12	1.01	1.10
$[2,7]$	4.42	4.53	2.24	2.10	1.02	1.07
$[3,5]$	4.45	4.52	2.26	2.14	1.01	1.06
$[3,7]$	4.35	4.49	2.20	2.10	1.03	1.05
$[4,6]$	4.38	4.54	2.22	2.18	1.03	1.02
$[5,6]$	4.38	4.62	2.22	2.21	1.06	1.00
$[6,7]$	4.08	4.27	2.05	1.83	1.05	1.12
mean μ	4.42	4.53	2.25	2.10	1.02	1.07
std dev σ	0.17	0.10	0.10	0.09	0.02	0.05
σ/μ	0.038	0.023	0.045	0.042	0.019	0.045

Table 4.3: Horton ratios for the Nile. Details are as per Table 4.3. (See Table D.5 for all data). Here $2 \le \omega_1 < \omega_2 < 7$. The data for the Nile comes from the United States Geological Survey's 30 arc second Hydro1K dataset, avaliable on the Internet at `edcftp.cr.usgs.gov`, which has a grid spacing of approximately 1000 meters. At this resolution, the Nile is an order $\Omega = 10$ basin.

to unity. For each quantity, we calculate the mean μ, standard deviation σ and normalized deviation σ/μ.

Note the variation of exponents with choice of order range. This is the largest source of error in the calculation of the Horton ratios. Therefore, rather than taking a single range of stream orders for the regression, we examine a collection of ranges. Also, the deviations for high and low orders observed in Figures 4.2(a) and 4.2(b) do of course affect measurements of the Horton ratios. In all cases, we have avoided using data for the smallest and largest orders.

For the three example networks given here, the statements $R_a \equiv R_n$ and $R_l \equiv R_{l(s)}$ are well supported. The majority of ranges give R_n/R_a and $R_l/R_{l(s)}$ very close to unity. The averages are also close to one and are different from unity mostly by within 1.0 and uniformly by within 1.5 standard deviations.

The normalized deviations, ie., σ/μ, for the four ratios are all below 0.05. No systematic ordering of the σ/μ is observed. Of all the data, the values for R_l in the case of the Mississippi are the most notably uniform having $\sigma/\mu = 0.015$. Throughout there is a slight trend for regression on lower orders to overestimate and on higher orders to underestimate the average ratios, while reasonable consistency is found at intermediate orders.
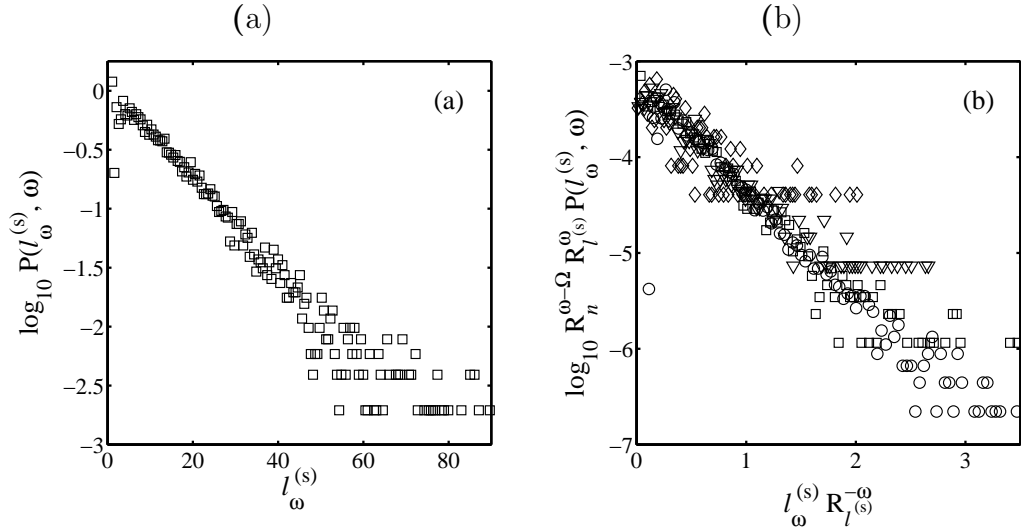
Figure 4.3: Plot (a) shows an example distribution of stream segment lengths, $P(l^{(s)}_\omega, \omega)$, for the Mississippi for order $\omega = 4$. The lengths here are in kilometers. The semi-logarithmic axes indicate the distribution is well approximated by an exponential. The value of the length scale ξ (see equation (4.8)) is estimated to be approximately 800 meters. Rescaled versions of the same stream segment length distributions for $\omega = 3$ (circles), $\omega = 4$ (squares), $\omega = 5$ (triangles), and $\omega = 6$ (diamonds), are shown in (b). The rescaling is done according to equation (4.4). The values of the Horton ratios used are $R_n = 4.69$ and $R_{l^{(s)}} = 2.33$ as determined from Table 4.1

Thus, overall the ranges chosen in the tables give a reasonably even set of estimates of the Horton ratios and we will use these averages as our estimates of the ratios.

4.5   Empirical evidence for Horton distributions

4.5.1   Stream segment length distributions

We now present Horton distributions for the Mississippi, Amazon, and Nile river basins as well as the Scheidegger model. Scheidegger networks may be thought of as collections of random-walker streams and are fully defined

in [32] and extensively studied in [34]. The forms of all distributions are observed to be the same in the real data and in the model.

   The first distribution is shown in Figure 4.3(a). This is the probability density function of $l^{(s)}{}_4$, fourth order stream segment lengths, for the Mississippi River. Distributions for different orders can be rescaled to show satisfactory agreement. This is done using the postulated Horton distribution of stream segment lengths given in equation (4.4). The rescaling is shown in Figure 4.3(b) and is for orders $\omega = 3, \dots, 6$. Note the effect of the exponential decrease in number of samples with order is evident for $\omega = 6$ since $P(l^{(s)}{}_6)$ is considerably scattered. Nevertheless, the figure shows the form of these distributions to be most closely approximated by exponentials. We observe similar exponential distributions for the Amazon, the Nile and the Scheidegger model. The fluctuation length scale ξ is found to be approximately 800 meters for the Mississippi, 1600 meters for the Amazon and 1200 meters for the Nile.

   Since ξ is based on the definition of stream ordering, comparisons of ξ are only sensible for networks that are measured on topographies with the same resolution. The above values of ξ are approximate and our confidence in them would be improved with higher resolution data. Nevertheless they do suggest that fluctuations in network structure increase as we move from the Mississippi through to the Nile and then the Amazon.

4.5.2   Main stream segment length distributions

The distributions of $\omega = 4$ main stream lengths for the Amazon River is shown in Figure 4.4(a). Since main stream lengths are sums of stream segment lengths, their distribution has a single peak away from the origin. However, these distributions will not tend towards a Gaussian because the individual stream length distributions do not satisfy the requirements of the central limit theorem [39]. This is because the moments of the stream segment length distributions grow exponentially with stream order. As the semi-logarithmic axes indicate, the tail may be reasonably well (but not exactly) modeled by exponentials. There is some variation in the distribution tails from region to region. For example, corresponding distributions for the Mississippi data do exhibit tails that are closer to exponentials. However, for the present work where we are attempting to characterize the basic forms of the Horton distributions, we consider these deviations to be of a higher order nature and belonging to the realm of further research.

   In accord with equation (4.5), Figure 4.4(b) shows the rescaling of the
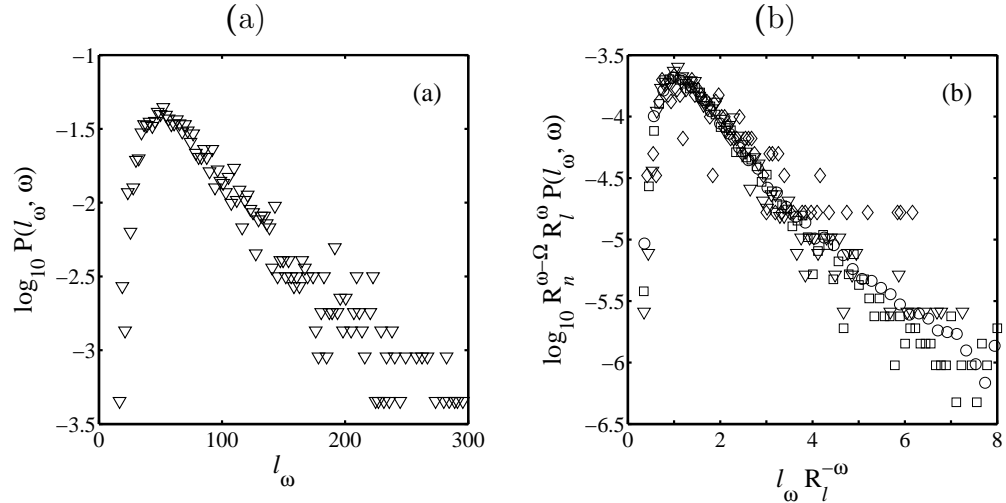
Figure 4.4: Plot (a) shows an example distribution for order $\omega = 5$ main stream lengths (measured in km) for the Amazon. The distribution is unimodal with what is a reasonable approximation of an exponential tail. In (b), distributions of main stream length for for $\omega = 3$ (circles), $\omega = 4$ (squares), $\omega = 5$ (triangles), and $\omega = 6$ (diamonds), are rescaled according to equation (4.5). The values of the Horton ratios used here are $R_n = 4.51$ and $R_{l(s)} = 2.17$, taken from Table 4.2.

main stream length distributions for $\omega = 3, \dots, 6$. The ratios used, $R_n = 4.49$ and $R_l = 2.19 (\simeq R_{l(s)} = 2.17)$ are taken from Table 4.2. Given the scatter of the distributions, it is unreasonable to perform minimization techniques on the rescaled data itself in order to estimate R_n and R_l. This is best done by examining means, as we have done, and higher order moments which we discuss below. Furthermore, varying R_n and R_l from the above values by, say, ± 0.05 does not greatly distort the visual quality of the "data collapse."

Similar results for the Scheidegger model are shown in Figure 4.5. The Scheidegger model may be thought of as a network defined on a triangular lattice where at each lattice site one of two directions is chosen as the stream path [32, 34]. Figure 4.5(a) gives a single example distribution for main stream lengths of order $\omega = 6$ basins. The tail is exponential as per the real world data. Figure 4.5(b) shows a collapse of main stream length distributions for orders $\omega = 4$ through 7. In contrast to the real data where an overall basin order is fixed (Ω), there is no maximum basin order here. The distributions in Figure 4.5(b) have an arbitrary normalization meaning
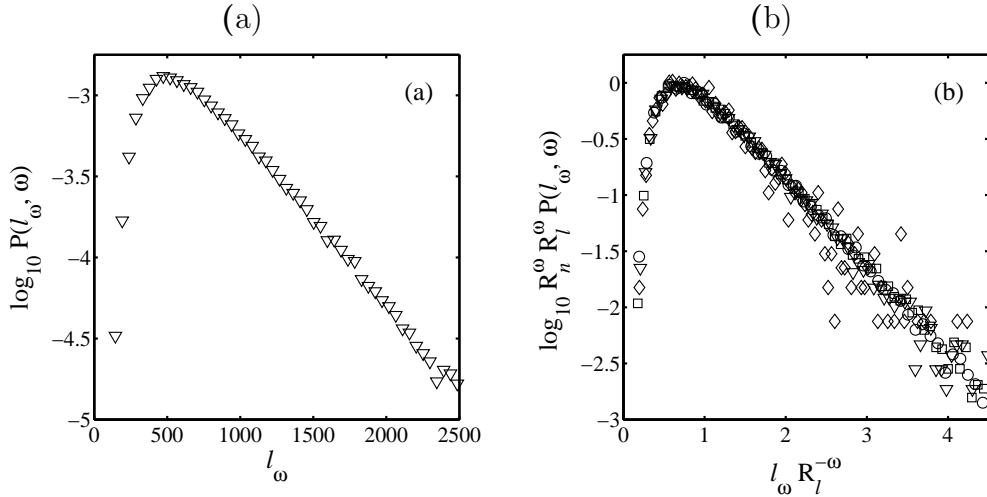
Figure 4.5: Given in (a) is an example distribution of order $\omega = 6$ main stream lengths for the Scheidegger model. The same form is observed as for real networks such as the Amazon (Figure 4.4). In the same way as Figure 4.4(b), (b) show rescaled distributions of main stream length for for $\omega = 4$ (circles), $\omega = 5$ (squares), $\omega = 6$ (triangles), and $\omega = 7$ (diamonds). Note that in (b), distributions are not normalized with respect to a fixed basin order Ω and hence the vertical offset is arbitrary. The values of the ratios used here are $R_n \simeq 5.20$ and $R_l \simeq 3.00$ [31].

the absolute values of the ordinate are also arbitrary. Otherwise, this is the same collapse as given in equation (4.5). For the Scheidegger model, our simulations yield $R_n \simeq 5.20$ and $R_{l(\mathrm{s})} \simeq 3.00$ [31]. For all distributions, we observe similar functional forms for real networks and the Scheidegger model, the only difference lying in parameters such as the Horton ratios.

4.5.3   Drainage area distributions

Figure 4.6 shows more Horton distributions, this time for drainage area as calculated for the Nile river basin. In Figure 4.6, an example distribution for $\omega = 4$ sub-basins is presented. The distribution is similar in form to those of main stream lengths of Figure 4.4, again showing a reasonably clear exponential tail. Rescaled drainage area distributions for $\omega = 3, \ldots, 6$ are presented in Figure 4.6(b). The rescaling now follows equation (4.6). Note
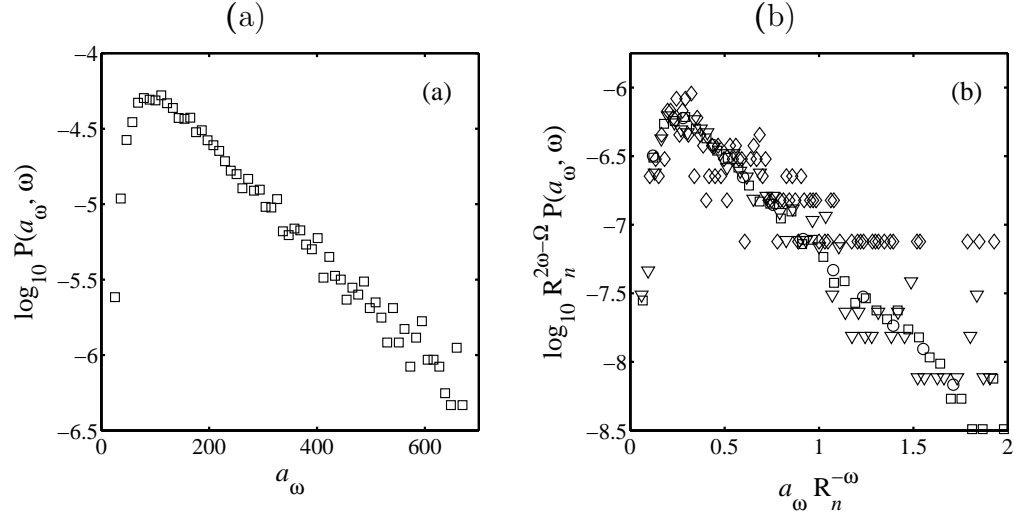
Figure 4.6: The distribution of drainage areas for $\omega = 4$ sub-basins of the Nile are shown in (a). All areas are measured in km^2. An exponential tail is observed as per the distributions of stream segment length (Figure 4.3) and main stream length (Figure 4.4). In (b), distributions of drainage area for for $\omega = 3$ (circles), $\omega = 4$ (squares), $\omega = 5$ (triangles), and $\omega = 6$ (diamonds), are rescaled according to equation (4.6). The rescaling uses the estimate $R_n = 4.42$ found in Table 4.3.

that if R_n and R_a were not equivalent, the rescaling would be of the form

$$P(a_\omega, \omega) = c_a (R_n R_a)^{-\omega} F_a(a_\omega R_a^{-\omega}). \tag{4.11}$$

Since we have asserted that $R_n \equiv R_a$, equation (4.11) reduces to equation (4.6). The Horton ratio used here is $R_n = 4.42$ which is in good agreement with $R_a = 4.53$, the respective standard deviations being 0.17 and 0.10. Both figures are taken from the data of Table 4.3.

4.5.4   Summing distributions to form power laws

As stated in Section 4.3, the Horton distributions of a_ω and l_ω must combine to form power law distributions for a and l (see equations 4.3 and 4.10). Figure 4.7 provides empirical support for this observation for the example main stream lengths of the Mississippi network. The distributions for $\omega = 3$, 4 and 5 main stream lengths are individually shown. Their combination together with the distribution of l_6 gives the reasonable approximation of
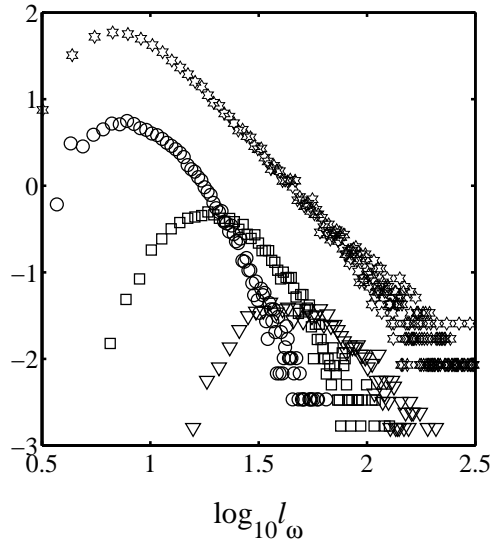
Figure 4.7: Summation of main stream length distributions for the Mississippi. Both axes are logarithmic,the unit of length is km and the vertical axis is probability density with units of km^{-1}. Distributions of l_ω for orders $\omega = 3$ (circles), $\omega = 4$ (squares), and $\omega = 5$ (triangles), are shown. As expected, the distributions sum together to give a power law tail (stars). The power law distribution (which is vertically offset by an order of magnitude for clarity) is the summation of the distributions below as well as the distribution for order $\omega = 6$ main stream lengths.

a power law as shown. The area distributions combine in the same way. Note that the distributions do not greatly overlap. Each point of the power law is therefore the addition of significant contributions from only two or three of the separate distributions. The challenge here then is to understand how rescaled versions of F_l, being the basic form of the $P(l_\omega, \omega)$, fit together in such a clean fashion. The details of this connection are established in Appendix A.1.2.

4.5.5   Connecting distributions of number and area

In considering the generalized Horton distributions for number and area, we observe two main points: a calculation in the vein of what we are able to do for main stream lengths is difficult; and, the Horton distributions for area and number are equivalent.

In principle, Horton area distributions may be derived from stream seg-

ment length distributions. This follows from an assumption of statistically uniform drainage density which means that the typical drainage area drained per unit length of any stream is invariant in space. Apart from the possibility of changing with space which we will preclude by assumption, drainage density does naturally fluctuate as well [32]. Thus, we can write $a \simeq \rho \sum_\omega l_\omega^{(\mathrm{s})}$ where the sum is over all orders and all stream segments and ρ is the average drainage density.

However, we need to know for an example basin, how many instances of each stream segment occur as a function of order. For example, the number of first order streams in an order Ω basins is $n_{\Omega,1}$. Given the distribution of this number, we can then calculate the distribution of the total contribution of drainage area due to first order streams. But the distributions of $n_{\Omega,\omega}$ are not independent so we cannot proceed in this direction.

We could potentially use the typical number of order ω streams, $(R_n)^{\Omega-\omega}$. Then the distribution of total area drained due to order ω streams would approach Gaussian because the individual distribution are identical and the central limit theorem would apply. However, because the fluctuations in total number of stream segments are so great, we lose too much information with this approach. Indeed, the distribution of area drained by order ω stream segments in a basin reflects variations in their number rather than length. Again, we meet up with the problem of the numbers of distinct orders of stream segment lengths being dependent.

One final way would be to use Tokunaga's law [31, 102, 144, 145, 146]. Tokunaga's law states that the number of order ν side branches along an (absorbing) stream segment of order μ is given by

$$T_k = T_1 (R_{l^{(\mathrm{s})}})^{k+1}. \tag{4.12}$$

where $k = \mu - \nu$. The parameter T_1 is the average number of side streams having order $\nu = \mu - 1$ for every order μ absorbing stream. This gives a picture of how a network fits together and may be seen to be equivalent to Horton's laws [31]. Now, even though we also understand the distributions underlying Tokunaga's law [32], similar technical problems arise. On descending into a network, we find the number of stream segments at each level to be dependent on all of the above.

Nevertheless, we can understand the relationship between the distributions for area and number. What follows is a generalization of the finding that $R_n \equiv R_a$. The postulated forms for these distributions were given in equations (4.6) and (4.7). Consider $n_{\Omega,1}$, the number of first order streams in an order Ω basin. Assuming that, on average, first order streams are
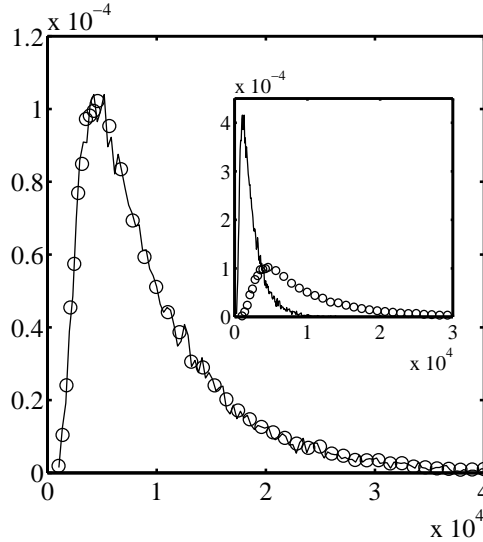
Figure 4.8: Comparison of number and area distributions for the Scheidegger model. Area is in terms of lattice units. In the inset plot, the raw distributions shown are $P(a_6|6)$ (circles) and $P(n_{6,1}|6)$ (continuous line). The latter is the probability of finding $n_{6,1}$ source streams in an order $\omega = 6$ basin. In the main plot, the number distribution has been rescaled to be $1/4P(n_{6,1}|6)$ as a function of $4n_{6,1}$ and the area distribution is unrescaled (the symbols are the same as for the inset plot). For the Scheidegger model, source streams occur at any site with probability of $1/4$, hence the rescaling by a factor of four.

distributed evenly throughout a network, then this number is simply proportional to a_Ω. As an example, Figure 4.8 shows data obtained for the Scheidegger model. For the Scheidegger model, first order streams are initiated with a $1/4$ probability when the flow at the two upstream sites is randomly directed away, each with probability $1/2$. Thus, for an area a_Ω, we expect and find $n_{\Omega,\omega} = a_\Omega/4$.

For higher internal orders, we can apply a simple renormalization. Assuming a system with exact scaling, the number of streams $n_{\Omega,\omega}$ is statistically equivalent to $n_{\Omega-\omega+1,1}$. Since the latter is proportional to $a_{\Omega-\omega+1}$ we have that

$$n_{\Omega,\omega} \simeq \rho_\omega a_{\Omega-\omega+1} \qquad (4.13)$$

where the constant of proportionality is the density of order ω streams, Clearly, this equivalence improves as number increases, i.e., the difference
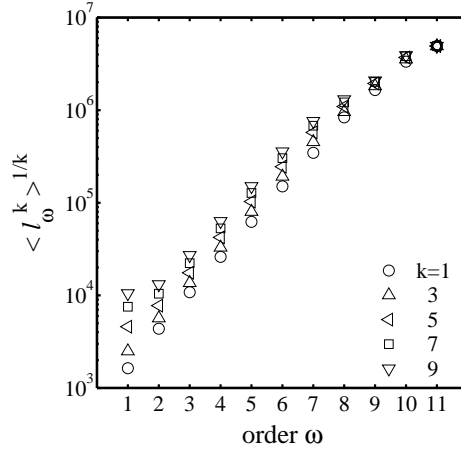
Figure 4.9: A comparison of moments calculated for main stream length distributions for the Mississippi River.

$\Omega - \omega$ increases.

While we do not have exact forms for the area or number distributions, we note that they are similar to the main stream length distributions. Since source streams are linear basins with the width of a grid cell, the distribution of a_1 is the same as the distribution of l_1 and $l^{(s)}{}_1$, a pure exponential. Hence, $n_{\Omega,\Omega-1}$ is also an exponential. For increasing ω, the distribution of a_ω becomes single peaked with an exponential tail, qualitatively the same as the main stream length distributions.

4.6   Higher order moments

Finally, we discuss the higher order moments for the generalized Horton distributions. Figure 4.9 presents moments for distributions of main stream lengths for the case of the Mississippi. These moments are calculated directly from the main stream length distributions. A regular logarithmic spacing is apparent in moments for orders ranging from 3 to 7.

To see whether or not this is expected, we detail a few small calculations concerning moments starting from the exponential form of stream segment lengths given in equation (4.8). As noted previously, for an exponential distribution, $F_{l^{(s)}}(u) = \xi^{-1}e^{-u/\xi}$, the mean is simply $\langle u \rangle = \xi$. In general, the

qth moment of an exponential distribution is

$$\langle u^q \rangle = \int_{u=0}^{\infty} \frac{u^q}{\xi} e^{-u/\xi} \mathrm{d}u$$
$$= \xi^q \int_{x=0}^{\infty} x^q e^{-x} \mathrm{d}x = q!\xi^q. \tag{4.14}$$

Assuming scaling holds exactly for across all orders, the above is precisely $\langle (l^{(\mathrm{s})}{}_1)^q \rangle$. Note that $\langle (l^{(\mathrm{s})}{}_1)^q \rangle = q!\langle l^{(\mathrm{s})}{}_1 \rangle^q$. Since the characteristic length of order ω streams is $(R_{l^{(\mathrm{s})}})^{\omega-1}$, we therefore have

$$\langle (l_\omega^{(\mathrm{s})})^q \rangle = q!\xi^q (R_{l^{(\mathrm{s})}})^{(\omega-1)q} = q! \langle l_\omega^{(\mathrm{s})} \rangle^q. \tag{4.15}$$

Since main stream lengths are sums of stream segment lengths, so are their respective moments. Hence,

$$\langle (l_\omega)^q \rangle = \sum_{k=1}^{\omega} \langle (l^{(\mathrm{s})}{}_k)^q \rangle,$$
$$= \sum_{k=1}^{\omega} q!\xi^q (R_{l^{(\mathrm{s})}})^{(k-1)q},$$
$$= q!\xi^q \sum_{k=1}^{\omega} (R_{l^{(\mathrm{s})}})^{(k-1)q},$$
$$= q!\xi^q \frac{(R_{l^{(\mathrm{s})}})^{q\omega} - 1}{R_{l^{(\mathrm{s})}} - 1}. \tag{4.16}$$

We can now determine the log-space separation of moments of main stream length. Using Stirling's approximation [50] that $\ln n! \sim (n+1/2)\ln n - n$ we have

$$\ln \langle (l_\omega)^q \rangle \sim q \left[\xi + (R_{l^{(\mathrm{s})}})^\omega + \ln q \right] + C, \tag{4.17}$$

where C is a constant. The $\ln q$ term inside the square brackets in equation 4.17 creates small deviations from linearity for $1 \le \omega \le 15$. Thus, in agreement with Figure 4.9, we expect approximately linear growth of moments in log-space.

4.7   Limitations on the predictive power of Horton's laws

In this last section, we briefly examine deviations from scaling within this generalized picture of Horton's laws. The basic question is given an approx-

imate scaling for quantities measured at intermediate stream orders, what
can we say about the features of the overall basin?
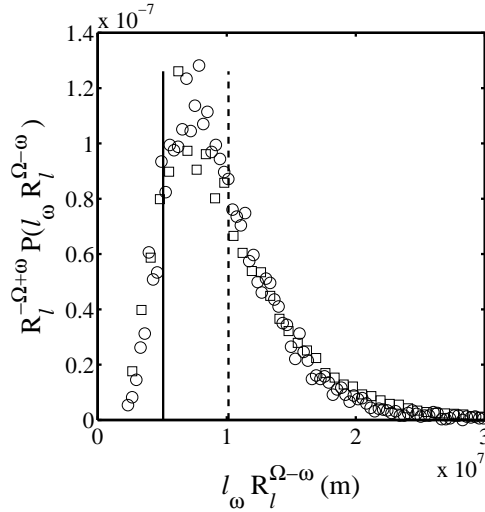
Figure 4.10: Comparing the generalized Horton length distribution rescaled to the
level of order $\Omega = 11$ basins with the Congo River itself. The two distributions
are for orders $\omega = 3$ (squares) and $\omega = 4$ (circles) stream lengths and the Horton
ratio is estimated to be $R_l = 2.39$ [33]. The dashed line represents the mean of
these scaled up distributions while the solid line marks $\bar{l}_{11}$, the measured length
of the Congo at a 1000 meter resolution. The actual length is within a standard
deviation of the mean being around 50% of $\bar{l}_{11}$. Table 4.4 shows comparisons for
various river networks for both area and length data.

   As noted in the previous section, all moments of the generalized Horton
distributions grow exponentially with order. Coupling this with the fact
that $n_\omega \propto R_n^{-\omega}$, i.e., the number of samples of order ω basins decreases
exponentially with ω, we observe that a basin's a and l will potentially differ
greatly from values predicted by Horton's laws.

   To illustrate this, Figure 4.10 specifically shows the distributions $P(l_3)$
and $P(l_4)$ scaled up to give $P(l_{11})$ for the Congo river. The actual Congo's
length measured at this 1000 meter resolution is represented by the solid line
and is around 57% of the distribution's mean as indicated by the dashed line.
Nevertheless, we see that the measured length is within a standard deviation
of the predicted value.

   In Table 4.4, we provide a comparison of predicted versus measured main
stream lengths and areas for the basins studied here. The mean for the scaled

basin:	l_Ω	$\bar{l}_\Omega$	σ_l	$l/\bar{l}_\Omega$	$\sigma_l/\bar{l}_\Omega$	a	$\bar{a}_\Omega$	σ_a	$a/\bar{a}_\Omega$	$\sigma_a/\bar{a}_\Omega$
Mississippi	4.92	11.10	5.60	0.44	0.51	2.74	7.55	5.58	0.36	0.74
Amazon	5.75	9.18	6.85	0.63	0.75	5.40	9.07	8.04	0.60	0.89
Nile	6.49	2.66	2.20	2.44	0.83	3.08	0.96	0.79	3.19	0.82
Congo	5.07	10.13	5.75	0.50	0.57	3.70	10.09	8.28	0.37	0.82
Kansas	1.07	2.37	1.74	0.45	0.73	0.14	0.49	0.42	0.28	0.86

Table 4.4: Comparison of predicted versus measured main stream lengths for large scale river networks. The dimensions of all lengths and areas are 10^6 m and 10^{12} m^2 respectively. Here, l_Ω, is the actual main stream length of the basin, $\bar{l}_\Omega$ the predicted mean value of l_Ω, σ_l the predicted variance and $\sigma_l/\bar{l}_\Omega$ the normalized deviation. The entries for the basin area data have corresponding definitions.

up distributions overestimates the actual values in all cases except for the Nile. Also, apart from the Nile, all values are within a standard deviation of the predicted mean. The coefficients of variation, $\sigma_a/\bar{a}_\Omega$ and $\sigma_l/\bar{l}_\Omega$, all indicate that fluctuations are on the order of the expected values of stream lengths and areas.

Thus, we see that by using a probabilistic point of view, this generalized notion of Horton's laws provides a way of discerning the strength of deviations about the expected mean. In general, stronger deviations would imply that geologic conditions play a more significant role in setting the structure of the network.

4.8   Conclusion

The objective of this work has been to explore the underlying distributions of river network quantities defined with stream ordering. We have shown that functional relationships generalize all cases of Horton's laws. We have identified the basic forms of the distributions for stream segment lengths (exponential) and main stream lengths (convolutions of exponentials) and shown a link between number and area distributions. Data from the continent-scale networks of the Mississippi, Amazon, and Nile river basins as well as from Scheidegger's model of directed random networks provide both agreement with and inspiration for the generalizations of Horton's laws. Finally, we have identified a fluctuation length scale ξ which is a reinterpretation of what was previously identified as only a mean value. We see the study of the

generalized Horton distributions as integral to increasing our understanding of river network structure. We also suggest that practical network analysis be extended to measurements of distributions and the length scale ξ with the aim of refining our ability to distinguish and compare network structure.

By taking account of fluctuations inherent in network scaling laws, we are able to see how measuring Horton's laws on low-order networks is unavoidably problematic. Moreover, as we have observed, the measurement of the Horton ratios is in general a delicate operation suggesting that many previous measurements are not without error.

The theoretical understanding of the growth and evolution of river networks requires a more thorough approach to measurement and a concurrent improvement in the statistical description of river network geometry. The present consideration of a generalization of Horton's laws is a necessary step in this process giving rise to stronger tests of both real and synthetic data. In the following paper [34], we round out this expanded picture of network structure by consdering the spatial distribution of network components.

Acknowledgements

CHAPTER 5

Fluctuations in network architecture

Abstract. River networks serve as a paradigmatic example of all branching
networks. Essential to understanding the overall structure of river networks
is a knowledge of their detailed architecture. Here we show that sub-branches
are distributed exponentially in size and that they are randomly distributed
in space, thereby completely characterizing the most basic level of river net-
work description. Specifically, an averaged view of network architecture is
first provided by a proposed self-similarity statement about the scaling of
drainage density, a local measure of stream concentration. This scaling of
drainage density is shown to imply Tokunaga's law, a description of the scal-
ing of side branch abundance along a given stream, as well as a scaling law
for stream lengths. This establishes the scaling of the length scale associated
with drainage density as the basic signature of self-similarity in river net-
works. We then consider fluctuations in drainage density and consequently
the numbers of side branches. Data is analyzed for the Mississippi River
basin and a model of random directed networks. Numbers of side streams
are found to follow exponential distributions as are stream lengths and inter-
tributary distances along streams. Finally, we derive the joint variation of
side stream abundance with stream length, affording a full description of
fluctuations in network structure. Fluctuations in side stream numbers are
shown to be a direct result of fluctuations in stream lengths. This is the last
paper in a series of three on the geometry of river networks.

5.1   Introduction

This is the last paper in a series of three on the geometry of river networks. In the first [32] we examine in detail the description of river networks by scaling laws [31, 35, 87, 110] and the evidence for universality. Additional introductory remarks concerning the motivation of the overall work are to found in this first paper. In the second article [33] we address distributions of the basic components of river networks, stream segments and sub-networks. Here, we provide an analysis complementary to the work of the second paper by establishing a description of how river network components fit together. As before, we are motivated by the premise that while relationships of mean quantities are primary in any investigation, the behavior of higher order moments potentially and often do encode significant information.

Our purpose then is to investigate the distributions of quantities which describe the architecture of river networks. The goal is to quantify these distributions and, where this is not possible, to quantify fluctuations. In particular, we center our attention on Tokunaga's law [144, 145, 146] which is a statement about network architecture describing the tributary structure of streams. Since Tokunaga's law can be seen as the main part of a platform from which all other river network scaling laws follow [31], it is an obvious starting point for the investigation of fluctuations in river network structure. We use data from the Schediegger model of random networks [112] and the Mississippi river. We find the distributions obtained from these two disparate sources agree very well in form. We are able to write down scaling forms of all distributions studied. We observe a number of distributions to be exponential, therefore requiring only one parameter for their description. As a result, we introduce a dimensionless scale ξ_t, finding it to be sufficient to describe the fluctuations present in Tokunaga's law and thus potentially all river network scaling laws. Significantly, we observe the spatial distribution of stream segments to be random implying we have reached the most basic description of network architecture.

Tokunaga's law is also intimately connected with drainage density, ρ, a quantity which will be used throughout the paper. Drainage density is a measure of stream concentration or, equivalently, how a network fills space. We explore this connection in detail, showing how simple assumptions regarding drainage density lead to Tokunaga's law.

The paper is structured as follows. We first outline Horton-Strahler stream ordering which provides the necessary descriptive taxonomy for river network architecture. We then define Tokunaga's law and introduce a scaling

law for a specific form of drainage density. We briefly describe Horton's laws for stream number and length and some simple variations. (Both stream ordering and Horton's laws are covered in more detail in [33]). We show that the scaling law of drainage density may be taken as an assumption from which all other scaling laws follow. We also briefly consider the variation of basin shapes (basin allometry) in the context of directedness. This brings us to the focal point of the paper, the identification of a statistical generalization of Tokunaga's law. We first examine distributions of numbers of tributaries (side streams) and compare these with distributions of stream segment lengths. We observe both distributions to be exponential leading to the notion that stream segments are distributed randomly throughout a network. The presence of exponential distributions also leads to the introduction of the characteristic number ξ_t and the single length-scale $\xi_{l^{(s)}} \propto \xi_t$. We then study the variation of tributary spacing along streams so as to understand fluctuations in drainage density and again find the signature of randomness. This leads us to develop a joint probability distribution connecting the length of a stream with the frequency of its side streams.

5.2   Definitions

5.2.1   Stream ordering

Horton-Strahler stream ordering[58, 128] breaks a river network down into a set of *stream segments*. The method can be thought of as an iterative pruning. First, we define a *source stream* as the stream section that runs from a channel head to the first junction with another stream. These source streams are classified as the *first-order* stream segments of the network. Next, we remove all source streams and identify the new source streams of the remaining network. These are the network's *second-order* stream segments. The process is repeated until one stream segment is left of order Ω. The order of the basin is then defined to be Ω (we will use the words basin and network interchangeably).

In discussing network architecture, we will speak of *side streams* and *absorbing streams*. A side stream is any stream that joins into a stream of higher order, the latter being the absorbing stream. We will denote the orders of absorbing and side streams by μ and ν but when referring to an isolated stream or streams where their relative rank is ambiguous, we will write stream order as ω, subscripted as seems appealing.

Central to our investigation of network architecture is stream segment length. As in [33], we denote this length by $l_\omega^{(\text{s})}$ for a stream segment of order ω. We will also introduce a number of closely related lengths which describe distances between side streams. When referring to streams throughout we will specifically mean stream segments of a particular order unless otherwise indicated. This is to avoid confusion with the natural definition of a stream which is the path from a point on a network moving upstream to the most distant source. For an order ω basin, we denote this *main stream length* by l_ω

Note also that we consider river networks in planform, i.e., as networks projected onto the horizontal (or gravitationally flat) plane. This simplification poses no great concern for the analysis of large scale networks such as the Mississippi but must be considered in the context of drainage basins with significant relief.

5.2.2   Tokunaga's law

Defining a stream ordering on a network allows for a number of well-defined measures of connectivity, stream lengths and drainage areas. Around a decade after the Strahler-improved stream ordering of Horton appeared, Tokunaga introduced the idea of measuring side stream statistics [144, 145, 146]. This technique arguably provides the most useful measurement based on stream ordering but has only recently received much attention [22, 31, 102, 147]. The idea is simply, for a given network, to count the average number of order ν side streams entering an order μ absorbing stream. This gives $\langle T_{\mu,\nu} \rangle$, a set of double-indexed parameters for a basin. Note that $\Omega \geq \mu > \nu \geq 1$, so we can view the Tokunaga ratios as a lower triangular matrix. An example for the Mississippi river is shown in Table 5.2.2 [1] The same data is represented pictorially in Figure 5.1 in what we refer to as a *Tokunaga graph*.

Tokunaga made several key observations about these side stream ratios. The first is that because of the self-similar nature of river networks, the $\langle T_{\mu,\nu} \rangle$ should not depend absolutely on either of μ or ν but only on the relative difference, i.e., $k = \mu - \nu$. The second is that in changing the value of $k = \mu - \nu$, the $\langle T_{\mu,\nu} \rangle$ must themselves change by a systematic ratio. These

---

[1]The network for the Mississippi was extracted from a topographic dataset constructed from three arc second USGS Digital Elevation Maps, decimated by averaging to approximately 1000 meter horizontal resolution (www.usgs.gov). At this grid scale, the Mississippi was found to be an order $\Omega = 11$ basin.
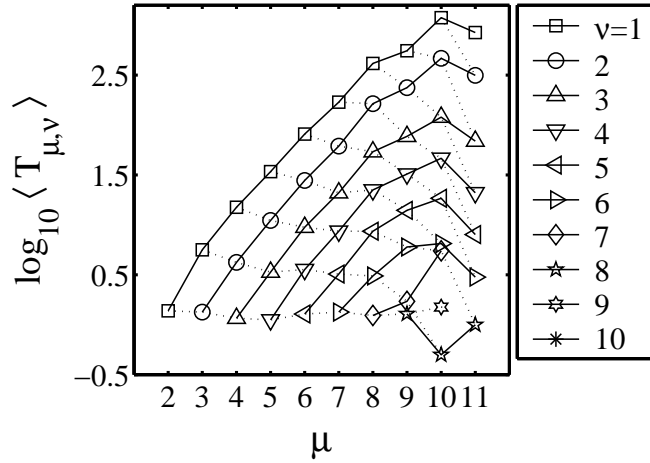
Figure 5.1: A Tokunaga graph for the Mississippi River. The values are given in Table 5.2.2. Each point represents a Tokunaga ratio $\langle T_{\mu,\nu} \rangle$. The solid lines follow variations in the order of the absorbing stream μ while the dotted lines follow unit increments in both μ and ν, the order of side streams. In comparison, the Tokunaga graph of an exactly self-similar network would have points evenly spaced at $\ln T_1 + (\mu + \nu - 1) \ln R_T$ where $1 \leq \nu < \mu = 2, 3, \dots, \Omega$, i.e., all lines in the plot would be straight and uniformly spaced, with the dotted lines being horizontal. The nature of deviations in scalings laws for river networks is addressed in [32].

	$\nu = 1$	2	3	4	5	6	7	8	9	10
$\mu = 2$	1.7									
3	4.9	1.3								
4	12	3.8	1.1							
5	29	9.1	2.9	1.0						
6	71	23	7.7	3.0	1.2					
7	190	56	19	7.8	3.3	1.1				
8	380	110	39	17	6.9	2.6	1.0			
9	630	170	64	28	11	4.5	3.0	0.60		
10	1100	270	66	29	13	4.3	2.7	1	1	
11	1400	510	120	66	25	12	9	3	1	1

Table 5.1: Tokunaga ratios for the Mississippi River. The row indices are the absorbing stream orders while the columns correspond to side stream orders. Each entry is the average number of order ν side streams per order μ absorbing stream.

statements lead to Tokunaga's law:

$$\langle T_{\mu,\nu} \rangle = \langle T_k \rangle = \langle T_1 \rangle \, (R_T)^{k-1}. \tag{5.1}$$

Thus, only two parameters are necessary to characterize the set of $T_{\mu,\nu}$: T_1 and R_T.

The parameter $T_1 > 0$ is the average number of side streams of one order lower than the absorbing stream, typically on the order of 1.0–1.5. Since these side streams of one order less are the dominant side streams of the basin, their number estimates the basin's breadth. In general, larger values of $\langle T_1 \rangle$ correspond to wider basins while smaller values are in keeping with basins with relatively thinner profiles.

The ratio $R_T > 1$ measures how the density of side streams of decreasing order increases. It is a measure of changing length scales and has a simple interpretation with respect to Horton's laws which we describe below. Thus, already inherent in Tokunaga's law is a generalization of drainage density ρ. the usual definition of which is given as follows. For a given region of landscape with area A with streams totalling in length L, $\rho = L/A$ and has the dimensions of an inverse length scale [58]. One may think of ρ as the inverse of the typical distance between streams, i.e., the characteristic scale beyond which erosion cannot more finely dissect the landscape [58]. In principle, drainage density may vary from landscape to landscape and also throughout a single region. Below, we will turn this observation about Tokunaga's law around to show that all river network scaling laws may be derived from an expanded notion of drainage density.

Even though the number of side streams entering any absorbing stream must of course be an integer, Tokunaga's ratios are under no similar obligation since they are averages. Nevertheless, Tokunaga's law provides a good sense of the structure of a network albeit at a level of averages. One of our main objectives here is to go further and consider fluctuations about and the full distributions underlying the $\langle T_{\mu,\nu} \rangle$.

Finally, a third important observation of Tokunaga is that two of Horton's laws follow from Tokunaga's law, which we next discuss.

5.2.3   Horton's laws

We review Horton's laws [31, 58, 116] and then show how self-similarity and drainage density lead to Tokunaga's law, Horton's laws and hence all other river network scaling laws.

The relevant quantities for Horton's relations are n_ω, the number of order ω streams, and $\langle l_\omega \rangle$, the average main stream length (as opposed to stream segment length $\langle l_\omega^{(s)} \rangle$) of order ω basins. The laws are simply that the ratio of these quantities from order to order remain constant:

$$\frac{n_{\omega+1}}{n_\omega} = 1/R_n \quad \text{and} \quad \frac{\langle l_{\omega+1} \rangle}{\langle l_\omega \rangle} = R_l, \tag{5.2}$$

for $\omega \geq 1$. Note the definitions are chosen so that all ratios are greater than unity. The number of streams decreases with order while all areas and lengths grow.

A similar law for basin areas [58, 116] states that $\langle a_{\omega+1} \rangle / \langle a_\omega \rangle = R_a$ where $\langle a_\omega \rangle$ is the average drainage area of an order ω basin. However, with the assumption of uniform drainage density it can be shown that $R_n \equiv R_a$ [31] so we are left with the two independent Horton laws of equation (5.2).

As in [33], we consider another Horton-like law for stream segment lengths:

$$\frac{\left\langle l_{\omega+1}^{(s)} \right\rangle}{\left\langle l_\omega^{(s)} \right\rangle} = R_{l^{(s)}}. \tag{5.3}$$

As we will show, the form of the distribution of the variable $T_{\mu,\nu}$ is a direct consequence of the distribution of $l_\omega^{(s)}$.

Tokunaga showed that Horton's laws of stream number and stream length follow from what we have called Tokunaga's law, equation (5.1). For example, the solution of a difference equation relating the n_ω and the T_k leads to the result $R_n = A_T + [A_T^2 - 2R_T]^{1/2}$ where $A_T = (2 + R_T + T_1)/2$ for $\Omega = \infty$ and a more complicated expression is obtained for finite Ω [31, 102, 145, 146]. In keeping with our previous remarks on T_1, this expression for R_n shows that an increase in T_1 will increase R_n which, since $R_a \equiv R_n$, corresponds to a network where basins tend to be relatively broader. Our considerations will expand significantly on this connection between the network descriptions of Horton and Tokunaga.

5.3   The implications of a scaling law for drainage density

We now introduce a law for drainage density based on stream ordering. We write $\rho_{\mu,\nu}$ for the number of side streams of order ν per unit length of order μ

absorbing stream. We expect these densities to be independent of the order of the absorbing stream and so we will generally use ρ_ν. The typical length separating order ν side streams is then $1/\rho_\nu$. Assuming self-similarity of river networks, we must have

$$\rho_{\nu+1}/\rho_\nu = 1/R_\rho \qquad (5.4)$$

where $R_\rho > 1$ independent of ν.

All river network scaling laws in the planform may be seen to follow from this relationship. Consider an absorbing stream of order μ. Self-similarity immediately demands that the number of side streams of order $\mu - 1$ must be statistically independent of μ. This number is of course $\langle T_1 \rangle$. Therefore, the typical length of an order μ absorbing stream must be

$$\left\langle l_\mu^{(\mathrm{s})} \right\rangle = \langle T_1 \rangle / \rho_{\mu-1}. \qquad (5.5)$$

Using equation (5.4) to replace $\rho_{\mu-1}$ in the above equation, we find

$$T_1/\rho_{\mu-1} = R_\rho T_1/\rho_{\mu-2}. \qquad (5.6)$$

Thus, $T_2 = R_\rho T_1$ and, in general $T_k = (R_\rho)^{k-1} T_1$. This is Tokunaga's law and we therefore have

$$R_\rho \equiv R_T. \qquad (5.7)$$

Equation (5.4) and equation (5.5) also give

$$\left\langle l_\mu^{(\mathrm{s})} \right\rangle = T_1/\rho_{\mu-1} = R_\rho T_1/\rho_{\mu-2} = R_\rho \left\langle l_{\mu-1}^{(\mathrm{s})} \right\rangle. \qquad (5.8)$$

On comparison with equation (5.3), we see that the above is our Hortonian law of stream segment lengths and that

$$R_\rho \equiv R_{l^{(\mathrm{s})}}. \qquad (5.9)$$

As $R_{l^{(\mathrm{s})}}$ is the basic length-scale ratio in the problem, we rewrite equation (5.4), our Hortonian law of drainage density, as

$$\rho_{\nu+1}/\rho_\nu = 1/R_{l^{(\mathrm{s})}}. \qquad (5.10)$$

The above statement becomes our definition of the self-similarity of drainage density.

5.4   Basin allometry

Given that we have suggested the need for only a single relevant length ratio, we must remark here on basin allometry. Allometry refers to the relative growth or scaling of a shape's dimensions and was originally introduced in the context of biology [62]. A growth or change being allometric usually implies it is not self-similar. A longstanding issue in the study of river networks has been whether or not basins are allometric [35, 54, 110].

Consider two basins described by (L_1, W_1) and (L_2, W_2) within the same system where L_i is a characteristic longitudinal basin length and W_i a characteristic width. The basins being allometric means that $(W_1/W_2) = (L_1/L_2)^H$ where $H < 1$. Thus, two length ratios are needed to describe the allometry of basins. If we consider basins defined by stream ordering then we have the Horton-like ratios R_L and $R_W = R_L^H$. Now, when rescaling an entire basin, streams roughly aligned with a basin's length will rescale with the factor R_L and those perpendicular to the basin's axis will rescale differently with R_W. This creates a conundrum: how can basins be allometric ($R_L \neq R_W$) and yet individual streams be self-similar ($R_L = R_W$) as implied by Horton's laws?

We contend the answer is that allometry must be restricted to *directed networks* and that self-similarity of basins must hold for *non-directed networks*. This is in agreement with Colaiori et al. [19] who also distinguish between self-similar and allometric river basins although we stress here the qualification of directedness. Directed networks have a global direction of flow in which the direction of each individual stream flow has a positive component. A basic example is the random model of Scheidegger [112] which we describe below. For a directed network, $R_L = R_l$, and the rescaling of basin sizes matches up with the rescaling of stream lengths regardless of how the basin's width rescales since all streams are on average aligned with the global direction of flow. Hence, our premise that streams rescale in a self-similar way is general enough to deal with systems whose basins rescale in an allometric fashion.

In considering the allometry of basins, we must also address the additional possibility that individual stream lengths may scale non-trivially with basin length. In this case, the main stream length l would vary with the longitudinal basin length L as $l \propto L^d$. This is typically a weak dependence with $1.0 < d < 1.15$ [87, 143]. Note that Horton's laws still apply in this case. The exponent d plays a part in determining whether or not a basin scales allometrically. The exponent H introduced in the discussion of basin allometry can be found in terms of Horton's ratios (or equivalently Tokunaga's

parameters) and d as $H = d \ln R_n / \ln R_l - 1$ [31].

Thus, for a directed network $d = 1$ and $H \leq 1$ (e.g., Scheidegger [112]) whereas for undirected, self-similar networks $H = 1$ and $d \geq 1$ (e.g., random undirected networks [84, 85]). River networks are in practice often neither fully directed or undirected. Scaling laws observed in such cases will show deviations from pure scaling that may well be gradual and difficult to detect [32].

5.5   Tokunaga distributions

The laws of Tokunaga and Horton relate averages of quantities. In the remainder of this paper, we investigate the underlying distributions from which these averages are made. We are able to find general scaling forms of a number of distributions and in many cases also identify the basic form of the relevant scaling function.
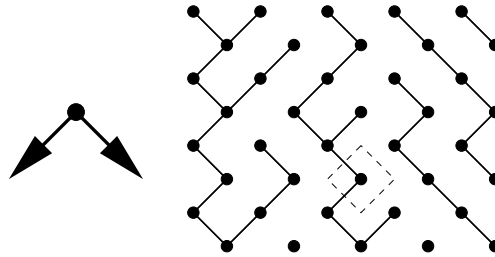
Figure 5.2: Scheidegger's random directed networks. Sites are arranged on a triangular lattice and stream flow is directed down the page. At each site, the flow direction is randomly chosen to be in one of the directions shown on the left. The dashed box indicates the area "drained" by the local site.

To aid and motivate our investigations, we examine, as we have done in both [32] and [33], a simple model of directed random networks that was first introduced by Scheidegger [112] Since we make much of use this model in the present work, we provide a self-contained discussion. Consider the triangular lattice of sites oriented as in Figure 5.2. At each site of the lattice a stream flow direction is randomly chosen between the two possible diagonal directions shown. It is therefore trivial to generate the model on a large scale, allowing for a thorough investigation of its river network statistics. The small, tilted box with a dashed boundary represents the area drained

by the enclosed site. As with many discrete-space models, the details of the underlying lattice are unimportant. On a square lattice, the model's streams would have three choices of flow, two diagonals and straight down the page. However, the choice of a triangular lattice does simplify implementation and calculation of statistics. For example, only one tributary can exist at each site along a stream and stream paths and basin boundaries are precisely those of the usual discrete-space random walk [39].

Since random walks are well understood, the exponents of many river network scaling laws are exactly known for the Scheidegger model [61, 138, 139, 140] and analogies may also be drawn with the Abelian sandpile model [26]. For example, a basin's boundaries being random walks means that a basin of length L will typically have a width $W \propto L^{1/2}$ which gives $H = 1/2$. Since the network is directed, stream length is the same as basin length, $l = L$, so we trivially have $d = 1$. Basin area a is estimated by $WL \propto L^{3/2} \propto l^{3/2}$ so $l \propto a^{2/3}$ giving Hack's law with an exponent of 2/3 [54].

Nevertheless, the Tokunaga parameters and the Horton ratios are not known analytically. Estimates from previous work [31] find $T_1 \simeq 1.35$, $R_l = R_T \simeq 3.00$ and $R_n \simeq 5.20$. Data for the present analysis was obtained on $L = 10^4$ by $W = 3 \times 10^3$ lattices with periodic boundaries. Given the self-averaging present in any single instance on these networks, ensembles of 10 were deemed sufficient.

We first examine the distributions of Tokunaga ratios $T_{\mu,\nu}$ and observe a strong link to the underlying distribution of $l_\mu^{(s)}$. Both are well described by exponential distributions. To understand this link, we next consider the distances between neighboring side streams of like order. This provides a measure of fluctuations in drainage density and again, exponential distributions appear. We are then in a position to develop theory for the joint probability distribution between the Tokunaga ratios and stream segment lengths and, as a result, the distribution for the quantity $T_{\mu,\nu}/l_\mu^{(s)}$ and its inverse. In the limit of large μ, the $T_{\mu,\nu}$ are effectively proportional to $l_\mu^{(s)}$ and all fluctuations of the former exactly follow those of the latter.

All investigations are initially carried out for the Scheidegger model where we may generate statistics of ever-improving quality. We find the same forms for all distributions for the Mississippi data (and for other river networks not presented here) and provide some pertinent examples. Perhaps the most significant benefit of the simple Scheidegger model is its ability to provide clean distributions whose form we can then search for in real data.

Figure 5.3 shows the distribution of the number of order $\nu = 2$ side
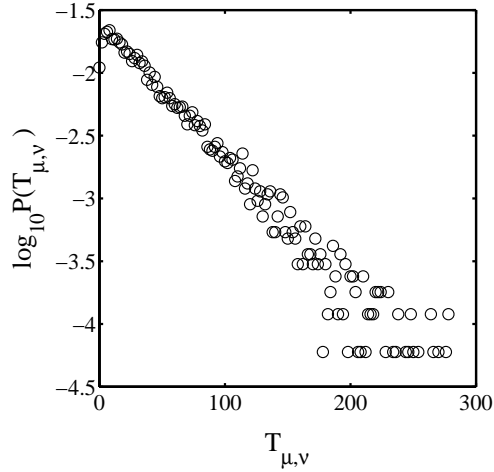
Figure 5.3: An example of a generalized Tokunaga distribution for the Scheidegger model. The Tokunaga ratio $T_{\mu,\nu}$ is the number of side streams of order ν entering an absorbing stream of order μ. For this particular example $\mu = 6$ and $\nu = 2$. The form is exponential and is a result of variations in stream segment length rather than significant fluctuations in side stream density.

streams entering an order $\mu = 6$ absorbing stream for the Scheidegger model. At first, it may seem surprising that this is not a single-peaked distribution centered around $\langle T_{\mu,\nu} \rangle$ dying off for small and large values of $T_{\mu,\nu}$.

The distribution of $T_{\mu,\nu}$ in Figure 5.3 is clearly well described by an exponential distribution. This can also be seen upon inspection of Figures 5.4(a) and 5.4(b). Figure 5.4(a) shows normalized distributions of $T_{\mu,\nu}$ for $\nu = 2$ and varying absorbing stream order $\mu = 4$, 5 and 6. These distributions (plus the one for absorbing stream order $\mu = 7$) are rescaled and presented in Figure 5.4(b). The single form thus obtained suggests a scaling form of the $T_{\mu,\nu}$ distribution is given by

$$P(T_{\mu,\nu}) = (R_{l^{(s)}})^{-\mu} F \left[T_{\mu,\nu} (R_{l^{(s)}})^{-\mu} \right]. \tag{5.11}$$

where F is an exponential scaling function. However, this only accounts for variations in μ, the order of the absorbing stream.

Figures 5.5(a) and 5.5(b) show that a similar rescaling of the distributions may be effected when ν is varied. In this case, the data is for the Mississippi. The rescaling is now by $R_{l^{(s)}}$ rather than $R_{l^{(s)}}^{-1}$ and equation (5.11) is improved
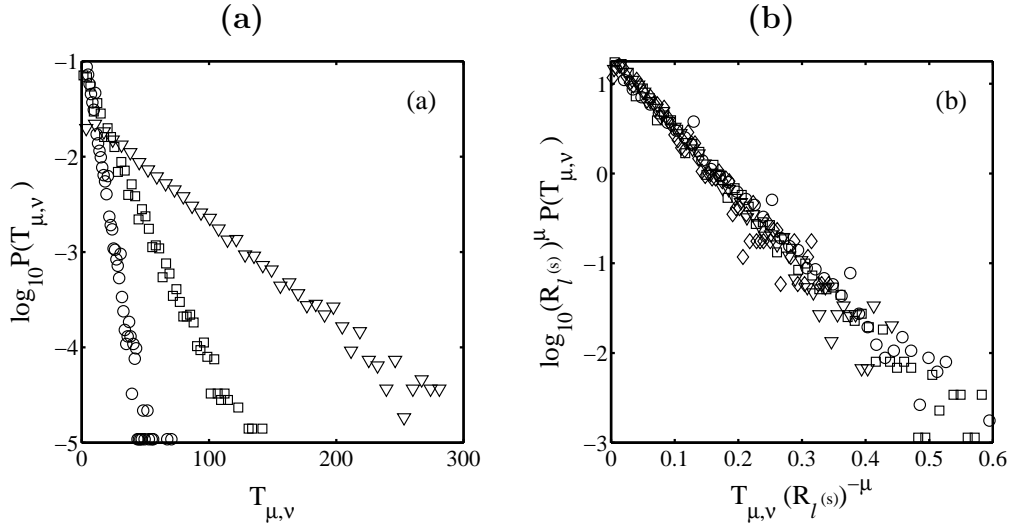
Figure 5.4:   Distributions for Tokunaga ratios for varying orders of absorbing stream and fixed side stream order of $\nu = 2$ for the Scheidegger network. In (a), examples of $T_{\mu,\nu}$ distributions for absorbing stream order $\mu = 4$ (circles), $\mu = 5$ (squares) and $\mu = 6$ (triangles). In (b), these distributions, as well as the $\mu = 7$ case, are rescaled according to equation (5.11). The resulting "data collapse" gives a single distribution. For the Scheidegger model, $R_{l^{(s)}} \simeq 3.00$.

to give

$$P(T_{\mu,\nu}) = (R_{l^{(s)}})^{\mu-\nu-1} P_T \left[T_{\mu,\nu}/(R_{l^{(s)}})^{\mu-\nu-1} \right]. \qquad (5.12)$$

The function P_T is a normalized exponential distribution independent of μ and ν,

$$P_T(z) = \frac{1}{\xi_t} e^{-z/\xi_t}, \qquad (5.13)$$

where ξ_t is the characteristic number of side streams of one order lower than the absorbing stream, i.e., $\xi_t = \langle T_1 \rangle$. For the Mississippi, we observe $\xi_t \simeq 1.1$ whereas for the Scheidegger model, $\xi_t \simeq 1.35$. As expected, the Tokunaga distribution is dependent only on $k = \mu - \nu$ so we can write

$$P(T_k) = (R_{l^{(s)}})^{k-1} P_T \left[T_{\mu,\nu}/(R_{l^{(s)}})^{k-1} \right]. \qquad (5.14)$$

with P_T as above.
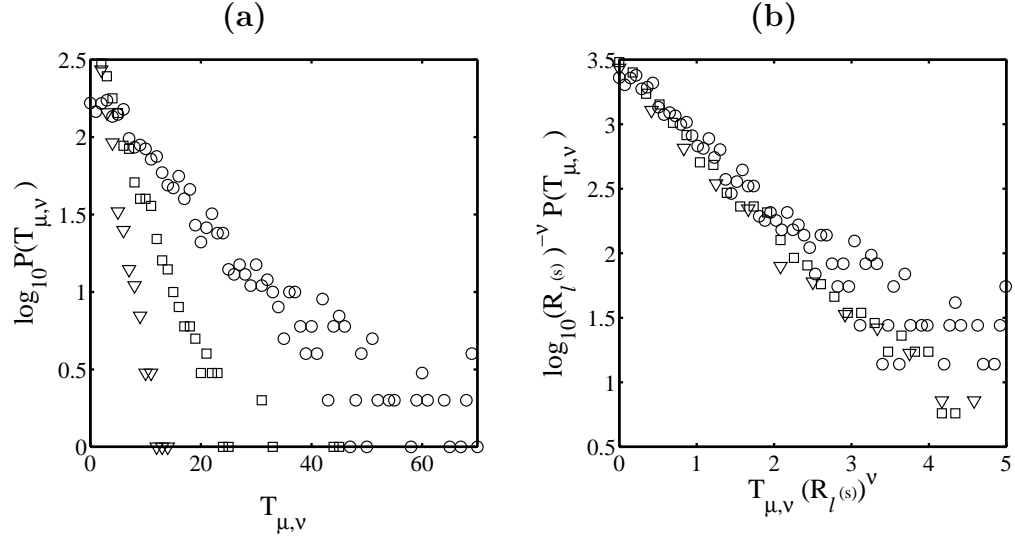
Figure 5.5: Tokunaga distributions for varying side stream orders for the Mississippi river basin. In both (a) and (b), the absorbing stream order is $\mu = 5$ and the side stream orders are $\nu = 2$ (circles), $\nu = 3$ (squares) and $\nu = 4$ (triangles). The raw distributions are shown in (a). In (b) the distributions are rescaled as per equation (5.12). For the Mississippi, the ratio is estimated to be $R_{l^{(s)}} \simeq 2.40$ [33].

5.6   Distributions of stream segment lengths and randomness

As we have suggested, the distributions of the Tokunaga ratios depend strongly on the distributions of stream segment lengths. Figure 5.6 is the indicates why this is so. The form of the underlying distribution is itself exponential. We have already examined this fact extensively in [33] and here we develop its relationship with the Tokunaga distributions.

Figures 5.6(a) and 5.6(b) show that the distributions of $l_\mu^{(s)}$ can be rescaled in the same way as the Tokunaga distributions. Thus, we write the distribution for stream segment lengths as [33]

$$P(l_\mu^{(s)}) = (R_{l^{(s)}})^{-\mu+1} P_{l^{(s)}} \left[l_\mu^{(s)} / (R_{l^{(s)}})^{-\mu+1} \right]. \tag{5.15}$$

As for P_T, the function $P_{l^{(s)}}$ is a normalized exponential distribution

$$P_{l^{(s)}}(z) = \frac{1}{\xi_{l^{(s)}}} e^{-z/\xi_{l^{(s)}}}, \tag{5.16}$$
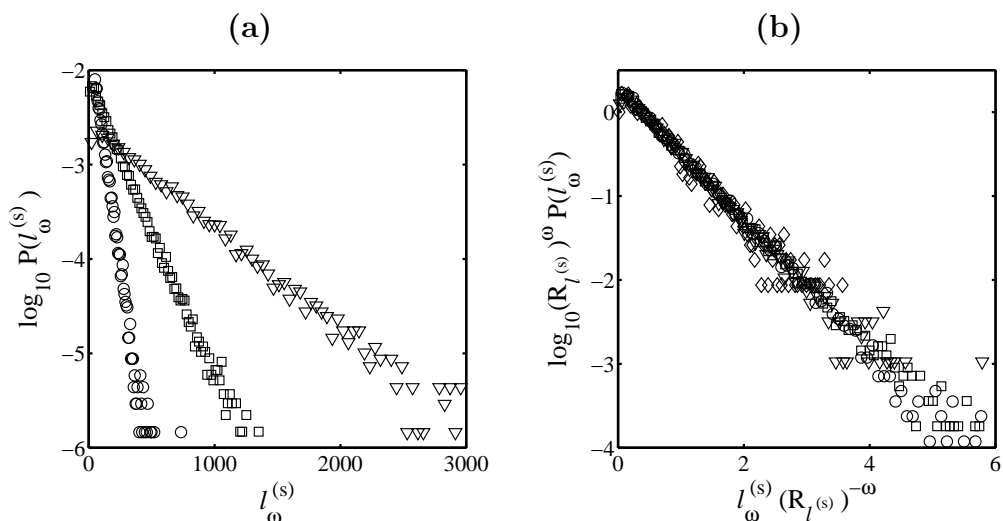
Figure 5.6: Stream segment length distributions for varying stream order for the Scheidegger model. Lengths are in units the lattice spacing. Shown in (a) are raw distributions for $\omega = 4$ (circles), $\omega = 5$ (squares) and $\omega = 6$. The linear forms on the semilogarithmic axes indication these distributions are well approximated by exponentials [33]. In (b), the distributions in (a) plus the distribution for $l_7^{(s)}$ (diamonds) are rescaled using equation (5.15).

where, in a strictly self-similar network, $\xi_{l^{(s)}}$ is the characteristic length of first-order stream segments, i.e., $\xi_{l^{(s)}} = \langle l_1^{(s)} \rangle$. (Note that in [33] we use ξ for $\xi_{l^{(s)}}$ for ease of notation). We qualify this by requiring the network to be exactly self-similar because in most models and all real networks this is certainly not the case. As should be expected, there are deviations from scaling for the largest and smallest orders. Therefore, $\xi_{l^{(s)}}$ is the characteristic size of a first-order stream as determined by scaling down the average lengths of those higher order streams that are in the self-similar structure of the network. It is thus in general different from $\langle l_1^{(s)} \rangle$.

We therefore see that the distributions of $T_{\mu,\nu}$ and $l_\mu^{(s)}$ are both exponential in form. Variations in $l_\mu^{(s)}$ largely govern the possible values of the $T_{\mu,\nu}$. However, $T_{\mu,\nu}$ is still only proportional to $l_\mu^{(s)}$ on average and later on we will explore the joint distribution from which these individual exponentials arise.

The connection between the characteristic number ξ_t and the length-scale

$\xi_{l^{(s)}}$ follows from equations (5.3), (5.5), and (5.10):

$$\xi_t = \rho_1 R_{l^{(s)}} \xi_{l^{(s)}}. \tag{5.17}$$

This presumes exact scaling of drainage densities and in the case where this is not so, ρ_1 would be chosen so that $(R_{l^{(s)}})^{\nu-1}\rho_1$ most closely approximates the higher order ρ_ν.

We come to an important interpretation of the exponential distribution as a composition of independent probabilities. Consider the example of stream segment lengths. We write $\tilde{p}_\mu$ as the probability that a stream segment of order μ meets with (and thereby terminates at) a stream of order at least μ. For simplicity, we assume only one side stream or none may join a stream at any site. We also take the lattice spacing α to be unity so that stream lengths are integers and therefore equate with the number of links between sites along a stream. For $\alpha \neq 1$, derivations similar to below will apply with $l_\mu^{(s)}$ replaced by $[l_\mu^{(s)}/\alpha]$, where $[\cdot]$ denotes rounding to the nearest integer. Note that extra complications arise when the distances between neighboring sites are not uniform.

Consider a single instance of an order μ stream segment. The probability of this segment having a length $l_\mu^{(s)}$ is given by

$$P(l_\mu^{(s)}) = \tilde{p}_\mu(1 - \tilde{p}_\mu)^{l_\mu^{(s)}}. \tag{5.18}$$

where $\tilde{p}_\mu$ is the probability that an order an order μ stream segment terminates on meeting a stream of equal or higher order. We can re-express the above equation as

$$P(l_\mu^{(s)}) \simeq \tilde{p}_\mu \exp\{-l_\mu^{(s)} \ln(1 - \tilde{p}_\mu)^{-1}\}, \tag{5.19}$$

and upon inspection of equations (5.15) and (5.16) we make the identification

$$(R_{l^{(s)}})^{\mu-1}\xi_{l^{(s)}} = [-\ln(1 - \tilde{p}_\mu)]^{-1}, \tag{5.20}$$

which has the inversion

$$\tilde{p}_\mu = 1 - e^{-1/(R_{l^{(s)}})^{\mu-1}\xi_{l^{(s)}}}. \tag{5.21}$$

For μ sufficiently large such that $\tilde{p}_\mu \ll 1$, we have the simplification

$$\tilde{p}_\mu \simeq 1/(R_{l^{(s)}})^{\mu-1}\xi_{l^{(s)}}. \tag{5.22}$$

We see that the probabilities satisfy the Horton-like scaling law

$$\tilde{p}_\mu/\tilde{p}_{\mu-1} = 1/R_{l^{(s)}}. \tag{5.23}$$

Thus, we begin to see the element of randomness in our expanded description of network architecture. The termination of a stream segment by meeting a larger branch is effectively a spatially random process.
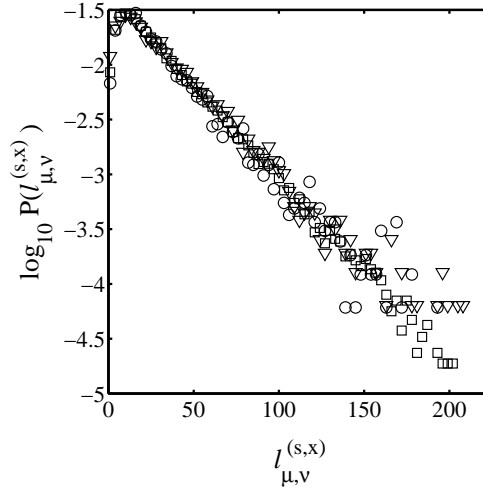
Figure 5.7: A comparison of inter-tributary length distributions for the Scheidegger model. The example here is for order $\mu = 6$ absorbing streams and order $\nu = 3$ side streams. Note that no rescaling of the distributions has been performed. The three length variables here correspond to x=b, x=i and x=e, i.e., $l_{\mu,\nu}^{(s,b)}$ (circles) $l_{\mu,\nu}^{(s,i)}$ (squares), and $l_{\mu,\nu}^{(s,e)}$ (triangles). These are the beginning, internal and end distances between entering side branches, defined fully in the text. No quantitative difference between these three lengths is observed.

5.7   Generalized drainage density

Having observed the similarity of the distributions of $T_{\mu,\nu}$ and $l_\mu^{(s)}$, we proceed to examine the exact nature of the relationship beteween the two. To do so, we introduce three new measures of stream length. These are $l_{\mu,\nu}^{(s,b)}$, the distance from the beginning of an order μ absorbing stream to the first order ν side stream; $l_{\mu,\nu}^{(s,i)}$, the distance between any two adjacent internal order ν side streams along an order μ absorbing stream; and $l_{\mu,\nu}^{(s,e)}$, the distance from the last order ν side stream to the end of an order μ absorbing stream. By analysis of these inter-tributary lengths, we will be able to discern the distribution of side stream location along absorbing streams. This leads directly to a more general picture of drainage density which we fully expand upon in the following section.

Figure 5.7 compares normalized distributions of $l_{\mu,\nu}^{(s,b)}$, $l_{\mu,\nu}^{(s,i)}$ and $l_{\mu,\nu}^{(s,e)}$ for the Scheidegger model. The data is for the distance between order $\nu = 3$ side streams entering order $\mu = 6$ absorbing streams. Once again, the
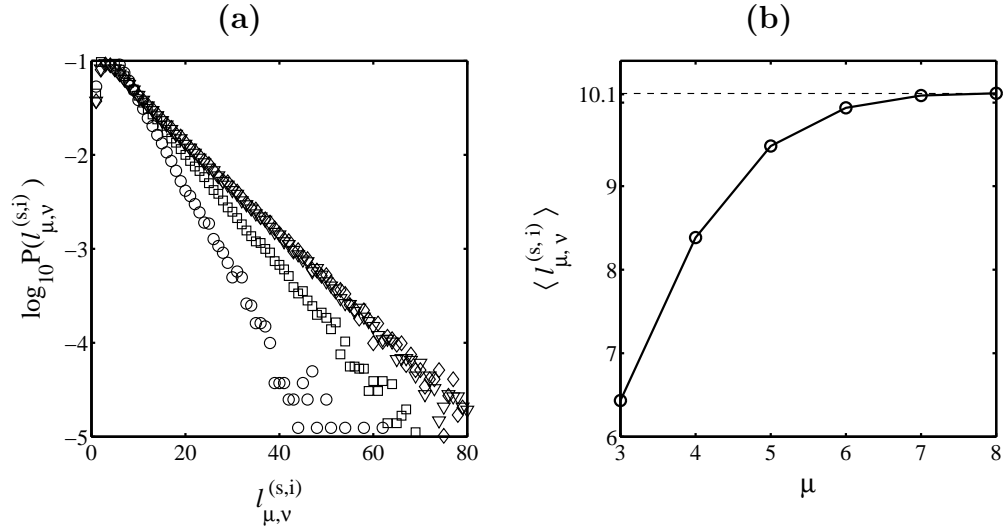
Figure 5.8: An examination of the asymptotic behavior of distributions of internal inter-tributary lengths. The data here is for the Scheidegger model for the case of fixed side stream order $\nu = 2$. The plot in (a) shows distributions for absorbing stream order $\mu = 3$ (circles), $\mu = 4$ (squares), $\mu = 6$ (triangles), and $\mu = 8$ (diamonds). As μ increases, the distributions, which are all individually exponential, tend towards a fixed exponential distribution. Since lower order stream segments have typically smaller lengths, they statistically block larger values of $l_{\mu,\nu}^{(s,i)}$, reducing the extent of the distribution tails for low μ. This is further evidenced in (b) which provides a plot of $\langle l_{\mu,\nu}^{(s,i)} \rangle$, the mean inter-tributary stream length, as a function of μ with $\nu = 2$. These mean values approach $\langle l_{\mu,\nu=2}^{(s,i)} \rangle = 1/\rho_2 \simeq 10.1$ where ρ_2 is the density of second-order side streams.

distributions are well approximated by exponential distributions. Moreover, they are indistinguishable. This indicates, at least for the Scheidegger model, that drainage density is independent of relative position of tributaries along an absorbing stream.

We now consider the effect on the distribution of internal inter-tributary distances $l_{\mu,\nu}^{(s,i)}$ following from variations in μ, the order of the absorbing stream. Figure 5.8(a) provides a comparison of $l_{\mu,\nu}^{(s,i)}$ distributions for $\nu = 2$ and $\mu = 3$ through $\mu = 8$. As μ increases, the distributions tend towards a limiting function. With increasing μ we are, on average, sampling absorbing streams of greater length and the full range of $l_{\mu,\nu}^{(s,i)}$ becomes accordingly more accessible. This approach to a fixed distribution is reflected in the means of

the distributions in Figure 5.8(a). Shown in Figure 5.8(b), the means $\langle l_{\mu,\nu}^{(s,i)} \rangle$ for $\nu = 2$ approach a value of around 10.1. The corresponding density of second-order streams for the Scheidegger model is thus $\rho_2 = 1/\langle l_{\mu,\nu=2}^{(s,i)} \rangle \simeq 0.01$. Higher drainage densities follow from equation (5.10). However, since deviations occur for small ν, there will also be an approach to uniform scaling to consider with drainage density.

5.8   Joint variation of Tokunaga ratios and stream segment length

We have so far observed that the individual distributions of the $l_\mu^{(s)}$ and $T_{\mu,\nu}$ are exponential and that they are related via the side-stream density $\rho_n u$. However, this is not an exact relationship. For example, given a collection of stream segments with a fixed length $l_\mu^{(s)}$ we expect to find fluctuations in the corresponding Tokunaga ratios $T_{\mu,\nu}$.

To investigate this further we now consider the joint variation of $T_{\mu,\nu}$ with $l_\mu^{(s)}$ from a number of perspectives. After discussing the full joint probability distribution $P(T_{\mu,\nu}, l_\mu^{(s)})$ we then focus on the quotient $v = T_{\mu,\nu}/l_\mu^{(s)}$ and its reciprocal $w = l_\mu^{(s)}/T_{\mu,\nu}$. The latter two quantities are measures of drainage density and inter-tributary length for an individual absorbing stream.

5.8.1   The joint probability distribution

We build the joint distribution of $P(T_{\mu,\nu}, l_\mu^{(s)})$ from our conception that stream segments are randomly distributed throughout a basin. In equation (5.18), we have the probability of a stream segment terminating after $l_\mu^{(s)}$ steps. We need to incorporate into this form the probability that the stream segment also has $T_{\mu,\nu}$ order ν side streams. Since we assume placement of these side streams to be random, we modify equation (5.18) to find

$$P(l_\mu^{(s)}, T_{\mu,\nu}) = \tilde{p}_\mu \binom{l_\mu^{(s)} - 1}{T_{\mu,\nu}} p_\nu^{T_{\mu,\nu}} (1 - p_\nu - \tilde{p}_\mu)^{l_\mu^{(s)} - T_{\mu,\nu} - 1}, \qquad (5.24)$$

where $\binom{n}{k} = n!/k!(n-k)!$ is the binomial coefficient and p_ν is the probability of absorbing an order ν side stream. The extra p_ν appears in the last factor $(1 - p_\nu - \tilde{p}_\mu)$ because this term is the probability that at a particular site the stream segment neither terminates nor absorbs an order ν side stream.

Also, it is simple to verify that the sum over $l_\mu^{(\mathrm{s})}$ and $T_{\mu,\nu}$ of the probability in equation (5.19) returns unity.

While equation (5.19) does precisely describe the joint distribution $P(l_\mu^{(\mathrm{s})}, T_{\mu,\nu})$, it is somewhat cumbersome to work with. We therefore find an analogous form defined for continuous rather than discrete variables. We simplify our notation by writing $p = p_\nu$, $q = (1 - p_\nu - \tilde{p}_\mu)$ and $\tilde{p} = \tilde{p}_\mu$. We also replace $(l_\mu^{(\mathrm{s})}, T_{\mu,\nu})$ by (x, y) where now $x, y \in \mathbb{R}$. Note that $0 \leq y \leq x - 1$ since the number of side streams cannot be greater than the number of sites within a stream segment.

Equation (5.19) becomes

$$P(x, y) = N\tilde{p}\frac{\Gamma(x)}{\Gamma(y+1)\Gamma(x-y)}(p)^y(q)^{x-y-1}, \tag{5.25}$$

where we have used $\Gamma(z + 1) = z!$ to generalize the binomial coefficient. We have included the normalization N to account for the fact that we have moved to continuous variables and the resulting probability may not be cleanly normalized. Also we must allow that $N = N(p, \tilde{p})$ and we will be able to identify this form more fully later on. Using Stirling's approximation [13], that $\Gamma(z + 1) \sim \sqrt{2\pi}z^{z+1/2}e^{-z}$, we then have

$$
\begin{aligned}
P(x, y) &= N\tilde{p}p^y q^{x-y-1}\frac{1}{\sqrt{2\pi}}\frac{(x-1)^{x-3/2}}{y^{y+1/2}(x-y-1)^{x-y-1/2}} \\
&= N\frac{\tilde{p}}{\sqrt{2\pi}q}p^y q^{x-y}(x-1)^{-1/2}\left(\frac{y}{x-1}\right)^{-y-1/2}\left(1 - \frac{y}{x-1}\right)^{-x+y+1/2} \\
&\simeq N'x^{-1/2}\left[F(y/x)\right]^x \tag{5.26}
\end{aligned}
$$

where we have absorbed N and all terms involving only p and $\tilde{p}$ into the prefactor $N' = N'(p, \tilde{p}) = N\tilde{p}/(\sqrt{2\pi}q)$. We have also assumed x is large such that $x - 1 \simeq x$ and $1 \gg 1/x \simeq 0$.

The function $F(v) = F(v; p, q)$ identified above has the form

$$F(v) = \left(\frac{1-v}{q}\right)^{-(1-v)}\left(\frac{v}{p}\right)^{-v}. \tag{5.27}$$

where $0 < v < 1$ (here and later, the variable v will refer to y/x). Note that for fixed x, the conditional probability $P(y \,|\, x)$ is proportional to $[F(y/x)]^x$. Figure 5.9(a) shows $[F(v)]^x$ for a range of powers x. The basic function has a single peak situated near $v = p$. For increasing x which corresponds to
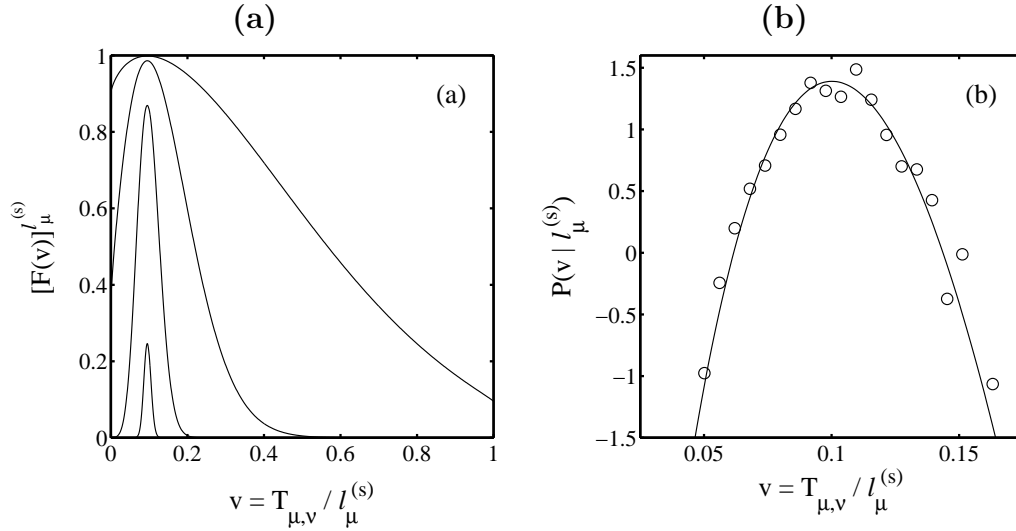
Figure 5.9: Form of the joint distribution of Tokunaga ratios and stream segment lengths. The distribution is given in equation (5.26) and is built around the function $F(v = T_{\mu,\nu}/l_\mu^{(s)})$ given in equation (5.27). Shown in (a) is $[F(v)]^{l_\mu^{(s)}}$ for $l_\mu^{(s)} = 1$, 10, 100 and 1000. Increasing $l_\mu^{(s)}$ corresponds to the focusing of the shape. In (b), the distribution $P(T_{\mu,\nu} \,|\, l_\mu^{(s)} \simeq 340)$ is compared between theory (smooth curve) and data from the Scheidegger model (circles). The Scheidegger model data is compiled for a range of values of $l_\mu^{(s)}$ rescaled as per equation (5.28).

increasing $l_\mu^{(s)}$, the peak becomes sharper approaching (when normalized) a delta function, i.e., $\lim_{x\to\infty}[F(v)]^x = \delta(v - p)$.

Figure 5.9(b) provides a comparison between data for the Scheidegger model and the analytic form of $P(l_\mu^{(s)}, T_{\mu,\nu})$. For this example, $\mu = 6$ and $\nu = 2$ which corresponds to $p \simeq 0.10$, $q \simeq 0.90$ and $\tilde{p} \simeq 0.001$ (using the results of the previous section). The smooth curve shown is the conditional probability $P(y \,|\, X)$ for the example value of $X = l_\mu^{(s)} \simeq 340$ following from equation (5.26). From simulations, we obtain a discretized approximation to $P(l_\mu^{(s)}, T_{\mu,\nu})$. For each fixed $x = l^{(s)}$ in the range $165 \lesssim l_\mu^{(s)} \lesssim 345$, we rescale the data using the following derived from equation (5.26),

$$P(X, y) = N' X^{-1/2} \left(N'^{-1} x^{1/2} P(x, y) \right)^{X/x}. \tag{5.28}$$

All rescaled data is then combined, binned and plotted as circles in Figure 5.9(b), showing excellent agreement with the theoretical curve.

5.8.2   Distributions of side branches per unit stream length

Having obtained the general form of $P(l_\mu^{(s)}, T_{\mu,\nu})$, we now delve further into its properties by investigating the distributions of the ratio $v = T_{\mu,\nu}/l_\mu^{(s)}$ and its reciprocal w.

The quantity $T_{\mu,\nu}/l_\mu^{(s)}$ is the number of side streams per length of a given absorbing stream and when averaged over an ensemble of absorbing streams gives

$$\left\langle T_{\mu,\nu}/l_\mu^{(s)} \right\rangle = \rho_\nu. \tag{5.29}$$

Accordingly, the reciprocal $l_\mu^{(s)}/T_{\mu,\nu}$ is the average separation of side streams of order ν.

First, we derive $P(T_{\mu,\nu}/l^{(s)})$ from $P(l_\mu^{(s)}, T_{\mu,\nu})$. We then consider some intuitive rescalings which will allow us to deduce the form of the normalization $N(p, q)$.

We rewrite equation (5.26) as

$$P(x, y) = N' x^{-1/2} \exp\left\{ -x \ln\left[-F(y/x) \right] \right\}. \tag{5.30}$$

We transform (x, y) to the modified polar coordinate system described by (u, v) with the relations

$$u^2 = x^2 + y^2 \qquad \text{and} \qquad v = y/x. \tag{5.31}$$

The inverse relations are $x = u/(1 + v^2)$ and $y = uv/(1 + v^2)$ and we also have $\mathrm{d}x\mathrm{d}y = x\mathrm{d}u\mathrm{d}v$. Equation (5.32) leads to

$$P(u, v) = N'\left(\frac{u}{1 + v^2}\right)^{1/2} \exp\left\{ -\frac{u}{1 + v^2} \ln\left[-F(v) \right] \right\}. \tag{5.32}$$

To find $P(v)$ we integrate out over the radial dimension u:

$$
\begin{aligned}
P(v) &= \int_{u=0}^{\infty} \mathrm{d}u\, P(u, v) \\
&= N' \int_{u=0}^{\infty} \mathrm{d}u \left(\frac{u}{1 + v^2}\right)^{1/2} \exp\left\{ -\frac{u}{1 + v^2} \ln\left[-F(v) \right] \right\} \\
&= N'(1 + v^2)(\ln[-F(v)])^{-3/2} \int_{z=0}^{\infty} \mathrm{d}z\, z^{1/2} e^{-z} \\
&= N'' \frac{1 + v^2}{(\ln[-F(v)])^{3/2}}. \tag{5.33}
\end{aligned}
$$
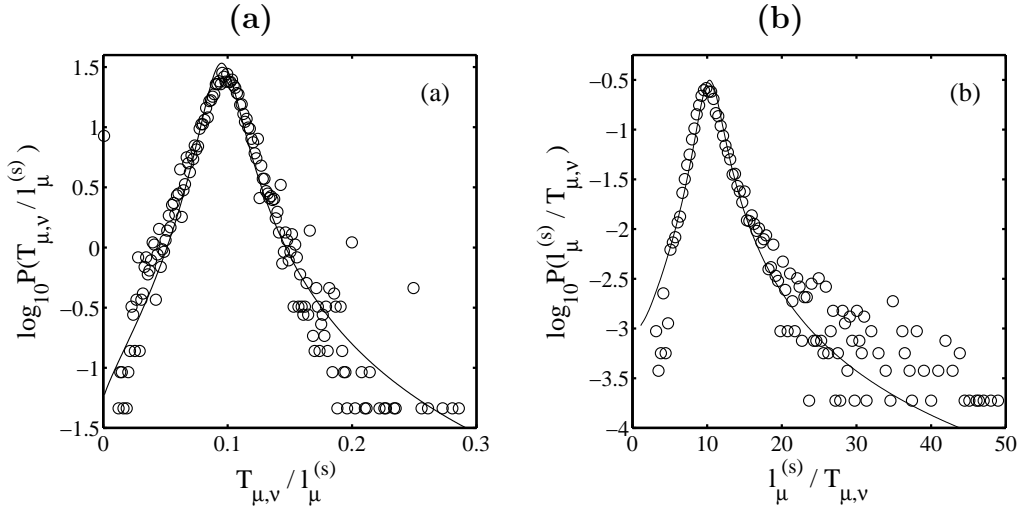
Figure 5.10: Comparison of theory with measurements of average inter-tributary distances for the Scheidegger model. The data in both (a) and (b) is for the case of order $\nu = 2$ side streams and order $\mu = 6$ absorbing streams. In (a), the distribution of $v = T_{\mu,\nu}/l_\mu^{(s)}$ obtained from the Scheidegger model (circles) is compared with the smooth curved predicted in equation (5.33). The same comparison is made for the reciprocal variable $w = l_\mu^{(s)}/T_{\mu,\nu}$, the predicted curve being given in equation (5.34).

Here, $N'' = N'\Gamma(3/2) = N'\sqrt{\pi}/2$ and we have used the substitution $z = u/(1+v^2)\ln[-F(v)]$.

The distribution for $w = l_\mu^{(s)}/T_{\mu,\nu} = 1/v$ follows simply from equation (5.33) and we find

$$P(w) = N''\frac{1+w^2}{w^4(\ln[-F(1/w)])^{3/2}}. \tag{5.34}$$

Figures 5.10(a) and 5.10(b) compare the predicted forms of $P(v)$ and $P(w)$ with data from the Scheidegger model. In both cases, the data is for order $\nu = 2$ side streams being absorbed by streams of order $\mu = 6$. Note that both distributions show an initially exponential-like decay away from a central peak. Moreover, the agreement is excellent, offering further support to the notion that the spatial distribution of stream segments is random.

Finally, we quantify how changes in the orders μ and ν affect the width of the distributions by considering some natural rescalings. Figure 5.11(a)
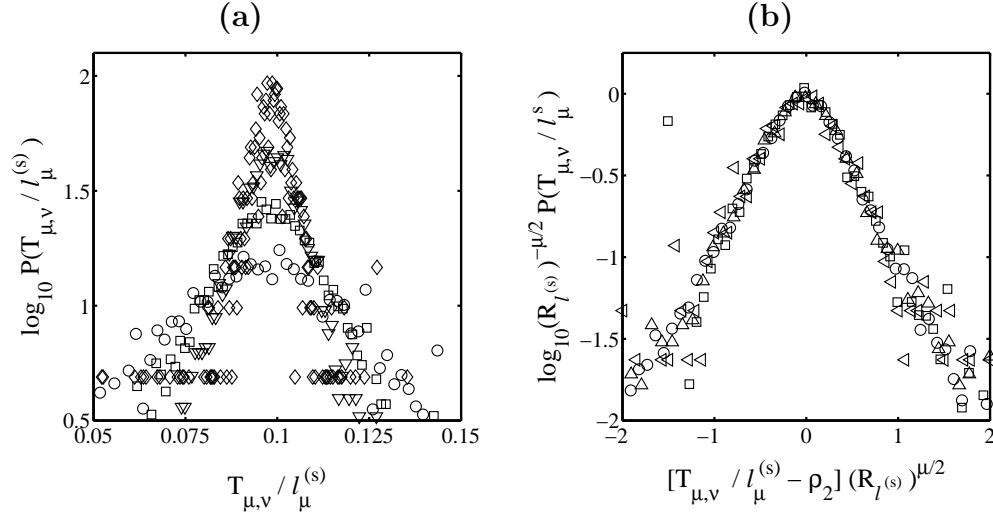
Figure 5.11: Distributions of the quantity $T_{\mu,\nu}/l_\mu^{(s)}$ for the Scheidegger model with μ, the order of the absorbing stream, varying and the side stream order fixed at $\nu = 2$. Given in (a) are unrescaled distributions for $\mu = 5$ (circles), $\mu = 6$ (squares), $\mu = 7$ (triangles), and $\mu = 8$ (diamonds). Note that as the order of the absorbing stream increases so does its typical length. This leads to better averaging and the standard deviation of the distribution decays as $R_l^{-\omega/2}$. The distributions are all centered near the typical density of order $\nu = 2$ side streams, $\rho_2 \simeq 0.10$. The rescaled versions of these distributions are given in (b) with the details as per equation (5.36).

shows binned, normalized distributions of $T_{\mu,\nu}/l_\mu^{(s)}$ for the Scheidegger model. Here, the side stream order is $\nu = 2$ and the absorbing stream orders range over $\mu = 5$ to $\mu = 8$. All distributions are centered around $\rho_2 \simeq 0.10$.

Because the average length of $l_\mu^{(s)}$ increases by a factor $R_{l^{(s)}}$ with μ, the typical number of side streams increases by the same factor. Since we can decompose $l_\mu^{(s)}$ as

$$l_\mu^{(s)} = l_{\mu,\nu}^{(s,\,b)} + l_{\mu,\nu}^{(s,\,i)} + \ldots + l_{\mu,\nu}^{(s,\,i)} + l_{\mu,\nu}^{(s,\,e)}, \qquad (5.35)$$

where there are $T_{\mu,\nu} - 1$ instances of $l_{\mu,\nu}^{(s,\,i)}$, $l_\mu^{(s)}$ becomes better and better approximated by $(T_{\mu,\nu} + 1)\langle l_{\mu,\nu}^{(s,\,i)}\rangle$.

Hence, the distribution of $T_{\mu,\nu}/l_\mu^{(s)}$ peaks up around ρ_2 as μ increases, the typical width reducing by a factor of $1/\sqrt{R_{l^{(s)}}}$ for every step in μ. Using this observation, Figure 5.11(b) shows a rescaling of the same distributions
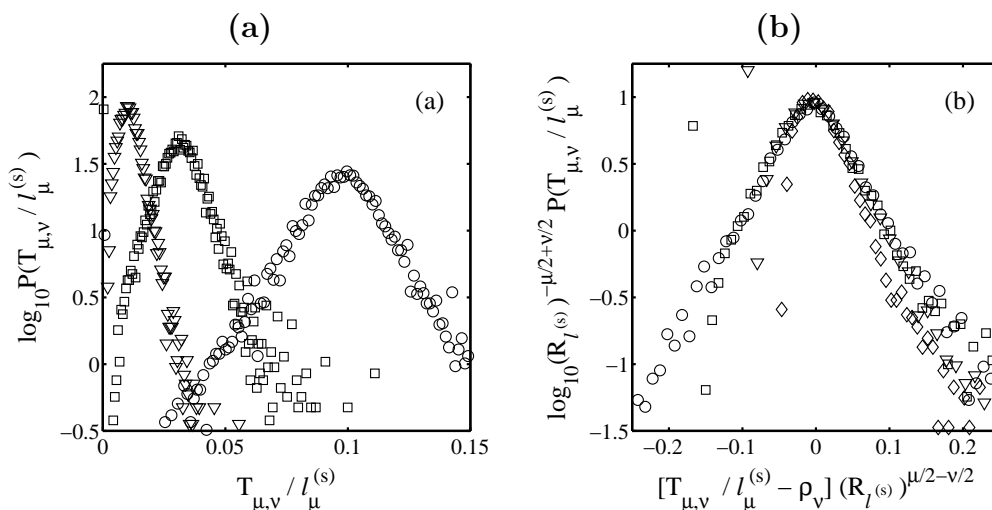
Figure 5.12: Distributions of number of side streams per unit length for the Scheidegger model with ν, the order of side streams, varying. For both (a) and (b), the absorbing stream order is $\mu = 6$. Shown in (a) are the unrescaled distributions for $\nu = 2$ (circles), $\nu = 3$ (squares), and $\nu = 4$ (triangles). Note that as ν increases, the mean number of side streams decreases as do the fluctuations. The distributions in (a) together with the distribution for $\nu = 5$ (diamonds) are shown rescaled in (b) as per equation (5.38).

shown in Figure 5.11(a). The form of this rescaling is

$$P(T_{\mu,\nu}/l_\nu^{(\mathrm{s})}) = (R_{l^{(\mathrm{s})}})^{\mu/2} G_1 \left([T_{\mu,\nu}/l_\nu^{(\mathrm{s})} - \rho_2](R_{l^{(\mathrm{s})}})^{\mu/2}\right) \qquad (5.36)$$

where the function is similar to the form of $P(v)$ given in equation (5.33). The mean drainage density of ρ_2 has been subtracted to center the distribution.

We are able to generalize this scaling form of the distribution further by taking into account side stream order. Figures 5.12(a) and 5.12(b) respectively show the unrescaled and rescaled distributions of $T_{\mu,\nu}/l_\mu^{(\mathrm{s})}$ with ν allowed to vary. This particular example taken from the Scheidegger model is for $\mu = 6$ and the range $\nu = 1$ to $\nu = 5$. Since ν is now changing, the centers are situated at the separate values of the ρ_ν. Also, the typical number of side streams changes with order ν so the widths of the distributions dilate as for the varying μ case by a factor $\sqrt{R_{l^{(\mathrm{s})}}}$. Notice that the rescaling works well for $\nu = 2, \ldots, 5$ but not $\nu = 1$. As we have noted, deviations from scaling
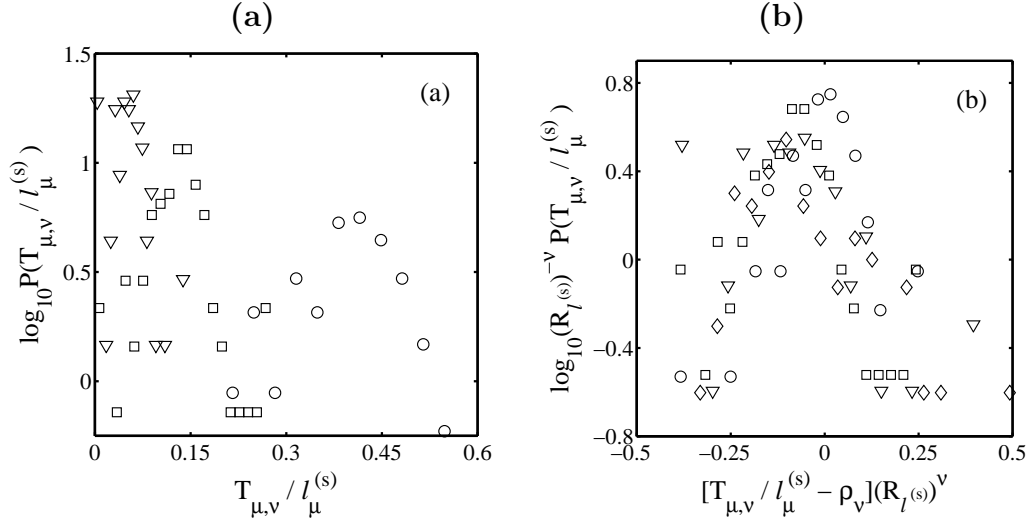
Figure 5.13: Tokunaga statistics for the Mississippi river basin. The distributions are as per Figure 5.12(a), distributions of number of side streams per unit length with ν, the order of side streams, varying. The absorbing stream order is $\mu = 7$ and the the individual distributions correspond to $\nu = 2$ (circles), $\nu = 3$ (squares) and $\nu = 4$ (triangles). All lengths are measured in meters. Rescalings of the distributions shown in (a) along with that for $\nu = 5$ (diamonds) are found in (b). Reasonable agreement with equation (5.38) is observed.

from small orders are to be expected. In this case, we are led to write down

$$P(T_{\mu,\nu}/l_\nu^{(s)})(R_{l^{(s)}})^{-\nu/2}G_2\left([T_{\mu,\nu}/l_\nu^{(s)} - \rho_\nu](R_{l^{(s)}})^{-\nu/2}\right) \qquad (5.37)$$

where, again, $G_2(z)$ is similar in form to $P(v)$.

We find the same rescalings apply for the Mississippi data. For example, Figure 5.13(a) shows unrescaled distributions of $T_{\mu,\nu}/l_\nu^{(s)}$ for varying ν. Figure 5.13(b) then shows reasonable agreement with the form of equation (5.37). In this case, the Scheidegger model clearly affords valuable guidance in our investigations of real river networks. The ratio $R_{l^{(s)}} = 2.40$ was calculated from an analysis of $l_\omega^{(s)}$ and l_ω. The density $\rho_2 \simeq 0.0004$ was estimated directly from the distributions of $T_{\mu,\nu}/l_\nu^{(s)}$ and means that approximately four second-order streams appear every ten kilometers.

Combining equations (5.38) and (5.38), we obtain the complete scaling form

$$P(T_{\mu,\nu}/l_\nu^{(s)}) = (R_{l^{(s)}})^{(\mu-\nu-1)/2}G\left([T_{\mu,\nu}/l_\nu^{(s)} - \rho_\nu](R_{l^{(s)}})^{(\mu-\nu-1)/2}\right). \qquad (5.38)$$

As per G_1 and G_2, the function G is similar in form to $P(v)$.

The above scaling form makes intuitive sense but is not obviously obtained from an inspection of (5.33). We therefore examine $P(v)$ by determining the position and magnitude of its maximum. Rather than solve $P'(v) = 0$ directly, we find an approximate solution by considering the argument of the denominator, $-\ln F(v)$, with $F(v)$ given in equation (5.27). Since the numerator of $P(v)$ is $1 + v^2$ and the maximum occurs for small v this is a justifiable step. Setting $dF/dv = 0$, we thus have

$$-\ln \frac{1-v}{q} + \ln vp = 0, \tag{5.39}$$

which gives $v_m = p/(q+p) = p/(1-\tilde{p})$. Note that for $\tilde{p} \ll 1$, we have $v_m \simeq p$.

Substituting $v = v_m = p/(1 - \tilde{p})$ into equation (5.33), we find

$$P(v_m) \simeq N'' \tilde{p}^{-3/2} = N\tilde{p}^{-1/2} 2^{-3/2} \tag{5.40}$$

presuming $p^2 \ll 1$ and $q \simeq 1$. Returning to the scaling form of equation (5.38), we see that the $\tilde{p}^{-1/2}$ factor in equation (5.40) accounts for the factors of $(R_{l^{(s)}})^{\mu/2}$ since $\tilde{p} = \tilde{p}_\mu$ scales from level to level by the ratio $R_{l^{(s)}}$. We therefore find the other factor $(R_{l^{(s)}})^{\nu/2}$ of equation (5.38) gives $N = cp^{1/2}$ where c is a constant. Since $p = p_\nu$, it is the only factor that can provide this variation. We thus have found the variation with stream order of the normalization N and have fully characterized, $P(x,y)$, the continuum approximation of $P(l_\mu^{(s)}, T_{\mu,\nu})$.

5.9   Concluding remarks

We have extensively investigated river network architecture as viewed in planform. We identify the self-similarity of a form of drainage density as the essence of the average connectivity and structure of networks. From previous work in [31], we then understand this to be a base from which all river network scaling laws may obtained.

We have extended the description of tributary structure provided by Tokunaga's law to find that side stream numbers are distributed exponentially. This in turn is seen to follow from the fact that the length of stream segments are themselves exponentially distributed. We interpret this to be consequence of randomness in the spatial distribution of stream segments. Furthermore, the presence of exponential distributions indicate fluctuations

in variables are significant being on the order of mean values. For the example of stream segment lengths, we thus identify $\xi_{l(\mathrm{s})}$, a single parameter needed to describe all moments. This is simply related to ξ_t, which describes the distributions of Tokunaga ratios. The exponential distribution becomes the null hypothesis for the distributions of these variables to be used in the examination of real river networks.

We are able to discern the finer details of the connection between stream segment length and tributary numbers. Analysis of the placement of side streams along a stream segment again reveals exponential distributions. We are then able to postulate a joint probability distribution for stream segment lengths and the Tokunaga ratios. The functional form obtained agrees well with both model and real network data. By further considering distributions of the number of side streams per unit length of individual stream segments, we are able to capture how variations in the separation of side streams are averaged out along higher-order absorbing streams.

By expanding our knowledge of the underlying distributions through empiricism, modeling and theory, we obtain a more detailed picture of network structure with which to compare real and theoretical networks. We have also further shown that the simple random network model of Scheidegger has an impressive ability to produce statistics whose form may then be observed in nature. Indeed, the only distinction between the two is the exact value of the scaling exponents and ratios involved since all distributions match up in functional form.

We end with a brief comment on the work of Cui et al. [22] who have recently also proposed a stochastic generalization of Tokunaga's law. They postulate that the underlying distribution for the $T_{\mu,\nu}$ is a negative binomial distribution. One parameter additional to T_1 and R_T, α, was introduced to reflect "regional variability," i.e., statistical fluctuations in network structure. This is in the same spirit as our identification of a single parameter ξ_t. However, our work disagrees on the nature of the underlying distribution of $T_{\mu,\nu}$. We have consistently observed exponential distributions for $T_{\mu,\nu}$ in both model and real networks.

In closing, by finding randomness in the spatial distribution of stream segments, we have arrived at the most basic description of river network architecture. Understanding the origin of the exact values of quantities such as drainage density remains an open problem.

Acknowledgements

CHAPTER **6**

Concluding remarks

The findings of the four papers that constitute this thesis provide a detailed framework through which to view river network geometry. Moreover, much of this framework has potential to be adapted to the analysis of other branching and non-branching networks. We have approached the study of river networks by combining what we identify as three principle avenues of scientific investigation: formulation of mathematical statements, numerical study of idealized models, and observation of empirical data. Ideas generated in each approach transfer to the others, speeding overall development.

The foundation of the thesis lies in our unification of river network scaling laws. From a few simple assumptions about the details of network architecture, we show that all scaling laws may be derived. The assumptions are that Tokunaga's law holds, individual stream paths may be self-affine and that networks are space-filling (drainage density is uniform). Importantly, we observe that the addition of the space-filling assumption implies that Horton's laws and Tokunaga's law are equivalent in their descriptive content. We show that Horton's laws reduce from three to two with the deduction that the stream number and area ratios are identical. Furthermore, we are able to revise previous notions of fractal dimensions for river networks.

This work also reduces the number of independent scaling exponents required to describe river networks to two. We have generally taken these to be (h, d), i.e., Hack's exponent and the scaling exponent for stream lengths. For most purposes, such as the identification of universality classes, this pair of exponents provides a suitable level of description. However, we also show that knowledge of scaling exponents cannot fully describe the details of network architecture. For example, Hack's exponent depends on the Horton ratios as $h = \ln R_l / \ln R_n$. Thus, we cannot retrieve the Horton ratios, or

equivalently, the Tokunaga parameters from knowledge of scaling laws only.

The thesis then proceeds to examine in depth a number of facets of this initial work. We first tackle Hack's law, the scaling of main stream length with area. We identify two major elements missing from a simple scaling law: fluctuations and deviations. We are able to go beyond fluctuations and postulate a form for the joint probability distribution of main stream lengths and areas, what we call the Hack distribution. As an aside, we find a form for the joint distribution of time to first return and area enclosed by a random walk. We further find fluctuations to be on the order of the mean values of mains stream lengths and basin areas. Reasonable but limited agreement with data from real world networks is observed. Regardless of the quality of the match, we identify the measurement of fluctuations as an important addition to the characterization of network structure.

The inclusion of fluctuations is a necessary first step towards the big picture view of Hack's law but we are still dealing with an idealized conception. We see the limitations to agreement with real world networks as being due to deviations from scaling. Focusing on the Kansas and Mississippi river basins, we find Hack's law to exhibit three distinctive behaviors at what we term small, intermediate and large scales.

At small scales, we find Hack's exponent to be unity due to the presence of long, narrow sub-networks. The extent of this regime will vary from landscape to landscape. We observe that the hillslope scale, of which the range of this linearity might feasibly be an estimate, is generally masked by larger, linear sub-networks.

A crossover in scaling links Hack's law at small scales to its form at intermediate scales. Here, where we expect to be able to measure Hack's exponent, we actually observe slow drifts in local measurements of the Hack exponent. So while the scaling appears to be robust at first glance, our deeper examination finds it to be only an approximate scaling. The existence of such trends bar us from assigning precise values of scaling exponents to these river networks. This also partly explains the variation of scaling exponents recorded in the literature. Without consideration of these slow trends and the deviations at small and large scales, the values of measured exponents must be reconsidered. Indeed, we observe the range of even this approximate scaling region is much reduced from the overall span of basin sizes. Moreover, we observe that the average value of Hack's exponent through this region varies from basin to basin. All of this is significant since we cannot then hope to identify a universality class to which all river networks belong.

At large scales, we are able to find suggestions of the origin of the slow

trends at intermediate scales. We find that local values of Hack's exponent fluctuate strongly at large scales. We observe that this is partly due to the statistical growth of fluctuations of main stream lengths and basin areas. However, we find these fluctuations are correlated with overall basin shape. In terms of stream ordering, the highest two differences in Hack's law show significant correlations in all cases we examine. This implies that internal basin shapes one to two orders of magnitude smaller in area than the overall basin can be affected by the outer shape.

We observe that basin shapes result from statistical fluctuations (chance) and geology with varying degrees of either component. Where the latter is dominant, we see that geology is not "washed out" of overall network structure but is subtly reflected in scaling law deviations. We see this as the beginning of a more complicated but ulimately more satisfactory approach to the understanding of river network statistics.

This takes us to the halfway point of the thesis. In the last two chapters we generalize Horton's laws and Tokunaga's law. The former is seen as a description of network components, how they change in number and size with stream order. We take these Horton relations of mean quantities and extend them to relations between probability distribution functions. We postulate the basic forms of these distributions and find good agreement between theory and observations of real data and the Scheidegger model. We start from the empirical observation that stream segment lengths have exponential distributions. From this, we develop analytic connections to distributions of main stream lengths for fixed stream order and then to power law distributions of main stream lengths without stream ordering. From a practical point of view, we put forward the utility of measuring fluctuations and higher order moments for all of these distributions.

Our observation that stream segment lengths are exponential connects well with our generalization of Tokunaga's law, the basic expression of network architecture. Here, we rephrase the work done in chapter 2 to place scaling of drainage density as the central assumption needed to derive Tokunaga's law and hence all other laws. Looking more deeply into network structure, we show that the presence of exponential distributions implies that stream segments are distributed randomly throughout a basin. We thus reach the lowest level at which description of network architecture is still meaningful.

In particular, we find side streams to be distributed randomly along absorbing streams which themselves terminate with fixed probability. This leads to a joint probability distribution between the number of side streams

and the length of an absorbing stream. We reduce this to a distribution of the ratio of these two variables and their inverse. In all cases, we find excellent agreement with our predictions and Scheidegger's model and, though the data is more sparse, with real networks.

Throughout the thesis, we find great motivation in the Scheidegger model. We consider this to be for river networks what the Ising model is for phase transitions, [49, 60]. Along with its connection to many problems in random walks, we find all forms of network statistics to be embodied by the Scheidegger model. Differences between it and the real world come down to parameters. We would hope that this thesis raises the Scheidegger model to a position of greater respect.

But a model is still a model and this thesis also makes substantial efforts to analyze real world river networks. Indeed, one of the attractions of studying river networks is the availability of large-scale topographic datasets. Nevertheless, even though we have been able to extract very good statistics, future higher resolution datasets promise to allow more and more refinement of our comparisons between reality and theory.

Ultimately, we hope that the advances made here and elsewhere in the quantification of river network geometry will be linked with dynamic theories of network evolution. Several directions of interest lie open.

We have shown that geology entwines itself with the forms of network scaling laws. Any simple theory of network evolution will have to contend with this issue. Here, we have been able to show overall basin shape correlates with large scale deviations of Hack's law. With more extensive studies of real networks, we may begin to further understand this entanglement and eventually be able to separate geology from simple physics.

A natural question about river networks regards their connection with their ambient topography. How does the structure of networks relate to the structure of a surface? The surface itself must encode a great deal more information than the network. By considering large-scale networks we have avoided this problem but for small-scale networks where vertical range is significant, this is an intriguing problem.

Beyond these considerations of static structures, there is the eventual need for dynamical theories of networks and surfaces whose time-dependent aspects may be tested by accessible data. The sticking point here is of course the availability of such data. Two possibilities arise here. If the geologic

history of a region are understood, it should be possible to identify basin shapes of, say, tectonic origins into which networks have grown. This gives an initial structure for models to be tested on. Comparisons would have to be done largely at a statistical level due to the randomness we have observed underlying any network structure.

Secondly, with constantly updated, inexpensive, remotely-sensed topographic data of sufficiently fine resolution, the recording of subtle changes in the earth's topography over long time scales becomes a possibility. This is possibly best done by tracking changes in mature river network structure. These changes occur largely in the position of channel heads and can be sensitive to, for example, changes in climate over small time-scales.

Some wandering thoughts on the maturity of a science. In my estimation, we enjoy a universe about which we have started to collate a concrete core of knowledge. Newton's laws, for example, have held firm within a broad realm of behavior. They have stood up to become kernels of isometric truth rather than be swept away by differing conceptions of reality. The extraordinary discoveries of quantum behavior and general relativity have come as extensions rather than refutations.

The creation of a firm, inner core of theory is one possible definition of a hardening of a science. There has long been a distinction made between hard and soft sciences, a distinction that has not always been taken as a pleasurable one. Indeed, there is the not unreasonable implication that hard is solid and right while soft is plastic and unformed.

But the further attachment of estimates of worth is unreasonable. For example, biology (piano) deals with problems of marvelous complexity that are fundamental in the understanding of consciousness and intelligence. General relativity (forte), sharing a happy kinship with mathematics as it does, thrives on exactness and rigidity. Which is more difficult? Is biology simply a younger science that will mature with time and be subsumed into physics departments?

From a general scientific perspective, we want to lay bare the underlying mechanisms that give rise to what we observe. For example, the mechanisms in fluid dynamics are, for the most part, encapsulated in the Navier-Stokes equations. In biology, there seems to be a molecule for every action, part of an enormous tool box generated by the experimentation of evolution. We are naturally led in biology to cataloging, working to locate broad patterns.

In all of science, we find many levels of description. Most desirable is to start at one level and, working by reason and logic, be able to describe the next higher one. We constantly descend further into the onion, looking for the axiomatic kernel that will lay bare the reasons for the onion itself. And maybe many other vegetables as well.

Perhaps a better alternative to the poles of hard and soft is to consider the universality of principles. How fragmented is a science's description? How many axioms are required to generate the patterns of a given level from the level below?

There is no magic in the world, just causal mechanisms. One of course cannot prove this but simply appeal to the idea of taking this as the most natural premise. And so it is an amusing and potent feature of consciousness that through billions of neural interconnections and the intricacies of history, we can nevertheless so easily map reality into a world of magical actions. The task of the scientist is often to unravel that which appears to involve illusion. And, for a lack of understanding of the mind, it is this task that, above everything else, most closely resembles sorcery.

Appendix A

Analytic treatment of generalized Horton's laws

A.1 Analytic connections between stream length distributions

In this appendix we consider a series of analytic calculations. These concern the connections between the distributions of stream segment lengths $l_\omega^{(s)}$, ordered basin main stream lengths l_ω and main stream lengths l. We will idealize the problem in places, assuming perfect scaling and infinite networks while making an occasional salubrious approximation. Also, we will treat the problem of lengths fully noting that derivations of distributions for areas follow similar but more complicated lines.

We begin by rescaling the form of stream segment length distributions

$$P(l_\omega^{(s)}, \omega) = (R_n - 1)(R_n R_{l^{(s)}})^{-\omega} F_{l^{(s)}}(l R_{l^{(s)}}^{-\omega}). \tag{A.1}$$

The normalization $c_{l^{(s)}} = R_n - 1$ stems from the requirement that

$$\int_{u=0}^{\infty} F_{l^{(s)}}(u) = 1, \tag{A.2}$$

which is made purely for aesthetic purposes. As we have suggested in equation (4.8) and demonstrated empirical support for, $F_{l^{(s)}}(u)$ is well approximated by the exponential distribution $\xi^{-1} e^{-u/\xi}$. For low u and also we have noted that deviations do of course occur but they are sufficiently insubstantial as to be negligible for a first order treatment of the problem.

A.1.1 Distributions of main stream lengths as a function of stream order

We now derive a form for the distribution of main stream lengths $P(l_\omega|\omega)$. As we have discussed, since $l_\omega = \sum_{i=1}^{\omega} l_\omega^{(\mathrm{s})}$, we have the convolution (4.9). The right-hand side of equation (4.9) consists of exponentials as per equation (4.8) so we now consider the function $K_\omega(u; \vec{a})$ given by

$$K_\omega(u; \vec{a}) = a_1 e^{-a_1 u} * a_2 e^{-a_2 u} * \cdots * a_\omega e^{-a_\omega u}, \tag{A.3}$$

where $\vec{a} = (a_1, a_2, \ldots, a_\omega)$. We are specifically interested in the case when no two of the a_i are equal, i.e., $a_i \neq a_j$ for all $i \neq j$. To compute this ω-fold convolution, we simply examine the $K_\omega(u; \vec{a})$ for $\omega = 2$ and $\omega = 3$ and identify the emerging pattern. For $\vec{a} = (a_1, a_2)$ we have, omitting the prefactors for the time being,

$$
\begin{aligned}
& e^{-a_1 u} * e^{-a_2 u} \\
&= \frac{e^{-a_1 u} - e^{-a_2 u}}{a_1 - a_2} = \frac{e^{-a_1 u}}{a_1 - a_2} + \frac{e^{-a_2 u}}{a_2 - a_1}
\end{aligned}
\tag{A.4}
$$

providing $a_1 \neq a_2$. Convolving this with $e^{-a_3 u}$ we obtain

$$
\begin{aligned}
e^{-a_1 u} * e^{-a_2 u} * e^{-a_3 u} &= \left(\frac{e^{-a_1 u} - e^{-a_2 u}}{a_1 - a_2} \right) * e^{-a_3 u} \\
&= \frac{e^{-a_1 u} - e^{-a_3 u}}{(a_1 - a_2)(a_1 - a_3)} - \frac{e^{-a_2 u} - e^{-a_3 u}}{(a_1 - a_2)(a_2 - a_3)}, \\
&= \frac{e^{-a_1 u}}{(a_1 - a_2)(a_1 - a_3)} + \\
& \quad \frac{e^{-a_2 u}}{(a_2 - a_1)(a_2 - a_3)} + \frac{e^{-a_3 u}}{(a_3 - a_1)(a_3 - a_2)}.
\end{aligned}
\tag{A.5}
$$

Generalizing from this point, we obtain

$$K_\omega(u; \vec{a}) = \left(\prod_{i=1}^{\omega} a_i \right) \sum_{i=1}^{\omega} \frac{e^{-a_i u}}{\prod_{j=1, j \neq i}^{\omega} (a_i - a_j)}. \tag{A.6}$$

Now, setting $a_i = 1/(\xi (R_{l^{(\mathrm{s})}})^{i-1})$ and carrying out some manipulations we

obtain the following expression for $P(l_\omega, \omega)$:

$$
\begin{aligned}
P(l_\omega, \omega) &= \frac{1}{(R_n)^\omega} \frac{1}{\prod_{j=1}^\omega \xi(R_{l^{(s)}})^{i-1}} \sum_{i=1}^\omega \frac{e^{-l_\omega/\xi(R_{l^{(s)}})^{i-1}}}{\prod_{j=1,j\neq i}^\omega (1/\xi(R_{l^{(s)}})^{i-1} - 1/\xi(R_{l^{(s)}})^{j-1})} \\
&= \frac{1}{(R_n)^\omega} \frac{1}{\xi^\omega \prod_{j=1}^\omega (R_{l^{(s)}})^{j-1}} \sum_{i=1}^\omega e^{-l_\omega/\xi(R_{l^{(s)}})^{i-1}} \xi^{\omega-1} \frac{\prod_{j=1,j\neq i}^\omega (R_{l^{(s)}})^{i-1} \prod_{j=1,j\neq i}^\omega (R_{l^{(s)}})^{j-1}}{\prod_{j=1,j\neq i}^\omega (R_{l^{(s)}})^{j-1} - (R_{l^{(s)}})^{i-1}}, \\
&= \frac{1}{(R_n)^\omega} \frac{\xi^{\omega-1}}{\xi^\omega} \sum_{i=1}^\omega e^{-l_\omega/\xi(R_{l^{(s)}})^{i-1}} \frac{(R_{l^{(s)}})^{-2(i-1)} \prod_{j=1}^\omega (R_{l^{(s)}})^{i-1} \prod_{j=1}^\omega (R_{l^{(s)}})^{j-1} \prod_{k=1}^\omega (R_{l^{(s)}})^{-(j-1)}}{(R_{l^{(s)}})^{-(\omega-1)} \prod_{j=1,j\neq i}^\omega (R_{l^{(s)}})^j - (R_{l^{(s)}})^i}, \\
&= \frac{1}{(R_n)^\omega} \frac{1}{\xi} \sum_{i=1}^\omega e^{-l_\omega/\xi(R_{l^{(s)}})^{i-1}} \frac{(R_{l^{(s)}})^{(i-1)(\omega-2)} (R_{l^{(s)}})^{\omega-2}/R_{l^{(s)}}}{\prod_{j=1,j\neq i}^\omega (R_{l^{(s)}})^j - (R_{l^{(s)}})^i}, \\
&= \frac{1}{(R_n)^\omega} \frac{1}{\xi R_{l^{(s)}}} \sum_{i=1}^\omega e^{-l_\omega/\xi(R_{l^{(s)}})^{i-1}} \frac{(R_{l^{(s)}})^{i(\omega-2)}}{\prod_{j=1,j\neq i}^\omega (R_{l^{(s)}})^j - (R_{l^{(s)}})^i}
\end{aligned}
\tag{A.7}
$$

Note that we have added in a factor of $1/(R_n)^\omega$ for the appropriate normalization. In addition, one observes that $P(0, \omega) = 0$ for all $\omega > 1$ since all convolutions of pairs of exponentials vanish at the origin. Furthermore, the tail of the distribution is dominated by the exponential corresponding to the largest stream segment.

The next step is to connect to the power law distribution of main stream lengths, $P(l)$ (see Figure 4.7 and the accompanying discussion). On considering equation (4.10) we see that the problem can possibly be addressed with some form of asymptotic analysis.

Before attacking this calculation however, we will simplify the notation keeping only the important details of the $P(l_\omega, \omega)$. Our main interest is to see how equation (4.10) gives rise to a power law. We transform the outcome of equation (A.7) by using $n = \omega$, $u = l_\omega/\xi$, $r = R_{l^{(s)}}$, and $s = R_n$, neglecting multiplicative constants and then summing over stream orders to obtain

$$
G(u) = \sum_{n=1}^\infty \frac{1}{s^n} \sum_{i=1}^n \frac{r^{(n-2)i} e^{-u/r^{i-1}}}{\prod_{j=1,j\neq i}^n (r^j - r^i)}.
\tag{A.8}
$$

The integration over l_ω has been omitted meaning that the result will be a power law with one power lower than expected.

A.1.2   Power law distributions of main stream lengths

We now show that this sum of exponentials $G(u)$ in equation (A.8) does in fact asymptotically tend to a power law. We first interchange the order of

summation replacing $\sum_{n=1}^{\infty} \sum_{i=1}^{n}$ with $\sum_{i=1}^{\infty} \sum_{n=i}^{n}$ to give

$$
\begin{aligned}
G(u) &= \sum_{i=1}^{\infty} e^{-u/r^{i-1}} \sum_{n=1}^{\infty} \frac{r^{(n-2)i}}{s^n \prod_{j=1,j\neq i}^{n}(r^j - r^i)}, \\
&= \sum_{i=1}^{\infty} C_i e^{-u/r^{i-1}}.
\end{aligned}
\tag{A.9}
$$

We thus simply have a sum of exponentials to contend with. The coefficients C_i appear unwieldy at first but do yield a simple expression after some algebra which we now perform:

$$
\begin{aligned}
C_i &= \sum_{n=1}^{\infty} \frac{r^{(n-2)i}}{s^n \prod_{j=1,j\neq i}^{n}(r^j - r^i)}, \\
&= \frac{1}{\prod_{j=1}^{i-1}(r^j - r^i)} \sum_{n=i}^{\infty} \frac{r^{(n-2)i}}{s^n \prod_{j=i+1}^{n}(r^j - r^i)}, \\
&= \frac{r^{(i-2)i}}{\prod_{j=1}^{i-1}(r^j - r^i)} \frac{1}{s^i} \sum_{n=i}^{\infty} \frac{s^i r^{(n-2)i} r^{-(i-2)i}}{s^n \prod_{j=i+1}^{n}(r^j - r^i)}, \\
&= \frac{1}{\prod_{j=1}^{i-1} r^{-i}(r^j - r^i)} \frac{r^{-i}}{s^i} \sum_{n=i}^{\infty} \frac{r^{(n-i)i}}{s^{n-i} \prod_{j=i+1}^{n}(r^j - r^i)}, \\
&= \frac{1}{\prod_{j=1}^{i-1}(r^{j-i} - 1)} \frac{1}{r^i s^i} \sum_{n=i}^{\infty} \frac{1}{\prod_{j=i+1}^{n} s r^{-i}(r^j - r^i)}, \\
&= \frac{1}{r^i s^i} \frac{1}{\prod_{j=1}^{i-1}(r^{j-i} - 1)} \sum_{n=i}^{\infty} \prod_{j=i+1}^{n} \frac{1}{s(r^{j-i} - 1)}, \\
&= \frac{1}{r^i s^i} \frac{1}{\prod_{j=1}^{i-1}(r^{j-i} - 1)} \sum_{n=i}^{\infty} \prod_{j=i+1}^{n} \frac{1}{s(r^{j-i} - 1)}, \\
&= \frac{1}{r^i s^i} \left(\frac{-1}{\prod_{k=1}^{i-1}(1 - r^{-k})} \right) \left(\sum_{m=1}^{\infty} \prod_{k=1}^{m} \frac{1}{s(r^k - 1)} \right).
\end{aligned}
\tag{A.10}
$$

In reaching the last line we have shifted the indices in several places. In the last bracketed term we have set $k = j - i$ and then $m = n - i$ while in the first bracketed term, we have used $-k = j - i$. Immediately of note is that the last term is independent of i and may thus be ignored.

The first bracketed term does depend on i but converges rapidly. Writing $D_i = \prod_{k=1}^{i-1}(1 - r^{-k})$ we have that $D_i = D_m \prod_{k=m}^{i-1}(1 - r^{-k})$. Taking m to be

fixed and large enough such that $1 - r^{-k}$ is approximated well by $\exp\{-r^{-k}\}$ for $k \geq m$, we then have

$$
\begin{aligned}
D_i &= D_m \exp\left\{\sum_{k=m}^{i-1} -r^{-k}\right\}, \\
&= D_m \exp\left\{\frac{r^{1-m}}{(r-1)}(1 - 1/r^{i-m-1})\right\}.
\end{aligned}
\tag{A.11}
$$

As $i \to \infty$, D_i clearly approaches a product of D_m and a constant. Therefore, the first bracketed term in equation (A.10) may also be neglected in an asymptotic analysis.

Hence, as $i \to \infty$, the coefficients C_i are simply given by

$$
C_i \propto \frac{1}{s^i r_i}.
\tag{A.12}
$$

and we can approximate $G(u)$ as, boldly using the equality sign,

$$
G(u) = AS(u) = A \sum_{i=0}^{\infty} \frac{e^{-u/r^i}}{r^{i(1+\gamma)}},
\tag{A.13}
$$

where A comprises the constant part of the C_i and factors picked up by shifting the lower limit of the index i from 1 to 0. We have also used here the identification

$$
s = r^{\gamma}.
\tag{A.14}
$$

We turn now to the asymptotic behavior of $S(u)$, this being the final stretch of our analysis

There are several directions one may take at this point. We will proceed by employing a transformation of $S(u)$ that is sometimes referred to as the Sommerfeld-Watson transformation and also as Watson's lemma [16, p. 239]. Given a sum over any set of integers I, say $S = \sum_{n \in I} f(n)$, it can be written as the following integral

$$
S = \frac{1}{2\pi i} \oint_C \frac{\pi \cos \pi z}{\sin \pi z} f(z) dz.
\tag{A.15}
$$

where C is a contour that contains the points on the real axis $n + i0$ where $n \in I$ and none of the points of the same form with $n \in \mathbb{Z}/I$. Calculation

of the residues of the simple poles of the integrand return us to the original sum.

Applying the transformation to $S(u)$ we obtain

$$S(u) = \frac{1}{2\pi i} \oint_C \frac{\pi \cos \pi z}{\sin \pi z} e^{-ur^{-z}} r^{-z(1+\gamma)} \mathrm{d}z. \tag{A.16}$$

The contour C is represented in Figure A.1.
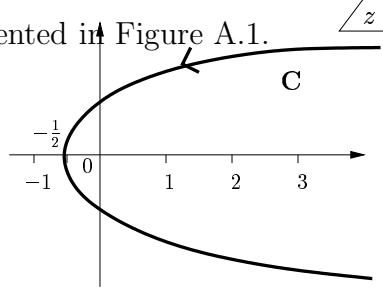
Figure A.1: Contour C used for evaluation of the integral given in equation (A.16). The poles are situated at $n + 0i$ where $n \in \{0, 1, 2, \dots\}$.

We first make a change of variables, $r^{-z} = \rho$. Substituting this and $\mathrm{d}z = -\mathrm{d}\rho/\rho \ln r$ into equation (A.16) we have

$$
\begin{aligned}
S(u) &= \frac{1}{2\pi i} \oint_C' \frac{\pi \cos -\pi \ln \rho / \ln r}{\sin -\pi \ln \rho / \ln r} e^{-u\rho} \rho^{(1+\gamma)} (-\mathrm{d}\rho/\rho \ln r) \\
&= \frac{1}{2i \ln r} \oint_C' \frac{\pi \cos \pi \ln \rho / \ln r}{\sin \pi \ln \rho / \ln r} e^{-u\rho} \rho^\gamma \mathrm{d}\rho.
\end{aligned} \tag{A.17}
$$

The transformed contour C' is depicted in Figure A.2.

As $u \to \infty$, the contribution to integral from the neighborhood of $\rho = 0$ dominates. The introduction of the sin and cos terms has created an interesting oscillation that has to be handled with with some care. We now deform the integration contour C' into the contour C'' of Figure A.3 focusing on the interval along the imaginary axis $[-i, i]$. Choosing this path will simplify the cos and sin expressions which at present have logs in their arguments.

The integral $S(u)$ is now given by $S(u) \simeq I(u) + \text{c.c.}$ where

$$I(u) = \frac{-1}{2i \ln r} \int_0^i \frac{\pi \cos \pi \ln \rho / \ln r}{\sin \pi \ln \rho / \ln r} e^{-u\rho} \rho^\gamma \mathrm{d}\rho. \tag{A.18}$$
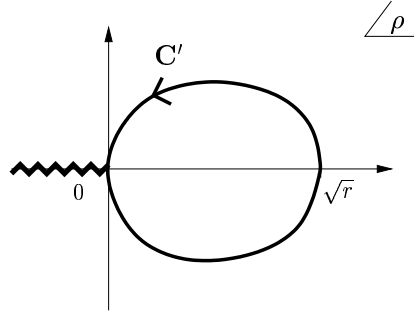
Figure A.2: Contour C' used for evaluation of the integral given in equation (A.17) as deduced from contour C (Figure A.1) with the transformation $\rho = r^{-z}$. The negative real axis is a branch cut.
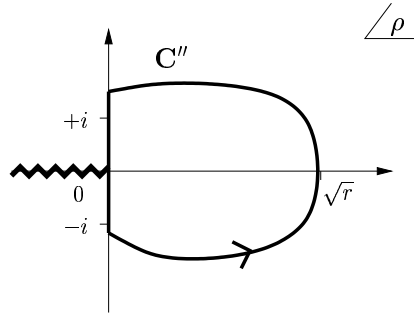
Figure A.3: Contour C'' used for evaluation of the integral given in equation (A.16). The poles are situated at $n + 0i$ where $n \in \{0, 1, 2, \dots\}$.

Writing $\rho = \sigma + i\tau$ with $\sigma = 0$, we have $\mathrm{d}\rho = i\mathrm{d}\tau$ and the following for the cos and sin terms:

$$
\begin{aligned}
\cos \pi \ln \rho / \ln r &= \frac{\rho^{i\pi/\ln r} + \rho^{-i\pi/\ln r}}{2}, \\
&= \frac{\tau^{i\pi/\ln r} e^{-\pi^2/2\ln r} + \tau^{-i\pi/\ln r} e^{\pi^2/2\ln r}}{2},
\end{aligned}
\tag{A.19}
$$

and

$$
\begin{aligned}
\sin \pi \ln \rho / \ln r &= \frac{\rho^{i\pi/\ln r} - \rho^{-i\pi/\ln r}}{2i}, \\
&= \frac{\tau^{i\pi/\ln r} e^{-\pi^2/2\ln r} - \tau^{-i\pi/\ln r} e^{\pi^2/2\ln r}}{2i}.
\end{aligned}
\tag{A.20}
$$

The cot term in the integrand becomes

$$
\begin{aligned}
\frac{\cos \pi \ln \rho / \ln r}{\sin \pi \ln \rho / \ln r} &= -i \frac{1 + \tau^{2i\pi/\ln r} e^{-\pi^2/\ln r}}{1 - \tau^{2i\pi/\ln r} e^{-\pi^2/\ln r}} \\
&= -i \frac{1 + \delta(\tau)}{1 - \delta(\tau)},
\end{aligned}
\tag{A.21}
$$

where $\delta(\tau) = \tau^{2i\pi/\ln r} e^{-\pi^2/\ln r}$. The integral $I(u)$ now becomes

$$
\begin{aligned}
I(u) &= \frac{i}{2 \ln r} \int_0^1 \frac{1 + \delta(\tau)}{1 - \delta(\tau)} e^{-iu\tau} \tau^\gamma e^{i\pi\gamma/2} \mathrm{d}\tau \\
&= \frac{e^{i\pi(1+\gamma)/2}}{2 \ln r} \int_0^1 e^{-iu\tau} \tau^\gamma \frac{1 + \delta(\tau)}{1 - \delta(\tau)} \mathrm{d}\tau.
\end{aligned}
\tag{A.22}
$$

Now, since $|\delta(\tau)| = e^{-\pi^2/\ln r} \lesssim 10^{-4}$ (taking $r = R_{l(\mathrm{s})} \approx 2.5$), we can expand the expression as follows

$$
\begin{aligned}
\frac{1 + \delta}{1 - \delta} &= (1 + \delta)(1 + \delta + \delta^2 + \dots) \\
&= 1 + 2\delta + 2\delta^2 + 2\delta^3 + \dots
\end{aligned}
\tag{A.23}
$$

The integral in turn becomes

$$
\begin{aligned}
I(u) = \frac{i^{1+\gamma}}{2 \ln r} \int_0^1 \mathrm{d}\tau \tau^\gamma e^{-iu\tau} \times \\
\left(1 + 2\tau^{2i\pi/\ln r} e^{-\pi^2/\ln r} + 2\tau^{4i\pi/\ln r} e^{-2\pi^2/\ln r} + \dots \right. \\
\left. + 2\tau^{2ni\pi/\ln r} e^{-n\pi^2/\ln r} + \dots \right)
\end{aligned}
\tag{A.24}
$$

The basic n-th integral in this expansion is

$$
I_n(u) = \int_0^1 \tau^{\gamma + 2ni\pi/\ln r} e^{-iu\tau} \mathrm{d}\tau.
\tag{A.25}
$$

Substituting $u\tau = w$ and replacing the upper limit $w = u$ with $w = \infty$ we have

$$
\begin{aligned}
I_n(u) &= u^{-(1+\gamma+2ni\pi/\ln r)} \int_0^\infty \mathrm{d}w\, w^{\gamma + 2ni\pi/\ln r} e^{-iw}, \\
&= (iu)^{-(1+\gamma+2ni\pi/\ln r)} \int_0^\infty i\mathrm{d}w (iw)^{\gamma + 2ni\pi/\ln r} e^{-iw}, \\
&= (iu)^{-(1+\gamma+2ni\pi/\ln r)} \int_0^\infty \mathrm{d}v (v)^{\gamma + 2ni\pi/\ln r} e^{-v}, \\
&= (iu)^{-(1+\gamma+2ni\pi/\ln r)} \Gamma(\gamma + 2ni\pi/\ln r).
\end{aligned}
\tag{A.26}
$$

Here, we have rotated the contour along the imaginary iw-axis to the real v-axis and identified the integral with the gamma function Γ [50]. The integral can now be expressed as

$$I(u) = \frac{1}{2\ln r u^{1+\gamma}} \left[1 + 2\sum_{n=1}^{\infty} u^{-2ni\pi/\ln r}\Gamma(\gamma + 2ni\pi/\ln r) \right]. \qquad (A.27)$$

We now need to show that the higher order terms are negligible. Note that their magnitudes do no vanish with increasing u but instead are highly oscillatory terms. Using the asymptotic form of the Gamma function [13]

$$\Gamma(z) = z^{z-1/2}e^{-z}\sqrt{2\pi}\left(1 + O(1/z)\right), \qquad (A.28)$$

we can estimate as follows for large n that

$$
\begin{aligned}
&|\Gamma(1 + \gamma + 2ni\pi/\ln r)| \\
&\sim \quad |(2i\pi n/\ln r + 1 + \gamma)^{2i\pi n/\ln r + 1/2 + \gamma}e^{-\gamma-1}\sqrt{2\pi}| \\
&= \quad |(e^{i\pi/2}2\pi n/\ln r)^{2i\pi n/\ln r + 1/2 + \gamma}e^{-\gamma-1}\sqrt{2\pi}| \\
&= \quad e^{-\pi^2 n/\ln r}n^{\gamma+1/2}(2\pi/e)^{1+\gamma}(\ln r)^{-1/2-\gamma}. \qquad (A.29)
\end{aligned}
$$

Hence, $\Gamma(1 + \gamma + 2ni\pi/\ln r)$ vanishes exponentially with n. For the first few values of n taking $\gamma = 3/2$ and $r = 2.5$, we have $\Gamma(1 + \gamma + 2i\pi/\ln r) \simeq 2.5\times 10^{-3}$ and $\Gamma(1+\gamma+4i\pi/\ln r) \simeq 2.1\times 10^{-6}$ showing that these corrections are negligible.

Hence we are able estimate $S(u)$ to first order as

$$S(u) \simeq \frac{1}{\ln r}u^{-1-\gamma}. \qquad (A.30)$$

Thus we have determined that a power law follows from the initial assumption that stream segment lengths follow exponential distributions.

This equivalence has been drawn as an asymptotic one, albeit one where convergences have been shown to be rapid. The calculation is clearly not the entire picture as the solution does contain small rapidly-oscillating corrections that do not vanish with increasing argument. A possible remaining problem and one for further investigation is to understand how the distributions for main stream lengths l_ω fit together over a range that is not to be considered asymptotic. Nevertheless, the preceding is one attempt at demonstrating this rather intriguing breakup of a smooth power law into a discrete family of functions built up from one fundamental scaling function.

Appendix B

Restricted partitions and the area-displacement distribution for random walks

Abstract. For the standard discrete random walk, the probability distribution of displacement from the origin has long been understood to be Gaussian. In 1+1 dimensions, the area or integral of the graph of a random walk is also readily seen to be Gaussian. Here we calculate the form of the joint probability distribution for displacement and the area. This distribution is found to be Gaussian with a simple form for the mean and an expression for the variance is obtained in closed form. The result is based on the observation of a connection to the theory of restricted partitions. In the case of a first return to the origin, we find the joint distribution for area and number of steps taken. Finally, we briefly discuss how this last result is significant in the study of river networks.

B.1   Introduction

Random walks and their continuum analog of Brownian motion have been studied and employed as basic models of detailed motion throughout physics, chemistry, mathematics and economics [39, 45] Einstein first deduced a molecular mechanism for Brownian motion in 1905 [36] and in the same year, Pearson introduced the discrete random walk as we think of it today [91, 100]. In this present paper, we endeavor to add to the vast literature that has developed since then by calculating the joint probability distribution for dis-

placement and area for the graph of a random walk in $1 + 1$ dimensions. This main result is achieved via a translation of the problem into one of enumeration of certain types of partitions of numbers.

The archetypal random walk may be defined in terms of a person, who has had too much to drink, stumbling home along a sidewalk. The disoriented walker moves a distance L along the sidewalk in a fixed time step. After each time step, our inebriated friend spontaneously and with an even chance turns about face or maintains the same course and then wanders another distance L only to repeat the same erratic decision process. The walker's position relative to the front door of his or her local establishment ($x_0 = 0$) is given by

$$x_n = x_{n-1} + s_{n-1} = \sum_{k=0}^{n-1} s_k \qquad (B.1)$$

where each $s_k = \pm L$ with equal probability. (L is set to unity for the rest of the paper). Now, as is well known, the probability distribution for x_k is asymptotically Gaussian with

$$P(x_n < x) \rightarrow \frac{1}{\sqrt{2\pi n}} \int_{-\infty}^{x} e^{-u^2/2n} du \qquad (B.2)$$

as $n \rightarrow \infty$.

A graph depicting the displacement of an example walk is shown in Figure B.1. Here we are concerned with two features: x_n, the displacement at time n, and a_n, the usual area obtained by integration of the graph. The latter is exactly given by

$$a_n = \sum_{k=1}^{n} x_k - x_n/2. \qquad (B.3)$$

In terms of the steps s_k, we therefore have using equations (B.1) and (B.3)
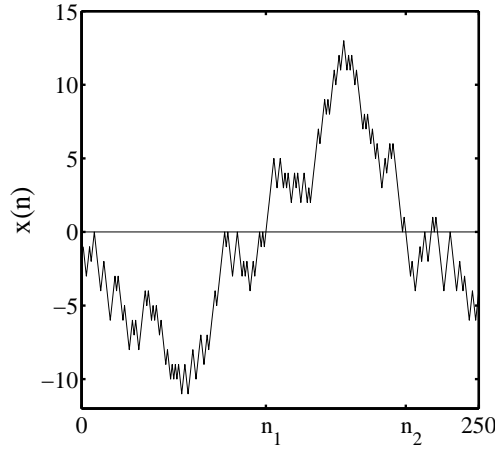
Figure B.1: An example random walk. A first return occurs at n_2 after the walk leaves the origin at n_1. Of interest is the joint probability distribution between the area subtended by this excursion and the $x = 0$ axis and the number of steps taken $n_2 - n_1$.

that

$$
\begin{aligned}
a_n &= \sum_{i=1}^{n} \sum_{j=0}^{i-1} s_j - x_n/2 \\
&= \sum_{j=0}^{n-1} \sum_{i=j+1}^{n} s_j - x_n/2 \\
&= \sum_{j=0}^{n-1} (n-j) s_j - x_n/2 \\
&= \sum_{k=1}^{n} k s_{n-k} - x_n/2 \\
&= \sum_{k=1}^{n} k \tilde{s}_k - x_n/2 \qquad \text{(B.4)}
\end{aligned}
$$

where $k = n - j$ has been substituted and we have introduced $\tilde{s}_k = s_{n-k}$.

The form of the area distribution may be obtained with a direct application of the central limit theorem [39]. Taking the independent variables to

be $\mathbf{X}_k = k\tilde{s}_k$ for $k = 1, \ldots, n$ and $\mathbf{X}_{n+1} = -x_n/2$ we have

$$\mu_k = \mathbf{E}(\mathbf{X}_k) = 0 \quad \text{and} \quad \sigma_k^2 = \text{Var}(\mathbf{X}_k) = k^2 \tag{B.5}$$

with $\mu_{n+1} = 0$ and $\sigma_{n+1}^2 = n/4$. The variance for the distribution of a_n is then given by

$$S_n^2 = \sum_{k=1}^{n+1} \sigma_k^2 = \sum_{k=1}^{n} k^2 + \frac{n}{4} \tag{B.6}$$

while the mean is clearly zero. For large n, we have

$$S_n^2 \sim \frac{n^3}{3} \tag{B.7}$$

since $\sum_{k=1}^{n} k^2 = n(n+1)(2n+1)/6$. The asymptotic form of the area distribution is therefore

$$P(a_n < a) \sim \sqrt{\frac{3}{2\pi n^3}} \int_{-\infty}^{a} e^{-3u^2/2n^3} du. \tag{B.8}$$

The same result may be obtained in the continuum case of Brownian motion with the use of cumulants. The variance for the area distribution is essentially obtained by integration of the variance of the displacement distribution [45].

B.2   Random walks and restricted partitions

Finding the form of $P(a_n, x_n, n)$, the joint distribution for area and displacement after n steps, requires some more effort. The approach is to fix x_n for some n and then determine the conditional distribution for a_n. Returning to equation (B.4) we can write

$$
\begin{aligned}
a_n &= \sum_{k=1}^{n} k\tilde{s}_k - x_n/2 \\
&= \frac{1}{2}n(n+1) - 2\sum_{k|\tilde{s}_k=-1} k - x_n/2 \\
&= \frac{1}{2}n(n+1) - 2r - x_n/2 \tag{B.9}
\end{aligned}
$$

Now, if a path reaches x_n then the sequence $\{s_k\}$ (and $\{\tilde{s}_k\}$) must contain $(n + x_n)/2$ instances of +1's and $(n - x_n)/2$ −1's (note that x_n and n are

either both odd or even). We will denote the number of such paths that reach x_n with area a_n by $\#(a_n = \frac{1}{2}n(n+1) - 2r - x_n/2, x_n)$. On examination of equation (B.9), this may then be identified with the number of partitions of the integer r into exactly $(n - x_n)/2$ distinct parts none of which can exceed n. We write this equality with the following notation

$$
\begin{aligned}
\#(a_n = \frac{1}{2}(n+1)(n+2) - 2r - x_n/2, x_n) \\
= \quad q(\leq n, =(n - x_n)/2, r) \\
= \quad q(\leq n, =(n - x_n)/2, \frac{1}{4}n(n+1) - x_n/4 - a_n/2) \quad \text{(B.10)}
\end{aligned}
$$

Now, $q(\leq N, =M, r)$ is in turn related to several other partition quantities and these connections will help our calculations. In the following, we build a link from the area of a random walk to $p(\leq N, \leq M, r)$ which is the number of partitions of r with at most M parts, none of which exceeds N.

Firstly, we have [6]

$$
p(\leq N, =M, r) = q(\leq N + M - 1, =M, r + \frac{1}{2}M(M - 1)) \quad \text{(B.11)}
$$

where $p(\leq N, = M, r)$ is the number of partitions of r with M parts each no greater than N. To see this, consider $(\alpha_1, \alpha_2, \ldots, \alpha_M)$, a partition of r with $1 \leq \alpha_1 \leq \alpha_2 \leq \cdots \leq \alpha_M \leq N$, thus being one of those partitions counted in $p(\leq N, =M, r)$. In correspondence to this is $(\alpha_1 + 0, \alpha_2 + 1, \ldots, \alpha_M + M - 1)$, a partition of $r + \frac{1}{2}M(M - 1)$ with M distinct parts. The relationship can be readily seen to be a bijection by considering the reverse mapping [6].

Next, we observe that

$$
p(\leq N, =M, r) = p(\leq N - 1, \leq M, r - M) \quad \text{(B.12)}
$$

Again we take $(\alpha_1, \alpha_2, \ldots, \alpha_M)$, a partition of r with $1 \leq \alpha_1 \leq \alpha_2 \leq \cdots \leq \alpha_M \leq N$. Now, a partition of $r - M$ may be constructed as $(\alpha_1 - 1, \alpha_2 - 1, \ldots, \alpha_M - 1)$. Removing those parts that are now zero, we have at most M parts all of which are less than $N - 1$. Again, consideration of the reverse mapping demonstrates a bijection between the two types of partitions [6].

So, combining equations (B.10), (B.11), and (B.12) we have the following identity:

$$
\#(a_n, x_n) = p(\leq N, \leq M, \rho) \quad \text{(B.13)}
$$

where

$$
\begin{aligned}
N &= \frac{n + x_n}{2} \\
M &= \frac{n - x_n}{2} \\
\rho &= \frac{1}{4}n(n+1) - \frac{1}{2}\frac{n - x_n}{2}\left(\frac{n - x_n}{2} + 1\right) - x_n/4 - a_n/2 \\
&= \frac{1}{4}n^2 - \frac{1}{2}\left(\frac{n - x_n}{2}\right)^2 - a_n/2.
\end{aligned}
\tag{B.14}
$$

With this relationship established we now move to an examination of the asymptotic properties of $p(\leq N, \leq M, \rho)$. Since a Gaussian distribution is to be expected, the principle results will be the calculation of the mean and the variance.

B.3   Asymptotics of restricted partitions

The restricted partitions measured by $p(\leq N, \leq M, \rho)$ have been well studied in partition theory. However, the particular regime of asymptotics that we will be interested in here has not been directly addressed and we will develop the results in this section. The method used here hinges on a standard saddle point approach developed by Hayman [56]. More specific applications of saddle point techniques for problems involving restricted partitions may be found in the work of Szekeres [133, 134].

Central to saddle point calculations are the canonical generating functions associated with partitions. We write

$$
G(\leq N, \leq M; \xi) = \sum_{\rho=0}^{\infty} p(\leq N, \leq M, \rho)\xi^\rho
\tag{B.15}
$$

and since $p(\leq M, \leq N, \rho) = 0$ for $\rho > MN$, G is a polynomial in ξ of order MN. The form of this generating function is explicitly known:

$$
G(\leq N, \leq M; \xi) = \frac{\prod_{k=1}^{N+M}(1 - \xi^k)}{\prod_{k=1}^{N}(1 - \xi^k)\prod_{k=1}^{M}(1 - \xi^k)}.
\tag{B.16}
$$

and is more generally referred to as a Gaussian polynomial.

The coefficients of Gaussian polynomials, i.e., the $p(\leq M, \leq N, \rho)$ themselves, are understood to be reciprocal and unimodal, the latter being a

non-trivial result [6]. Here we show that they are also approximated by a Gaussian distribution centered around $MN/2$.

For a given generating function $f(z) = \sum_{\rho=1}^{\infty} f_\rho z^\rho$ we would like to estimate f_ρ. To do this we employ Cauchy's formula which gives

$$f_\rho = \int_C z^{-1-\rho} f(z)\, dz \tag{B.17}$$

where C is the contour $|z| = c_0$ and $z = u + iv$. Although any contour containing the origin may be used, it turns out that the contour $|z| = c_0$ provides an integral that may be successfully estimated with Laplace's method. This observation holds for functions that for some range of u (as detailed below) $f(u) = \max_{|z|=u} f(z)$ and in general, a unique minimum along the real z axis will be found at $u = c_0$. Saddle point methods may now be applied.

The integral in equation (B.17) can be rewritten as

$$f_\rho = \int_C e^{\ln\left(f(z)/z^\rho\right)}\, d(\ln z). \tag{B.18}$$

For ρ fixed, minimizing the argument of the exponential along $z = \xi + i0$ with respect to $\ln z$ gives

$$\xi f'(\xi)/f(\xi) = \rho. \tag{B.19}$$

The position of the saddle point, $z = c_0$, is thus a solution to this equation.

We now draw on the work of Hayman, who obtained a general result using the saddle point method for a particular class of functions [56]. Here we use Odlyzko's interpretation of Hayman's theorem as reproduced below [51].

Definition 1 *Functions of the form*

$$f(z) = \sum_{\rho=0}^{\infty} f_\rho z^\rho \tag{B.20}$$

are said to be H-admissible (H for Hayman) if (writing $z = \xi + i\nu$)

- *$f(z)$ is analytic in $|z| < \Xi$ where $0 < \Xi < \infty$,*

- *$f(\xi)$ is real for $|\xi| < \Xi$,*

- *for $\Xi_0 < \xi < \Xi$, $\max_{|z|=\xi} |f(z)| = f(\xi)$,*

and, defining

$$a(\xi) = \xi\frac{f'(\xi)}{f(\xi)},$$

$$b(r) = \xi a'(\xi) = \xi\frac{f'(\xi)}{f(\xi)} + \xi^2\frac{f''(\xi)}{f(\xi)} - \xi^2\left(\frac{f'(\xi)}{f(\xi)}\right)^2 \qquad \text{(B.21)}$$

it is required that, modulo some technical details, that $b(\xi) \to \infty$ as $\xi \to \Xi$.

For such functions we then have the following theorem due to Hayman [56]

Theorem 2 *Given a function $f(z)$, H-admissible in $|z| < R$, then, as $\xi \to \infty$,*

$$f_\rho = (2\pi b(\xi))^{-1/2}f(\xi)\xi^{-\rho}\left(e^{-(a(\xi)-\rho)^2/b(\xi)} + o(1)\right) \qquad \text{(B.22)}$$

The form of equation (B.22) can be recast to show that the values of the f_ρ follow the form of a normal distribution:

$$
\begin{aligned}
f_\rho &\sim (2\pi b(\xi))^{-1/2}f(\xi)e^{-\left(a(\xi)^2 - (a - \frac{b(\xi)}{2}\ln\xi)^2\right)/b(\xi)} \\
&\quad \times \exp\left\{-\frac{1}{b(\xi)}\left(\frac{2a(\xi) - b(\xi)\ln(\xi)}{2}\right)^2\right\} \\
&= \frac{c(\xi)}{(2\pi\sigma(\xi))^{1/2}}\exp\left\{-\frac{(\rho - \mu(\xi))^2}{2\sigma(\xi)^2}\right\} \qquad \text{(B.23)}
\end{aligned}
$$

where the mean and variance are given by

$$\mu(\xi) = \frac{2a(\xi) - b(\xi)\ln(\xi)}{2} \quad \text{and} \quad \sigma(\xi)^2 = b(\xi)/2. \qquad \text{(B.24)}$$

Since we are interested in the form of the $p(\leq N, \leq M, \rho)$ around the center $\rho = MN/2$, we will require that

$$\mu(\xi) = \frac{2a(\xi) - b(\xi)\ln(\xi)}{2} = MN/2 \qquad \text{(B.25)}$$

and this will determine the ξ at which we will apply the theorem. Thus, up to a normalization factor we have

$$p(\leq N, \leq M, \rho) \propto \frac{1}{(2\pi\sigma(\xi))^{1/2})}\exp\left\{-\frac{(\rho - \mu(\xi))^2}{2\sigma(\xi)^2}\right\} \qquad \text{(B.26)}$$

with ξ, $\mu(\xi)$, $\sigma(\xi)$ determined by equations (B.21), (B.24) and (B.25).

Returning to the generating function of equation (B.16), we may now determine $a(\xi)$ for the present case.

$$
\begin{aligned}
a(\xi) &= \xi \frac{G'(\leq N, \leq M; \xi)}{G(\leq N, \leq M; \xi)} \\
&= \sum_{k=1}^{N} \frac{k\xi^k}{1 - \xi^k} + \sum_{k=1}^{M} \frac{k\xi^k}{1 - \xi^k} - \sum_{k=1}^{N+M} \frac{k\xi^k}{1 - \xi^k}
\end{aligned}
\tag{B.27}
$$

The sums in equation (B.27) can be evaluated for large, increasing M and N using a Riemann integral approximation [13]:

$$
\begin{aligned}
\sum_{k=1}^{N} \frac{k\xi^k}{1 - \xi^k} &= s^2 \sum_{k=1}^{N} \frac{k}{s} \frac{e^{-k/s}}{1 - e^{-k/s}} \frac{1}{r} \\
&\sim s^2(\gamma^2 - I(N/s))
\end{aligned}
\tag{B.28}
$$

where we have identified $\xi = e^{-1/s}$,

$$
I(x) = \int_x^{\infty} \frac{t}{e^t - 1} \, dt
\tag{B.29}
$$

and $\gamma^2 = \pi^2/6 = I(0)$. We observe that s will be of the order of N (and M) which means that the quantities such as N/s must be retained.

Therefore, $a(\xi)$ is now given by

$$
a(\xi) = s^2 \left(c^2 + I\left(\frac{M + N}{s}\right) - I\left(\frac{N}{s}\right) - I\left(\frac{M}{s}\right) \right)
\tag{B.30}
$$

where $s = (-\ln \xi)^{-1}$. The form for $b(\xi)$ is then obtained via the definition $b(\xi) = \xi a'(\xi)$.

The requirement that the mean $\mu(\xi) = MN/2$ (equation (B.25)) then gives

$$
\begin{aligned}
MN/2 = \quad & \\
& 2s^2 \left(\gamma^2 + I\left(\frac{M + N}{s}\right) - I\left(\frac{N}{s}\right) - I\left(\frac{M}{s}\right) \right) \\
& + \frac{1}{2} \left[\frac{(M + N)^2}{e^{-(M+N)/s} - 1} - \frac{N^2}{e^{-N/s} - 1} - \frac{M^2}{e^{-M/s} - 1} \right].
\end{aligned}
\tag{B.31}
$$

For convenience, we now consider pairs of M and N related as $M = N(1 + \alpha)$. Expecting that s is of the order of M and N we set $s = \lambda N$. Equation (B.31) becomes

$$
\begin{aligned}
(1 + \alpha)/2 = \\
2\lambda^2 \left(\gamma^2 + I\left(\frac{2+\alpha}{\lambda}\right) - I\left(\frac{1}{\lambda}\right) - I\left(\frac{1+\alpha}{\lambda}\right) \right) \\
+ \quad \frac{1}{2} \left[\frac{(2+\alpha)^2}{e^{-(2+\alpha)/s} - 1} - \frac{1}{e^{-1/\lambda} - 1} - \frac{(1+\alpha)^2}{e^{-(1+\alpha)/\lambda} - 1} \right]
\end{aligned}
\tag{B.32}
$$

which implicitly determines λ as a function of α.

Since by design, $\mu(\xi) = MN/2$ we have only to determine the variance $\sigma(\xi)^2 = b(\xi)/2$ (equation (B.24)). Inverting equation (B.25) we have

$$
b(\xi)/2 = \frac{1}{\ln \xi}(a(\xi) - MN/2)
\tag{B.33}
$$

Using the form of $a(\xi)$ found in equation (B.30) along with $s = \lambda N$ and $M = (1 + \alpha)N$ we find

$$
\sigma(\xi)^2 = b(\xi)/2 = \beta^2 (MN)^{3/2}
\tag{B.34}
$$

where

$$
\begin{aligned}
\beta^2 = \frac{\lambda}{(1+\alpha)^{1/2}} \\
\times \quad \left[\frac{1}{2} - \frac{\lambda^2}{1+\alpha} \left(\gamma^2 + I(\frac{2+\alpha}{\lambda}) - I(\frac{1+\alpha}{\lambda}) - I(\frac{1}{\lambda}) \right) \right]
\end{aligned}
\tag{B.35}
$$

B.4 The area-displacement distribution of a random walk

The asymptotic form for $p(\leq N, \leq M, \rho)$ may now be transformed back to the random walk setting. Equations (B.13), (B.13), (B.26) (B.25) and (B.34) combine to give

$$
\begin{aligned}
\#(a_n, x_n) = p(\leq N, \leq M, \rho) \\
\sim \quad \frac{C}{\sqrt{2\pi}\sigma(x_n, n)} \exp\left\{ \frac{-(a_n - \mu(x_n, n))^2}{2\sigma(x_n, n)^2} \right\}
\end{aligned}
\tag{B.36}
$$

where

$$\mu(x_n, n) = nx_n/2 \quad \text{and} \quad \sigma(x_n, n)^2 = \frac{\beta^2}{2}(n^2 - x_n^2)^{3/2}. \tag{B.37}$$

The mean $\mu(x_n, n)$ is simply the area of the triangle formed by a walk that moves directly from the origin to the point (x_n, n). Even though the asymptotic form is not assured to have any validity at for x_n far from the origin, it is nevertheless of note that the variance vanishes at $x_n = \pm n$. At each of these end points, only one walk is possible and the distribution becomes a delta function.

The normalization factor C in equation (B.36) is easily deduced by noting that

$$\sum_{a_n} \#(a_n, x_n) = \#(x_n) \tag{B.38}$$

where $\#(x_n)$ is the frequency of walks that pass through x_n. From equation (B.2) we have that

$$\#(x_n) \sim \frac{1}{\sqrt{2\pi n}} e^{-x_n^2/2n} \tag{B.39}$$

and therefore

$$
\begin{aligned}
\#(a_n, & x_n) \\
&\sim \frac{1}{2\pi\sqrt{n}\sigma(x_n, n)} \exp\left\{ -\frac{(a_n - \mu(x_n, n))^2}{2\sigma(x_n, n)^2} - \frac{x_n^2}{2n} \right\} \\
&= \frac{1}{\sqrt{2n}\pi\beta(n^2 - x_n^2)^{3/4}} \exp\left\{ -\frac{(a_n - nx_n/2)^2}{\beta^2(n^2 - x_n^2)^{3/2}} - \frac{x_n^2}{2n} \right\} \tag{B.40}
\end{aligned}
$$

as $n \to \infty$.

B.5 The area distribution for the point of first return

We now consider walks which first return to the origin after n steps. Given the main result of this paper, this section provides, at least, a numerical route to the distribution of areas for such walks. We start with walks that return to the origin after n steps, without the condition that it be their first

return. For these walks, we have $x_n = 0$ and that n must be even. The area distribution of equation (B.40) reduces to

$$\#(a_n, 0) = \frac{1}{\sqrt{2}\pi\beta n^2} e^{-a_n^2/\beta^2 n^3} \tag{B.41}$$

We introduce $f(a, n)$ and $u(a, n)$, the probabilities of returning to the origin after n steps with area a for the first time and for any number of times respectively. We also define $f(a, 0) = 0$ and $u(a, 0) = \delta_{a,0}$. The probability $u(a, n)$ is of course asymptotically given by $\#(a_n, 0)$ as per equation (B.41).

Generalizing a straightforward result for first return problems without area [39] we have

$$u(a, n) = \delta_{a,0}\delta_{n,0} + \sum_{j=-\infty}^{\infty} \sum_{k=2}^{n} u(a - j, n - k)f(j, k) \tag{B.42}$$

where j and k are restricted to even numbers within the given limits (a_n and n are also both even). Multiplying each side by $v^a w^n$ and summing over a and n then yields a relationship involving the generating functions of u and f:

$$U(v, w) = 1 + U(v, w)F(v, w) \tag{B.43}$$

where the double sum being a convolution affords a product of the generating functions U and F. Rearranging equation (B.43) gives

$$F(v, w) = \frac{U(v, w) - 1}{U(v, w)}. \tag{B.44}$$

The area distribution for walks that first return at n may therefore be obtained by inverse transform of equation (B.44).

Acknowledgements

Appendix C

Analysis of Digital Elevation Maps

This appendix briefly outlines the method used in this thesis for extracting networks from digitized topography. Since the actual datasets used will be outmoded in the not too distant future, the details of the code developed are largely irrelevant. Here, we simply record the basic ideas involved.

There are two main problems to contend with: the coordinate system of the datasets and the problems confronted by local minima.

Large-scale datasets are typically stored in spherical coordinates, though some are available in a format projected onto a uniform grid. With the latter, the major concern is the quality of the projection that has been used. In the case of the former, one must take care of the fact that individual grid cells are not uniform in shape. Data that is recorded at fixed intervals of latitude and longitude will mean when moving away from the equator cells become thinner in the direction of the radial parameter. Another potential problem is that the earth is not a sphere and that the data may have been stored in reference to a non-spherical shape. However, this is much less of a concern as the corrections in area and length calculations are of secondary order.

The second issue of local minima is the one that creates much work and the method used here is certainly debatable. Local minima arise partly due as artifacts of resolution. Relatively flat regions can also cause algorithms trouble. And, of course, there are real lakes to contend with.

Out of a number of possible methods, a type of filling routine was created. Sequentially at every point on a landscape, a walker (unit of precipitation) is placed. The walker descends down the direction of steepest descent as far as possible. If the edge of the dataset is reached then we start again at the next

initial site. However if a site where there is no clear direction is reached (i.e., every way is up or more than two directions are at the same level which may easily occur for rounded data) the walker has to take stock of the situation. All local sites that are of equal height are first scouted out. The lowest points of this region are then examined to see if an outlet (a point lower than the region) exists. If not, the region is raised to the height of its lowest boundary neighbor and the process is repeated: all equal heights are found and raised if necessary. When an outlet is detected, a filling algorithm begins that adds infinitesimal heights to points in the raised region. The amount added is increased monotonically with distance from the outlet as measured within the region (i.e., a "chemical distance" not a direct distance). It is ensured that the region is not raised above its higher boundary neighbors. If several outlets are present the same height additions are made from all of them.

After passing through the whole grid we have a filled topography that has been constructed so that a walker starting at any site will reach the edge of the grid. This is the most computationally expensive part of the calculations although determination of drainage area does take some time as well. Once the topography has been filled, we can readily extract a network, i.e., a matrix of directions, and from there our computations become more straightforward. Note that when calculating lengths and areas the height of the topography is necessary for exact calculations. However, a mean height is generally sufficient for this purpose.

Appendix D

Miscellaneous observations of real river networks

In this last appendix we provide some data taken from real river networks. Several major river basins are analyzed including the Mississippi, the Amazon, the Nile, the Congo, and the Kansas River. For each network, a table of Horton ratios as well as a table of Tokunaga ratios are presented.

ω range	R_n	R_a	R_l	$R_{l(s)}$	$\frac{R_a}{R_n}$	$\frac{R_l}{R_{l(s)}}$	$\frac{\ln R_l}{\ln R_a}$
$[2,3]$	5.27	5.26	2.48	2.30	1.00	1.07	0.55
$[2,4]$	4.99	5.08	2.44	2.32	1.02	1.05	0.56
$[2,5]$	4.86	4.96	2.42	2.31	1.02	1.05	0.56
$[2,6]$	4.81	4.92	2.42	2.33	1.02	1.04	0.56
$[2,7]$	4.77	4.88	2.40	2.31	1.02	1.04	0.56
$[2,8]$	4.69	4.85	2.39	2.33	1.03	1.03	0.57
$[3,4]$	4.72	4.91	2.41	2.34	1.04	1.03	0.57
$[3,5]$	4.70	4.82	2.40	2.31	1.03	1.04	0.57
$[3,6]$	4.70	4.83	2.40	2.35	1.03	1.03	0.57
$[3,7]$	4.69	4.82	2.38	2.31	1.03	1.03	0.56
$[3,8]$	4.60	4.79	2.38	2.34	1.04	1.02	0.57
$[4,5]$	4.67	4.72	2.39	2.28	1.01	1.05	0.57
$[4,6]$	4.69	4.81	2.40	2.36	1.02	1.02	0.57
$[4,7]$	4.68	4.80	2.37	2.30	1.03	1.03	0.56
$[4,8]$	4.57	4.77	2.38	2.34	1.05	1.01	0.57
$[5,6]$	4.72	4.90	2.42	2.43	1.04	0.99	0.57
$[5,7]$	4.68	4.83	2.36	2.29	1.03	1.03	0.56
$[5,8]$	4.51	4.77	2.37	2.35	1.06	1.01	0.57
$[6,7]$	4.63	4.76	2.30	2.16	1.03	1.07	0.54
$[6,8]$	4.39	4.71	2.36	2.35	1.07	1.00	0.58
$[7,8]$	4.16	4.67	2.41	2.56	1.12	0.94	0.62
mean μ	4.69	4.85	2.40	2.33	1.04	1.03	0.57
std dev σ	0.21	0.13	0.04	0.07	0.03	0.03	0.01
σ/μ	0.045	0.027	0.015	0.031	0.024	0.027	0.025

Table D.1: Horton ratios for the Mississippi River. (This is the full version of Table 4.1). For each range, estimates of the ratios are obtained via simple regression analysis. For each quantity, a mean μ, standard deviation σ and coefficient of variation σ/μ are calculated. The values obtained for R_l are especially robust while some variation is observed for the estimates of R_n and R_a. Good agreement is observed between the ratios R_n and R_a and also between R_l and $R_{l(s)}$. The network was extracted from a topography dataset composed of digital elevations models obtained from the United States Geological Survey (www.usgs.gov). The dataset is decimated so as to have horizontal resolution of approximately 1000 meters leading to an order $\Omega = 11$ network.

	$\nu = 1$	2	3	4	5	6	7	8	9	10
$\mu = 2$	1.38	0	0	0	0	0	0	0	0	0
3	5.62	1.34	0	0	0	0	0	0	0	0
4	15.03	4.22	1.16	0	0	0	0	0	0	0
5	34.16	11.06	3.36	1.12	0	0	0	0	0	0
6	81.32	27.84	9.47	3.57	1.28	0	0	0	0	0
7	169.7	61.5	20.97	8.65	3.22	1.34	0	0	0	0
8	413.6	163.8	54.04	22.4	8.64	3.08	1.24	0	0	0
9	555.6	236.9	77	32.29	14	6	1.71	1.29	0	0
10	1190	466	120	46.5	18.5	6.5	5.5	0.5	1.5	0
11	845	315	69	21	8	3	0	1	0	0

Table D.2: Tokunaga ratios for the Mississippi.

ω range	R_n	R_a	R_l	$R_{l(\mathrm{s})}$	$\frac{R_a}{R_n}$	$\frac{R_l}{R_{l(\mathrm{s})}}$	$\frac{\ln R_l}{\ln R_a}$
$[2,3]$	5.05	4.69	2.10	1.65	0.93	1.28	0.46
$[2,4]$	4.79	4.71	2.10	1.82	0.98	1.16	0.48
$[2,5]$	4.65	4.64	2.11	1.92	1.00	1.10	0.49
$[2,6]$	4.62	4.64	2.14	2.03	1.01	1.05	0.50
$[2,7]$	4.54	4.63	2.16	2.11	1.02	1.03	0.51
$[2,8]$	4.51	4.57	2.17	2.14	1.01	1.01	0.51
$[3,4]$	4.54	4.73	2.10	2.01	1.04	1.05	0.49
$[3,5]$	4.49	4.60	2.11	2.06	1.03	1.03	0.50
$[3,6]$	4.51	4.62	2.15	2.15	1.02	1.00	0.51
$[3,7]$	4.45	4.61	2.18	2.22	1.04	0.98	0.52
$[3,8]$	4.44	4.55	2.19	2.23	1.02	0.98	0.52
$[4,5]$	4.44	4.48	2.12	2.10	1.01	1.01	0.51
$[4,6]$	4.52	4.59	2.18	2.24	1.02	0.97	0.52
$[4,7]$	4.42	4.59	2.21	2.30	1.04	0.96	0.53
$[4,8]$	4.42	4.51	2.21	2.27	1.02	0.97	0.53
$[5,6]$	4.59	4.71	2.24	2.38	1.02	0.94	0.53
$[5,7]$	4.39	4.62	2.25	2.39	1.05	0.94	0.55
$[5,8]$	4.40	4.49	2.22	2.31	1.02	0.96	0.54
$[6,7]$	4.19	4.55	2.26	2.40	1.09	0.94	0.57
$[6,8]$	4.34	4.37	2.21	2.25	1.01	0.98	0.54
$[7,8]$	4.50	4.21	2.15	2.12	0.94	1.02	0.51
mean μ	4.51	4.58	2.17	2.15	1.01	1.02	0.52
std dev σ	0.17	0.12	0.05	0.19	0.03	0.08	0.03
σ/μ	0.038	0.026	0.024	0.089	0.034	0.078	0.050

Table D.3: Horton ratios for the Amazon. (This is the full version of Table 4.2). Details are as per Table D.1. The topography dataset used here was obtained from the National Imagery and Mapping Agency (`www.nima.mil`). The dataset has a horizontal resolution of approximately 1000 meters yielding and order $\Omega = 11$ network for the Amazon.

	$\nu = 1$	2	3	4	5	6	7	8	9	10
$\mu = 2$	1.68	0	0	0	0	0	0	0	0	0
3	4.87	1.25	0	0	0	0	0	0	0	0
4	12.13	3.78	1.11	0	0	0	0	0	0	0
5	28.68	9.07	2.87	1.03	0	0	0	0	0	0
6	71.4	22.65	7.69	2.98	1.16	0	0	0	0	0
7	185.6	55.99	18.85	7.75	3.28	1.12	0	0	0	0
8	383.9	114.3	39.38	16.84	6.88	2.63	1.03	0	0	0
9	633.3	174.8	63.9	28.2	10.8	4.5	3	0.6	0	0
10	1050	266.3	66	28.67	13.33	4.33	2.67	1	1	0
11	1403	505	121	66	25	12	9	3	1	1

Table D.4: Tokunaga ratios for the Amazon.

ω range	R_n	R_a	R_l	$R_{l(\mathrm{s})}$	$\frac{R_a}{R_n}$	$\frac{R_l}{R_{l(\mathrm{s})}}$	$\frac{\ln R_l}{\ln R_a}$
$[2,3]$	4.78	4.71	2.47	2.08	0.99	1.19	0.58
$[2,4]$	4.64	4.64	2.38	2.10	1.00	1.13	0.57
$[2,5]$	4.55	4.58	2.32	2.12	1.01	1.10	0.56
$[2,6]$	4.50	4.57	2.29	2.14	1.02	1.07	0.55
$[2,7]$	4.42	4.53	2.24	2.10	1.02	1.07	0.54
$[2,8]$	4.31	4.42	2.18	2.02	1.03	1.08	0.53
$[3,4]$	4.51	4.58	2.30	2.12	1.02	1.08	0.55
$[3,5]$	4.45	4.52	2.26	2.14	1.01	1.06	0.54
$[3,6]$	4.42	4.54	2.24	2.16	1.03	1.04	0.54
$[3,7]$	4.35	4.49	2.20	2.10	1.03	1.05	0.54
$[3,8]$	4.23	4.36	2.13	2.00	1.03	1.07	0.53
$[4,5]$	4.39	4.46	2.22	2.15	1.01	1.03	0.54
$[4,6]$	4.38	4.54	2.22	2.18	1.03	1.02	0.54
$[4,7]$	4.29	4.46	2.17	2.07	1.04	1.04	0.53
$[4,8]$	4.15	4.30	2.09	1.95	1.04	1.07	0.52
$[5,6]$	4.38	4.62	2.22	2.21	1.06	1.00	0.54
$[5,7]$	4.23	4.44	2.13	2.01	1.05	1.06	0.53
$[5,8]$	4.05	4.21	2.04	1.86	1.04	1.10	0.51
$[6,7]$	4.08	4.27	2.05	1.83	1.05	1.12	0.51
$[6,8]$	3.88	4.01	1.95	1.71	1.03	1.14	0.49
$[7,8]$	3.70	3.77	1.86	1.59	1.02	1.17	0.47
mean μ	4.32	4.43	2.19	2.03	1.03	1.08	0.53
std dev σ	0.25	0.22	0.14	0.16	0.02	0.05	0.02
σ/μ	0.058	0.050	0.064	0.080	0.016	0.045	0.044

Table D.5: Horton ratios for the Nile. (This is the full version of Table 4.1). Details are as per Table D.1. The data used here comes from the United States Geological Survey's 30 arc second Hydro1K dataset (`edcftp.cr.usgs.gov`), which has a grid spacing of approximately 1000 meters. At this resolution, the Nile is an order $\Omega = 10$ basin.

	$\nu = 1$	2	3	4	5	6	7	8	9
$\mu = 2$	2.04	0	0	0	0	0	0	0	0
3	6.03	1.2	0	0	0	0	0	0	0
4	14.31	3.45	1.12	0	0	0	0	0	0
5	31.76	8.22	2.99	1.06	0	0	0	0	0
6	67.3	18.36	6.86	3.01	1.18	0	0	0	0
7	122	35.34	14.48	5.68	2.47	1.01	0	0	0
8	150.4	54.24	21.36	9	3.3	1.36	0.79	0	0
9	482.6	157.4	61	26.29	9.43	4.57	2.29	1.57	0
10	3314	968	398	223	118	54	14	8	5

Table D.6: Tokunaga ratios for the Nile.

ω range	R_n	R_a	R_l	$R_{l(\mathrm{s})}$	$\frac{R_a}{R_n}$	$\frac{R_l}{R_{l(\mathrm{s})}}$	$\frac{\ln R_l}{\ln R_a}$
$[2,3]$	5.00	4.53	2.16	1.78	0.91	1.21	0.48
$[2,4]$	4.79	4.60	2.16	1.96	0.96	1.10	0.49
$[2,5]$	4.79	4.63	2.17	2.05	0.97	1.06	0.49
$[2,6]$	4.80	4.72	2.21	2.16	0.98	1.02	0.51
$[2,7]$	4.68	4.72	2.24	2.20	1.01	1.02	0.52
$[2,8]$	4.56	4.64	2.23	2.16	1.02	1.03	0.53
$[3,4]$	4.60	4.67	2.16	2.16	1.02	1.00	0.51
$[3,5]$	4.72	4.67	2.17	2.17	0.99	1.00	0.50
$[3,6]$	4.78	4.79	2.24	2.29	1.00	0.98	0.51
$[3,7]$	4.62	4.76	2.27	2.29	1.03	0.99	0.54
$[3,8]$	4.48	4.63	2.25	2.21	1.03	1.02	0.54
$[4,5]$	4.85	4.68	2.18	2.19	0.96	1.00	0.49
$[4,6]$	4.86	4.87	2.28	2.37	1.00	0.96	0.52
$[4,7]$	4.58	4.78	2.32	2.33	1.04	0.99	0.55
$[4,8]$	4.40	4.60	2.26	2.20	1.04	1.03	0.55
$[5,6]$	4.86	5.07	2.39	2.57	1.04	0.93	0.55
$[5,7]$	4.40	4.79	2.37	2.37	1.09	1.00	0.58
$[5,8]$	4.24	4.51	2.26	2.16	1.07	1.05	0.57
$[6,7]$	3.99	4.52	2.36	2.19	1.13	1.08	0.62
$[6,8]$	4.00	4.26	2.19	1.97	1.07	1.11	0.56
$[7,8]$	4.00	4.01	2.03	1.77	1.00	1.14	0.51
mean μ	4.57	4.64	2.23	2.17	1.02	1.03	0.53
std dev σ	0.30	0.21	0.09	0.19	0.05	0.06	0.04
σ/μ	0.066	0.046	0.038	0.087	0.048	0.063	0.066

Table D.7: Horton ratios for the Congo plus the usual comparisons. The data is obtained from the same dataset as the Nile, see Table D.5.

	$\nu = 1$	2	3	4	5	6	7	8	9	10
$\mu = 2$	1.55	0	0	0	0	0	0	0	0	0
3	4.46	1.23	0	0	0	0	0	0	0	0
4	11.44	3.78	1.11	0	0	0	0	0	0	0
5	26.88	9.52	3.13	1.13	0	0	0	0	0	0
6	74.48	27.33	9.7	3.96	1.22	0	0	0	0	0
7	158.7	60.38	23.03	9.67	3.5	1	0	0	0	0
8	272.6	112.7	35.81	17.19	6.38	2.15	0.88	0	0	0
9	534.3	214	70.86	29.29	11.86	3.14	2.86	1	0	0
10	1031	526	164	67.5	22.5	9.5	3	2.5	1.5	0
11	538	255	58	24	22	6	3	0	0	0

Table D.8: Tokunaga ratios for the Congo.

ω range	R_n	R_a	R_l	$R_{l(\mathrm{s})}$	$\frac{R_a}{R_n}$	$\frac{R_l}{R_{l(\mathrm{s})}}$	$\frac{\ln R_l}{\ln R_a}$
[2, 3]	4.61	4.16	2.16	1.64	0.90	1.32	0.50
[2, 4]	4.76	4.36	2.07	1.69	0.92	1.22	0.47
[2, 5]	4.78	4.59	2.09	1.86	0.96	1.12	0.47
[2, 6]	4.75	4.68	2.13	1.99	0.99	1.07	0.48
[2, 7]	4.78	4.73	2.16	2.07	0.99	1.05	0.49
[2, 8]	4.82	4.84	2.23	2.15	1.00	1.03	0.51
[2, 9]	4.85	4.91	2.29	2.20	1.01	1.04	0.52
[3, 4]	4.91	4.58	1.98	1.75	0.93	1.13	0.43
[3, 5]	4.84	4.82	2.07	2.01	1.00	1.03	0.46
[3, 6]	4.77	4.84	2.13	2.14	1.02	1.00	0.49
[3, 7]	4.80	4.86	2.19	2.19	1.01	1.00	0.50
[3, 8]	4.85	4.96	2.27	2.27	1.02	1.00	0.52
[3, 9]	4.88	5.01	2.33	2.30	1.03	1.01	0.53
[4, 5]	4.78	5.08	2.16	2.31	1.06	0.93	0.49
[4, 6]	4.69	4.94	2.21	2.34	1.05	0.95	0.51
[4, 7]	4.78	4.91	2.25	2.32	1.03	0.97	0.52
[4, 8]	4.86	5.04	2.34	2.38	1.04	0.98	0.54
[4, 9]	4.90	5.08	2.41	2.39	1.04	1.01	0.55
[5, 6]	4.61	4.80	2.27	2.37	1.04	0.96	0.54
[5, 7]	4.81	4.85	2.30	2.32	1.01	0.99	0.53
[5, 8]	4.92	5.07	2.41	2.41	1.03	1.00	0.55
[5, 9]	4.95	5.11	2.48	2.41	1.03	1.03	0.57
[6, 7]	5.02	4.89	2.33	2.28	0.97	1.02	0.52
[6, 8]	5.07	5.23	2.50	2.45	1.03	1.02	0.56
[6, 9]	5.04	5.22	2.56	2.43	1.04	1.05	0.58
[7, 8]	5.13	5.60	2.67	2.63	1.09	1.01	0.60
[7, 9]	5.03	5.34	2.66	2.47	1.06	1.08	0.60
[8, 9]	4.94	5.08	2.64	2.32	1.03	1.14	0.61
mean μ	4.85	4.91	2.30	2.22	1.01	1.04	0.52
std dev σ	0.13	0.29	0.19	0.25	0.04	0.08	0.04
σ/μ	0.026	0.059	0.081	0.111	0.043	0.080	0.085

Table D.9: Horton ratios for the Kansas river along with various comparisons. The data comes from the same dataset as the Mississippi, see Table D.1.

	$\nu = 1$	2	3	4	5	6	7	8	9	10	11
$\mu = 2$	1.7	0	0	0	0	0	0	0	0	0	0
3	3.76	1	0	0	0	0	0	0	0	0	0
4	8.82	2.97	1.09	0	0	0	0	0	0	0	0
5	26.48	9.87	3.63	1.16	0	0	0	0	0	0	0
6	69.07	28.92	10.6	3.26	1.09	0	0	0	0	0	0
7	170.3	79.59	29.39	10	3.15	1.11	0	0	0	0	0
8	479.2	238.6	90.43	28.22	11.24	4.3	1.29	0	0	0	0
9	1146	585.1	225.4	73.75	31.06	12.5	3.63	1.38	0	0	0
10	1563	817.7	296.8	93.83	38	20.33	7.83	1.67	0.33	0	0
11	3684	1619	708	209	88.5	48.5	18.5	7	0.5	0.5	0
12	1274	627	216	55	27	14	3	1	1	1	0

Table D.10: Tokunaga ratios for the Kansas.

List of Figures

193

List of Tables

Bibliography

[1] A. D. Abrahams. Channel networks: a geomorphological perspective. *Water Resour. Res.*, 20(2):161–188, February 1984.

[2] S. Aharinejad, W. Schreiner, and F. Neumann. Morphometry of human coronary arterial trees. *Anat. Rec.*, 251(1):50–59, 1998.

[3] R. Albert, H. Jeong, and A.-L. Barabasi. Diameter of the world-wide web. *Nature*, 401(6749):130–131, September 1999.

[4] B. Alder and T. Wainwright. Decay of the velocity autocorrelation function. *Phys. Rev. Lett.*, 1:18–21, 1970.

[5] J. M. Allman. *Evolving brains*. Scientific American Library, New York, 1999.

[6] G. E. Andrews. *The Theory of Partitions*, volume 2 of *Encyclopedia of Mathematics and Its Applications*. Addison-Wesley, Reading, Massachusetts, 1976.

[7] P. Bak. *How Nature Works: the Science of Self-Organized Criticality*. Springer-Verlag, New York, 1996.

[8] P. Ball. *The Self-Made Tapestry*. Oxford, UK, January 1998.

[9] J. R. Banavar, F. Colaiori, A. Flammini, A. Giacometti, A. Maritan, and A. Rinaldo. Sculpting of a fractal river basin. *Phys. Rev. Lett.*, 78: 4522–4525, 1997.

[10] A.-L. Barabasi and H. E. Stanley. *Fractal Concepts in Surface Growth*. Cambridge University Press, Great Britain, 1995.

[11] G. I. Barenblatt. *Scaling, self-similarity, and intermediate asymptotics*, volume 14 of *Cambridge Texts in Applied Mathematics*. Cambridge University Press, 1996.

[12] J. Bartlett. *Bartlett's Familiar Quotations*. Little, Brown & Company, Canada, 16th edition, 1992.

[13] C. M. Bender and S. A. Orszag. *Advanced mathematical methods for scientists and engineers*. International series in pure and applied mathematics. McGraw-Hill, New York, 1978.

[14] J. Bolker. *Writing Your Dissertation in Fifteen Minutes a Day*. Henry Holt and Company, New York, 1998.

[15] G. Caldarelli, A. Giacometti, A. Maritan, I. Rodríguez-Iturbe, and A. Rinaldo. Randomly pinned landscape evolution. *Phys. Rev. E*, 55 (5):4865–8, May 1997.

[16] G. F. Carrier, M. Krook, and C. E. Pearson. *Functions of a complex variable; theory and technique*. McGraw-Hill, New York, 1966.

[17] C. Cherniak, M. Changizi, and D. Kang. Large-scale optimization of neuron arbors. *Phys. Rev. E*, 59(5), 1999.

[18] M. Cieplak, A. Giacometti, A. Maritan, A. Rinaldo, I. Rodríguez-Iturbe, and J. R. Banavar. Models of fractal river basins. *J. Stat. Phys.*, 91(1/2):1–15, January 1998.

[19] F. Colaiori, A. Flammini, A. Maritan, and J. R. Banavar. Analytical and numerical study of optimal channel networks. *Phys. Rev. E*, 55(2): 1298, 1310 1997.

[20] S. N. Coppersmith, C.-h. Liu, S. Majumdar, O. Narayan, and T. A. Witten. Model for force fluctuations in bead packs. *Phys. Rev. E*, 53 (5):4673–4685, May 1996.

[21] M. C. Costa-Cabral and S. J. Burges. Sensitivity of channel network planform laws and the question of topologic randomness. *Water Resour. Res.*, 33(9):2179–2197, September 1997.

[22] G. Cui, B. Williams, and G. Kuczera. A stochastic Tokunaga model for stream networks. *Water Resour. Res.*, 35(10):3139–3147, 1999.

[23] C. Dawson, G. Krenz, K. Karau, S. Haworth, C. Hanger, and J. Linehan. Structure-function relationships in the pulmonary arterial tree. *J. Appl. Physiol.*, 86(2):569–583, February 1999.

[24] H. de Vries, T. Becker, and B. Eckhardt. Power law distribution of discharge in ideal networks. *Water Resour. Res.*, 30(12):3541–3543, December 1994.

[25] D. Dhar. Sandpiles and self-organized criticality. *Physica A*, 186:82–87, 1992.

[26] D. Dhar. The abelian sandpile and related models. *Physica A*, 263: 4–25, 1999.

[27] D. Dhar and S. N. Majumdar. Abelian sandpile model on the Bethe lattice. *J. Phys. A: Math. Gen.*, 23:4333–4350, 1990.

[28] W. Dietrich and D. Montgomery. Hillslopes, channels, and landscape scale. In G. Sposito, editor, *Scale Dependence and Scale Invariance in Hydrology*, pages 30–60. Cambridge University Press, Cambridge, United Kingdom, 1998.

[29] W. E. Dietrich and T. Dunne. The channel head. In K. Beven and M. Kirkby, editors, *Channel Network Hydrology*, chapter 7, pages 175–219. John Wiley & Sons Ltd, New York, 1993.

[30] P. S. Dodds, R. Pastor-Satorras, and D. H. Rothman. Fluctuation in river network scaling laws. In preparation, 1999.

[31] P. S. Dodds and D. H. Rothman. Unified view of scaling laws for river networks. *Phys. Rev. E*, 59(5):4865–4877, May 1999.

[32] P. S. Dodds and D. H. Rothman. Geometry of river networks I: Scaling, fluctuations, and deviations. submitted to PRE, 2000.

[33] P. S. Dodds and D. H. Rothman. Geometry of river networks II: Distributions of component size and number. submitted to PRE, 2000.

[34] P. S. Dodds and D. H. Rothman. Geometry of river networks III: Characterization of component connectivity. submitted to PRE, 2000.

[35] P. S. Dodds and D. H. Rothman. Scaling, universality, and geomorphology. *Annu. Rev. Earth Planet. Sci.*, 28:571–610, 2000.

[36] A. Einstein. Motion of suspended particles in the kinetic theory. *Ann. Phys.*, 17:549–, 1905.

[37] J. Feder. *Fractals.* Plenum Press, New York, 1988.

[38] M. J. Feigenbaum. Universal behavior in nonlinear systems. *Los Alamos Science*, 1:4–27, 1980.

[39] W. Feller. *An Introduction to Probability Theory and Its Applications*, volume I. John Wiley & Sons, New York, third edition, 1968.

[40] W. Feller. *An Introduction to Probability Theory and Its Applications*, volume II. John Wiley & Sons, New York, third edition, 1968.

[41] J. J. Flint. Stream gradient as a function of order, magnitude, and discharge. *Water Resour. Res.*, 10(5):969–973, 1974.

[42] Y.-C. B. Fung. *Biomechanics: motion, flow, stress, and growth.* Springer-Verlag, New York, 1990.

[43] R. Gan, Y. Tian, R. Yen, and G. Kassab. Morphometry of the dog pulmonary venous tree. *J. Appl. Physiol.*, 75(1):432–440, 1993.

[44] R. Gan and R. Yen. Vascular impedance analysis in dog lung with detailed morphometric and elasticity data. *J. Appl. Physiol.*, 77(2): 706–717, 1994.

[45] C. W. Gardiner. *Handbook of Stochastic Methods for Physics, Chemistry and the Natural Sciences.* Springer, New York, second edition, 1985.

[46] V. Gardiner. Univariate distributional characterics of some morphometric variables. *Geogr. Ann.*, 55A(3–4):147–153, 1973.

[47] A. Giacometti. Local minimal energy landscapes in river networks. Preprint, 2000.

[48] W. S. Glock. The development of drainage systems: A synoptic view. *The Geogr. Rev.*, 21:475–482, 1931.

[49] N. Goldenfeld. *Lectures on Phase Transitions and the Renormalization Group*, volume 85 of *Frontiers in Physics*. Addison-Wesley, Reading, Massachusetts, 1992.

[50] I. Gradshteyn and I. Ryzhik. *Table of Integrals, Series, and Products.* Academic Press, San Diego, fifth edition, 1994.

[51] R. L. Graham, M. Grötschel, and L. Lovász, editors. *Handbook of Combinatorics*, volume II. MIT Press, Cambridge, MA, 1995.

[52] D. M. Gray. Interrelationships of watershed characteristics. *J. Geophys. Res.*, 66(4):1215–1223, 1961.

[53] H. Gray. *Gray's anatomy: the anatomical basis of medicine and surgery*. Churchill Livingstone, New York, 38th edition, 1995.

[54] J. T. Hack. Studies of longitudinal stream profiles in Virginia and Maryland. *U.S. Geol. Surv. Prof. Pap.*, 294-B:45–97, 1957.

[55] P. Haggett and R. J. Chorley. *Network Analysis in Geography*. Edward Arnold, London, 1969.

[56] W. K. Hayman. A generalization of Stirling's formula. *J. Reine Angew. Math.*, 196:67–95, 1956.

[57] E. Hinch. Hydrodynamics at low Reynolds numbers: a brief and elementary introduction. In E. Guyon, J.-P. Nadal, and Y. Pomeau, editors, *Disorder and Mixing*, volume 152 of *ASI series E: Applied Sciences*, pages 43–55. NATO, Kluwer Academic Press, 1988.

[58] R. E. Horton. Erosional development of streams and their drainage basins; hydrophysical approach to quatitative morphology. *Bull. Geol. Soc. Am*, 56(3):275–370, March 1945.

[59] A. D. Howard. Simulation of stream networks by headward growth and branching. *Geogr. Anal.*, 3:29–50, 1971.

[60] K. Huang. *Statistical Mechanics*. Wiley, New York, second edition, 1987.

[61] G. Huber. Scheidegger's rivers, takayasu's aggregates and continued fractions. *Physica A*, 170:463–470, 1991.

[62] J. S. Huxley and G. Teissier. Terminology of relative growth. *Nature*, 137:780–781, 1936.

[63] E. J. Ijjasz-Vasquez, R. L. Bras, and I. Rodríguez-Iturbe. Self-affine scaling of fractal river courses and basin boundaries. *Physica A*, 109: 288–300, 1994.

[64] N. Izumi and G. Parker. Inception of channelization and drainage basin formation: upstream-driven theory. *Journal of Fluid Mechanics*, 283: 341–363, 1995.

[65] H. Jaeger, S. Nagel, and R. Behringer. Granular solids, liquids, and gases. *Rev. Mod. Phys.*, 68(4):1259–1273, 1996.

[66] L. Kadanoff. Granular flows. *Rev. Mod. Phys.*, 71(1):435–444, January 1999.

[67] L. P. Kadanoff. Scaling and universality in statistical physics. *Physica A*, 163:1–14, 1990.

[68] L. P. Kadanoff, W. Gotze, D. Hamblen, R. Hecht, E. A. S. Lewis, V. V. Palciauskas, M. Rayl, and J. Swift. Static phenomena near critical points: theory and experiment. *Rev. Mod. Phys.*, 39:1–431, 1966.

[69] G. S. Kassab and Y.-C. B. Fung. Topology and dimensions of pig coronary capillary networks. *Am. J. Physiol.*, 267:H319–H325, 1994.

[70] G. S. Kassab, D. H. Lin, and Y.-C. B. Fung. Morphometry of pig coronary venous system. *Am. J. Physiol.*, 267:H2100–H2113, 1994.

[71] G. S. Kassab, C. A. Rider, T. N. J., and Y. B. Fung. Morphometry of pig coronary arterial trees. *Am. J. Physiol.*, 265:H350–H365, 1993.

[72] J. W. Kirchner. Statistical inevitability of Horton's laws and the apparent randomness of stream channel networks. *Geology*, 21:591–594, July 1993.

[73] S. Kramer and M. Marder. Evolution of river networks. *Phys. Rev. Lett.*, 68(2):205–208, January 1992.

[74] P. La Barbera and R. Rosso. On the fractal dimension of stream networks. *Water Resour. Res.*, 25(4):735–741, April 1989.

[75] P. La Barbera and R. Rosso. Reply. *Water Resour. Res.*, 26(9):2245–2248, September 1990.

[76] P. La Barbera and G. Roth. Invariance and scaling properties in the distributions of contributing area and energy in drainage basins. *Hydrol. Processes*, 8:125–135, 1994.

[77] H. Lamb. *Hydrodynamics*. Dover, New York, 6th edition, 1945.

[78] W. B. Langbein. Topographic characteristics of drainage basins. *U.S. Geol. Surv. Water-Supply Pap.*, W 0968-C:125–157, 1947.

[79] R. L. Leheny. Simple model for river network evolution. *Phys. Rev. E*, 52(5):5610–5620, November 1995.

[80] R. L. Leheny and S. R. Nagel. Model for the evolution of river networks. *Phys. Rev. Lett.*, 71(9):1470–73, August 1993.

[81] E. L. Lehman. *Nonparametrics : statistical methods based on ranks.* Holden-Day, San Francisoc, 1975.

[82] L. B. Leopold and W. B. Langbein. The concept of entropy in landscape evolution. *U.S. Geol. Surv. Prof. Pap.*, 500-A:1–20, 1962.

[83] B. B. Mandelbrot. *The Fractal Geometry of Nature*. Freeman, San Francisco, 1983.

[84] S. S. Manna, D. Dhar, and S. N. Majumdar. Spanning trees in two dimensions. *Phys. Rev. A*, 46:4471–4474, 1992.

[85] S. S. Manna and B. Subramanian. Quasirandom spanning tree model for the early river network. *Phys. Rev. Lett.*, 76(18):3460–3463, April 1996.

[86] A. Maritan, F. Colaiori, A. Flammini, M. Cieplak, and J. R. Banavar. Universality classes of optimal channel networks. *Science*, 272:984–986, May 1996.

[87] A. Maritan, A. Rinaldo, R. Rigon, A. Giacometti, and I. Rodríguez-Iturbe. Scaling laws for river networks. *Phys. Rev. E*, 53(2):1510–1515, February 1996.

[88] P. Meakin, J. Feder, and T. Jøssang. Simple statistical models for river networks. *Physica A*, 176:409–429, 1991.

[89] M. A. Melton. A derivation of Strahler's channel-ordering system. *J. Geol.*, 67:345–346, 1959.

[90] D. R. Montgomery and W. E. Dietrich. Channel initiation and the problem of landscape scale. *Science*, 255:826–30, 1992.

[91] E. W. Montroll and M. F. Shlesinger. *On the wonderful world of random walks*, volume XI of *Studies in statistical mechanics*, chapter 1, pages 1–121. New-Holland, New York, 1984.

[92] J. W. Moon. On the expected diameter of random channel networks. *Water Resour. Res.*, 16(6):1119–1120, December 1980.

[93] M. E. Morisawa. Quantitatitive geomorphology of some watersheds in the Appalachian Plateau. *Geological Society of America Bulletin*, 73: 1025–1046, September 1962.

[94] M. P. Mosley and R. S. Parker. Re-evalution of the relationship of master streams and drainage basins: Discussion. *Geological Society of America Bulletin*, 84:3123–3126, September 1973.

[95] J. E. Mueller. Re-evaluation of the relationship of master streams and drainage basins. *Geological Society of America Bulletin*, 83:3471–3473, November 1972.

[96] J. E. Mueller. Re-evaluation of the relationship of master streams and drainage basins: Reply. *Geological Society of America Bulletin*, 84: 3127–3130, September 1973.

[97] W. I. Newman, D. L. Turcotte, and A. M. Gabrielov. Fractal trees with side branching. *Fractals*, 5(4):603–614, December 1997.

[98] R. Pastor-Satorras and D. H. Rothman. Scaling of a slope: the erosion of tilted landscapes. *J. Stat. Phys.*, 93:477–500, 1998.

[99] R. Pastor-Satorras and D. H. Rothman. Stochastic equation for the erosion of inclined topography. *Phys. Rev. Lett.*, 80(19):4349–4352, May 1998.

[100] K. Pearson. The problem of the random walk. *Nature*, 72:294–, 1905.

[101] S. Peckham and V. Gupta. A reformulation of horton's laws for large river networks in terms of statistical self-similarity. *Water Resour. Res.*, 35(9):2763–2777, 1999.

[102] S. D. Peckham. New results for self-similar trees with applications to river networks. *Water Resour. Res.*, 31(4):1023–1029, April 1995.

[103] J. Pelletier and D. Turcotte. Shapes of river networks and leaves: are they statistically similar? *Philos. T. Roy. Soc. B*, 355(1394):307–311, 2000.

[104] W. H. Press, S. A. Teukolsky, W. T. Vetterling, and B. P. Flannery. *Numerical Recipes in C*. Cambridge University Press, second edition, 1992.

[105] F. Reif. *Fundamentals of Statistical and Thermal Physics*. McGraw-Hill, New York, 1965.

[106] R. Rigon, I. Rodríguez-Iturbe, A. Maritan, A. Giacometti, D. G. Tarboton, and A. Rinaldo. On Hack's law. *Water Resour. Res.*, 32(11): 3367–3374, November 1996.

[107] R. Rigon, I. Rodríguez-Iturbe, and A. Rinalod. Feasible optimality implies Hack's law. *Water Resour. Res.*, 34(11):3181–3189, November 1998.

[108] A. Rinaldo, I. Rodríguez-Iturbe, and R. Rigon. Channel networks. *Annu. Rev. Earth Planet. Sci*, 26:289–327, 1998.

[109] A. Rinaldo, I. Rodríguez-Iturbe, R. Rigon, E. Ijjasz-Vasquez, and R. L. Bras. Self-organized fractal river networks. *Phys. Rev. Lett.*, 70(6):822–5, February 1993.

[110] I. Rodríguez-Iturbe and A. Rinaldo. *Fractal River Basins: Chance and Self-Organization*. Cambridge University Press, Great Britain, 1997.

[111] R. Rosso, B. Bacchi, and P. La Barbera. Fractal relation of mainstream length to catchment area in river networks. *Water Resour. Res.*, 27(3): 381–387, March 1991.

[112] A. E. Scheidegger. A stochastic model for drainage patterns into an intramontane trench. *Bull. Int. Assoc. Sci. Hydrol.*, 12(1):15–20, 1967.

[113] A. E. Scheidegger. Horton's law of stream lengths and drainage areas. *Water Resour. Res.*, 4(5):1015–1021, October 1968.

[114] A. E. Scheidegger. *Theoretical Geomorphology*. Springer-Verlag, New York, third edition, 1991.

[115] A. E. Scheidegger. *Theoretical Geomorphology*. Springer-Verlag, New York, third edition, 1991.

[116] S. A. Schumm. Evolution of drainage systems and slopes in badlands at Perth Amboy, New Jersey. *Bull. Geol. Soc. Am*, 67:597–646, May 1956.

[117] R. L. Shreve. Statistical law of stream numbers. *J. Geol.*, 74:17–37, 1966.

[118] R. L. Shreve. Infinite topologically random channel networks. *J. Geol.*, 75:178–186, 1967.

[119] K. Sinclair and R. C. Ball. Mechanism for global optimization of river networks from local erosion rules. *Phys. Rev. Lett.*, 76(18):3360–3363, April 1996.

[120] J. S. Smart. A comment on Horton's law of stream numbers. *Water Resour. Res.*, 3(3):773–776, 1967.

[121] T. R. Smith and F. P. Bretherton. Stability and the conservation of mass in drainage basin evolution. *Water Resour. Res.*, 3(6):1506–28, 1972.

[122] E. Somfai and L. M. Sander. Scaling and river networks: A Landau theory for erosion. *Phys. Rev. E*, 56(1):R5–R8, 1997.

[123] P. Sprent. *Applied Nonparametric Statistical Methods*. Chapman & Hall, New York, second edition, 1993.

[124] C. P. Stark. An invasion percolation model of drainage network evolution. *Nature*, 352:405–409, 1991.

[125] C. P. Stark. Stream networks on a bethe lattice: Cayley trees, invasion percolation and branching ratios. Preprint, 1997.

[126] D. Stauffer and A. Aharony. *Introduction to Percolation Theory*. Taylor & Francis, Washington, D.C., second edition, 1992.

[127] A. N. Strahler. Hypsometric (area altitude) analysis of erosional topography. *Bull. Geol. Soc. Am*, 63:1117–1142, 1952.

[128] A. N. Strahler. Quantitative analysis of watershed geomorphology. *EOS Trans. AGU*, 38(6):913–920, December 1957.

[129] S. H. Strogatz. *Nonlinear Dynamics and Chaos*. Addison Wesley, Reading, Massachusetts, 1994.

[130] T. Sun, P. Meakin, and T. Jøssang. Minimum energy dissipation model for river basin geometry. *Phys. Rev. E*, 49(6):4865–4872, June 1994.

[131] T. Sun, P. Meakin, and T. Jøssang. The topography of optimal drainage basins. *Water Resour. Res.*, 30(9):2599–2619, September 1994.

[132] T. Sun, P. Meakin, and T. Jøssang. Minimum energy dissipation river networks with fractal boundaries. *Phys. Rev. E*, 51(6):5353–5359, June 1995.

[133] G. Szekeres. Asymptotic distribution of the number and size of parts in unequal partitions. *Bull. Austral. Math. Soc.*, 36(1):89–97, 1987.

[134] G. Szekeres. Asymptotic distribution of partitions by number and size of parts. In K. Győry and G. Halász, editors, *Number theory, Vol. I (Budapest, 1987)*, pages 527–538. North-Holland, Amsterdam, 1990.

[135] H. Takayasu. Steady-state distribution of generalized aggregation system with injection. *Physcial Review Letters*, 63(23):2563–2565, December 1989.

[136] H. Takayasu. *Fractals in the Physical Sciences*. Manchester University Press, Manchester, 1990.

[137] H. Takayasu and H. Inaoka. New type of self-organized criticality in a model of erosion. *Phys. Rev. Lett.*, 68(7):966–9, February 1992.

[138] H. Takayasu, I. Nishikawa, and H. Tasaki. Power-law mass distribution of aggregation systems with injection. *Phys. Rev. A*, 37(8):3110–3117, April 1988.

[139] H. Takayasu, M. Takayasu, A. Provata, and G. Huber. Statistical properties of aggregation with injection. *J. Stat. Phys.*, 65(3/4):725–, 1991.

[140] M. Takayasu and H. Takayasu. Apparent independency of an aggregation system with injection. *Phys. Rev. A*, 39(8):4345–4347, April 1989.

[141] D. G. Tarboton, R. L. Bras, and I. Rodríguez-Iturbe. The fractal nature of river networks. *Water Resour. Res.*, 24(8):1317–22, August 1988.

[142] D. G. Tarboton, R. L. Bras, and I. Rodríguez-Iturbe. Scaling and elevation in river networks. *Water Resour. Res.*, 25(9):2037–51, September 1989.

[143] D. G. Tarboton, R. L. Bras, and I. Rodríguez-Iturbe. Comment on "On the fractal dimension of stream networks" by Paolo La Barbera and Renzo Rosso. *Water Resour. Res.*, 26(9):2243–4, September 1990.

[144] E. Tokunaga. The composition of drainage network in Toyohira River Basin and the valuation of Horton's first law. *Geophys. Bull. Hokkaido Univ.*, 15:1–19, 1966.

[145] E. Tokunaga. Consideration on the composition of drainage networks and their evolution. *Geogr. Rep., Tokyo Metrop. Univ.*, 13:1–27, 1978.

[146] E. Tokunaga. Ordering of divide segments and law of divide segment numbers. *Trans. Jpn. Geomorphol. Union*, 5(2):71–77, 1984.

[147] D. L. Turcotte, J. D. Pelletier, and W. I. Newman. Networks with side branching in biology. *J. Theor. Biol.*, 193:577–592, 1998.

[148] D. J. Watts. *Small Worlds : The Dynamics of Networks Between Order and Randomness*. Princeton Studies in Complexity. Princeton University Press, Princeton, 1999.

[149] D. J. Watts and S. J. Strogatz. Collective dynamics of 'small-world' networks. *Nature*, 393:440–442, June 1998.

[150] E. Waymire. On the main channel length-magnitude formula for random networks: A solution to moon's conjecture. *Water Resour. Res.*, 25(5):1049–1050, May 1989.

[151] G. B. West, J. H. Brown, and B. J. Enquist. A general model for the origin of allometric scaling laws in biology. *Science*, 276:122–126, April 1997.

[152] G. Willgoose, R. L. Bras, and I. Rodríguez-Iturbe. A coupled channel network growth and hillslope evolution model; 1. theory. *Water Resour. Res.*, 27(7):1671–1684, July 1991.

[153] G. Willgoose, R. L. Bras, and I. Rodríguez-Iturbe. A coupled channel network growth and hillslope evolution model; 2. nondimensionsalization and applications. *Water Resour. Res.*, 27(7):1685–1696, July 1991.

[154] G. Willgoose, R. L. Bras, and I. Rodríguez-Iturbe. Results from a new model of river basin evolution. *Earth Surf. Proc. Landforms*, 16: 237–254, 1991.

[155] K. G. Wilson and J. B. Kogut. The renormalization group and the epsilon expansion. *Phys. Rep.*, 12C:75–200, 1974.

[156] M. Zamir. On fractal properties of arterial trees. *J. Theor. Biol.*, 197: 517–526, 1999.

[157] M. Zamir, S. M. Wrigley, and B. L. Langille. Arterial bifurcations in the cardiovascular system of a rat. *J. Gen. Physiol.*, 81:325–335, 1983.

[158] W. Zinsser. *On Writing Well*. HarperCollins, sixth edition, 1998.

Citation Index

[1] Abrahams (1984), 44, 98
[2] Aharinejad et al. (1998), 99
[3] Albert et al. (1999), 13, 68
[4] Alder and Wainwright (1970), 25
[5] Allman (1999), 13
[6] Andrews (1976), 171, 173
[7] Bak (1996), 35
[8] Ball (1998), 68
[9] Banavar et al. (1997), 32, 68
[10] Barabasi and Stanley (1995), 21
[11] Barenblatt (1996), 26
[12] Bartlett (1992), 14
[13] Bender and Orszag (1978), 140, 165, 175
[14] Bolker (1998), 6
[15] Caldarelli et al. (1997), 68
[16] Carrier et al. (1966), 161
[17] Cherniak et al. (1999), 13, 68
[18] Cieplak et al. (1998), 60, 68
[19] Colaiori et al. (1997), 60, 129
[20] Coppersmith et al. (1996), 68, 75
[21] Costa-Cabral and Burges (1997), 31
[22] Cui et al. (1999), 124, 148
[23] Dawson et al. (1999), 13
[24] de Vries et al. (1994), 45, 46, 50, 60, 101
[25] Dhar (1992), 75
[26] Dhar (1999), 75, 131
[27] Dhar and Majumdar (1990), 75
[28] Dietrich and Montgomery (1998), 86
[29] Dietrich and Dunne (1993), 86
[30] Dodds et al. (1999), 49, 52
[31] Dodds and Rothman (1999), 69–71, 74, 89, 90, 98, 100, 101, 103, 111, 114, 122, 124, 126, 127, 130, 131, 147
[32] Dodds and Rothman (2000), 23, 98, 99, 109, 110, 114, 122, 125, 130
[33] Dodds and Rothman (2000), 23, 69, 72, 89, 118, 122–124, 127, 130, 134, 135
[34] Dodds and Rothman (2000), 23, 69, 72, 99, 102, 103, 106, 109, 110, 120
[35] Dodds and Rothman (2000), 16, 68, 69, 71, 86, 98, 100, 122, 129
[36] Einstein (1905), 167
[37] Feder (1988), 56
[38] Feigenbaum (1980), 26
[39] Feller (1968), 20, 22, 75, 79, 109, 131, 167, 169, 178
[40] Feller (1968), 76
[41] Flint (1974), 32
[42] Fung (1990), 99

[96] Mueller (1973), 39, 70
[97] Newman et al. (1997), 39
[98] Pastor-Satorras and Rothman (1998), 68
[99] Pastor-Satorras and Rothman (1998), 68
[100] Pearson (1905), 167
[101] Peckham and Gupta (1999), 89, 98
[102] Peckham (1995), 39, 46, 53, 54, 114, 124, 127
[103] Pelletier and Turcotte (2000), 13
[104] Press et al. (1992), 93
[105] Reif (1965), 25
[106] Rigon et al. (1996), 23, 38, 44, 49, 62, 68, 70, 73
[107] Rigon et al. (1998), 70, 73
[108] Rinaldo et al. (1998), 32, 68, 98
[109] Rinaldo et al. (1993), 98
[110] Rodríguez-Iturbe and Rinaldo (1997), 32, 35–37, 39, 43, 45, 49, 50, 60, 68, 74, 98, 122, 129
[111] Rosso et al. (1991), 50, 53, 55, 56, 58
[112] Scheidegger (1967), 16, 27, 36, 42, 68, 72, 74, 98, 122, 129, 130
[113] Scheidegger (1968), 41
[114] Scheidegger (1991), 13
[115] Scheidegger (1991), 36, 42
[116] Schumm (1956), 42, 89, 98, 99, 126, 127
[117] Shreve (1966), 30, 31, 35
[118] Shreve (1967), 30, 31, 45, 46
[119] Sinclair and Ball (1996), 32, 68

[120] Smart (1967), 51
[121] Smith and Bretherton (1972), 68
[122] Somfai and Sander (1997), 35, 68
[123] Sprent (1993), 93
[124] Stark (1991), 35, 68, 98
[125] Stark (1997), 56
[126] Stauffer and Aharony (1992), 30
[127] Strahler (1952), 35
[128] Strahler (1957), 36, 89, 99, 123
[129] Strogatz (1994), 26
[130] Sun et al. (1994), 35, 68, 98
[131] Sun et al. (1994), 35
[132] Sun et al. (1995), 68
[133] Szekeres (1987), 172
[134] Szekeres (1990), 172
[135] Takayasu (1989), 42, 44
[136] Takayasu (1990), 42, 44
[137] Takayasu and Inaoka (1992), 68
[138] Takayasu et al. (1988), 23, 42, 44, 74, 75, 131
[139] Takayasu et al. (1991), 42, 44, 131
[140] Takayasu and Takayasu (1989), 42, 44, 131
[141] Tarboton et al. (1988), 35, 39, 43, 45, 56, 59, 60, 101
[142] Tarboton et al. (1989), 45
[143] Tarboton et al. (1990), 35, 39, 45, 56, 57, 71, 101, 129
[144] Tokunaga (1966), 18, 39, 40, 51, 69, 114, 122, 124
[145] Tokunaga (1978), 18, 31, 39, 44–46, 48, 69, 114, 122, 124, 127

[146] Tokunaga (1984), 18, 39, 69,
        114, 122, 124, 127
[147] Turcotte et al. (1998), 99, 124
[148] Watts (1999), 13
[149] Watts and Strogatz (1998),
        13, 68
[150] Waymire (1989), 31
[151] West et al. (1997), 63
[152] Willgoose et al. (1991), 35
[153] Willgoose et al. (1991), 35
[154] Willgoose et al. (1991), 35
[155] Wilson and Kogut (1974), 26
[156] Zamir (1999), 68, 99
[157] Zamir et al. (1983), 99
[158] Zinsser (1998), 6

Notation

Subject Index